EC 8751 – OPTICAL COMMUNICATION

UNIT – 1

INTRODUCTION TO OPTICAL FIBERS

INTRODUCTION

Communication may be broadly defined as the transfer of information from one point to another. When the information is to be conveyed over any distance a communication system is usually required. Within a communication system the information transfer is frequently achieved by superimposing or modulating the information onto an electromagnetic wave which acts as a carrier for the information signal. This modulated carrier is then trans- mitted to the required destination where it is received and the original information signal is obtained by demodulation. Sophisticated techniques have been developed for this process using electromagnetic carrier waves operating at radio frequencies as well as microwave and millimeter wave frequencies. However, 'communication' may also be achieved using an electromagnetic carrier which is selected from the optical range of frequencies.

The general system:

An optical fiber communication system is similar in basic concept to any type of communication system. A block schematic of a general communication system is shown in Figure 1.2(a), the function of which is to convey the signal from the information source over the transmission medium to the destination. The communication system therefore consists of a transmitter or modulator linked to the information source, the transmission medium, and a receiver or demodulator at the destination point. In electrical communications the information source provides an electrical signal, usually derived from a message signal which is not electrical (e.g. sound), to a transmitter comprising electrical and electronic components which converts the signal into a suitable form for propagation over the transmission medium. This is often achieved by modulating a carrier, which, as mentioned pre- viously, may be an electromagnetic wave.

For optical fiber communications the system shown in Figure 1.1(a) may be considered in slightly greater detail, as given in Figure 1.1(b). In this case the information source pro- vides an electrical signal to a transmitter comprising an electrical stage which drives an optical source to give modulation of the light wave carrier. The optical source which pro- vides the electrical–optical conversion may be either a semiconductor laser or light-emitting diode (LED).

The transmission medium consists of an optical fiber cable and the receiver consists of an optical detector which drives a further electrical stage and hence provides demodulation of the optical carrier. Photodiodes (*p–n*, *p–i–n* or avalanche) and, in some instances, phototransistors and photoconductors are utilized for the detection of the optical signal and the optical–electrical conversion. Thus there is a requirement for electrical interfacing at either end of the optical link and at present the signal processing is usually performed electrically.*

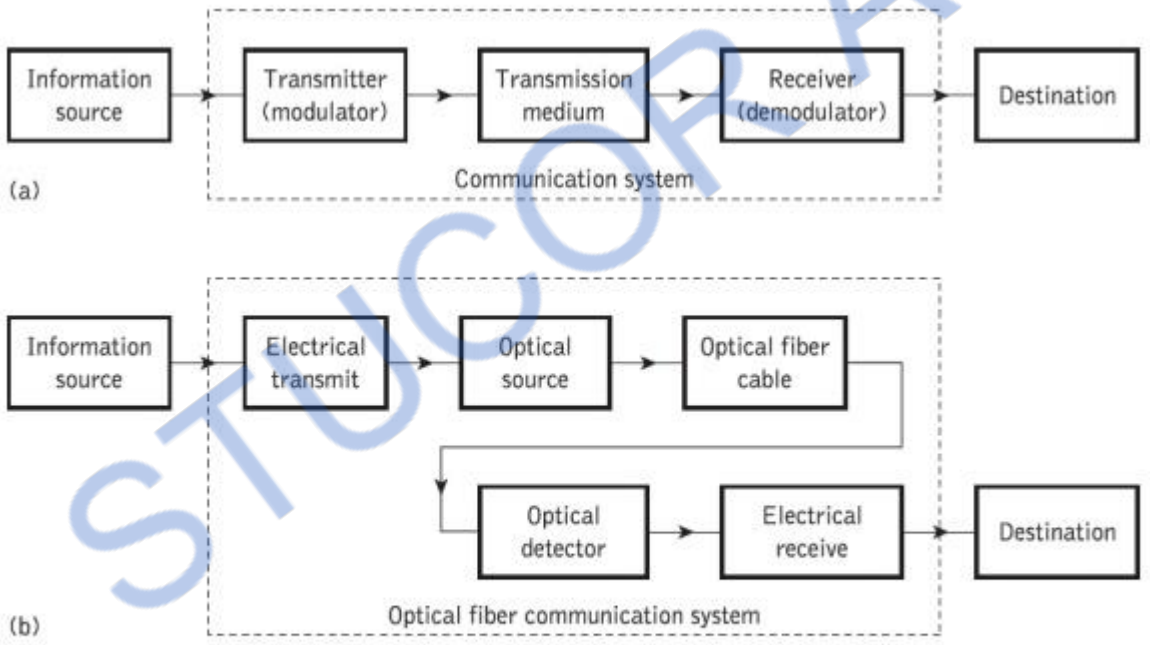

Figure 1.1 (a) The general communication system. (b) The optical fiber communication system

The optical carrier may be modulated using either an analog or digital information signal. In the system shown in Figure 1.1(b) analog modulation involves the variation of the light emitted from the optical source in a continuous manner. With digital modulation, however, discrete changes in the light intensity are obtained (i.e. on–off

pulses). Although often simpler to implement, analog modulation with an optical fiber communication sys- tem is less efficient, requiring a far higher signal-to-noise ratio at the receiver than digital modulation. Also, the linearity needed for analog modulation is not always provided by semiconductor optical sources, especially at high modulation frequencies. For these reasons, analog optical fiber communication links are generally limited to shorter distances and lower bandwidth operation than digital links.

Introduction

The transmission of light via a dielectric waveguide structure was first proposed and investigated at the beginning of the twentieth century. In 1910 Hondros and Debye conducted a theoretical study, and experimental work was reported by Schriever in 1920. However, a transparent dielectric rod, typically of silica glass with a refractive index of around 1.5, surrounded by air, proved to be an impractical waveguide due to its unsupported structure (especially when very thin waveguides were considered in order to limit the number of optical modes propagated) and the excessive losses at any dis- continuities of the glass–air interface. Nevertheless, interest in the application of dielectric optical waveguides in such areas as optical imaging and medical diagnosis (e.g. endoscopes) led to proposals for a clad dielectric rod in the mid-1950s in order to overcome these problems. This structure is illustrated in Figure 2.1, which shows a trans- parent core with a refractive index n_1 surrounded by a transparent cladding of slightly lower refractive index n_2. Theinvention of the clad waveguide structure led to the first serious proposals by Kao and Hockham and Werts, in 1966, to utilize optical fibers as a communications medium, even though they had losses in excess of 1000 dB km^{-1}.

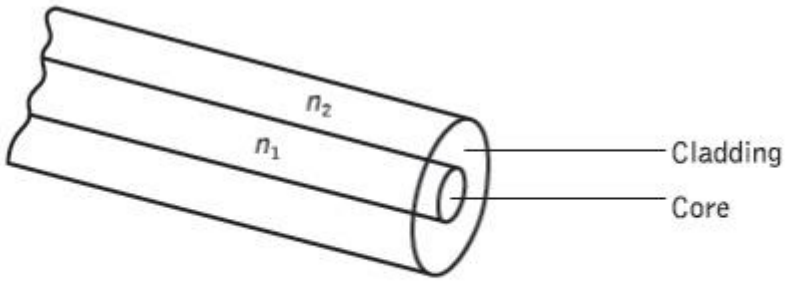

Figure 1.1 (c) Optical fiber waveguide showing the core of refractive index $n1$, surrounded by the cladding of slightly lower refractive index $n2$

These proposals stimulated tremendous efforts to reduce the attenuation by purification of the materials. This has resulted in improved conventional glass refining techniques giving fibers

with losses of around 4.2 dB km. Also, progress in glass refining processes such as depositing vapor-phase reagents to form silice allowed fibers with losses below 1 dB km to be fabricated.

Most of this work was focused on the 0.8 to 0.9 μm wavelength band because the first generation of optical sources fabricated from gallium aluminum arsenide alloys operated in this region. However, as silica fibers were studied in further detail it became apparent that transmission at longer wavelengths (1.1 to 1.6 μm) would result in lower losses and reduced signal dispersion. This produced a shift in optical fiber source and detector technology in order to provide operation at these longer wavelengths. Hence at longer wavelengths, especially around 1.55 μm, typical high-performance fibers have losses of 0.2 dB km.

As such losses are very close to the theoretical lower limit for silicate glass fiber, there is interest in glass-forming systems which can provide low-loss transmission in the mid infrared (2 to 5 μm) optical wavelength regions. Although a system based on fluoride glass offers the potential for ultra-low-loss transmission of 0.01 dB kmat a wavelength of 2.55 μm, such fibers still exhibit losses of at least 0.65 dB km properties of silica fibers.

In order to appreciate the transmission mechanism of optical fibers with dimensions approximating to those of a human hair, it is necessary to consider the optical

waveguideing of a cylindrical glass fiber. Such a fiber acts as an open optical waveguide, which may be analyzed utilizing simple ray theory. However, the concepts of geometric optics are not sufficient when considering all types of optical fiber, and electromagnetic mode theory must be used to give a complete picture. The following sections will therefore outline the transmission of light in optical fibers prior to a more detailed discussion of the various types of fiber.

Ray theory transmission

1. Total internal reflection

To consider the propagation of light within an optical fiber utilizing the ray theory model it is necessary to take account of the refractive index of the dielectric medium. The refractive index of a medium is defined as the ratio of the velocity of light in a vacuum to the velocity of light in the medium.

A ray of light travels more slowly in an optically dense medium than in one that is less dense, and the refractive index gives a measure of this effect. When a ray is incident on the interface between two dielectrics of differing refractive indices (e.g. glass–air), refraction occurs, as illustrated in Figure 1.2(a). It may be observed that the ray approaching the interface is propagating in a dielectric of refractive index n and is at an angle φ to the normal at the surface of the interface. If the dielectric on the other side of the interface has a refractive index $n$which is less than n_1, then the refraction is such that the ray path in this lower index medium is at an angle to the normal, where is greater than . The angles of incidence and refraction are related to each other and to the refractive indices of the dielectrics by Snell's law of refraction, which states that:

$$n_1 \sin \phi_1 = n_2 \sin \phi_2$$

Or

$$\frac{\sin \phi_1}{\sin \phi_2} = \frac{n_2}{n_1} \qquad (1.1)$$

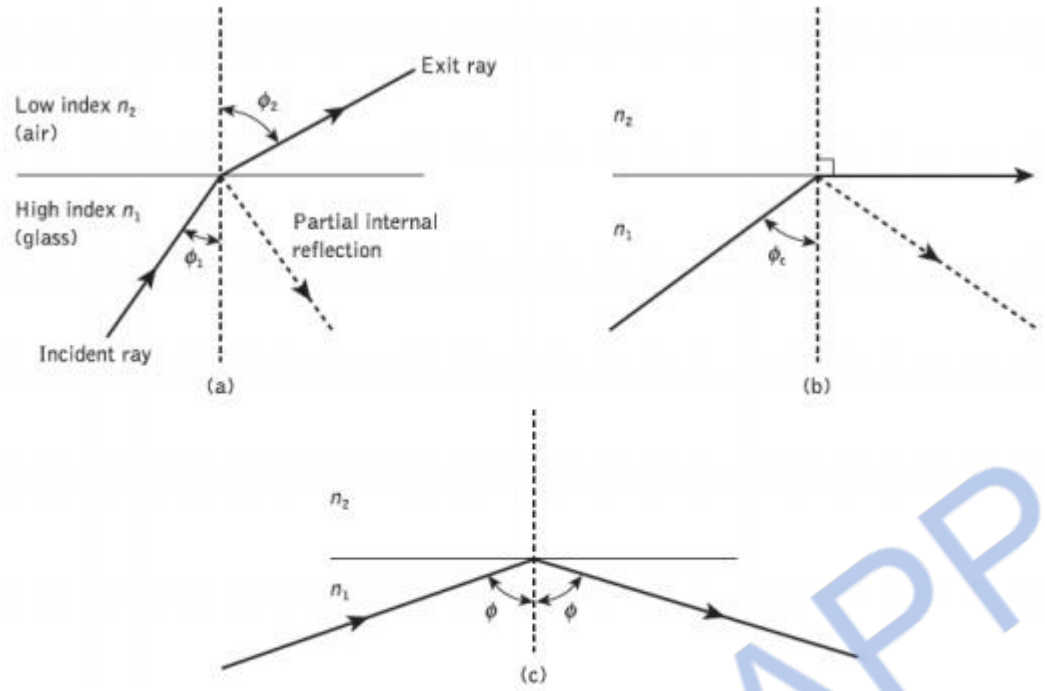

Figure 1.2 Light rays incident on a high to low refractive index interface (e.g. glass air): (a) refraction; (b) the limiting case of refraction showing the critical ray at an angle φ_c (c) total internal reflection where $\varphi > \varphi_c$

It may also be observed in Figure 1.2(a) that a small amount of light is reflected back into the originating dielectric medium (partial internal reflection). As *n*is greater than *n*, the angle of refraction is always greater than the angle of incidence. Thus when the angle of refraction is 90° and the refracted ray emerges parallel to the interface between the dielectrics, the angle of incidence must be less than 90°. This is the limiting case of refraction and the angle of incidence is now known as the critical angle φc, as shown in Figure 1.2(b). From Eq. (1.1) the value of the critical angle is given by

$$\sin \phi_c = \frac{n_2}{n_1} \tag{1.2}$$

At angles of incidence greater than the critical angle the light is reflected back into the originating dielectric medium (total internal reflection) with high efficiency (around 99.9%). Hence, it may be observed in Figure 1.2(c) that total internal reflection occurs at the inter- face between two dielectrics of differing refractive indices when light is incident on the dielectric of lower index from the dielectric of higher index, and the

angle of incidence of the ray exceeds the critical value. This is the mechanism by which light at a sufficiently shallow angle (less than 90° − may be considered to propagate down an optical fiber with low loss.

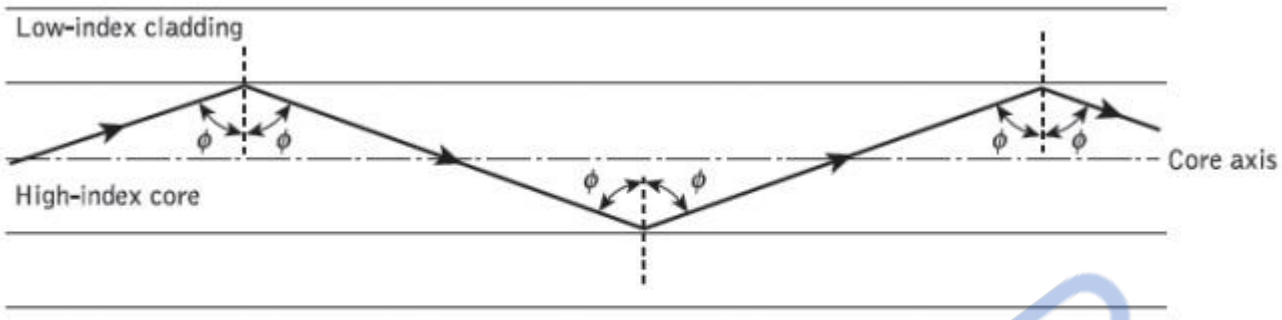

Figure 1.3 The transmission of a light ray in a perfect optical fiber

Figure 1.3 illustrates the transmission of a light ray in an optical fiber via a series of total internal reflections at the interface of the silica core and the slightly lower refractive index silica cladding. The ray has an angle of incidence φ at the interface which is greater than the critical angle and is reflected at the same angle to the normal.

The light ray shown in Figure 1.3 is known as a meridional ray as it passes through the axis of the fiber core. This type of ray is the simplest to describe and is generally used when illustrating the fundamental transmission properties of optical fibers. It must also be noted that the light transmission illustrated in Figure 1.3 assumes a perfect fiber, and that any discontinuities or imperfections at the core–cladding interface would probably result in refraction rather than total internal reflection, with the subsequent loss of the light ray into the cladding.

2. Acceptance angle

Having considered the propagation of light in an optical fiber through total internal reflection at the core–cladding interface, it is useful to enlarge upon the geometric optics approach with reference to light rays entering the fiber. Since only rays with a sufficiently shallow grazing angle (i.e. with an angle to the normal greater than φ_c) at the core–cladding interface are transmitted by total internal reflection, it is clear that not all rays entering the fiber core will continue to be propagated down its length.

The geometry concerned with launching a light ray into an optical fiber is shown in Figure1.4, which illustrates a meridional ray *A* at the critical angle φ_c within the fiber at the core– cladding interface. It may be observed that this ray enters the fiber core at an angle θ_a to the fiber axis and is refracted at the air–core interface before transmission to the core–cladding interface at the critical angle. Hence, any rays which are incident into the fiber core at an angle greater than θ_a will be transmitted to the core–cladding interface at an angle less than φ_c, and will not be totally internally reflected. This situation is also illustrated in Figure 2.4, where the incident ray *B* at an angle greater than θ_a is refracted into the cladding and eventually lost by radiation. Thus for rays to be transmitted by total internal reflection within the fiber core they must be incident on the fiber core within an acceptance cone defined by the conical half angle θ_a.

Hence θa is the maximum angle to the axis at which light may enter the fiber in order to be propagated, and is often referred to as the acceptance angle for the fiber.

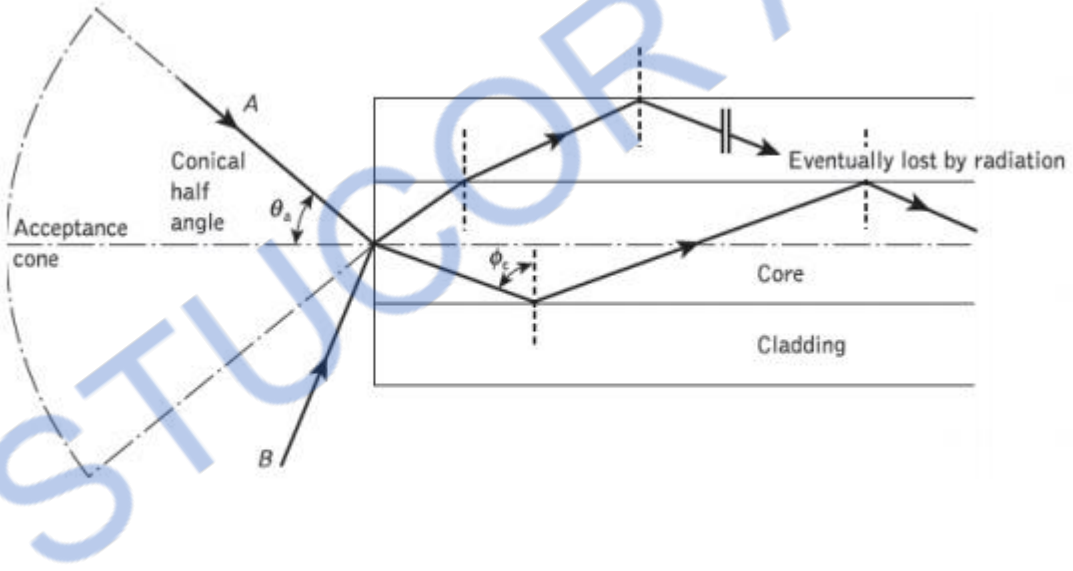

Figure 1.4 The acceptance angle θ_a when launching light into an optical fiber

If the fiber has a regular cross-section (i.e. the core–cladding interfaces are parallel and there are no discontinuities) an incident meridional ray at greater than the critical angle will continue to be reflected and will be transmitted through the fiber. From symmetry considerations it may be noted that the output angle to the axis will be equal to the input angle for the ray, assuming the ray emerges into a medium of the same refractive index from which it was input.

3. Numerical aperture

The acceptance angle for an optical fiber was defined in the preceding section. However, it is possible to continue the ray theory analysis to obtain a relationship between the acceptance angle and the refractive indices of the three media involved, namely the core, cladding and air. This leads to the definition of a more generally used term, the numerical aperture of the fiber. It must be noted that within this analysis, as with the preceding discussion of acceptance angle, we are concerned with meridional rays within the fiber. Figure 1.5 shows a light ray incident on the fiber core at an angle θ_1 to the fiber axis which is less than the acceptance angle for the fiber θ_a. The ray enters the fiber from a medium (air) of refractive index n_0, and the fiber core has a refractive index n_1, which is slightly greater than the cladding refractive index n_2.

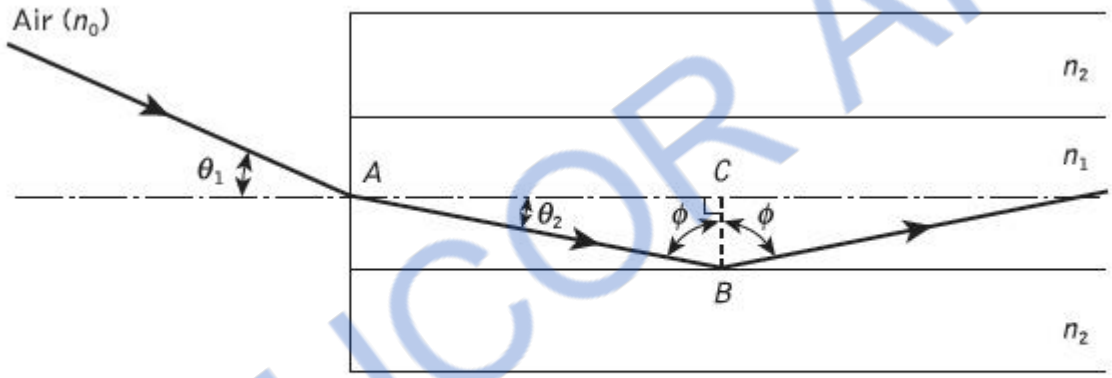

Figure 2.5 The ray path for a meridional ray launched into an optical fiber in air at an input angle less than the acceptance angle for the fiber

Assuming the entrance face at the fiber core to be normal to the axis, then considering the refraction at the air–core interface and using Snell's law given by Eq. (1.1):

$$n_0 \sin \theta_1 = n_1 \sin \theta_2 \tag{1.3}$$

Considering the right-angled triangle *ABC* indicated in Figure 2.5, then:

$$\phi = \frac{\pi}{2} - \theta_2 \tag{1.4}$$

where φ is greater than the critical angle at the core–cladding interface. Hence Eq. (1.3) becomes:

$$n_0 \sin \theta_1 = n_1 \cos \phi \tag{1.5}$$

Using the trigonometrical relationship $\sin^2 \varphi + \cos^2 \varphi = 1$, Eq. (1.5) may be written in the form:

$$n_0 \sin \theta_1 = n_1 (1 - \sin^2 \phi)^{\frac{1}{2}} \tag{1.6}$$

When the limiting case for total internal reflection is considered, φ becomes equal to the critical angle for the core–cladding interface and is given by Eq. (1.2). Also in this limiting case θ_1 becomes the acceptance angle for the fiber θ_a. Combining these limiting cases into Eq. (1.6) gives:

$$n_0 \sin \theta_a = (n_1^2 - n_2^2)^{\frac{1}{2}} \tag{1.7}$$

Equation (1.7), apart from relating the acceptance angle to the refractive indices, serves as the basis for the definition of the important optical fiber parameter, the numerical aperture (*NA*). Hence the *NA* is defined as:

$$NA = n_0 \sin \theta_a = (n_1^2 - n_2^2)^{\frac{1}{2}} \tag{1.8}$$

Since the *NA* is often used with the fiber in air where n_0 is unity, it is simply equal to sin θ_a. It may also be noted that incident meridional rays over the range $0 \leq \theta_1 \leq \theta_a$ will be propagated within the fiber. The *NA* may also be given in terms of the relative refractive index difference between the core and the cladding which is defined as:

$$\Delta = \frac{n_1^2 - n_2^2}{2n_1^2}$$

$$\simeq \frac{n_1 - n_2}{n_1} \qquad \text{for } \Delta \ll 1 \tag{1.9}$$

Hence combining Eq. (1.8) with Eq. (1.9) we can write:

$$NA = n_1(2\Delta)^{\frac{1}{2}} \tag{1.10}$$

The relationships given in Eqs (1.8) and (1.10) for the numerical aperture are a very useful measure of the light-collecting ability of a fiber. They are independent of the fiber core diameter and will hold for diameters as small as 8 μm. However, for smaller diameters they break down as the geometric optics approach is invalid. This is because the ray theory model is only a partial description of the character of light. It describes the direction a plane wave component takes in the fiber but does not take into account interference between such components. When interference phenomena are considered it is found that only rays with certain discrete characteristics propagate in the fiber core. Thus the fiber will only support a discrete number of guided modes. This becomes critical in small- core-diameter fibers which only support one or a few modes. Hence electromagnetic mode theory must be applied in these cases.

4. Skew rays

In the preceding sections we have considered the propagation of meridional rays in the optical waveguide. However, another category of ray exists which is transmitted without passing through the fiber axis. These rays, which greatly outnumber the meridional rays, follow a helical path through the fiber, as illustrated in Figure 1.6, and are called skew rays.

It is not easy to visualize the skew ray paths in two dimensions, but it may be observed from Figure 1.6(b) that the helical path traced through the fiber gives a change in direction of 2γ at each reflection, where γ is the angle between the projection of the ray in two dimensions and the radius of the fiber core at the point of reflection. Hence, unlike meridional rays, the point of emergence of skew rays from the fiber in air will

depend upon the number of reflections they undergo rather than the input conditions to the fiber. When the light input to the fiber is non uniform, skew rays will therefore tend to have a smoothing effect on the distribution of the light as it is transmitted, giving a more uniform output. The amount of smoothing is dependent on the number of reflections encountered by the skew rays. A further possible advantage of the transmission of skew rays becomes apparent when their acceptance conditions are considered

In order to calculate the acceptance angle for a skew ray it is necessary to define the direction of the ray in two perpendicular planes. The geometry of the situation is illustrated in Figure 1.7 where a skew ray is shown incident on the fiber core at the point *A*, at an angle θ_s to the normal at the fiber end face. The ray is refracted at the air–core interface before traveling to the point *B* in the same plane. The angles of incidence and reflection at the point*B* are φ, which is greater than the critical angle for the core–cladding interface.

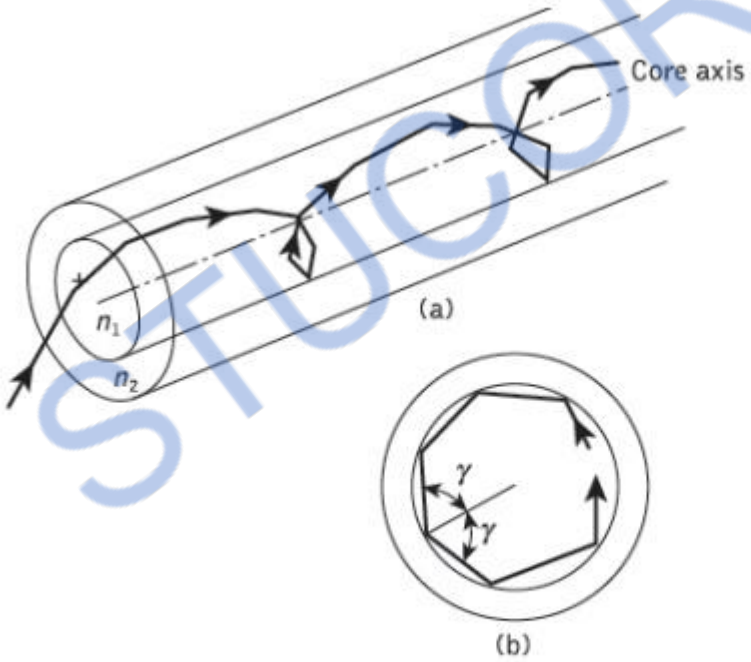

Figure 1.6 The helical path taken by a skew ray in an optical fiber: (a) skew ray path down the fiber; (b) cross-sectional view of the fiber

When considering the ray between *A* and *B* it is necessary to resolve the direction of the ray path *AB* to the core radius at the point *B*. As the incident and reflected rays at the

point *B* are in the same plane, this is simply cos φ. However, if the two perpendicular planes through which the ray path *AB*traverses are considered, then γ is the angle between the core radius and the projection of the ray onto a plane *BRS* normal to the core axis, and θ is the angle between the ray and a line *AT* drawn parallel to the core axis. Thus to resolve the ray path *AB* relative to the radius *BR* in these two perpendicular planes requires multiplication by cos γ and sin θ

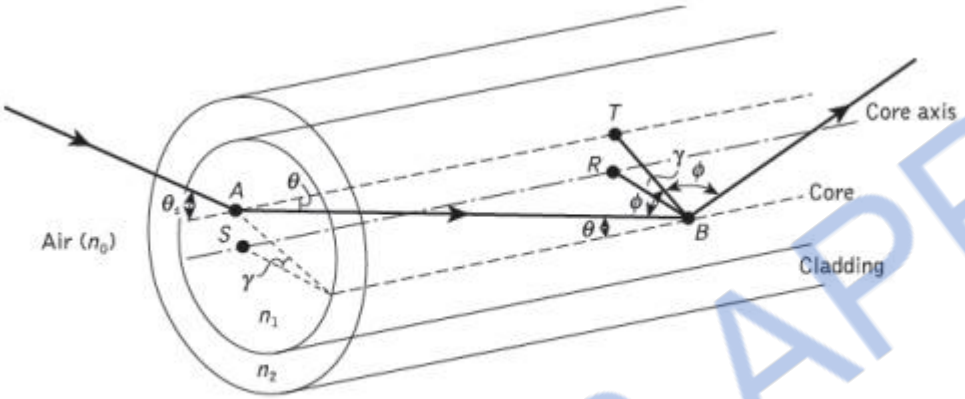

Figure 1.7 The ray path within the fiber core for a skew ray incident at an angle θ_S to the

Hence, the reflection at point *B* at an angle φ may be given by:

$$\cos\gamma \sin\theta = \cos\varphi \tag{1.11}$$

Using the trigonometrical relationship $\sin^2\varphi + \cos^2\varphi = 1$, Eq. (2.11) becomes:

$$\cos\gamma \sin\theta = \cos\phi = (1 - \sin^2\phi)^{\frac{1}{2}} \tag{1.12}$$

If the limiting case for total internal reflection is now considered, then φ becomes equal to the critical angle φ_c for the core–cladding interface and, following Eq. (2.2), is given by $\sin\varphi_c = n_2/n_1$. Hence, Eq. (2.12) may be written as:

$$\cos\gamma \sin\theta \leq \cos\phi_c = \left(1 - \frac{n_2^2}{n_1^2}\right)^{\frac{1}{2}} \tag{1.13}$$

Furthermore, using Snell's law at the point *A*, following Eq. (2.1) we can write:

$$n_0 \sin\theta_a = n_1 \sin\theta \tag{1.14}$$

where θ_a represents the maximum input axial angle for meridional rays, as expressed in Section 1.2.2, and θ is the internal axial angle. Hence substituting for sin θ from Eq.(1.13) into Eq. (1.14) gives:

$$\sin \theta_{as} = \frac{n_1}{n_0} \frac{\cos \phi_c}{\cos \gamma} = \frac{n_1}{n_0 \cos \gamma} \left(1 - \frac{n_2^2}{n_1^2}\right)^{\frac{1}{2}} \tag{1.15}$$

where θ_{as} now represents the maximum input angle or acceptance angle for skew rays. It may be noted that the inequality shown in Eq. (1.13) is no longer necessary as all the terms in Eq. (1.15) are specified for the limiting case. Thus the acceptance conditions for skew rays are:

$$n_0 \sin \theta_{as} \cos \gamma = (n_1^2 - n_2^2)^{\frac{1}{2}} = NA \tag{1.16}$$

and in the case of the fiber in air ($n_0 = 1$):

$$\sin \theta_{as} \cos \gamma = NA \tag{1.17}$$

Therefore by comparison with Eq. (1.8) derived for meridional rays, it may be noted that skew rays are accepted at larger axial angles in a given fiber than meridional rays, depending upon the value of cos γ. In fact, for meridional rays cos γ is equal to unity and θ_{as} becomes equal to θ_a. Thus although θ_a is the maximum conical half angle for the acceptance of meridional rays, it defines the minimum input angle for skew rays. Hence, as may be observed from Figure 1.6, skew rays tend to propagate only in the annular region near the outer surface of the core, and do not fully utilize the core as a transmission medium. However, they are complementary to meridional rays and increase the light-gathering capacity of the fiber. This increased light-gathering ability may be significant for large *NA* fibers, but for most communication design purposes the expressions given in Eqs (1.8) and (1.10) for meridional rays are considered adequate.

Electromagnetic mode theory for optical propagation

1. Electromagnetic waves

In order to obtain an improved model for the propagation of light in an optical fiber, elec-tromagnetic wave theory must be considered. The basis for the study of electromagnetic wave propagation is provided by Maxwell's equations [Ref. 13]. For a medium with zero conductivity these vector relationships may be written in terms of the electric field **E**, magnetic field **H**, electric flux density **D** and magnetic flux density **B** as the curl equations:

$$\Delta \times \mathbf{E} = -\frac{\partial \mathbf{B}}{\partial t} \tag{1.18}$$

$$\nabla \times \mathbf{H} = \frac{\partial \mathbf{D}}{\partial t} \tag{2.19}$$

and the divergence conditions:

$$\nabla \cdot \mathbf{D} = 0 \qquad \text{(no free charges)} \tag{1.20}$$

$$\nabla \cdot \mathbf{B} = 0 \qquad \text{(no free poles)} \tag{1.21}$$

where ∇ is a vector operator.

The four field vectors are related by the relations:

$$\mathbf{D} = \varepsilon \mathbf{E} \tag{1.22}$$

$$\mathbf{B} = \mu \mathbf{H}$$

where ε is the dielectric permittivity and μ is the magnetic permeability of the medium. Substituting for **D** and **B** and taking the curl of Eqs (1.18) and 1.19) gives:

$$\nabla \times (\nabla \times \mathbf{E}) = -\mu\varepsilon \frac{\partial^2 \mathbf{E}}{\partial t^2} \tag{1.23}$$

$$\nabla \times (\nabla \times \mathbf{H}) = -\mu\varepsilon \frac{\partial^2 \mathbf{H}}{\partial t^2} \tag{1.24}$$

Then using the divergence conditions of Eqs (1.20) and (1.21) with the vector identity:

$$\nabla \times (\nabla \times \mathbf{Y}) = \nabla(\nabla \cdot \mathbf{Y}) - \nabla^2(\mathbf{Y})$$

We obtain the nondispersive wave equations:

$$\nabla^2 \mathbf{E} = \mu\varepsilon \frac{\partial^2 \mathbf{E}}{\partial t^2} \tag{1.25}$$

And

$$\nabla^2 \mathbf{H} = \mu\varepsilon \frac{\partial^2 \mathbf{H}}{\partial t^2} \tag{1.26}$$

where∇2 is the Laplacian operator. For rectangular Cartesian and cylindrical polar coordinates the above wave equations hold for each component of the field vector, every component satisfying the scalar wave equation

$$\nabla^2 \psi = \frac{1}{v_p^2} \frac{\partial^2 \psi}{\partial t^2} \tag{1.27}$$

Where ψ may represent a component of the **E** or **H** field and up is the phase velocity (velocity of propagation of a point of constant phase in the wave) in the dielectric medium. It follows that:

$$v_p = \frac{1}{(\mu\varepsilon)^{\frac{1}{2}}} = \frac{1}{(\mu_r \mu_0 \varepsilon_r \varepsilon_0)^{\frac{1}{2}}} \tag{1.28}$$

Where μr and εr are the relative permeability and permittivity for the dielectric medium and μ0 and ε0 are the permeability and permittivity of free space. The velocity of light in free spacecis therefore:

$$c = \frac{1}{(\mu_0 \varepsilon_0)^{\frac{1}{2}}} \tag{1.29}$$

If planar waveguides, described by rectangular Cartesian coordinates (x, y, z), or circular fibers, described by cylindrical polar coordinates (r, φ, z), are considered, then the Laplacian operator takes the form:

$$\nabla^2\psi = \frac{\partial^2\psi}{\partial x^2} + \frac{\partial^2\psi}{\partial y^2} + \frac{\partial^2\psi}{\partial z^2} \tag{1.30}$$

Or

$$\nabla^2\psi = \frac{\partial^2\psi}{\partial r^2} + \frac{1}{r}\frac{\partial\psi}{\partial r} + \frac{1}{r^2}\frac{\partial^2\psi}{\partial\phi^2} + \frac{\partial^2\psi}{\partial z^2} \tag{1.31}$$

respectively.

It is necessary to consider both these forms for a complete treatment of optical propagation in the fiber, although many of the properties of interest may be dealt with using Cartesian coordinates.

The basic solution of the wave equation is a sinusoidal wave, the most important form of which is a uniform plane wave given by

$$\psi = \psi_0 \exp[\mathrm{j}(\omega t - \mathbf{k}\cdot\mathbf{r})] \tag{1.32}$$

where ω is the angular frequency of the field, t is the time, $\mathbf{k}$ is the propagation vector which gives the direction of propagation and the rate of change of phase with distance, while the components of $\mathbf{r}$ specify the coordinate point at which the field is observed. When λ is the optical wavelength in a vacuum, the magnitude of the propagation vector or the vacuum phase propagation constant k (where $k = |\mathbf{k}|$) is given by:

$$k = \frac{2\pi}{\lambda} \tag{1.33}$$

It should be noted that in this case k is also referred to as the free space wave number.

2. Modes in a planar guide

The planar guide is the simplest form of optical waveguide. We may assume it consists of a slab of dielectric with refractive index n_1 sandwiched between two regions of lower refractive index n_2. In order to obtain an improved model for optical propagation it is useful to consider theinterference of plane wave components within this dielectric waveguide.

The conceptual transition from ray to wave theory may be aided by consideration of a plane monochromatic wave propagating in the direction of the ray path within the guide (see Figure 1.8(a)). As the refractive index within the guide is n_1, the optical wavelength in this region is reduced to λ/n_1, while the vacuum propagation constant is increased to n_1k. When θ is the angle between the wave propagation vector or the equivalent ray and the guide axis, the plane wave can be resolved into two component plane waves propagating in the z and x directions, as shown in Figure 1.8(a).

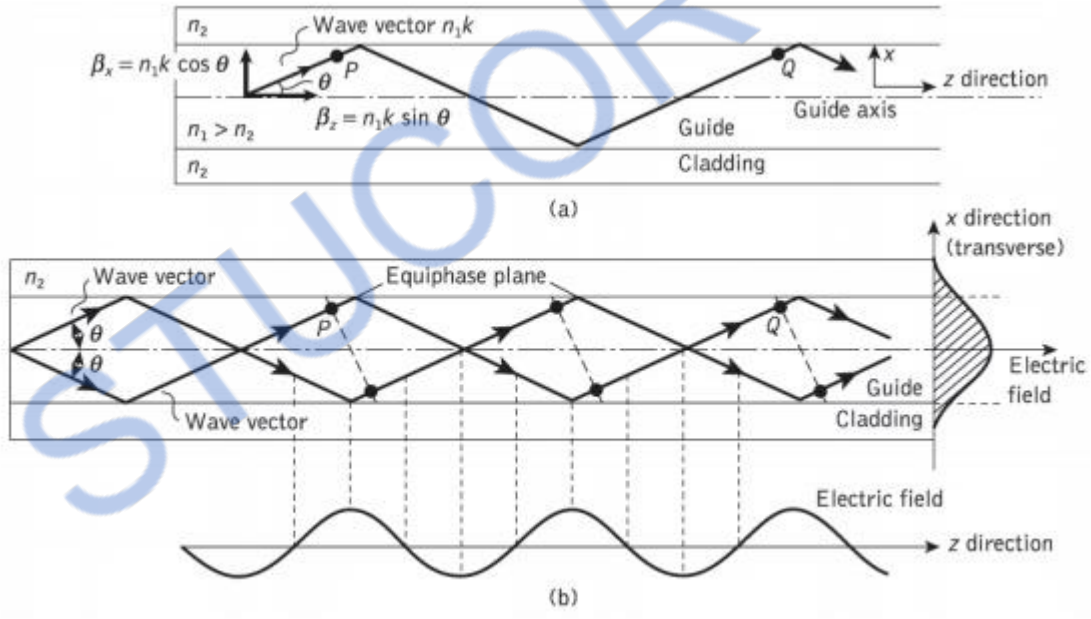

Figure 1.8 The formation of a mode in a planar dielectric guide: (a) a plane wavepropagating in the guide shown by its wave vector or equivalent ray – the wave vector is resolved into components in the z and x directions; (b) the interference of plane waves in the guide forming the lowest order mode (m = 0)

The component of the phase propagation in the Z direction is given by:

$$\beta_z = n_1 k \cos\theta \tag{1.34}$$

The component of the phase propagation constant in the x direction β_x is:

$$\beta_x = n_1 k \sin\theta \tag{1.35}$$

The component of the plane wave in the x direction is reflected at the interface between the higher and lower refractive index media. When the total phase change* after two successive reflections at the upper and lower interfaces (between the points P and Q) is equal to $2m\pi$ radians, where m is an integer, then constructive interference occurs and a standing wave is obtained in the x direction. This situation is illustrated in Figure 1.8(b), where the interference of two plane waves is shown. In this illustration it is assumed that the interference forms the lowest order (where $m = 0$) standing wave, where the electric field is a maximum at the center of the guide decaying towards zero at the boundary between the guide and cladding. However, it may be observed from Figure 1.8(b) that the electric field penetrates some distance into the cladding, a phenomenon which is discussed in Section 1.3.4.

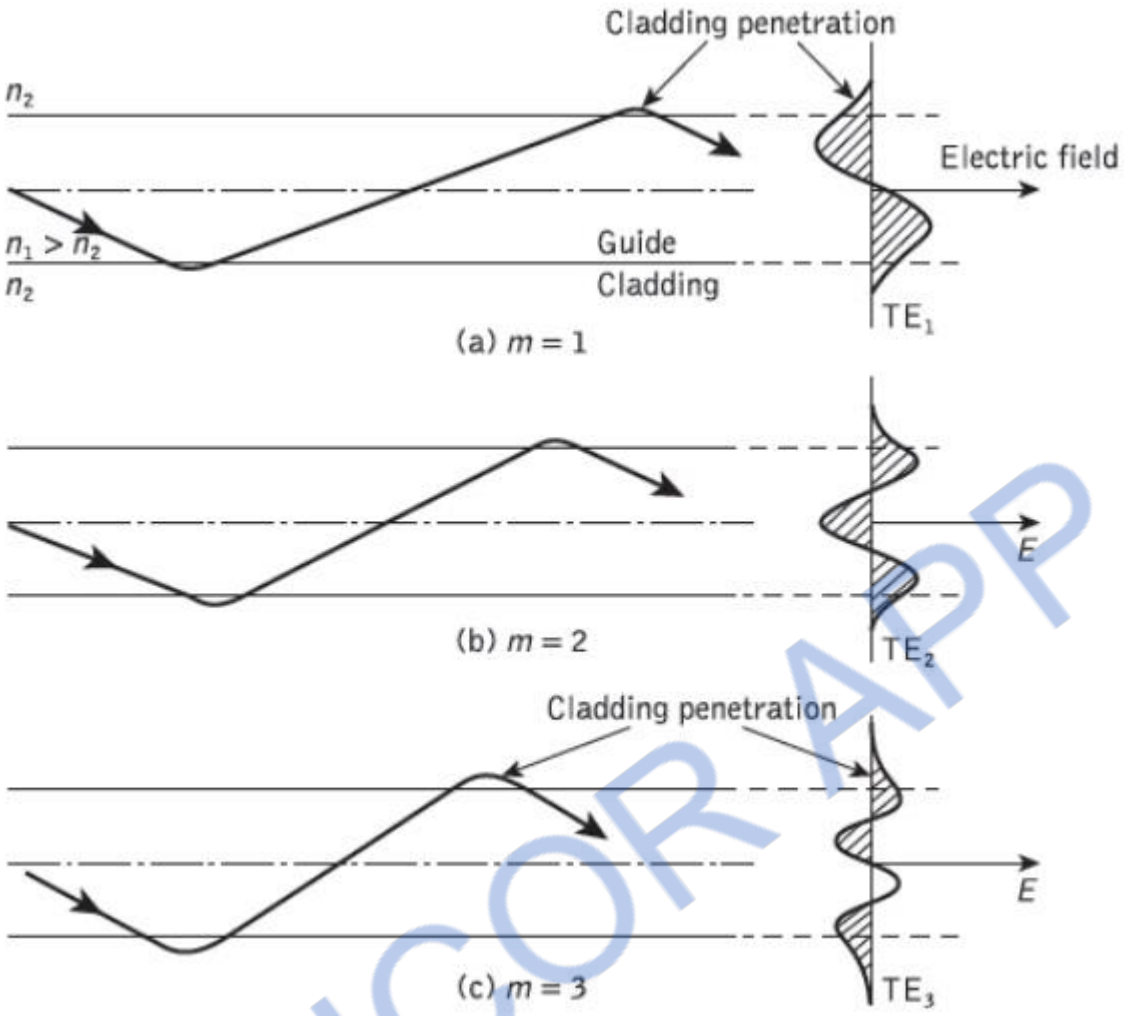

Figure 1.9 *Physical model showing the ray propagation and the corresponding transverse electric (TE) field patterns of three lower order models (m =1, 2, 3) in the planar dielectric guide*

Nevertheless, the optical wave is effectively confined within the guide and the electric field distribution in the *x* direction does not change as the wave propagates in the *z* direction. The sinusoidally varying electric field in the *z* direction is also shown in Figure 1.8(b). The stable field distribution in the*x* direction with only a periodic *z*dependence is known as a mode. A specific mode is obtained only when the angle between the propagation vectors or the rays and the interface have a particular value, as indicated in Figure 1.8(b). In effect, Eqs (1.34) and (1.35) define a group or congruence of rays which in the case described represents the lowest order mode. Hence the light

propagating within the guide is formed into discrete modes, each typified by a distinct value of θ.

To visualize the dominant modes propagating in the *z* direction we may consider plane waves corresponding to rays at different specific angles in the planar guide. These plane waves give constructive interference to form standing wave patterns across the guide following a sine or cosine formula. Figure 2.9 shows examples of such rays for $m = 1, 2, 3$, together with the electric field distributions in the *x* direction. It may be observed that *m*denotes the number of zeros in this transverse field pattern. In this way *m* signifies the order of the mode and is known as the mode number.

When light is described as an electromagnetic wave it consists of a periodically varying electric field **E** and magnetic field **H** which are orientated at right angles to each other. The transverse modes shown in Figure 1.9 illustrate the case when the electric field is perpendicular to the direction of propagation and hence $E_z = 0$, but a corresponding component of the magnetic field **H** is in the direction of propagation. In this instance the modes are said to be transverse electric (TE). Alternatively, when a component of the **E** field is in the direction of propagation, but $H_z = 0$, the modes formed are called transverse magnetic (TM). The mode numbers are incorporated into this nomenclature by referring to the Te_m and TM_m modes, as illustrated for the transverse electric modes shown in Figure 1.9. When the total field lies in the transverse plane, transverse electromagnetic (TEM) waves exist where both E_z and H_z are zero. However, although TEM waves occur in metallic conductors (e.g. coaxial cables) they are seldom found in optical waveguides.

3. Phase and group velocity

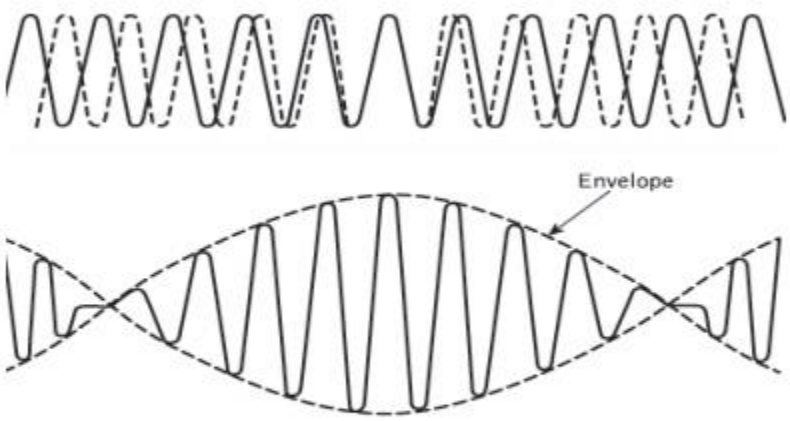

Figure 1.10 The formation of a wave packet from the combination of two waves with nearly equal frequencies.

The envelope of the wave package or group of waves travels at a group velocity υg With in all electromagnetic waves, whether plane or otherwise, there are points of constant phase. For plane waves these constant phase points form a surface which is referred to as a wavefront. As a monochromatic lightwave propagates along a waveguide in the *z* direction these points of constant phase travel at a phase velocity υ_p given by

$$\upsilon_p = \frac{\omega}{\beta} \tag{1.36}$$

where ω is the angular frequency of the wave. However, it is impossible in practice to produce perfectly monochromatic lightwaves, and light energy is generally composed of a sum of plane wave components of different frequencies. Often the situation exists where a group of waves with closely similar frequencies propagate so that their resultant forms a packet of waves. The formation of such a wave packet resulting from the combination of two waves of slightly different frequency propagating together is illustrated in Figure 1.10. This wave packet does not travel at the phase velocity of the individual waves but is observed to move at a group velocity υg given by :

$$\upsilon_g = \frac{\delta\omega}{\delta\beta} \tag{1.37}$$

The group velocity is of greatest importance in the study of the transmission characteristics of optical fibers as it relates to the propagation characteristics of observable wave groups or packets of light. If propagation in an infinite medium of refractive index n_1 is considered, then the propagation constant may be written as:

$$\beta = n_1 \frac{2\pi}{\lambda} = \frac{n_1 \omega}{c} \tag{1.38}$$

where c is the velocity of light in free space. Equation (1.38) follows from Eqs (1.33) and (1.34) where we assume propagation in the z direction only and hence cos θ is equal to unity. Using Eq. (1.36) we obtain the following relationship for the phase velocity:

$$v_p = \frac{c}{n_1} \tag{1.39}$$

Similarly, employing Eq. (1.37), where in the limit δω/δβ becomes dω/dβ, the group velocity:

$$\begin{aligned} v_g &= \frac{d\lambda}{d\beta} \cdot \frac{d\omega}{d\lambda} = \frac{d}{d\lambda}\left(n_1 \frac{2\pi}{\lambda}\right)^{-1} \left(\frac{-\omega}{\lambda}\right) \\ &= \frac{-\omega}{2\pi\lambda}\left(\frac{1}{\lambda}\frac{dn_1}{d\lambda} - \frac{n_1}{\lambda^2}\right)^{-1} \\ &= \frac{c}{\left(n_1 - \lambda \dfrac{dn_1}{d\lambda}\right)} = \frac{c}{N_g} \end{aligned} \tag{1.40}$$

The parameter N_g is known as the group index of the guide.

Cylindrical fiber

1. Modes

The exact solution of Maxwell's equations for a cylindrical homogeneous core dielectric waveguide* involves much algebra and yields a complex result. Although the presentation of thismathematics is beyond the scope of this text, it is useful to consider the resulting modal fields. In common with the planar guide (Section 1.3.2), TE

(where $E_z = 0$) and TM (where $H_z = 0$) modes are obtained within the dielectric cylinder. The cylindrical waveguide, however, is bounded in two dimensions rather than one. Thus two integers, l and m, are necessary in order to specify the modes, in contrast to the single integer (m) required for the planar guide.

For the cylindrical waveguide we therefore refer to TE_{lm} and TM_{lm} modes. These modes correspond to meridional rays (see Section 1.2.1) traveling within the fiber. However, hybrid modes where E_z and H_z are nonzero also occur within the cylindrical waveguide. These modes, which result from skew ray propagation (see Section 1.2.4) within the fiber, are designated HE_{lm} and EH_{lm} depending upon whether the components of **H** or **E** make the larger contribution to the transverse (to the fiber axis) field. Thus an exact description of the modal fields in a step index fiber proves somewhat complicated.

Fortunately, the analysis may be simplified when considering optical fibers for communication purposes. These fibers satisfy the weakly guiding approximation where the relative index difference $\Delta 1$. This corresponds to small grazing angles θ in Eq. (1.34). In fact is usually less than 0.03 (3%) for optical communications fibers. For weakly guiding structures with dominant forward propagation, mode theory gives dominant transverse field components. Hence approximate solutions for the full set of HE, EH, TE and TM modes may be given by two linearly polarized components.

These linearly polarized (LP) modes are not exact modes of the fiber except for the fundamental (lowest order) mode. However, as in weakly guiding fibers is very small, then HE– EH mode pairs occur which have almost identical propagation constants. Such modes are said to be degenerate. The superpositions of these degenerating modes characterized by a common propagation constant correspond to particular LP modes regardless of their HE, EH, TE or TM field configurations. This linear combination of degenerate modes obtained from the exact solution produces a useful simplification in the analysis of weakly guiding fibers.

The relationship between the traditional HE, EH, TE and TM mode designations and the LP_{lm} mode designations is shown in Table 1.1. The mode subscripts l and m are related to the electric field intensity profile for a particular LP mode (see Figure 1.11(d)). There are in general $2l$ field maxima around the circumference of the fiber core and m field

maxima along a radius vector. Furthermore, it may be observed from Table 1.1 that the notation for labeling the HE and EH modes has changed from that specified for the exact solution in the cylindrical waveguide mentioned previously.

Table 1.1 Correspondence between the lower order in linearly polarized modes and the traditional exact modes from which they are formed

Linearly polarized	*Exact*
LP_{01}	HE_{11}
LP_{11}	HE_{21}, TE_{01}, TM_{01}
LP_{21}	HE_{31}, EH_{11}
LP_{02}	HE_{12}
LP_{31}	HE_{41}, EH_{21}
LP_{12}	HE_{22}, TE_{02}, TM_{02}
LP_{lm}	HE_{2m}, TE_{0m}, TM_{0m}
LP_{lm} ($l \neq 0$ or 1)	$HE_{l+1,m}$, $EH_{l-1,m}$

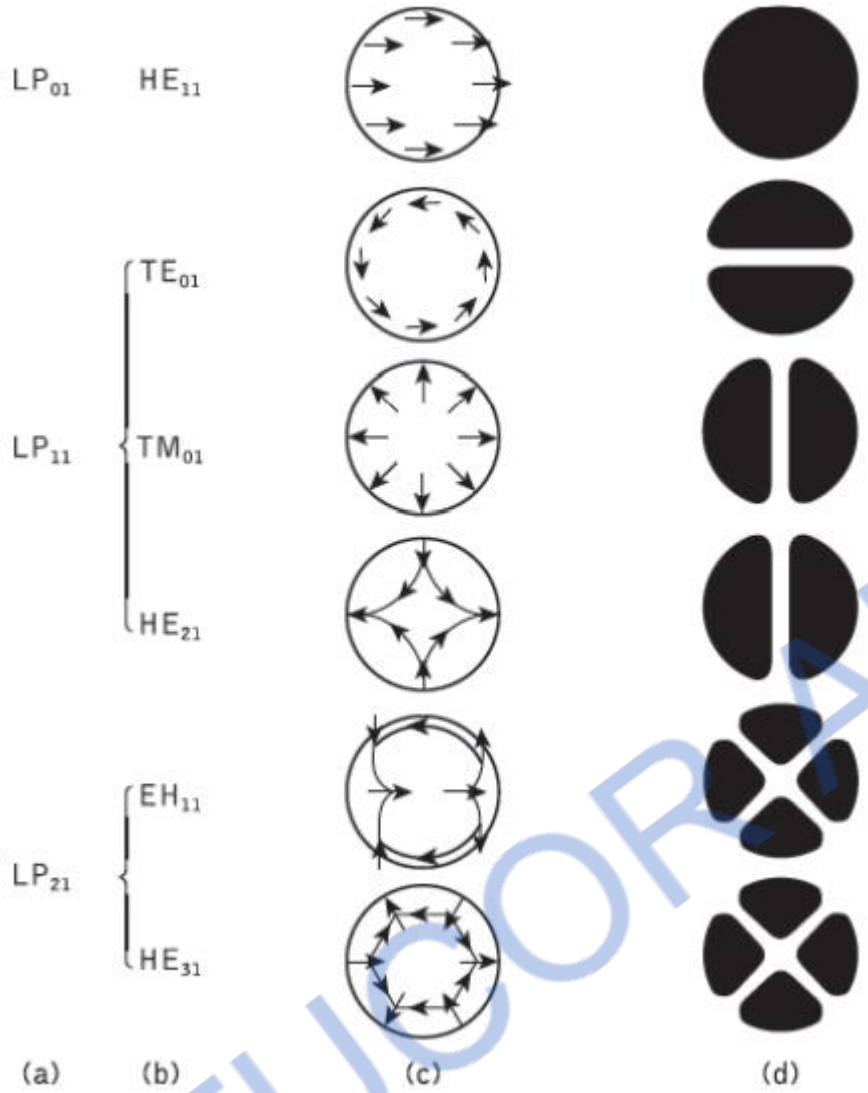

Figure 1.11 The electric field configurations for the three lowest LP modes illustrated in terms oftheir constituent exact modes: (a) LP mode designations; (b) exact mode designations; (c) electric field distribution of the exact modes; (d) intensity distribution of Ex for the exact modes indicating the electric field intensity profile for the corresponding LP modes

The subscript l in the LP notation now corresponds to HE and EH modes with labels $l + 1$ and $l - 1$ respectively. The electric field intensity profiles for the lowest three LP modes, together with the electric field distribution of their constituent exact modes, are shown in Figure 1.11.

It may be observed from the field configurations of the exact modes that the field strength in the transverse direction (E_x or E_y) is identical for the modes which belong to the same LP mode.

Hence the origin of the term 'linearly polarized'.

Using Eq. (1.31) for the cylindrical homogeneous core waveguide under the weak guidance conditions outlined above, the scalar wave equation can be written in the form

$$\frac{d^2\psi}{dr^2}+\frac{1}{r}\frac{d\psi}{dr}+\frac{1}{r^2}\frac{d^2\psi}{d\phi^2}+(n_1^2k^2-\beta^2)\psi=0 \tag{1.41}$$

where ψ is the field (**E** or **H**), n_1 is the refractive index of the fiber core, k is the propagation constant for light in a vacuum, and r and φ are cylindrical coordinates. The propagation constants of the guided modes β lie in the range:

$$n_2k<\beta<n_1k \tag{1.42}$$

where n_2 is the refractive index of the fiber cladding. Solutions of the wave equation for the cylindrical fiber are separable, having the form:

$$\psi=E(r)\left[\frac{\cos l\phi}{\sin l\phi}\exp(\omega t-\beta z)\right] \tag{1.43}$$

where in this case ψ represents the dominant transverse electric field component. The periodic dependence on φ following cos$l$φ or sin lφ gives a mode of radial order l. Hence the fiber supports a finite number of guided modes of the form of Eq. (1.43).

Introducing the solutions given by Eq. (1.43) into Eq. (1.41) results in a differential equation of the form:

$$\frac{d^2\mathbf{E}}{dr^2}+\frac{1}{r}\frac{d\mathbf{E}}{dr}+\left[(n_1k^2-\beta^2)-\frac{l^2}{r^2}\right]\mathbf{E}=0 \tag{1.45}$$

For a step index fiber with a constant refractive index core, Eq. (1.43) is a Bessel differential equation and the solutions are cylinder functions. In the core region the solutions are Bessel functions denoted by J_l.

A graph of these gradually damped oscillatory functions (with respect to r) is shown in Figure 1.12(a). It may be noted that the field is finite at $r = 0$ and may be represented by the zero-order Bessel function $J0$. However, the field vanishes as r goes to infinity and the solutions in the cladding are therefore modified Bessel functions denoted by K_l. These modified functions decay exponentially with respect to r, as illustrated in Figure 1.12(b). The electric field may therefore be given by:

$$\begin{aligned} \mathbf{E}(r) &= GJ_l(UR) && \text{for } R<1 \text{ (core)} \\ &= GJ_l(U)\frac{K_l(WR)}{K_l(W)} && \text{for } R>1 \text{ (cladding)} \end{aligned} \tag{1.45}$$

Where G is the amplitude coefficient and $R = r/a$ is the normalized radial coordinate when a is the radius of the fiber core; U and W, which are the eigenvalues in the core and cladding respectively,* are defined as:

$$U = a(n_1^2k^2 - \beta^2)^{\frac{1}{2}} \tag{1.46}$$

$$W = a(\beta^2 - n_2^2k^2)^{\frac{1}{2}} \tag{1.47}$$

2. Mode coupling

We have thus far considered the propagation aspects of perfect dielectric waveguides. However, waveguide perturbations such as deviations of the fiber axis from straightness, variations in the core diameter, irregularities at the core–cladding interface and refractive index variations may change the propagation characteristics of the fiber. These will have the effect of coupling energy traveling in one mode to another depending on the specific perturbation. Ray theory aids the understanding of this phenomenon, as shown in Figure 1.13, which illustrates two types of perturbation. It may be observed that in both cases the ray no longer maintains the same angle with the axis. In electromagnetic wave theory this corres- ponds to a change in the propagating mode for the light. Thus

individual modes do not normally propagate throughout the length of the fiber without large energy transfers to adjacent modes, even when the fiber is exceptionally good quality and is not strained or bent by its surroundings. This mode conversion is known as mode coupling or mixing. It is usually analyzed using coupled mode equations which can be obtained directly from Maxwell's equations.

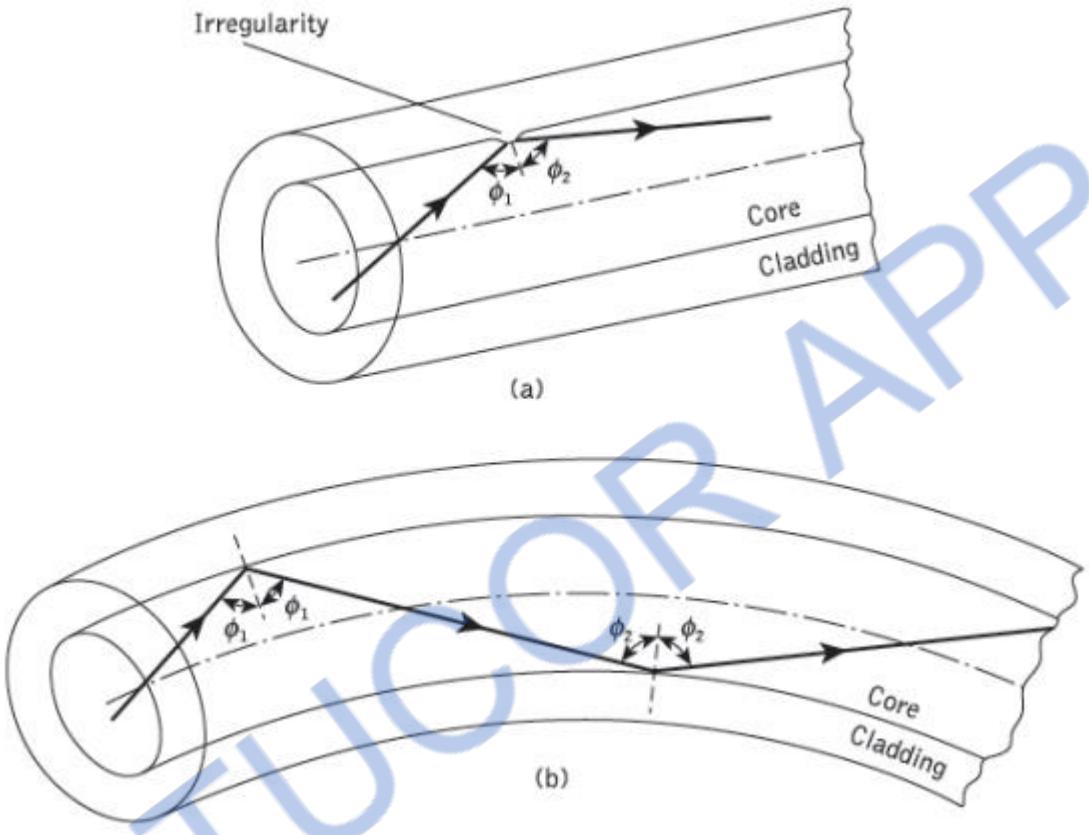

Figure 1.13 *Ray theory illustrations showing two of the possible fiber perturbations which give mode coupling: (a) irregularity at the core–cladding interface; (b) fiber bend*

3. Step index fibers

The optical fiber considered in the preceding sections with a core of constant refractive index n_1 and a cladding of a slightly lower refractive index $n_2$is known as step index fiber. This is because the refractive index profile for this type of fiber makes a step change at the core–cladding interface, as indicated in Figure 1.14, which illustrates the two major types of step index fiber.

The refractive index profile may be defined as:

$$n(r) = \begin{cases} n_1 & r < a \quad \text{(core)} \\ n_2 & r \geq a \quad \text{(cladding)} \end{cases} \tag{1.48}$$

in both cases.

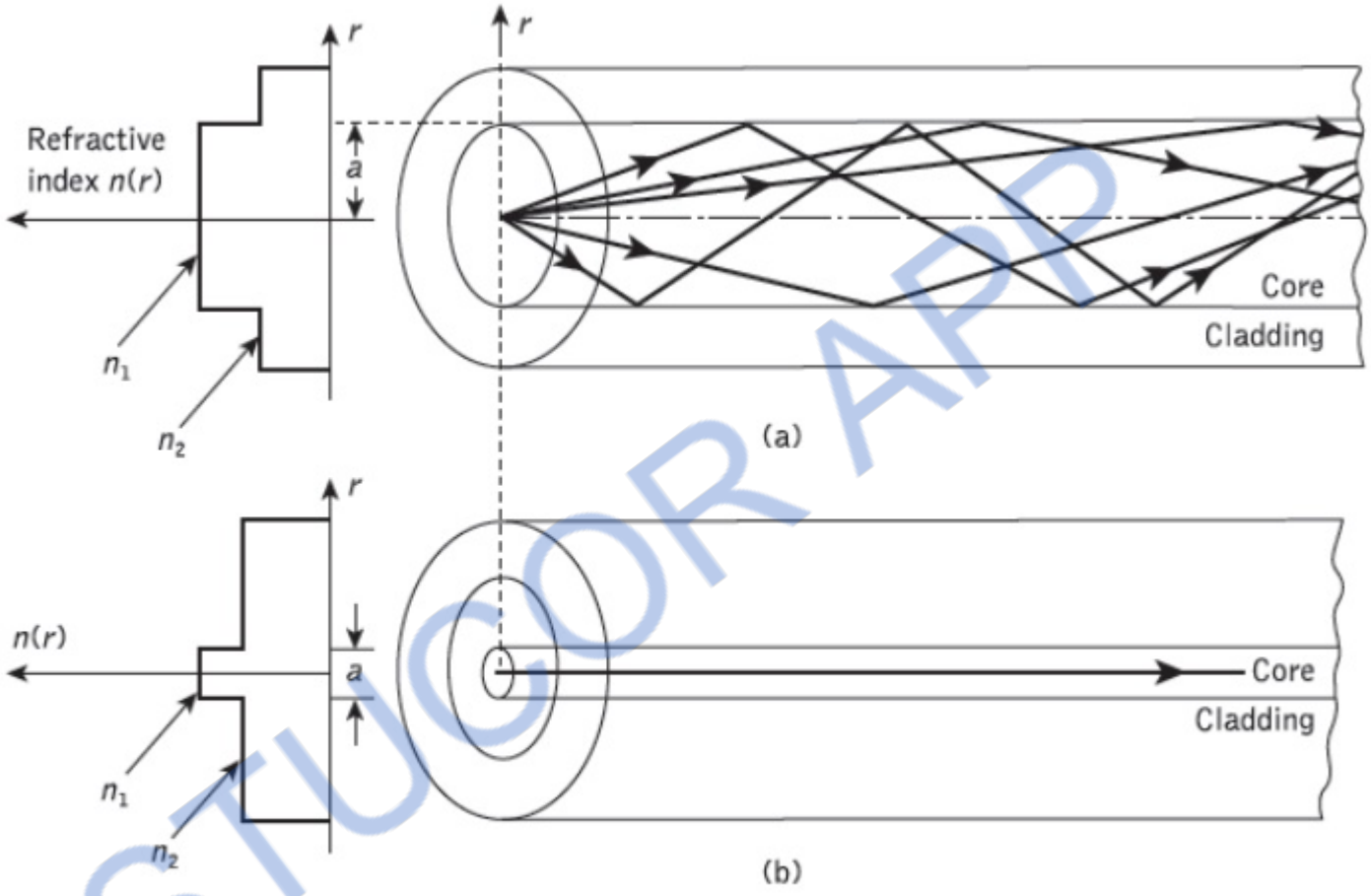

Figure 1.14 The refractive index profile and ray transmission in step index fibers: (a) multimode step index fiber; (b) single-mode step index fiber

Figure 1.14(a) shows a multimode step index fiber with a core diameter of around 50μm or greater, which is large enough to allow the propagation of many modes within the fiber core. This is illustrated in Figure 1.14(a) by the many different possible ray paths through the fiber. Figure 1.14(b) shows a single-mode or monomode step index fiber which allows the propagation of only one transverse electromagnetic mode (typically HE11), and hence the core diameter must be of the order of 2 to 10μm. The propagation

of a single mode is illustrated in Figure 1.14(b) as corresponding to a single ray path only (usually shown as the axial ray) through the fiber.

The single-mode step index fiber has the distinct advantage of low intermodal dispersion (broadening of transmitted light pulses), as only one mode is transmitted, whereas with multimode step index fiber considerable dispersion may occur due to the differing group velocities of the propagating modes. This in turn restricts the maximum bandwidth attainable with multimode step index fibers, especially when com- pared with single-mode fibers. However, for lower bandwidth applications multimode fibers have several advantages over single-mode fibers. These are:

a) The use of spatially incoherent optical sources (e.g. most light-emitting diodes) which cannot be efficiently coupled to single-mode fibers.

b) Larger numerical apertures, as well as core diameters, facilitating easier coupling to optical sources

c) Lower tolerance requirements on fiber connectors

Multimode step index fibers allow the propagation of a finite number of guided modes along the channel. The number of guided modes is dependent upon the physical para- meters (i.e. relative refractive index difference, core radius) of the fiber and the wavelengths of the transmitted light which are included in the normalized frequency V for the fiber. Mode propagation does not entirely cease below cutoff. Modes may propagate as unguided or leaky modes which can travel considerable distances along the fiber. Nevertheless, it is the guided modes which are of paramount importance in optical fiber communications as these are confined to the fiber over its full length. that the total number of guided modes or mode volume M_s for a step index fiber is related to the V value for the fiber by the approximate expression

$$M_s \simeq \frac{V^2}{2} \tag{1.49}$$

Which allows an estimate of the number of guided modes propagating in a particular multimode step index fiber.

4. Graded index fibers

Graded index fibers do not have a constant refractive index in the core* but a decreasing core index $n(r)$ with radial distance from a maximum value ofn_1 at the axis to a constant value n_2 beyond the core radius a in the cladding. This index variation may be represented as:

$$n(r) = \begin{cases} n_1(1 - 2\Delta(r/a)^{\alpha})^{\frac{1}{2}} & r < a \quad \text{(core)} \\ n_1(1 - 2\Delta)^{\frac{1}{2}} = n_2 & r \geq a \quad \text{(cladding)} \end{cases} \tag{1.50}$$

where Δ is the relative refractive index difference and α is the profile parameter which gives the characteristic refractive index profile of the fiber core. Equation (1.50) which is a convenient method of expressing the refractive index profile of the fiber core as a variation of α, allows representation of the step index profile when α = ∞, a parabolic profile when α = 2 and a triangular profile when α = 1. This range of refractive index profiles is illustrated in Figure 1.15

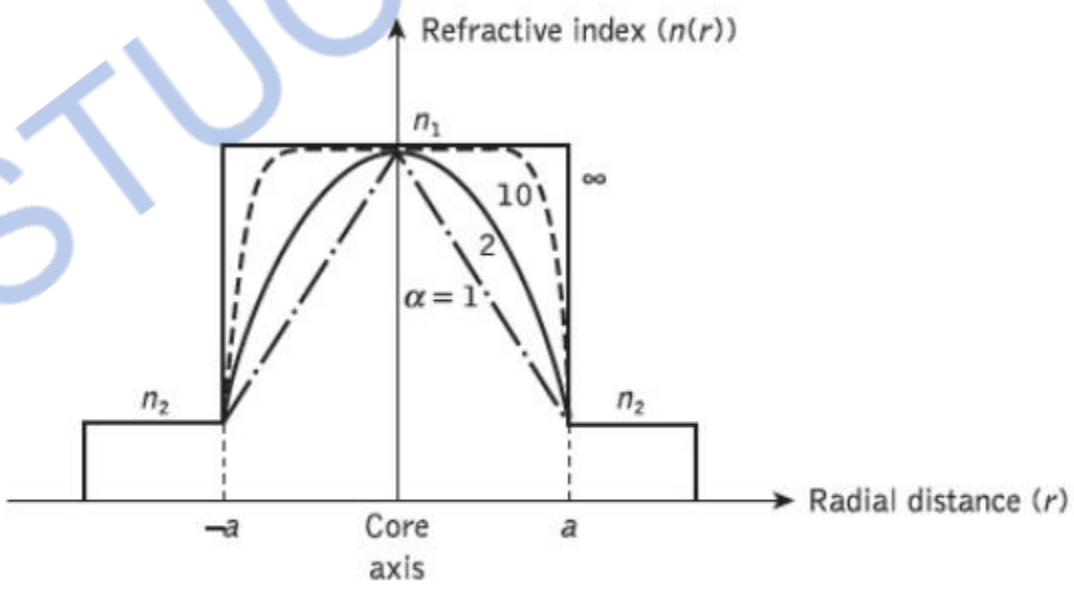

Figure 1.15 Possible fiber refractive index profiles for different values of α (given in Eq. (1.50)

The graded index profiles which at present produce the best results for multimode optical propagation have a near parabolic refractive index profile core with $\alpha \sim\sim 2$. Fibers with such core index profiles are well established and consequently when the term 'graded index' is used without qualification it usually refers to a fiber with this profile.

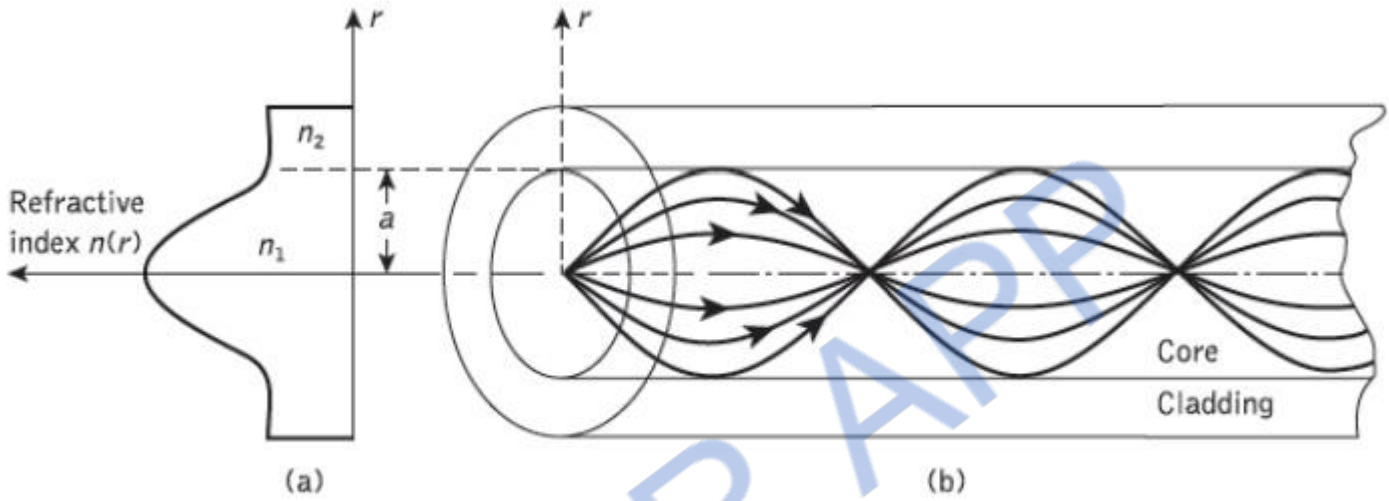

Figure 1.16 The refractive index profile and ray transmission in a multimode graded index fiber

For this reason in this section we consider the waveguiding properties of graded index fiber with a parabolic refractive index profile core.

A multimode graded index fiber with a parabolic index profile core is illustrated in Figure 1.16. It may be observed that the meridional rays shown appear to follow curved paths through the fiber core. Using the concepts of geometric optics, the gradual decrease in refractive index from the center of the core creates many refractions of the rays as they are effectively incident on a large number or high to low index interfaces. This mechanism is illustrated in Figure 1.17 where a ray is shown to be gradually curved, with an ever- increasing angle of incidence, until the conditions for total internal reflection are met, and the ray travels back towards the core axis, again being continuously refracted.

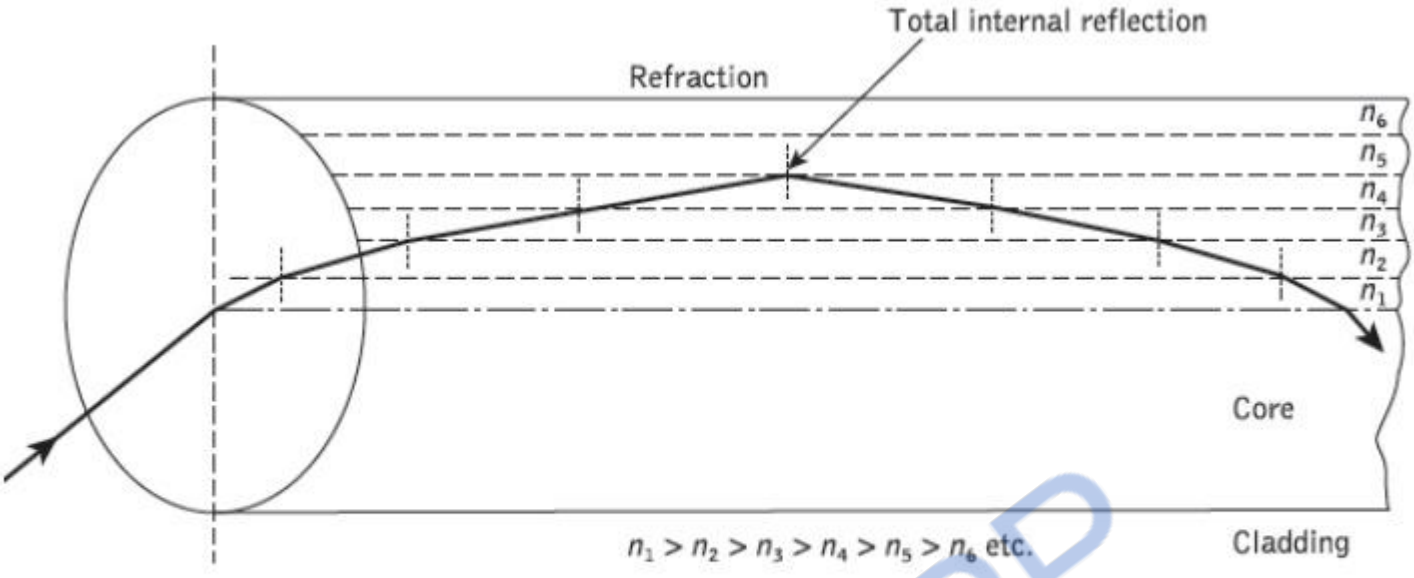

Figure 1.17 An expanded ray diagram showing refraction at the various high to low index interfaces within a graded index fiber, giving an overall curved ray path into the outer regions of the core.

Multimode graded index fibers exhibit far less intermodal dispersion than multimode step index fibers due to their refractive index profile. Although many different modes are excited in the graded index fiber, the different group velocities of the modes tend to be normalized by the index grading. Again considering ray theory, the rays traveling close to the fiber axis have shorter paths when compared with rays which travel

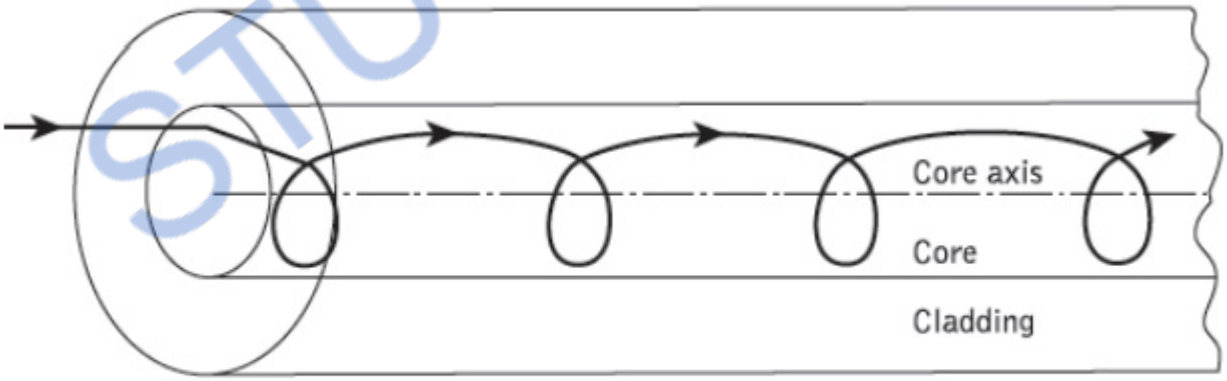

Figure 1.18 A helical skew ray path within a graded index fiber

However, the near axial rays are transmitted through a region of higher refractive index and therefore travel with a lower velocity than the more extreme rays. This compensates for the shorter path lengths and reduces dispersion in the fiber. A similar situation exists

for skew rays which follow longer helical paths, as illus- trated in Figure 1.18. These travel for the most part in the lower index region at greater speeds, thus giving the samemechanism of mode transit time equalization. Hence, multi- mode graded index fibers with parabolic or near-parabolic index profile cores have trans- mission bandwidths which may be orders of magnitude greater than multimode step index fiber bandwidths. Consequently, although they are not capable of the bandwidths attain- able with single-mode fibers, such multimode graded index fibers have the advantage of large core diameters (greater than 30 μm) coupled with bandwidths suitable for long- distance communication.

The parameters defined for step index fibers (i.e. NA, Δ, V) may be applied to graded index fibers and give a comparison between the two fiber types. However, it must be noted that for graded index fibers the situation is more complicated since the numerical aperture is a function of the radial distance from the fiber axis. Graded index fibers, therefore, accept less light than corresponding step index fibers with the same relative refractive index difference.

Single-mode fiber

The advantage of the propagation of a single mode within an optical fiber is that the signal dispersion caused by the delay differences between different modes in a multimode fiber may be avoided. Multimode step index fibers do not lend themselves to the propagation of a single mode due to the difficulties of maintaining single-mode operation within the fiber when mode conversion (i.e. coupling) to other guided modes takes place at both input mismatches and fiber imperfections.

Hence, for the transmission of a single mode the fiber must be designed to allow propagation of only one mode, while all other modes are attenuated by leakage or absorption. Following the preceding discussion of multimode fibers, this may be achieved through choice of a suitable normalized frequency for the fiber. For single-mode operation, only the fundamental LP_{01} mode can exist. Hence the limit of single-mode operation depends on the lower limit of guided propagation for the LP_{11} mode. The cutoff normalized frequency for the LP_{11} mode in step index fibers occurs at $V_c = 2.405$. Thus single-mode propagation of the LP_{01} mode in step index fibers is possible over the range:

$$0 \leq V < 2.405 \tag{1.51}$$

as there is no cutoff for the fundamental mode. It must be noted that there are in fact two modes with orthogonal polarization over this range, and the term single-mode applies to propagation of light of a particular polarization. Also, it is apparent that the normalized frequency for the fiber may be adjusted to within the range given in Eq. (1.51) by reduction of the core radius.

1. Cutoff wavelength

It may be noted that single-mode operation only occurs above a theoretical cutoff wavelength λ_c given by:

$$\lambda_c = \frac{2\pi a n_1}{V_c}(2\Delta)^{\frac{1}{2}} \tag{1.52}$$

where V_c is the cutoff normalized frequency. Hence λ_c is the wavelength above which a particular fiber becomes single-moded.

Dividing Eq. (1.52) by $V = \frac{2\pi}{\lambda} a n_1 (2\Delta)^{\frac{1}{2}}$

$$\frac{\lambda_c}{\lambda} = \frac{V}{V_c} \tag{1.53}$$

Thus for step index fiber where $V_c = 2.405$, the cutoff wavelength is given by:

$$\lambda_c = \frac{V\lambda}{2.405} \tag{1.54}$$

An effective cutoff wavelength has been defined by the ITU-T which is obtained from a 2 m length of fiber containing a single 14 cm radius loop. This definition was produced because the first higher order LP_{11} mode is strongly affected by fiber length and curvature near cutoff. Recommended cutoff wavelength values for primary coated fiber range from 1.1 to 1.28 μm for single-mode fiber designed for operation in the 1.3μm wavelength region in order to avoid modal noise and dispersion problems. Moreover,

practical transmission systems are generally operated close to the effective cutoff wavelength in order to enhance the fundamental mode confinement, but sufficiently distant from cutoff so that no power is transmitted in the second-order LP_{11} mode.

2. Mode-field diameter and spot size

Many properties of the fundamental mode are determined by the radial extent of its electromagnetic field including losses at launching and jointing, micro bend losses, waveguide dispersion and the width of the radiation pattern. Therefore, the MFD is an important parameter for characterizing single-mode fiber properties which takes into account the wavelength-dependent field penetration into the fiber cladding. In this context it is a better measure of the functional properties of single-mode fiber than the core diameter. For step index and graded (near parabolic profile) single-mode fibers operating near the cutoff wavelength λ_c, the field is well approximated by a Gaussian distribution. In this case the MFD is generally taken as the distance between the opposite $1/e = 0.37$ field amplitude points and the power $1/e^2 = 0.135$ points in relation to the corresponding values on the fiber axis.

Another parameter which is directly related to the MFD of a single-mode fiber is the spot size (or mode-field radius) ω_0. Hence MFD = $2\omega_0$, where $\omega_0$is the nominal half width of the input excitation.

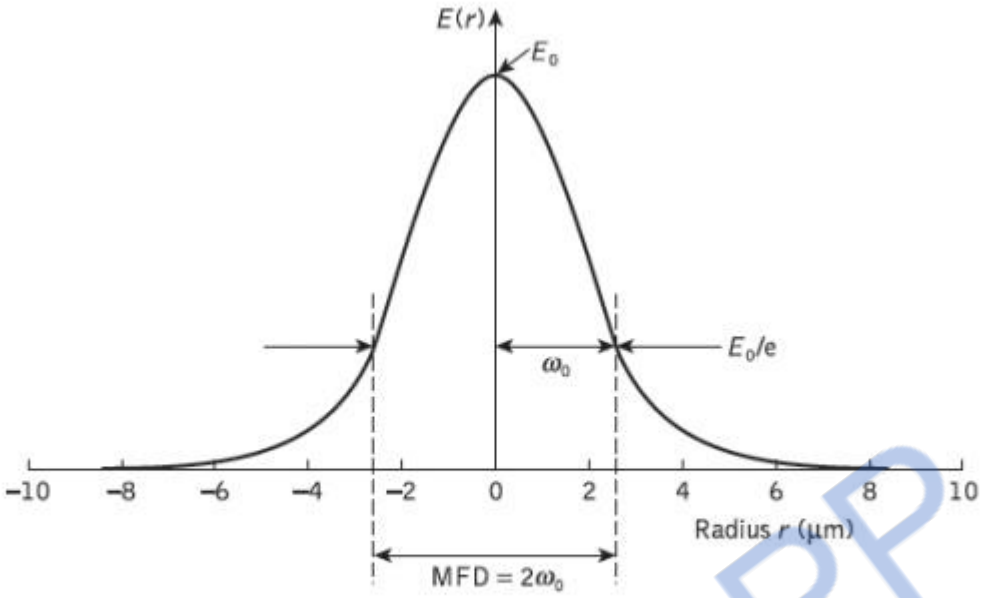

Figure 1.19 Field amplitude distribution $E(r)$ of the fundamental mode in a single-mode fiber illustrating the mode-field diameter (MFD) and spot size (ω_0)

The MFD can therefore be regarded as the single- mode analog of the fiber core diameter in multimode fibers. However, for many refractive index profiles and at typical operating wavelengths the MFD is slightly larger than the single-mode fiber core diameter.

Often, for real fibers and those with arbitrary refractive index profiles, the radial field distribution is not strictly Gaussian and hence alternative techniques have been proposed. However, the problem of defining the MFD and spot size for non-Gaussian field dis- tributions is a difficult one and at least eight definitions exist.

3. Effective refractive index

The rate of change of phase of the fundamental LP_{01} mode propagating along a straight fiber is determined by the phase propagation constant . It is directly related to the wavelength of the LP01 mode λ01 by the factor 2π, since β gives the increase in phase angle per unit length. Hence:

$$\beta\lambda_{01} = 2\pi \quad \text{or} \quad \lambda_{01} = \frac{2\pi}{\beta} \tag{1.55}$$

Moreover, it is convenient to define an effective refractive index for single-mode fiber, sometimes referred to as a phase index or normalized phase change coefficient n_{eff}, by the ratio of the propagation constant of the fundamental mode to that of the vacuum propagation constant:

$$n_{eff} = \frac{\beta}{k} \tag{1.56}$$

Hence, the wavelength of the fundamental mode λ_{01} is smaller than the vacuum wavelength λ by the factor $1/n_{eff}$ where:

$$\lambda_{01} = \frac{\lambda}{n_{eff}} \tag{1.57}$$

It should be noted that the fundamental mode propagates in a medium with a refractive index $n(r)$ which is dependent on the distance r from the fiber axis. The effective refractive index cantherefore be considered as an average over the refractive index of this medium.

Within a normally clad fiber, not depressed-cladded fibers, at long wavelengths (i.e. small V values) the MFD is large compared to the core diameter and hence the electric field extends farinto the cladding region. In this case the propagation constant β will be approximately equal to n_2k (i.e. the cladding wave number) and the effective index will be similar to the refractive indexof the cladding n_2. Physically, most of the power is transmitted in the cladding material.

At short wavelengths, however, the field is concentrated in the core region and the propagation constant β approximates to the maximum wave numbern_1k. Following this discussion, and as indicated previously, then the propagation constant in single-mode fiber varies over the interval $n_2k < \beta < n_1k$. Hence, the effective refractive index will vary over the range $n_2 < n_{eff} < n_1$. In addition, a relationship between the effective refractive index and the normalized propagation constant b defined as:

$$b = \frac{(\beta/k)^2 - n_2^2}{n_1^2 - n_2^2} = \frac{\beta^2 - n_2^2 k^2}{n_1 k^2 - n_2^2 k^2} \tag{1.58}$$

may be obtained. Making use of the mathematical relation $A2 - B2 = (A + B)(A - B)$, Eq. (1.58) can be written in the form:

$$b = \frac{(\beta + n_2 k)(\beta - n_2 k)}{(n_1 k + n_2 k)(n_1 k - n_2 k)} \tag{1.59}$$

However, taking regard of the fact that $\beta \cong n_1 k$, then

$$b \simeq \frac{\beta - n_2 k}{n_1 k - n_2 k} = \frac{\beta/k - n_2}{n_1 - n_2}$$

Finally, in Eq. (1.56) n_{eff} is equal to β/k, therefore:

$$b \simeq \frac{n_{eff} - n_2}{n_1 - n_2} \tag{1.60}$$

The dimensionless parameter b which varies between 0 and 1 is particularly useful in the theory of single-mode fibers because the relative refractive index difference is very small, giving only a small range for β. Moreover, it allows a simple graphical representation of results to be presented as illustrated by the characteristic shown in Figure 2.32 of the normalized phase constant of β as a function of normalized frequency V in a step index fiber.* It should also be noted that $b(V)$ is a universal function which does not depend explicitly on other fiber parameters.

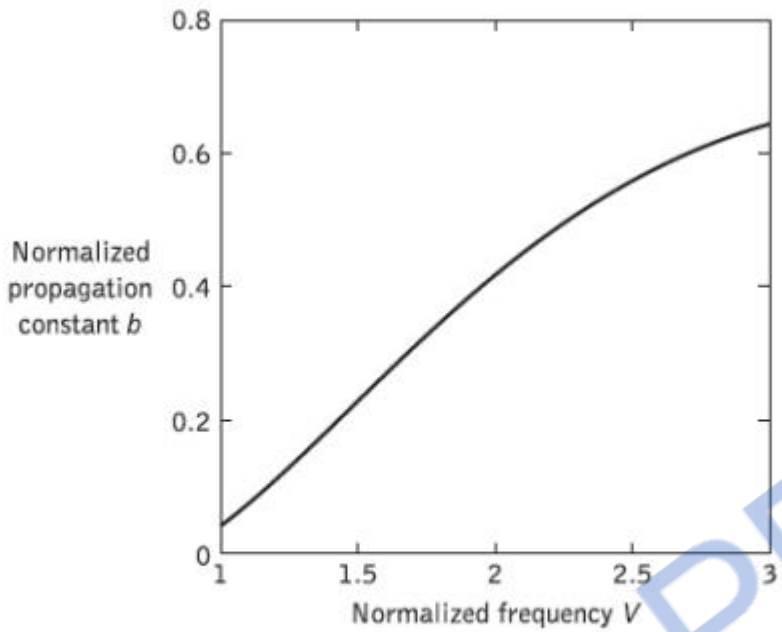

Figure 1.20 The normalized propagation constant (b) of the fundamental mode in a step index fiber shown as a function of the normalized frequency (V)

4. Group delay and mode delay factor

The transit time or group delay τ_g for a light pulse propagating along a unit length of fiber is the inverse of the group velocity υ_g . Hence:

$$\tau_g = \frac{1}{\upsilon_g} = \frac{d\beta}{d\omega} = \frac{1}{c}\frac{d\beta}{dk} \tag{1.61}$$

The group index of a uniform plane wave propagating in a homogeneous medium has been determined as:

$$N_g = \frac{c}{\upsilon_g}$$

However, for a single-mode fiber, it is usual to define an effective group index* N_{ge} By:

$$N_{ge} = \frac{c}{\upsilon_g} \tag{1.62}$$

Where υ_g is considered to be the group velocity of the fundamental fiber mode. Hence, the specific group delay of the fundamental fiber mode becomes:

$$\tau_g = \frac{N_{ge}}{c} \tag{1.63}$$

Moreover, the effective group index may be written in terms of the effective refractive index n_{eff} defined in Eq. (1.56) as:

$$N_{ge} = n_{eff} - \lambda \frac{dn_{eff}}{d\lambda} \tag{1.64}$$

$$\beta = k[(n_1^2 - n_2^2)b + n_2^2] \simeq kn_2[1 + b\Delta] \tag{1.65}$$

Furthermore, approximating the relative refractive index difference as $(n_1 - n_2)/n_2$, for a weakly guiding fiber where $\Delta << 1$, we can use the approximation :

$$\frac{n_1 - n_2}{n_2} \simeq \frac{N_{g1} - N_{g2}}{N_{g2}} \tag{1.66}$$

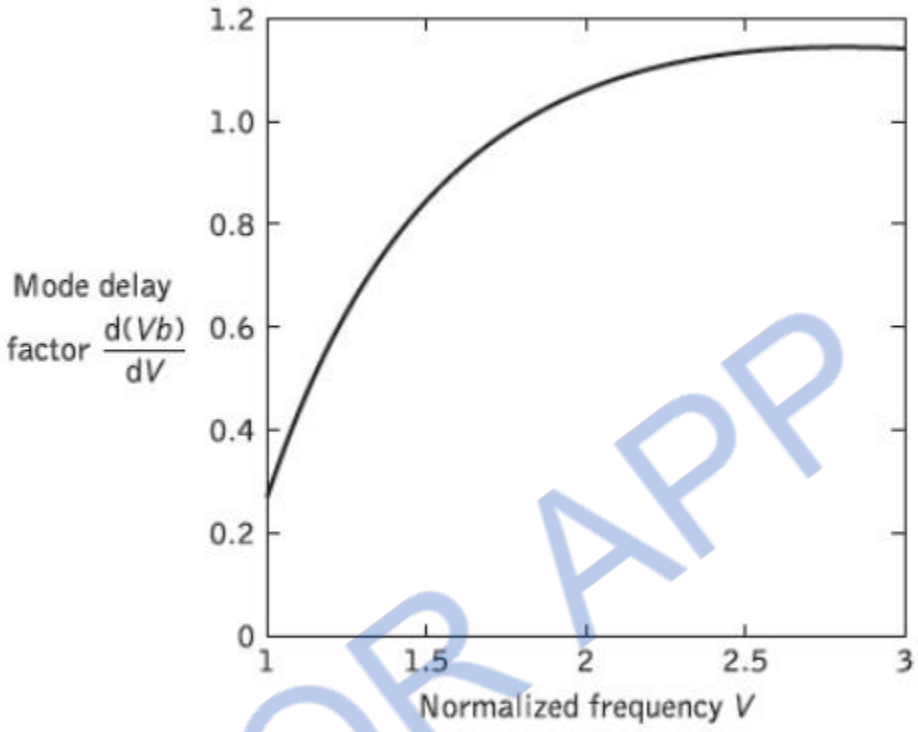

Figure 1.21 The mode delay factor (d(Vb)/dV) for the fundamental mode in a step index fiber shown as a function of normalized frequency (V)

Where N_{g1} and N_{g2} are the group indices for the fiber core and cladding regions respectively. Substituting Eq. (1.65) for β into Eq. (1.67) and using the approximate expression given in Eq. (1.66), we obtain the group delay per unit distance as:

$$\tau_g = \frac{1}{c}\left[N_{g2} + (N_{g1} - N_{g2})\frac{d(Vb)}{dV}\right] \tag{1.67}$$

The dispersive properties of the fiber core and the cladding are often about the same and therefore the wavelength dependence of can be ignored. Hence the group delay can be written as:

$$\tau_g = \frac{1}{c}\left[N_{g2} + n_2\Delta\frac{d(Vb)}{dV}\right] \tag{1.68}$$

The initial term in Eq. (1.68) gives the dependence of the group delay on wavelength caused when a uniform plane wave is propagating in an infinitely extended medium with a refractive index which is equivalent to that of the fiber cladding. However, the second term results from the waveguiding properties of the fiber only and is determined by the mode delay factor d(Vb)/dV, which describes the change in group delay caused by the changes in power distribution between the fiber core and cladding. The mode delay factor [Ref. 50] is a further universal parameter which plays a major part in the theory of single- mode fibers. Its variation with normalized frequency for the fundamental mode in a step index fiber is shown in Figure 1.21.

5. The Gaussian approximation

The field shape of the fundamental guided mode within a single-mode step index fiber for two values of normalized frequency is displayed in Figure 1.22.

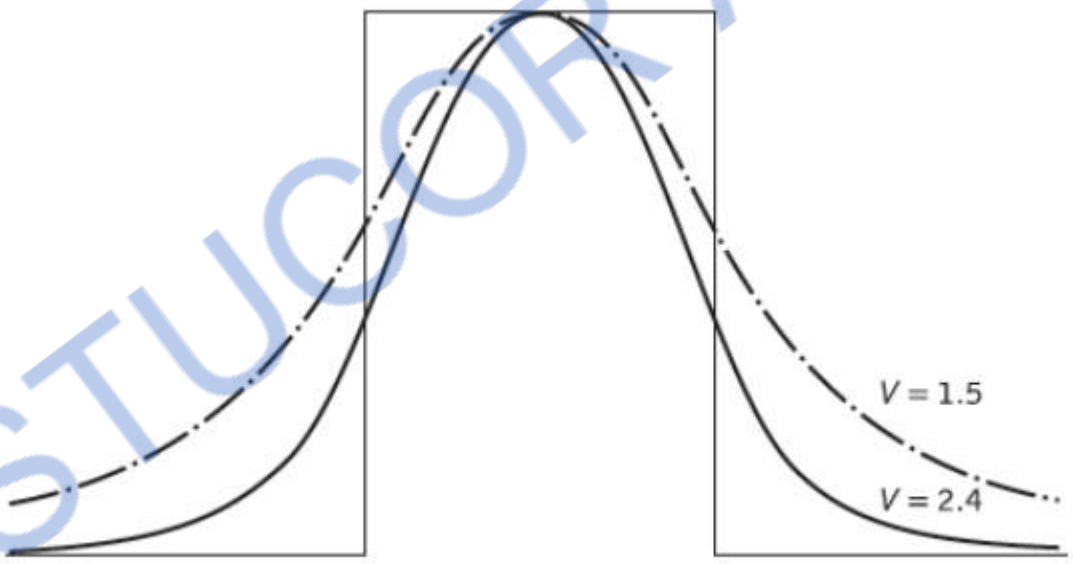

Figure 1.22 Field shape of the fundamental mode for normalized frequencies, V =1.5and V =2.4

As may be expected, considering the discussion in Section 2.4.1, it has the form of a Bessel function ($J_0(r)$) in the core region matched to a modified Bessel function ($K_0(r)$) in the cladding. Depending on the value of the normalized frequency, a significant proportion of the modal power is propagated in the cladding region, as mentioned earlier. Hence, even at the cutoff value (i.e. V_c) only about 80% of the power propagates within the fiber core.

It may be observed from Figure 1.22 that the shape of the fundamental LP01 mode is similar to a Gaussian shape, which allows an approximation of the exact field distribution by a Gaussian function.* The approximation may be investigated by writing the scalar wave equation in the form:

$$\nabla^2\psi + n^2k^2\psi = 0 \tag{1.69}$$

where k is the propagation vector defined in Eq. (1.33) and $n(x, y)$ is the refractive index of the fiber, which does not generally depend on z, the coordinate along the fiber axis. It should be noted that the time dependence $\exp(j\omega t)$ has been omitted from the scalar wave equation to give the reduced wave equation† in Eq. (1.69). This representation is valid since the guided modes of a fiber with a small refractive index difference have one predominant transverse field component, for example E_y. By contrast

Ex and the longitudinal component are very much smaller.

The field of the fundamental guided mode may therefore be considered as a scalar quantity and need not be described by the full set of Maxwell's equations. Hence Eq. (1.69) may be written as:

$$\nabla^2\phi + n^2k^2\phi = 0 \tag{1.70}$$

where φ represents the dominant transverse electric field component.

The near-Gaussian shape of the predominant transverse field component of the fundamental mode has been demonstrated for fibers with a wide range of refractive index distributions. This proves to be the case not only for the LP01 mode of the step index fiber, but also for the modes with fibers displaying arbitrary graded refractive index distributions.

6. Equivalent step index method

Another strategy to obtain approximate values for the cutoff wavelength and spot size in graded index single-mode fibers (or arbitrary refractive index profile fibers) is to define

an equivalent step index (ESI) fiber on which to model the fiber to be investigated. Various methods have been proposed in the literature which commence from the observation that the fields in the core regions of graded index fibers often appear similar to the fields within step index fibers. Hence, as step index fiber characteristics are well known, it is convenient to replace the exact methods for graded index single-mode fibers by approximate techniques based on step index fibers. In addition, such ESI methods allow the propagation characteristics of single-mode fibers to be represented by a few parameters.

Several different suggestions have been advanced for the choice of the core radius a_{ESI}, and the relative index difference $_{ESI}$, of the ESI fiber which lead to good approximations for the spot size (and hence joint and bend losses) for the actual graded index fiber. They are all conceptually related to the Gaussian approximation in that they utilize the close resemblance of the field distribution of the LP_{01} mode to the Gaussian distribution within single-mode fiber.

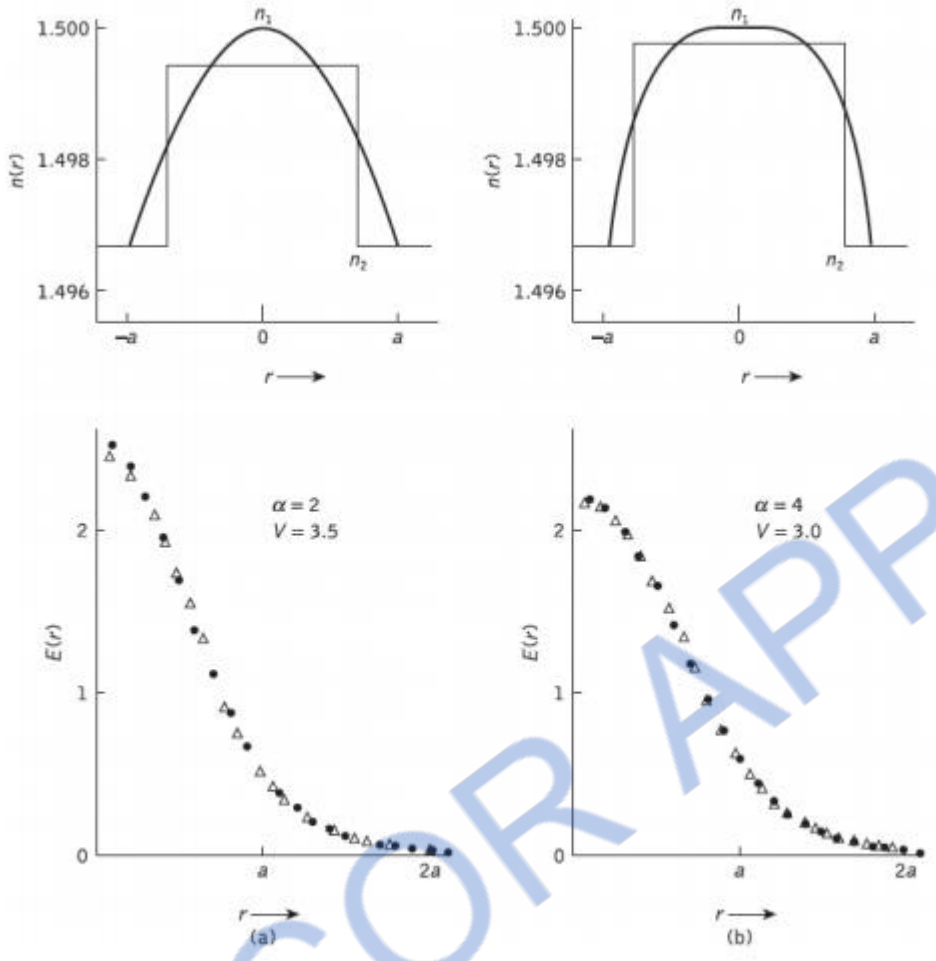

Figure 1.23 Refractive index distributions $n(r)$ and electric field distributions $E(r)$ for graded index fibers and their ESI fibers for: (a) α=2, V =3.5; (b) α=4, V =3.0.

An early proposal for the ESI method involved transformation of the basic fiber parameters following/:

$$a_s = Xa \qquad V_s = YV \qquad NA_s = (Y/X)NA$$

where the subscript s is for the ESI fiber and X, Y are constants which must be determined. However, these ESI fiber representations are only valid for a particular value of normalized frequency V and hence there is a different X, Y pair for each wavelength differences. Figure 1.23 compares the refractive index profiles and the electric field distri- butions for two graded index fibres (α = 2, 4) and their ESI fibers. It may be observed that their fields differ slightly only near the axis.

INTRODUCTION

1. Write the expression for the refractive index in graded index fibers.

$n(r) = n1[1-2\Delta(r/a)^{\alpha}]^{1/2}$ for $0<=r<=a$

$n1(1-2\Delta)^{1/2} \simeq n1(1-\Delta) = n2$ for $r>=a$

r radial distance from fiber axis a core radius

n1 refractive index at the core

n2 refractive index at the cladding

α shape of the index profile

Δ index difference

2. Define Mode-field diameter.

The fundamental parameter of a single mode fiber is the mode-field diameter. This can be determined from the mode field distribution of the fundamental LPo1 mode.

3. Give the expression for linearly polarized waves.

The electric or magnetic field of a train of plane polarized waves travelling in a direction k can be represented in the general form

$A(x,t) = eiAoexp[j(wt-k.x)]$

With x=xex+yey+zez representing a general position vector and k=kxex+kyey+kzez representing the wave propagation vector.

4. What is Snell's law?

The relationship at the interface is known as Snell's law and is given by

$n_1 \sin\Phi_1 = n_2 \sin\Phi_2$

5. What is the necessity of cladding for an optical fiber?

a) To provide proper light guidance inside the core

b) To avoid leakage of light from the fiber

c) To avoid mechanical strength for the fiber

d) To protect the core from scratches and other mechanical damages

6. What are the uses of optical fibers?

a) To transmit the information which are in the form of coded signals of the telephone communication, computer data, etc.

b) To transmit the optical images (Example : Endoscopy)

c) To act as a light source at the inaccessible places.

d) To act as sensors to do mechanical, electrical and magnetic measurements.

7. What is the principle used in the working of fibers as light guides?

The phenomenon of total internal reflection is used to guide the light in the optical fiber. To get total internal reflection, the ray should travel from denser to rarer i.e. from core to clad region of the fiber and the angle of incidence in the denser medium should be greater than the critical angle of that medium.

8. What are step index and graded index fibers?

In the case of graded index fiber, the refractive index of a core is a constant and is larger than the refractive index of the cladding. The light propagation is mainly by meridional rays. In the case of graded index fiber (GRIN fiber) the refractive index of the core varies parabolically from the center of the core having maximum refractive index to the core-cladding interface having constant minimum refractive index. Here the light propagation is by skew rays.

9. Why do we prefer step index single mode fiber for long distance communication?

Step index single mode fiber has

a) Low attenuation due to smaller core diameter

b) Higher bandwidth and

c) Very low dispersion.

10. Define relative refractive index difference.

$$\Delta = \frac{n_1^2 - n_2^2}{2n_1^2} = \frac{n_1 - n_2}{n_1}$$

Thus relative refractive index difference is the ratio between the refractive index difference (of core and cladding) and refractive index of core.

11. What are meridional rays?

Meridional rays are the rays following Zig Zag path when they travel through fiber and for every reflection it will cross the fiber axis.

12. What are skew rays?

Skew rays are the rays following the helical path around the fiber axis when they travel through the fiber and they would not cross the fiber axis at any time.

13. What is V number of fiber or normalized frequency of fiber?

V number of fiber or normalized frequency of fiber is used to find the number of propagating modes through the fiber.

$V = 2\prod a\,(N.A) / \lambda$

In step index fiber number of modes propagating through the fiber=$V^2/2$

Taking the two possible polarizations, total number of possible modes propagating through the fiber = $[V^2/2\ ] * 2 = V^2$

14. What are the conditions for total internal reflection?

a) Light should travel from denser medium to rarer medium.

b) The angle of incidence should be greater than the critical angle of the denser medium.

15. Give the relation between numerical aperture of skew rays and meridional rays.

$(N.A)_{skew} = \cos\gamma\,(N.A)_{meridional}$ when the fiber is placed in air. Here γ is the half of the angular change in every reflection.

16. State Goos-Haenchen effect.

Goos-Haenchen effect states that there is a lateral shift of the reflected ray at the point of incidence at the core-cladding interface. This lateral shift is called the Goos-Haenchen shift.

17. When do you have phase shift during total internal reflection of light?

When the light ray travels from denser medium to rarer medium, if the angle of incidence is greater than the critical angle of core medium, there is a phase shift for both TE and TM waves.

18. What are hybrid modes? Give two examples.

Hybrid modes are the mixture of TE and TM modes that can be traveled through the optical fiber.

Examples:

1. HE1m modes in which |Ez|>|Hz|
2. EH1m modes in which |Hz|>|Ez|

19. Define cutoff wavelength of the fiber.

The cutoff wavelength is defined as the minimum value of wavelength that can be transmitted through the fiber. The wavelengths greater than the cutoff wavelength can be transmitted.

λ cutoff = $2\prod a (N.A) / V$

20. Mention the rule distinguishing 'mode' and 'order'.

The rule states that the smaller the modes propagating angle, the lower the order of the mode. Hus the mode traveling precisely along the fiber's central axis is zero mode.

21. What is fiber birefringence?

Imperfections in the fiber are common such as asymmetrical lateral stress, non-circular imperfect variations of refractive index profile. These imperfections break the circular

symmetry of ideal fiber and mode propagate with different phase velocity and the difference between their refractive index is called fiber birefringence.

$B=k_o(n_y-n_x)$

22. Give the expression for numerical aperture in graded index fibers.

$N.A(r)=N.A.(0)\ (1-(r/a)^{\alpha})^{1/2}$ for r<=a

where N.A(0) = axial numerical aperture = $(n1^2-n2^2)1/2$ a is core radius and α is the refractive index profile.

Glossary

Mode-field diameter.

The fundamental parameter of a single mode fiber is the mode-field diameter. This can be determined from the mode field distribution of the fundamental LPo1 mode.

2. Snell's law.

The relationship at the interface is known as Snell's law and is given by

$n_1 \sin\Phi_1 = n_2 \sin\Phi_2$

3. cladding for an optical fiber

a) To provide proper light guidance inside the core

b) To avoid leakage of light from the fiber

c) To avoid mechanical strength for the fiber

d) To protect the core from scratches and other mechanical damages

4. Step index and graded index fibers.

In the case of graded index fiber, the refractive index of a core is a constant and is larger than the refractive index of the cladding. The light propagation is mainly by meridional rays. In the case of graded index fiber (GRIN fiber) the refractive index of the core varies parabolically from the center of the core having maximum refractive index to the core-cladding interface having constant minimum refractive index. Here the light propagation is by skew rays.

5. Relative refractive index difference.

$$\Delta = \frac{n_1^2 - n_2^2}{2n_1^2} = \frac{n_1 - n_2}{n_1}$$

Thus relative refractive index difference is the ratio between the refractive index difference (of core and cladding) and refractive index of core.

6. Meridional rays.

Meridional rays are the rays following ZigZag path when they travel through fiber and for every reflection it will cross the fiber axis.

skew rays.

Skew rays are the rays following the helical path around the fiber axis when they travel through the fiber and they would not cross the fiber axis at any time.

8. V number of fiber or normalized frequency of fiber.

V number of fiber or normalized frequency of fiber is used to find the number of propagating modes through the fiber.

$V = [2\pi a/ \lambda] (N.A)$

9. Goos-Haenchen effect.

Goos-Haenchen effect states that there is a lateral shift of the reflected ray at the point of incidence at the core-cladding interface. This lateral shift is called the Goos-Haenchen shift.

10. Hybrid modes.

Hybrid modes are the mixture of TE and TM modes that can be traveled through the optical fiber.

Examples:

1. HE1m modes in which |Ez|>|Hz|
2. EH1m modes in which |Hz|>|Ez|

11. Cutoff wavelength of the fiber.

The cutoff wavelength is defined as the minimum value of wavelength that can be transmitted through the fiber. The wavelengths greater than the cutoff wavelength can be transmitted.

λ cutoff = [2$\prod$a/ V] (N.A)

12. fiber birefringence.

Imperfections in the fiber are common such as asymmetrical lateral stress, non-circular imperfect variations of refractive index profile. These imperfections break the circular symmetry of ideal fiber and mode propagate with different phase velocity and the difference between their refractive index is called fiber birefringence.

$B=ko(n_y-n_x)$

UNIT – 2

TRANSMISSION CHARACTERISTIC OF OPTICAL FIBER

Attenuation

The attenuation or transmission loss of optical fibers has proved to be one of the most important factors in bringing about their wide acceptance in telecommunications. As channel attenuation largely determined the maximum transmission distance prior to signal restoration, optical fiber communications became especially attractive when the transmission losses of fibers were reduced below those of the competing metallic conductors (less than 5 dB km^{-1}).

Signal attenuation within optical fibers, as with metallic conductors, is usually expressed in the logarithmic unit of the decibel. The decibel, which is used for comparing two power levels, may be defined for a particular optical wavelength as the ratio of the input (transmitted) optical power *P*i into a fiber to the output (received) optical power *P*o from the fiber as:

$$\text{Number of decibels (dB)} = 10 \log_{10} \frac{P_i}{P_o} \tag{2.1}$$

This logarithmic unit has the advantage that the operations of multiplication and division reduce to addition and subtraction, while powers and roots reduce to multiplication and division. However, addition and subtraction require a conversion to numerical values which may be obtained using the relationship:

$$\frac{P_i}{P_o} = 10^{(\text{dB}/10)} \tag{2.2}$$

In optical fiber communications the attenuation is usually expressed in decibels per unit length (i.e. dB km^{-1}) following:

$$\alpha_{\text{dB}} L = 10 \log_{10} \frac{P_i}{P_o} \tag{2.3}$$

where αdB is the signal attenuation per unit length in decibels which is also referred to as the fiber loss parameter and L is the fiber length. A number of mechanisms are responsible for the signal attenuation within optical fibers. These mechanisms are influenced by the material composition, the preparation and purification technique, and the waveguide structure. They may be categorized within several major areas which include material absorption, material scattering (linear and nonlinear scattering), curve and microbending losses, mode coupling radiation losses and losses due to leaky modes.

Material absorption losses in silica glass fibers

Material absorption is a loss mechanism related to the material composition and the fabrication process for the fiber, which results in the dissipation of some of the transmitted optical power as heat in the waveguide. The absorption of the light may be intrinsic (caused by the interaction with one or more of the major components of the glass) or extrinsic (caused by impurities within the glass).

1. Intrinsic absorption

An absolutely pure silicate glass has little intrinsic absorption due to its basic material structure in the near-infrared region. However, it does have two major intrinsic absorption mechanisms at optical wavelengths which leave a low intrinsic absorption window over the 0.8 to 1.7 µm wavelength range, as illustrated in Figure 2.1, which shows a possible optical attenuation against wavelength characteristic for absolutely pure glass.

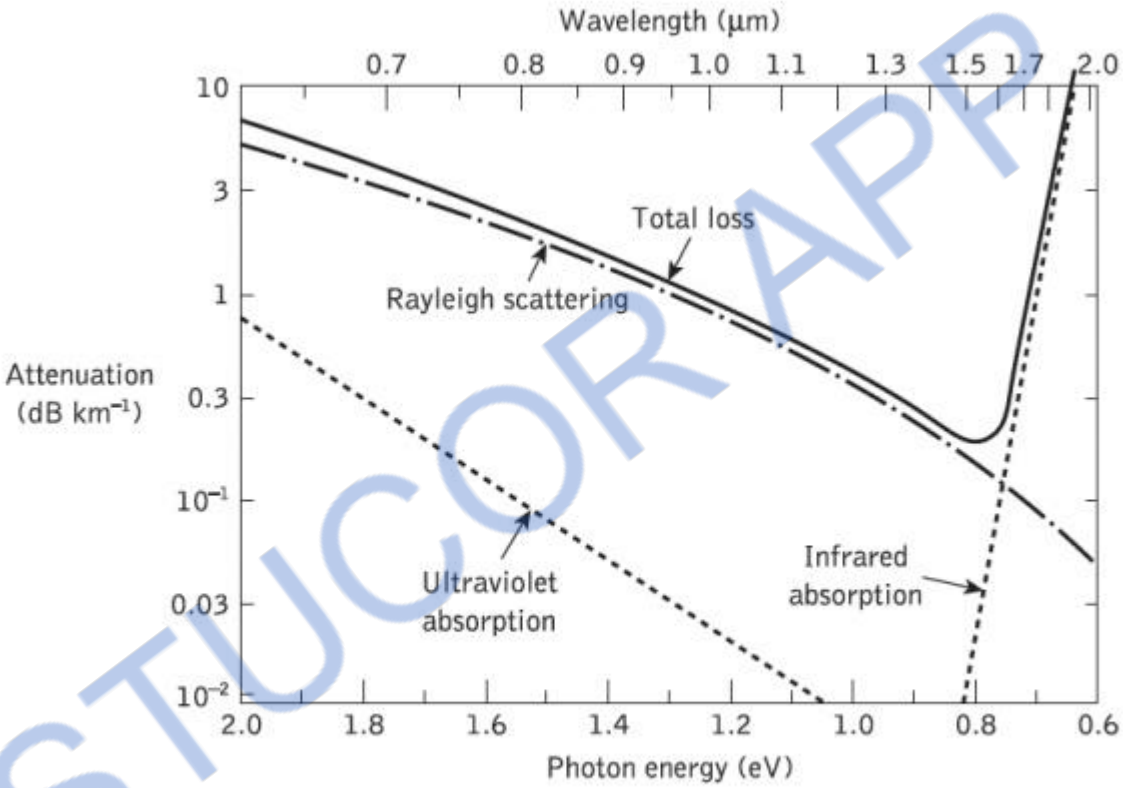

Figure 2.1 The attenuation spectra for the intrinsic loss mechanisms in pure GeO2–SiO2 glass

It may be observed that there is a fundamental absorption edge, the peaks of which are centered in the ultraviolet wavelength region. This is due to the stimulation of electron transitions within the glass by higher energy excitations.

The tail of this peak may extend into the window region at the shorter wavelengths, as illustrated in Figure 2.1. Also in the infrared and far infrared, normally at wavelengths above 7 µm, fundamentals of absorption bands from the interaction of photons with molecular vibrations within the glass occur.

These give absorption peaks which again extend into the window region. The strong absorption bands occur due to oscillations of structural units such as Si–O (9.2 µm), P–O (8.1 µm), B–O (7.2 µm) and Ge–O (11.0µm) within the glass. Hence, above 1.5 µm the tails of these largely far-infrared absorption peaks tend to cause most of the pure glass losses.

However, the effects of both these processes may be minimized by suitable choice of both core and cladding compositions. For instance, in some non oxide glasses such as fluorides and chlorides, the infrared absorption peaks occur at much longer wavelengths which are well into the far infrared (up to 50 µm), giving less attenuation to longer wavelength transmission compared with oxide glasses.

2. Extrinsic absorption

In practical optical fibers prepared by conventional melting techniques, a major source of signal attenuation is extrinsic absorption from transition metal element impurities.

Some of the more common metallic impurities found in glasses are shown in the Table 2.1, together with the absorption losses caused by one part in 109

Table 2.1 Absorption losses caused by some of the more common metallic ionimpurities in glasses, together with the absorption peak wavelength

	Peak wavelength (nm)	*One part in 10^9 (dB km^{-1})*
Cr^{3+}	625	1.6
C^{2+}	685	0.1
Cu^{2+}	850	1.1
Fe^{2+}	1100	0.68
Fe^{3+}	400	0.15
Ni^{2+}	650	0.1
Mn^{3+}	460	0.2
V^{4+}	725	2.7

It may be noted that certain of these impurities, namely chromium and copper, in their worst valence state can cause attenuation in excess of 1 dB km−1 in the near-infrared region. Transition element contamination may be reduced to acceptable levels (i.e. one

part in 1010) by glass refining techniques such as vapor-phase oxidation, which largely eliminates the effects of these metallic impurities.

However, another major extrinsic loss mechanism is caused by absorption due to water (as the hydroxyl or OH ion) dissolved in the glass. These hydroxyl groups are bonded into the glass structure and have fundamental stretching vibrations which occur at wavelengths between 2.7 and 4.2μm depending on group position in the glass network. The fundamental vibrations give rise to overtones appearing almost harmonically at 1.38, 0.95 and 0.72 μm, as illustrated in Figure 2.2. This shows the absorption spectrum for the hydroxyl group in silica.

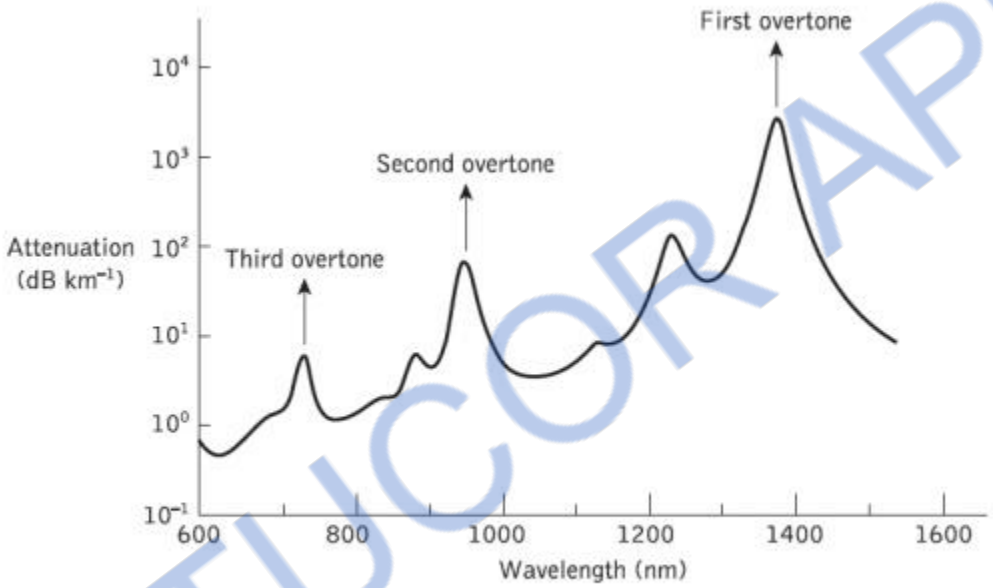

Figure 2.2 The absorption spectrum for the hydroxyl (OH) group in silica.

Furthermore, combinations between the overtones and the fundamental SiO2 vibration occur at 1.24, 1.13 and 0.88 μm, completing the absorption spectrum shown in Figure 2.2.It may also be observed in Figure 3.2 that the only significant absorption band in the region below a wavelength of

1 μm is the second overtone at 0.95 μm which causes attenuation of about 1 dB km−1 for one part per million (ppm) of hydroxyl.

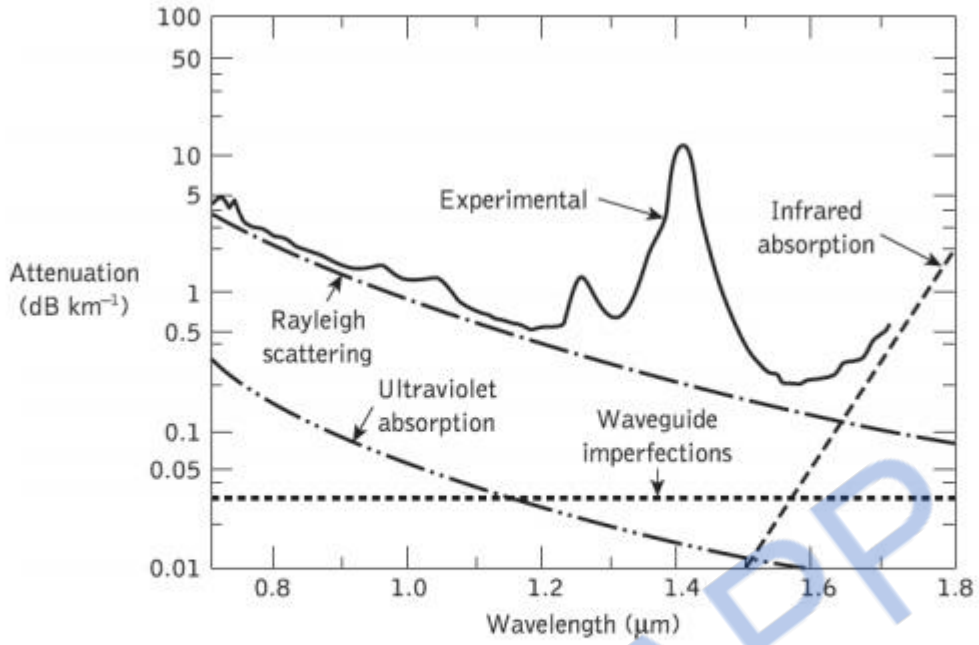

Figure 2.3 The measured attenuation spectrum for an ultra-low-loss single-mode fiber (solid line) with the calculated attenuation spectra for some of the loss mechanisms contributing to the overall fiber attenuation

At longer wavelengths the first overtone at 1.383 μm and its sideband at 1.24 μm are strong absorbers giving attenuation of about 2 dB km−1 ppm and 4 dB km−1 ppm respectively. Since most resonances are sharply peaked, narrow windows exist in the longer wavelength region around 1.31 and 1.55 μm which are essentially unaffected by OH absorption once the impurity level has been reduced below one part in 107. This situation is illustrated in Figure 2.3, which shows the attenuation spectrum of a low-loss single-mode fiber produced in 1979. It may be observed that the lowest attenuation for this fiber occurs at a wavelength of 1.55 μm and is 0.2 dB km−1. Despite this value approaching the minimum possible attenuation of around 0.18 dB km−1 at the 1.55 μm wavelength, it should be noted that the transmission loss of an ultra-low-loss pure silica core fiber was more recently measured as 0.1484 dB km−1 at the slightly longer wavelength of 1.57μm.

Although in standard, modern single-mode fibers the loss caused by the primary OH peak at 1.383 μm has been reduced below 1 dB km−1, it still limits operation over significant distances to the lower loss windows at 1.31 and 1.55 μm.

Linear scattering losses

Linear scattering mechanisms cause the transfer of some or all of the optical power contained within one propagating mode to be transferred linearly (proportionally to the mode power) into a different mode. This process tends to result in attenuation of the transmitted light as the transfer may be to a leaky or radiation mode which does not continue to propagate within the fiber core, but is radiated from the fiber. It must be noted that as with all linear processes, there is no change of frequency on scattering.

Linear scattering may be categorized into two major types: Rayleigh and Mie scattering. Both result from the nonideal physical properties of the manufactured fiber which are difficult and, in certain cases, impossible to eradicate at present.

1. Rayleigh scattering

Rayleigh scattering is the dominant intrinsic loss mechanism in the low-absorption window between the ultraviolet and infrared absorption tails. It results from inhomogeneities of a random nature occurring on a small scale compared with the wavelength of the light.

These inhomogeneities manifest themselves as refractive index fluctuations and arise from density and compositional variations which are frozen into the glass lattice on cooling. The compositional variations may be reduced by improved fabrication, but the index fluctuations caused by the freezing-in of density inhomogeneities are fundamental and cannot be avoided.

The subsequent scattering due to the density fluctuations, which is in almost all directions, produces an attenuation proportional to 1/λ4 following the Rayleigh scattering formula. For a single-component glass this is given by:

$$\gamma_R = \frac{8\pi^3}{3\lambda^4} n^8 p^2 \beta_c K T_F \qquad (2.4)$$

where γR is the Rayleigh scattering coefficient, λ is the optical wavelength, *n* is the refractive index of the medium, *p* is the average photoelastic coefficient, βc is the isothermal compressibility at a fictive temperature *T*F, and *K* is Boltzmann's constant. The fictive temperature is defined as the temperature at which the glass can reach a state

of thermal equilibrium and is closely related to the anneal temperature. Furthermore, the Rayleigh scattering coefficient is related to the transmission loss factor (transmissivity) of the fiber following the relation:

$$\mathscr{L} = \exp(-\gamma_R L) \tag{2.5}$$

where L is the length of the fiber. It is apparent from Eq. (2.4) that the fundamental component of Rayleigh scattering is strongly reduced by operating at the longest possible wavelength.

2. Mie scattering

Linear scattering may also occur at inhomogeneities which are comparable in size with the guided wavelength. These result from the nonperfect cylindrical structure of the waveguide and may be caused by fiber imperfections such as irregularities in the core–cladding interface, core–cladding refractive index differences along the fiber length, diameter fluctuations, strains and bubbles. When the scattering inhomogeneity size is greater than λ/10, the scattered intensity which has an angular dependence can be very large.

The scattering created by such inhomogeneities is mainly in the forward direction and is called Mie scattering. Depending upon the fiber material, design and manufacture, Mie scattering can cause significant losses. The inhomogeneities may be reduced by:

✓⋯removing imperfections due to the glass manufacturing process;

✓⋯carefully controlled extrusion and coating of the fiber;

✓⋯increasing the fiber guidance by increasing the relative refractive index difference.

By these means it is possible to reduce Mie scattering to insignificant levels

Nonlinear scattering losses

Optical waveguides do not always behave as completely linear channels whose increase in output optical power is directly proportional to the input optical power. Several

nonlinear effects occur, which in the case of scattering cause disproportionate attenuation, usually at high optical power levels.

This nonlinear scattering causes the optical power from one mode to be transferred in either the forward or backward direction to the same, or other modes, at a different frequency. It depends critically upon the optical power density within the fiber and hence only becomes significant above threshold power levels.

The most important types of nonlinear scattering within optical fibers are stimulated Brillouin and Raman scattering, both of which are usually only observed at high optical power densities in long single-mode fibers. These scattering mechanisms in fact give optical gain but with a shift in frequency, thus contributing to attenuation for light transmission at a specific wavelength. However, it may be noted that such nonlinear phenomena can also be used to give optical amplification in the context of integrated optical techniques

1. Stimulated Brillouin scattering

Stimulated Brillouin scattering (SBS) may be regarded as the modulation of light through thermal molecular vibrations within the fiber. The scattered light appears as upper and lower sidebands which are separated from the incident light by the modulation frequency. The incident photon in this scattering process produces a phonon* of acoustic frequency as well as a scattered photon. This produces an optical frequency shift which varies with the scattering angle because the frequency of the sound wave varies with acoustic wavelength.

The frequency shift is a maximum in the backward direction, reducing to zero in the forward direction, making SBS a mainly backward process. As indicated previously, Brillouin scattering is only significant above a threshold power density. Assuming that the polarization state of the transmitted light is not maintained, it may be shown that the threshold power *P*B is given by:

$$P_B = 4.4 \times 10^{-3} d^2 \lambda^2 \alpha_{dB} \nu \text{ watts} \qquad (2.6)$$

where d and λ are the fiber core diameter and the operating wavelength, respectively, both measured in micrometers, αdB is the fiber attenuation in decibels per kilometer and ν is the source bandwidth (i.e. injection laser) in gigahertz. The expression given in Eq. (2.6) allows the determination of the threshold optical power which must be launched into a single-mode optical fiber before SBS occurs

2. Stimulated Raman scattering

Stimulated Raman scattering (SRS) is similar to SBS except that a high-frequency optical phonon rather than an acoustic phonon is generated in the scattering process. Also, SRS can occur in both the forward and backward directions in an optical fiber, and may have an optical power threshold of up to three orders of magnitude higher than the Brillouin threshold in a particular fiber.

Using the same criteria as those specified for the Brillouin scattering threshold given in Eq. (2.6), it may be shown that the threshold optical power for SRS PR in a long single-mode fiber is given by:

$$P_R = 5.9 \times 10^{-2} d^2 \lambda \alpha_{dB} \text{ watts} \quad (2.7)$$

Fiber bend loss

Optical fibers suffer radiation losses at bends or curves on their paths. This is due to the energy in the evanescent field at the bend exceeding the velocity of light in the cladding and hence the guidance mechanism is inhibited, which causes light energy to be radiated from the fiber. An illustration of this situation is shown in Figure 2.5. The part of the mode which is on the outside of the bend is required to travel faster than that on the inside so that a wavefront perpendicular to the direction of propagation is maintained.

Hence, part of the mode in the cladding needs to travel faster than the velocity of light in that medium. As this is not possible, the energy associated with this part of the mode is lost through radiation. The loss can generally be represented by a radiation attenuation coefficient which has the form:

$$\alpha_r = c_1 \exp(-c_2 R)$$

Where R is the radius of curvature of the fiber bend and $c1$, $c2$ are constants which are independent of R. Furthermore, large bending losses tend to occur in multimode fibers at a critical radius of curvature Rc which may be estimated from:

$$R_c \simeq \frac{3n_1^2\lambda}{4\pi(n_1^2 - n_2^2)^{\frac{3}{2}}} \tag{2.8}$$

It may be observed from the expression given in Eq. (2.8) that potential macrobending losses may be reduced by:

✓…designing fibers with large relative refractive index differences;

✓…operating at the shortest wavelength possible.

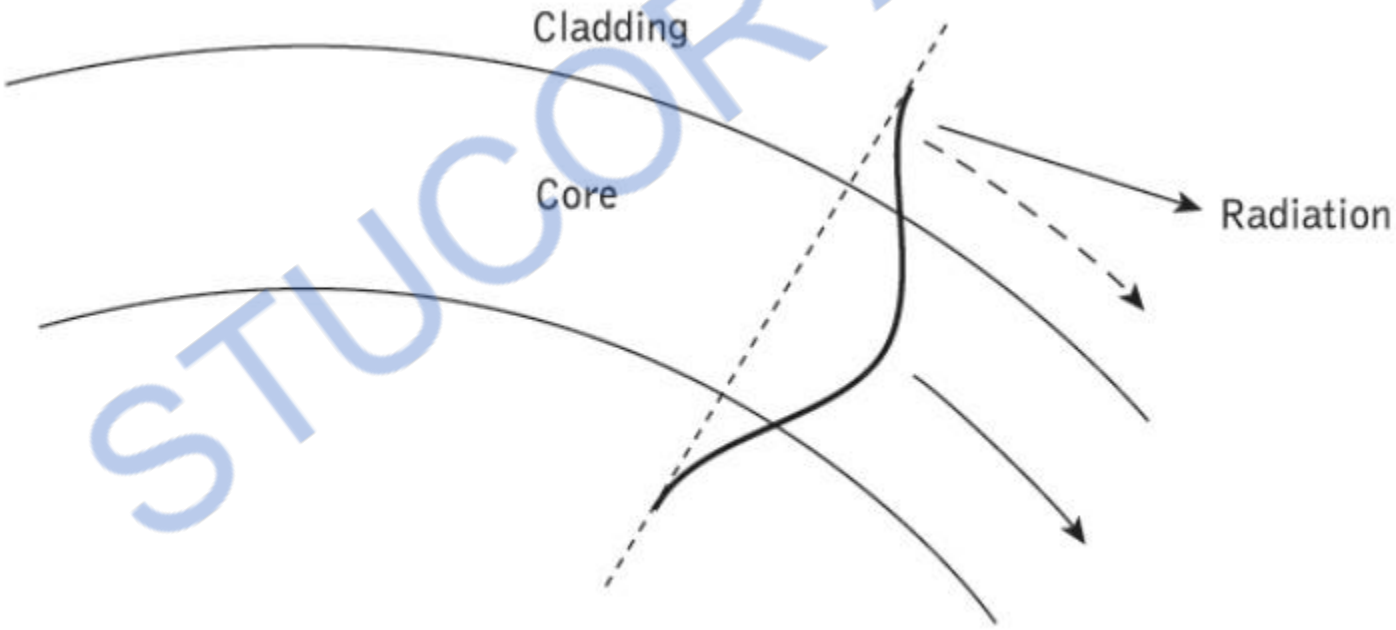

Figure 2.5 An illustration of the radiation loss at a fiber bend.

The above criteria for the reduction of bend losses also apply to single-mode fibers. One theory, based on the concept of a single quasi-guided mode, provides an expression from which the critical radius of curvature for a single-mode fiber Rcs can be estimated as

$$R_{cs} \simeq \frac{20\lambda}{(n_1 - n_2)^{\frac{3}{2}}}\left(2.748 - 0.996\frac{\lambda}{\lambda_c}\right)^{-3} \quad (2.9)$$

where λc is the cutoff wavelength for the single-mode fiber. Hence again, for a specific single-mode fiber (i.e. a fixed relative index difference and cutoff wavelength), the critical wavelength of the radiated light becomes progressively shorter as the bend radius is decreased.

Mid-infrared and far-infrared transmission

In the near-infrared region of the optical spectrum, fundamental silica fiber attenuation is dominated by Rayleigh scattering and multiphonon absorption from the infrared absorption edge (see Figure 2.2). Therefore, the total loss decreases as the operational transmission wavelength increases until a crossover point is reached around a wavelength of 1.55 μm where the total fiber loss again increases because at longer wavelengths the loss is dominated by the phonon absorption edge. Since the near fundamental attenuation limits for near-infrared silicate class fibers have been achieved, more recently researchers have turned their attention to the mid-infrared (2 to 5 μm) and the far-infrared (8 to 12 μm) optical wavelengths.

In order to obtain lower loss fibers it is necessary to produce glasses exhibiting longer infrared cutoff wavelengths. Potentially, much lower losses can be achieved if the transmission window of the material can be extended further into the infrared by utilizing constituent atoms of higher atomic mass and if it can be drawn into fiber exhibiting suitable strength and chemical durability. The reason for this possible loss reduction is due to Rayleigh scattering which displays a λ−4 dependence and hence becomes much reduced as the wavelength is increased. For example, the scattering loss is reduced by a factor of 16 when the optical wavelength is doubled.

Thus it may be possible to obtain losses of the order of 0.01 dB km−1 at a wavelength of 2.55 μm, with even lower losses at wavelengths of between 3 and 5 μm. Candidate glass-forming systems for mid-infrared transmission are fluoride, fluoride–chloride, chalcogenide and oxide.

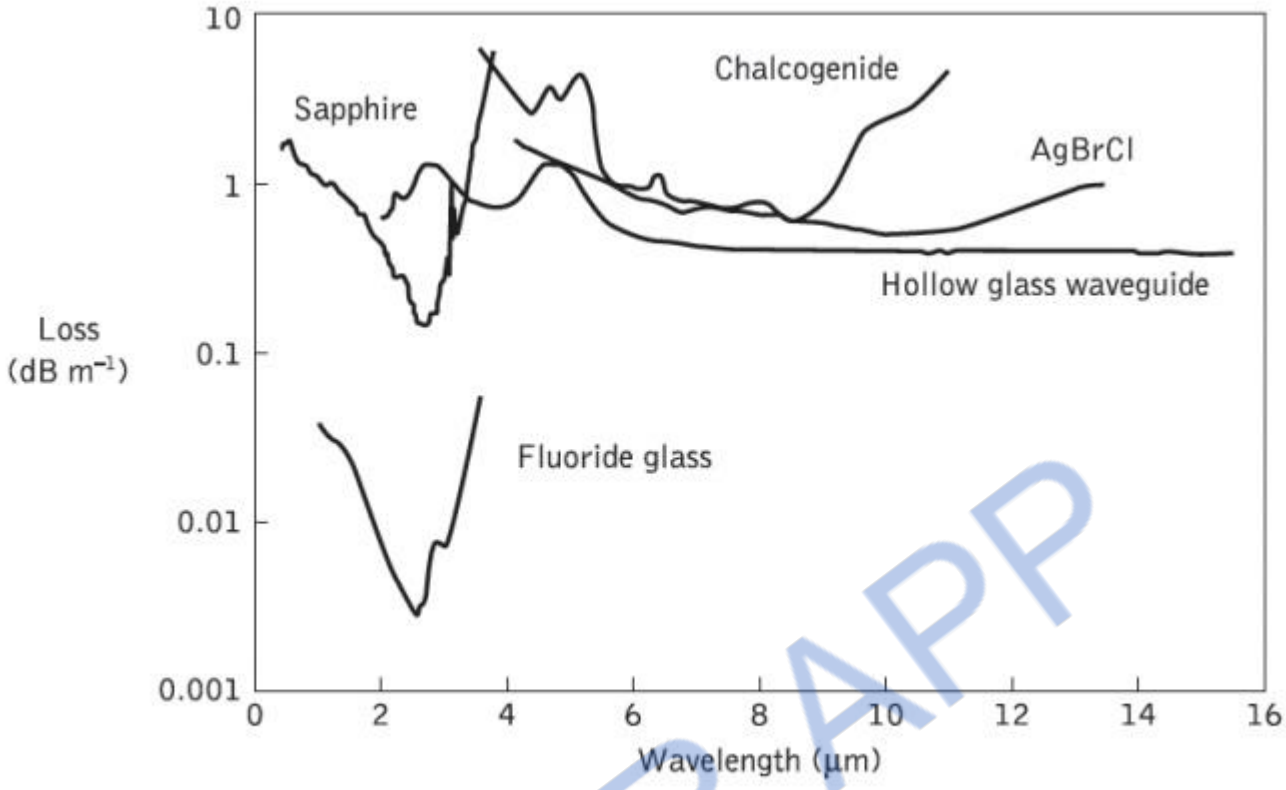

Figure 2.6 Attenuation spectra for some common mid- and far-infrared fibers

In particular, oxide glasses such as Al2O3 (i.e. sapphire) offer a near equivalent transmittance range to many of the fluoride glasses and have benefits of high melting points, chemical inertness, and the ability to be readily melted and grown in air. Chalcogenide glasses, which generally comprise one or more elements Ge, Si, As and Sb, are capable of optical transmission in both the mid-infrared and far-infrared regions.

A typical chalcogenide fiber glass is therefore arsenide trisulfide (As2S3). However, research activities into far-infrared transmission using chalcogenide glasses, halide glasses, polycrystalline halide fibers (e.g. silver and thallium) and hollow glass waveguides are primarily concerned with radiometry, infrared imaging, optical wireless, optical sensing and optical power transmission rather than telecommunications

The loss spectrum for a single-crystal sapphire fiber which also transmits in the midinfrared is also shown in Figure 2.6. Although they have robust physical properties, including a Young's modulus six times greater as well as a thermal expansion some ten times higher than that of silica, these fibers lend themselves to optical power delivery applications [Ref. 27], not specifically optical communications. Chalcogenide glasses

which have their lowest losses over both the mid- and far-infrared ranges are very stable, durable and insensitive to moisture. Arsenic trisulfide fiber, being one of the simplest, has a spectral range from 0.7 to around 6 μm. Hence it has a cut off at long wavelength significantly before the chalcogenide fibers containing heavier elements such as Te, Ge and Se, an attenuation spectrum for the latter being incorporated in Figure 2.6. In general, chalcogenide glass fibers have proved to be useful in areas such as optical sensing, infrared imaging and for the production of fiber infrared lasers and amplifiers.

Dispersion

Dispersion of the transmitted optical signal causes distortion for both digital and analog transmission along optical fibers. When considering the major implementation of optical fiber transmission which involves some form of digital modulation, then dispersion mechanisms within the fiber cause broadening of the transmitted light pulses as they travel along the channel. The phenomenon is illustrated in Figure 2.7, where it may be observed that each pulse broadens and overlaps with its neighbors, eventually becoming indistinguishable at the receiver input. The effect is known as intersymbol interference (ISI). Thus an increasing number of errors may be encountered on the digital optical channel as the ISI becomes more pronounced. The error rate is also a function of the signal attenuation on the link and the subsequent signal-to-noise ratio (SNR) at the receiver.

For no overlapping of light pulses down on an optical fiber link the digital bit rate BT must be less than the reciprocal of the broadened (through dispersion) pulse duration (2τ).

Hence:

$$B_T \leq \frac{1}{2\tau} \tag{2.10}$$

The conversion of bit rate to bandwidth in hertz depends on the digital coding format used. For metallic conductors when a nonreturn-to-zero code is employed, the binary 1 level is held for the whole bit period τ. In this case there are two bit periods in one

wavelength (i.e. 2 bits per second per hertz), as illustrated in Figure 2.8(a). Hence the maximum bandwidth B is one-half the maximum data rate or:

$$B_T(\max) = 2B \tag{2.12}$$

However, when a return-to-zero code is considered, as shown in Figure 2.8(b), the binary 1 level is held for only part (usually half) of the bit period. For this signaling scheme the data rate is equal to the bandwidth in hertz (i.e. 1 bit per second per hertz) and thus $BT = B$.

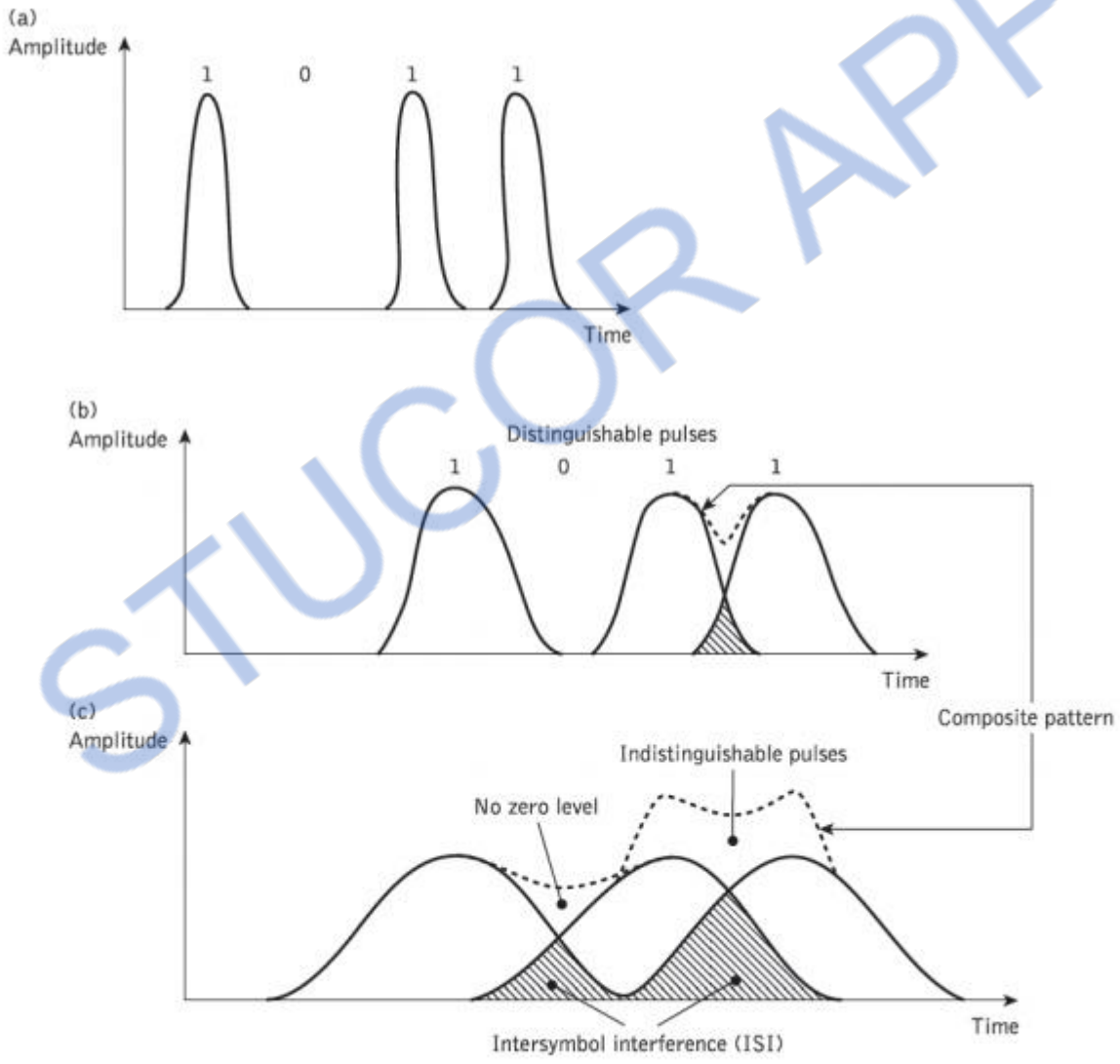

Figure 2.7 An illustration using the digital bit pattern 1011 of the broadening of light pulses as they are transmitted along a fiber: (a) fiber input; (b) fiber output at a distance $L1$; (c) fiber output at a distance $L2 > L1$

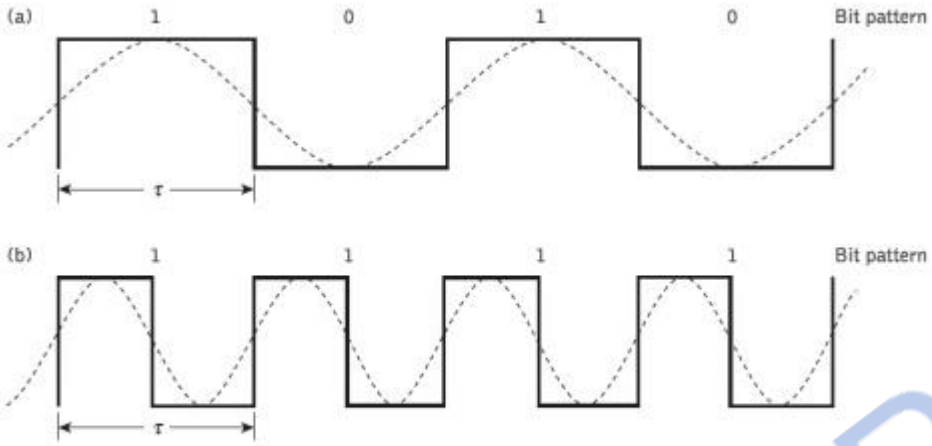

Figure 2.8 Schematic illustration of the relationships of the bit rate to wavelength for digital codes: (a) nonreturn-to-zero (NRZ); (b) return-to-zero (RZ)

The bandwidth *B* for metallic conductors is also usually defined by the electrical 3 Db points (i.e. the frequencies at which the electric power has dropped to one-half of its constant maximum value). However, when the 3 dB optical bandwidth of a fiber is considered it is significantly larger than the corresponding 3 dB electrical bandwidth. Hence, when the limitations in the bandwidth of a fiber due to dispersion are stated (i.e. optical bandwidth *B*opt), it is usually with regard to a return to zero code where the bandwidth in hertz is considered equal to the digital bit rate. Within the context of dispersion the bandwidths expressed in this chapter will follow this general criterion unless otherwise stated.

when electro-optic devices and optical fiber systems are considered it is more usual to statethe electrical 3 dB bandwidth, this being the more useful measurement when interfacing an optical fiber link to electrical terminal equipment.

Intramodal Dispersion

Chromatic or intramodal dispersion may occur in all types of optical fiber and results from the finite spectral linewidth of the optical source. Since optical sources do not emit just a single frequency but a band of frequencies (in the case of the injection laser corresponding to only a fraction of a percent of the center frequency, whereas for the

LED it is likely to be a significant percentage), then there may be propagation delay differences between the different spectral components of the transmitted signal. This causes broadening of each transmitted mode and hence intramodal dispersion. The delay differences may be caused by the dispersive properties of the waveguide material (material dispersion) and also guidance effects within the fiber structure (waveguide dispersion).

1. Material dispersion

Pulse broadening due to material dispersion results from the different group velocities of the various spectral components launched into the fiber from the optical source. It occurs when the phase velocity of a plane wave propagating in the dielectric medium varies nonlinearly with wavelength, and a material is said to exhibit material dispersion when the second differential of the refractive index with respect to wavelength is not zero.

Hence the group delay is given by:

$$\tau_g = \frac{d\beta}{d\omega} = \frac{1}{c}\left(n_1 - \lambda\frac{dn_1}{d\lambda}\right) \tag{2.13}$$

Where n_1 is the refractive index of the core material. The pulse delay τ_m due to material dispersion in a fiber of length L is therefore:

$$\tau_m = \frac{L}{c}\left(n_1 - \lambda\frac{dn_1}{d\lambda}\right) \tag{2.14}$$

For a source with rms spectral width $\sigma\lambda$ and a mean wavelength λ, the rms pulse broadening due to material dispersion σ_m may be obtained from the expansion of Eq. (2.14) in a

Taylor series about λ where:

$$\sigma_m = \sigma_\lambda \frac{d\tau_m}{d\lambda} + \sigma_\lambda \frac{2d^2\tau_m}{d\lambda^2} + \ldots \tag{2.15}$$

As the first term in Eq. (2.15) usually dominates, especially for sources operating over the 0.8 to 0.9

μm wavelength range, then:

$$\sigma_m \simeq \sigma_\lambda \frac{d\tau_m}{d\lambda} \tag{2.16}$$

Hence the pulse spread may be evaluated by considering the dependence of τm on λ, where from Eq. (2.14):

$$\frac{d\tau_m}{d\lambda} = \frac{L\lambda}{c}\left[\frac{dn_1}{d\lambda} - \frac{d^2 n_1}{d\lambda^2} - \frac{dn_1}{d\lambda}\right]$$

$$= \frac{-L\lambda}{c}\frac{d^2 n_1}{d\lambda^2} \tag{2.17}$$

Therefore, substituting the expression obtained in Eq. (2.17) into Eq. (2.16), the rms pulse broadening due to material dispersion is given by:

$$\sigma_m \simeq \frac{\sigma_\lambda L}{c}\left|\lambda \frac{d^2 n_1}{d\lambda^2}\right| \tag{2.18}$$

The material dispersion for optical fibers is sometimes quoted as a value for $|\lambda^2(d^2 n_1/d\lambda^2)|$ or simply $|d^2 n_1/d\lambda^2|$.

However, it may be given in terms of a material dispersion parameter M which is defined as:

$$M = \frac{1}{L}\frac{d\tau_m}{d\lambda} = \frac{\lambda}{c}\left|\frac{d^2 n_1}{d\lambda^2}\right| \tag{2.19}$$

and which is often expressed in units of ps nm−1 km−1.

2. Waveguide dispersion

The waveguiding of the fiber may also create chromatic dispersion. This results from the variation in group velocity with wavelength for a particular mode. Considering the ray

theory approach, it is equivalent to the angle between the ray and the fiber axis varying with wavelength which subsequently leads to a variation in the transmission times for the rays, and hence dispersion. For a single mode whose propagation constant is β, the fiber exhibits waveguide dispersion when $d^2\beta/d\lambda^2 \neq 0$. Multimode fibers, where the majority of modes propagate far from cutoff, are almost free of waveguide dispersion and it is generally negligible compared with material dispersion (≈0.1 to 0.2 ns/ km).

However, with single-mode fibers where the effects of the different dispersion mechanisms are not easy to separate, waveguide dispersion may be significant.

Intermodal dispersion

Pulse broadening due to intermodal dispersion (sometimes referred to simply as modal or mode dispersion) results from the propagation delay differences between modes within a multimode fiber. As the different modes which constitute a pulse in a multimode fiber travel along the channel at different group velocities, the pulse width at the output is dependent upon the transmission times of the slowest and fastest modes. This dispersion mechanism creates the fundamental difference in the overall dispersion for the three types of fiber. Thus multimode step index fibers exhibit a large amount of intermodal dispersion which gives the greatest pulse broadening. However, intermodal dispersion in multimode fibers may be reduced by adoption of an optimum refractive index profile which is provided by the near-parabolic profile of most graded index fibers.

Hence, the overall pulse broadening in multimode graded index fibers is far less than that obtained in multimode step index fibers (typically by a factor of 100). Thus graded index fibers used with a multimode source give a tremendous bandwidth advantage over multimode step index fibers. Under purely single-mode operation there is no intermodal dispersion and therefore pulse broadening is solely due to the intramodal dispersion mechanisms. In theory, this is the case with single-mode step index fibers where only a single mode is allowed to propagate. Hence they exhibit the least pulse broadening and have the greatest possible bandwidths, but in general are only usefully operated with single-mode sources.

In order to obtain a simple comparison for intermodal pulse broadening between multimode step index and multimode graded index fibers, it is useful to consider the geometric optics picture for the two types of fiber.

1. Multimode step index fiber

Using the ray theory model, the fastest and slowest modes propagating in the step index fiber may be represented by the axial ray and the extreme meridional ray (which is incident at the core–cladding interface at the critical angle φc) respectively. The paths taken by these two rays in a perfectly structured step index fiber are shown in Figure 2.9. The delay difference between these two rays when traveling in the fiber core allows estimation of the pulse broadening resulting from intermodal dispersion within the fiber. As both rays are traveling at the same velocity within the constant refractive index fiber core, then the delay difference is directly related to their respective path lengths within the fiber. Hence the time taken for the axial ray to travel along a fiber of length L gives the minimum delay time TMin and:

$$T_{\text{Min}} = \frac{\text{distance}}{\text{velocity}} = \frac{L}{(c/n_1)} = \frac{Ln_1}{c} \tag{2.20}$$

where n_1 is the refractive index of the core and c is the velocity of light in a vacuum.

The extreme meridional ray exhibits the maximum delay time TMax where:

$$T_{\text{Max}} = \frac{L/\cos\theta}{c/n_1} = \frac{Ln_1}{c\cos\theta} \tag{2.21}$$

Using Snell's law of refraction at the core–cladding interface following Eq. (2.2):

$$\sin\phi_c = \frac{n_2}{n_1} = \cos\theta \tag{2.22}$$

where n_2 is the refractive index of the cladding. Furthermore, substituting into Eq. (2.21) for cosθ gives:

$$T_{\text{Max}} = \frac{Ln_1^2}{cn_2} \tag{2.23}$$

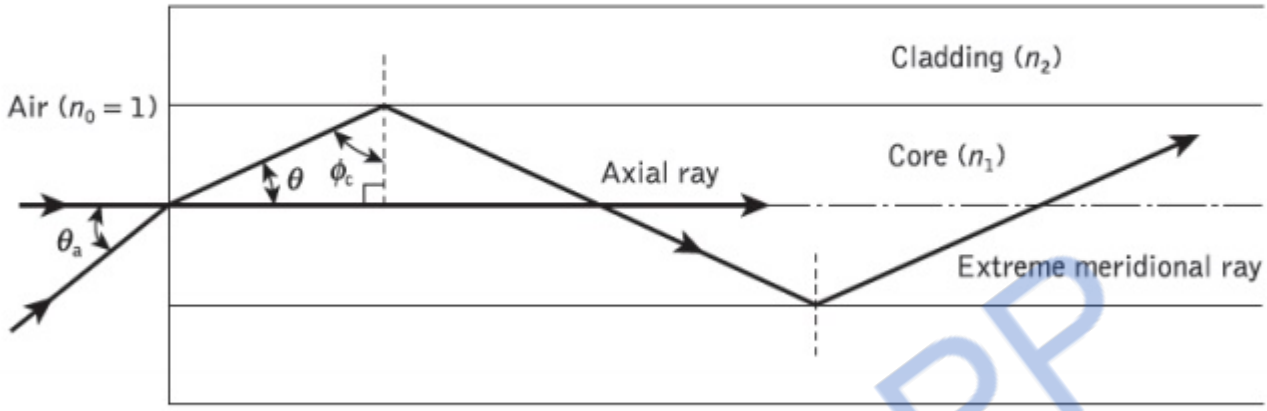

Figure 2.9 The paths taken by the axial and an extreme meridional ray in a perfect multimode step index fiber

The delay difference δT_s between the extreme meridional ray and the axial ray may be obtained by:

$$\delta T_s = T_{\text{Max}} - T_{\text{Min}} = \frac{Ln_1^2}{cn_2} - \frac{Ln_1}{c}$$

$$= \frac{Ln_1^2}{cn_2}\left(\frac{n_1 - n_2}{n_1}\right) \tag{2.24}$$

$$\simeq \frac{Ln_1^2\Delta}{cn_2} \quad \text{when } \Delta \ll 1 \tag{2.25}$$

where Δ is the relative refractive index difference. However, when $\Delta << 1$, then from the definition given by Eq. (2.9), the relative refractive index difference may also be given approximately by:

$$\Delta \simeq \frac{n_1 - n_2}{n_2} \tag{2.26}$$

Hence rearranging Eq. (3.24):

$$\delta T_s = \frac{L n_1}{c}\left(\frac{n_1 - n_2}{n_2}\right) \simeq \frac{L n_1 \Delta}{c} \tag{2.27}$$

Also substituting for Δ from Eq. (2.10) gives:

$$\delta T_s \simeq \frac{L(NA)^2}{2 n_1 c} \tag{2.28}$$

where *NA* is the numerical aperture for the fiber. The approximate expressions for the delay difference given in Eqs (2.27) and (2.28) are usually employed to estimate the maximum pulse broadening in time due to intermodal dispersion in multimode step index fibers. Again considering the perfect step index fiber, another useful quantity with regard to intermodal dispersion on an optical fiber link is the rms pulse broadening resulting from this dispersion mechanism along the fiber. When the optical input to the fiber is a pulse *p*i(*t*) of unit area, as illustrated in Figure 2.10, then

$$\int_{-\infty}^{\infty} p_i(t)\, dt = 1 \tag{2.29}$$

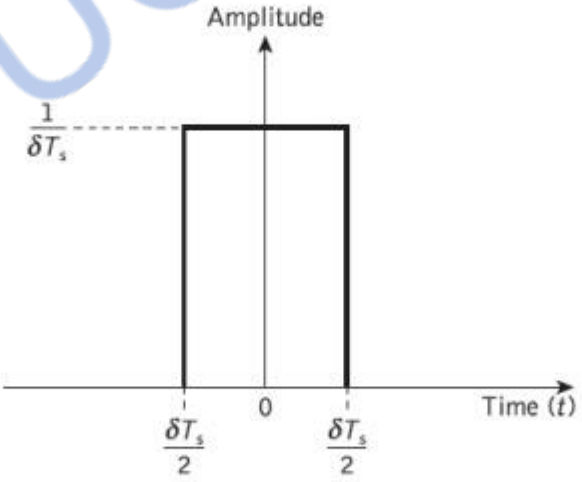

Figure 2.10 An illustration of the light input to the multimode step index fiber consisting of an ideal pulse or rectangular function with unit area

It may be noted that *p*i(*t*) has a constant amplitude of 1/δ*T*s over the range:

$$\frac{-\delta T_s}{2} \le p(t) \le \frac{\delta T_s}{2}$$

The rms pulse broadening at the fiber output due to intermodal dispersion for the multimode step index fiber σs (i.e. the standard deviation) may be given in terms of the variance σs2:

$$\sigma_s^2 = M_2 - M_1^2 \tag{2.30}$$

Where *M*1 is the first temporal moment which is equivalent to the mean value of the pulse and *M*2, the second temporal moment, is equivalent to the mean square value of the pulse.

Hence:

$$M_1 = \int_{-\infty}^{\infty} t p_i(t)\, dt \tag{2.31}$$

And:

$$M_2 = \int_{-\infty}^{\infty} t^2 p_i(t)\, dt \tag{2.32}$$

The mean value *M*1 for the unit input pulse of Figure 2.10 is zero, and assuming this is maintained for the output pulse, then from Eqs (2.30) and (2.32):

$$\sigma_s^2 = M_2 = \int_{-\infty}^{\infty} t^2 p_i(t)\, dt \tag{2.33}$$

Integrating over the limits of the input pulse (Figure 3.12) and substituting for *p*i(*t*) in Eq. (2.33) over this range gives:

$$\sigma_s^2 = \int_{-\delta T_s/2}^{\delta T_s/2} \frac{1}{\delta T_s} t^2 \, dt$$

$$= \frac{1}{\delta T_s}\left[\frac{t^3}{3}\right]_{-\delta T_s/2}^{\delta T_s/2} = \frac{1}{3}\left(\frac{\delta T_s}{2}\right)^2 \tag{2.34}$$

Hence substituting from Eq. (2.27) for δTs gives:

$$\sigma_s \simeq \frac{L n_1 \Delta}{2\sqrt{3}c} \simeq \frac{L(NA)^2}{4\sqrt{3}n_1 c} \tag{2.35}$$

Equation (2.35) allows estimation of the rms impulse response of a multimode step index fiber if it is assumed that intermodal dispersion dominates and there is a uniform distribution of light rays over the range $0 \leq \theta \leq \theta a$ The pulse broadening is directly proportional to the relative refractive index difference Δ and the length of the fiber L. The latter emphasizes the bandwidth–length trade-off that exists, especially with multimode step index fibers, and which inhibits their use for wideband long-haul (between repeaters) systems. Furthermore, the pulse broadening is reduced by reduction of the relative refractive index difference Δ for the fiber.

Intermodal dispersion may be reduced by propagation mechanisms within practical fibers. For instance, there is differential attenuation of the various modes in a step index fiber. This is due to the greater field penetration of the higher order modes into the cladding of the waveguide. These slower modes therefore exhibit larger losses at any core–cladding irregularities, which tends to concentrate the transmitted optical power into the faster lower order modes. Thus the differential attenuation of modes reduces intermodal pulse broadening on a multimode optical link.

Another mechanism which reduces intermodal pulse broadening in nonperfect (i.e. practical) multimode fibers is the mode coupling or mixing. The coupling between guided modes transfers optical power from the slower to the faster modes, and vice versa. Hence, with strong coupling the optical power tends to be transmitted at an average speed, which is the mean of the various propagating modes. This reduces the intermodal dispersion on the link and makes it advantageous to encourage mode coupling within multimode fibers.

The expression for delay difference given in Eq. (2.27) for a perfect step index fiber may be modified for the fiber with mode coupling among all guided modes to:

$$\delta T_{sc} \simeq \frac{n_1 \Delta}{c} (L L_c)^{\frac{1}{2}} \tag{2.36}$$

2. Multimode graded index fiber

Intermodal dispersion in multimode fibers is minimized with the use of graded index fibers. Hence, multimode graded index fibers show substantial bandwidth improvement over multimode step index fibers. The reason for the improved performance of graded index fibers may be observed by considering the ray diagram for a graded index fiber shown in Figure 2.11. The fiber shown has a parabolic index profile with a maximum at the core axis, as illustrated in Figure 2.11(a). Analytically, the index profile is given by:

$$\begin{aligned} n(r) &= n_1[1 - 2\Delta(r/a)^2]^{\frac{1}{2}} \qquad r < a \text{ (core)} \\ &= n_1(1 - 2\Delta)^{\frac{1}{2}} = n_2 \qquad r \geq a \text{ (cladding)} \end{aligned} \tag{2.37}$$

Figure 2.11(b) shows several meridional ray paths within the fiber core. It may be observed that apart from the axial ray, the meridional rays follow sinusoidal trajectories of different path lengths which result from the index grading. However, the local group velocity is inversely proportional to the local refractive index and therefore the longer sinusoidal paths are compensated for by higher speeds in the lower index medium away from the axis.

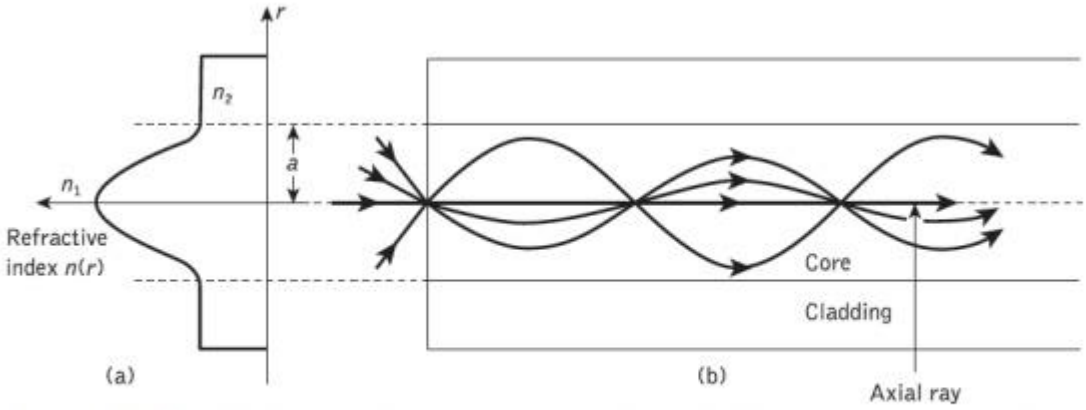

Figure 2.11 A multimode graded index fiber: (a) parabolic refractive index profile; (b) meridional ray paths within the fiber core

Hence there is an equalization of the transmission times of the various trajectories towards the transmission time of the axial ray which travels exclusively in the high-index region at the core axis, and at the slowest speed. As these various ray paths may be considered to represent the different modes propagating in the fiber, then the graded profile reduces the disparity in the mode transit times.

The dramatic improvement in multimode fiber bandwidth achieved with a parabolic or near-parabolic refractive index profile is highlighted by consideration of the reduced delay difference between the fastest and slowest modes for this graded index fiber δTg. Using a ray theory approach the delay difference is given by:

$$\delta T_g \simeq \frac{L n_1 \Delta^2}{2c} \simeq \frac{(NA)^4}{8 n_1^3 c} \tag{2.38}$$

However, a more rigorous analysis using electromagnetic mode theory gives an absolute temporal width at the fiber output of :

$$\delta T_g = \frac{L n_1 \Delta^2}{8c} \tag{2.39}$$

which corresponds to an increase in transmission time for the slowest mode of $\Delta 2/8$ over the fastest mode. The expression given in Eq. (2.39) does not restrict the bandwidth to pulses with time slots corresponding to δTg as 70% of the optical power is concentrated in the first half of the interval. Hence the rms pulse broadening is a useful parameter for

assessment of intermodal dispersion in multimode graded index fibers. It may be shown that the rms pulse broadening of a near-parabolic

index profile graded index fiber σg is reduced compared with similar broadening for the corresponding step index fiber σs (i.e. with the same relative refractive index difference) following

$$\sigma_g = \frac{\Delta}{D}\sigma_s \tag{2.40}$$

where *D* is a constant between 4 and 10 depending on the precise evaluation and the exact optimum profile chosen.

The best minimum theoretical intermodal rms pulse broadening for a graded index fiber with an optimum characteristic refractive index profile for the core αop of

$$\alpha_{op} = 2 - \frac{12\Delta}{5} \tag{2.41}$$

is given by combining Eqs (2.27) and (2.40) as:

$$\sigma_g = \frac{Ln_1\Delta^2}{20\sqrt{3}c} \tag{2.42}$$

Overall fiber dispersion

1. Multimode fibers

The overall dispersion in multimode fibers comprises both chromatic and intermodal terms. The total rms pulse broadening σT is given (see Appendix D) by:

$$\sigma_T = (\sigma_c^2 + \sigma_n^2)^{\frac{1}{2}} \tag{2.44}$$

where σc is the intramodal or chromatic broadening and σn is the intermodal broadening caused by delay differences between the modes (i.e. σs for multimode step index fiber and σg for multimode graded index fiber). The chromatic term σc consists of pulse broadening due to both material and waveguide dispersion. However, since waveguide

dispersion is generally negligible compared with material dispersion in multimode fibers, thenσc =σm.

2. Single-mode fibers

The pulse broadening in single-mode fibers results almost entirely from chromatic or intramodal dispersion as only a single-mode is allowed to propagate.* Hence the bandwidth is limited by the finite spectral width of the source. Unlike the situation in multimode fibers, the mechanisms giving chromatic dispersion in single-mode fibers tend to be interrelated in a complex manner. The transit time or specific group delay σg for a light pulse propagating along a unit length of single-mode fiber may be given as:

$$\tau_g = \frac{1}{c}\frac{d\beta}{dk} \tag{2.45}$$

where *c* is the velocity of light in a vacuum, β is the propagation constant for a mode within the fiber core of refractive index *n*1 and *k* is the propagation constant for the mode in a vacuum.

The total first-order dispersion parameter or the chromatic dispersion of a single-mode fiber, *D*T, is given by the derivative of the specific group delay with respect to the vacuum wavelength λ□as:

$$D_T = \frac{d\tau_g}{d\lambda} \tag{2.46}$$

In common with the material dispersion parameter it is usually expressed in units of ps nm−1 km−1. When the variable λ is replaced by ω, then the total dispersion parameter becomes:

$$D_T = -\frac{\omega}{\lambda}\frac{d\tau_g}{d\omega} = -\frac{\omega}{\lambda}\frac{d^2\beta}{d\omega^2} \tag{2.47}$$

The fiber exhibits intramodal dispersion when β varies nonlinearly with wavelength. β may be expressed in terms of the relative refractive index difference Δ and the normalized propagation constant *b* as

$$\beta = kn_1[1 - 2\Delta(1 - b)]^{\frac{1}{2}} \tag{2.48}$$

The rms pulse broadening caused by chromatic dispersion down a fiber of length L is given by the derivative of the group delay with respect to wavelength as [Ref. 45]:

$$\text{Total rms pulse broadening} = \sigma_\lambda L \left| \frac{d\tau_g}{d\lambda} \right| = \frac{\sigma_\lambda L 2\pi}{c\lambda^2} \frac{d^2\beta}{dk^2} \tag{2.49}$$

where σλ is the source rms spectral linewidth centered at a wavelength λ. When Eq. (2.44) is substituted into Eq. (2.45), detailed calculation of the first and second derivatives with respect to k gives the dependence of the pulse broadening on the fiber material's properties and the normalized propagation constant b. This gives rise to three interrelated effects which involve complicated cross-product terms. However, the final expression may be separated into three composite dispersion components in such a way that one of the effects dominates each terms. The dominating effects are as follows:

✓⋯The material dispersion parameter DM defined by λ/c | d2n/dλ| where n = n1 or n2 for the core or cladding respectively.

✓⋯The waveguide dispersion parameter DW, which may be obtained from Eq. (3.47) by substitution from Eq. (2.114) for τg, is defined as:

$$D_W = -\left(\frac{n_1 - n_2}{\lambda c}\right) V \frac{d^2(Vb)}{dV^2} \tag{2.50}$$

where V is the normalized frequency for the fiber. Since the normalized propagation constant b for a specific fiber is only dependent on V, then the normalized waveguide dispersion coefficient Vd2(Vb)/dV2 also depends on V. This latter function is another universal parameter which plays acentral role in the theory of singlemode fibers.

A profile dispersion parameter DP which is proportional to dΔ/dλ

This situation is different from multimode fibers where the majority of modes propagate far from cutoff and hence most of the power is transmitted in the fiber core. In the multimode case the composite dispersion components may be simplified and separated into two chromatic terms which depend on either material or waveguide dispersion. Also, especially when considering step index multimode fibers, the effect of profile dispersion is negligible. Strictly speaking, in single-mode fiber with a power-law refractive index profile the composite dispersion terms should be employed. Nevertheless, it is useful to consider the total first-order dispersion DT in a practical single-mode fiber as comprising:

$$D_T = D_M + D_W + D_P \qquad (\text{ps nm}^{-1}\ \text{km}^{-1}) \tag{2.51}$$

Polarization

Cylindrical optical fibers do not generally maintain the polarization state of the light input for more than a few meters, and hence for many applications involving optical fiber transmission some form of intensity modulation of the optical source is utilized. The optical signal is thus detected by a photodiode which is insensitive to optical polarization or phase of the lightwave within the fiber. Nevertheless, systems and applications have been investigated which could require the polarization states of the input light to be maintained over significant distances, and fibers have been designed for this purpose. These fibers are single mode and the maintenance of the polarization state is described in terms of a phenomenon known as fiber birefringence.

1. Fiber birefringence

Single-mode fibers with nominal circular symmetry about the core axis allow the propagation of two nearly degenerate modes with orthogonal polarizations. They are therefore bimodal supporting HEx11 and HEy11 modes where the principal axes x and y are determined by the symmetry elements of the fiber cross section. Hence in an optical fiber with an ideal optically circularly symmetric core both polarization modes propagate with identical velocities.

Manufactured optical fibers, however, exhibit some birefringence resulting from differences in the core geometry (i.e. ellipticity) resulting from variations in the internal and external stresses, and fiber bending. The fiber therefore behaves as a birefringent medium due to the difference in the effective refractive indices, and hence phase velocities, for these two orthogonally polarized modes. The modes therefore have different propagation constants βx and βy which are dictated by the anisotropy of the fiber cross section. In this case βx and βy are the propagation constants for the slow mode and the fast mode respectively. When the fiber cross-section is independent of the fiber length L in the z direction, then the modal birefringence$B$F for the fiber is given by:

$$B_F = \frac{(\beta_x - \beta_y)}{(2\pi/\lambda)} \tag{2.52}$$

Where λ is the optical wavelength. Light polarized along one of the principal axes will retain its polarization for all L. The difference in phase velocities causes the fiber to exhibit a linear retardation $\Phi(z)$ which depends on the fiber length L in the z direction and is given by:

$$\Phi(z) = (\beta_x - \beta_y)L \tag{2.53}$$

assuming that the phase coherence of the two mode components is maintained. The phase coherence of the two mode components is achieved when the delay between the two transit times is less than the coherence time of the source. the coherence time for the source is equal to the reciprocal of the uncorrelated source frequency width ($1/\delta f$).

It may be shown that birefringent coherence is maintained over a length of fiber Lbc (i.e. coherence length) when:

$$L_{bc} \simeq \frac{c}{B_F \delta f} = \frac{\lambda^2}{B_F \delta \lambda} \tag{2.54}$$

where$c$ is the velocity of light in a vacuum and $\delta\lambda$ is the source linewidth.

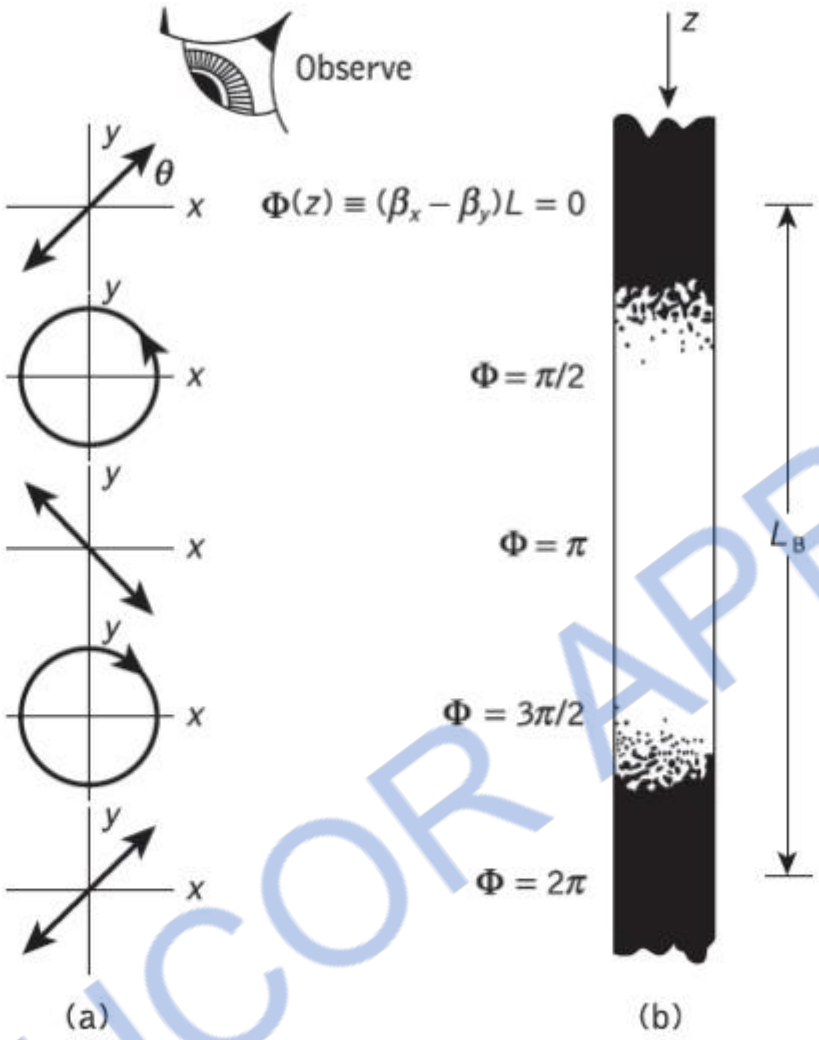

Figure 2.14 An illustration of the beat length in a single-mode optical fiber: (a) the polarization states against Φ(*z*); (b) the light intensity distribution over the beat length within the fiber

However, when phase coherence is maintained (i.e. over the coherence length) Eq. (2.58) leads to a polarization state which is generally elliptical but which varies periodically along the fiber. This situation is illustrated in Figure 2.14(a) where the incident linear polarization which is at 45° with respect to the *x* axis becomes circular polarization at $\Phi = \pi/2$ and linear again at $\Phi = \pi$. The process continues through another circular polarization at $\Phi = 3\pi/2$ before returning to the initial linear polarization at $\Phi = 2\pi$. The characteristic length L_B for this process corresponding to the propagation distance for which a 2π phase difference accumulates between the two modes is known as the beat length. It is given by:

$$L_B = \frac{\lambda}{B_F} \tag{2.55}$$

Substituting for BF from Eq. (2.47) gives:

$$L_B = \frac{2\pi}{(\beta_x - \beta_y)} \tag{2.56}$$

It may be noted that Eq. (2.56) may be obtained directly from Eq. (2.58) where:

$$\Phi(L_B) = (\beta_x - \beta_y)L_B = 2\pi \tag{2.57}$$

Typical single-mode fibers are found to have beat lengths of a few centimeters, and the effect may be observed directly within a fiber via Rayleigh scattering with use of a suitable visible source (e.g. He–Ne laser). It appears as a series of bright and dark bands with a period corresponding to the beat length, as shown in Figure 2.14.(b).

The modal birefringence BF may be determined from these observations of beat length. In a nonperfect fiber various perturbations along the fiber length such as strain or variations in the fiber geometry and composition lead to coupling of energy from one polarization to the other. These perturbations are difficult to eradicate as they may easily occur in the fiber manufacture and cabling. The energy transfer is at a maximum when the perturbations have a period Λ, corresponding to the beat length, and defined by:

$$\Lambda = \frac{\lambda}{B_F} \tag{2.58}$$

However, the cross-polarizing effect may be minimized when the period of the perturbations is less than a cutoff period Λc (around 1 mm). Hence polarization-maintaining fibers may be designed by either:

(a) high (large) birefringence: the maximization of the fiber birefringence, may be achieved by reducing the beat length LB to around 1 mm or less; or

(b) low (small) birefringence: the minimization of the polarization coupling perturbations with a period of Λ. This may be achieved by increasing Λc giving a large beat length of around 50 m or more.

2. Polarization-maintaining fibers

Although the polarization state of the light arriving at a conventional photodetector is not distinguished and hence of little concern, it is of considerable importance in coherent lightwave systems in which the incident signal is superimposed on the field of a local oscillator (see Section 13.3). Moreover, interference and delay differences between the orthogonally polarized modes in birefringent fibers may cause polarization modal noise and PMD respectively (see Section 3.13.2). Finally, polarization is also of concern when a single-mode fiber is coupled to a modulator or other waveguide device (see Section 11.4.2) that can require the light to be linearly polarized for efficient operation. Hence, there are several reasons why it may be desirable to use fibers that will permit light to pass through while retaining its state of polarization. Such polarization-maintaining (PM) fibers

can be classified into two major groups: namely, high-birefringence (HB) and low-birefringence (LB) fibers.

The birefringence of conventional single-mode fibers is in the range BF = 10-6 to 10-5. An HB fiber requires BF > 10-5 and a value better than 10-4 is a minimum for polarization maintenance. HB fibers can be separated into two types which are generally referred to as two-polarization fibers and single-polarization fibers. In the latter case, in order to allow only one polarization mode to propagate through the fiber, a cutoff condition is imposed on the other mode by utilizing the difference in bending loss between the two polarization modes.

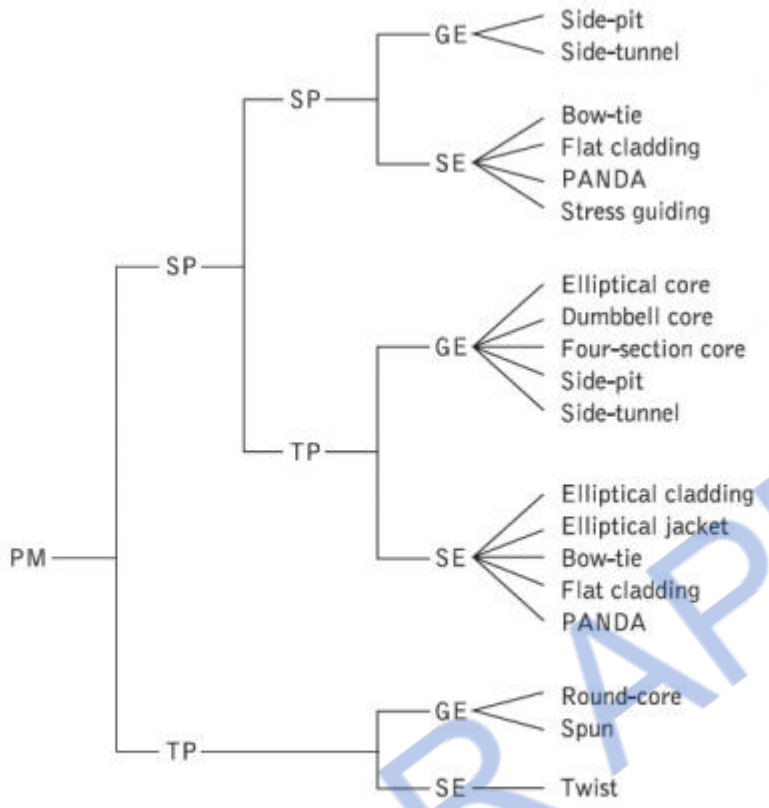

Figure 2.15 Polarization-maintaining fiber types classified from a linear polarization maintenance viewpoint. PM: polarization-maintaining, HB: high-birefringence, LB: low-birefringence, SP: single-polarization, TP: two-polarization, GE: geometrical effect, SE: stress effect

The various types of PM fiber, classified in terms of their linear polarization maintenance, are shown in Figure 2.16

Nonlinear effects

Usually lightwaves or photons transmitted through a fiber have little interaction with each other, and are not changed by their passage through the fiber (except for absorption and scattering). There are exceptions, however, arising from the interactions between lightwaves and the material transmitting them, which can affect optical signals. These processes are normally referred to as nonlinear effects or phenomena because their strength typically depends on the square (or some higher power) of the optical intensity. Hence nonlinear effects are weak at low powers but they can become much stronger at high optical intensities. This situation can result either when the power is increased, or when it is concentrated in a small area such as the core of a single-mode optical fiber.

Although the nonlinear effects in optical fibers are small, they accumulate as light passes through many kilometers of single-mode fiber. The small core diameters, together with the long transmission distances that may be obtained with these fibers, have enabled the occurrence of nonlinear phenomena at power levels of a few milliwatts which are well within the capability of semiconductor lasers. Furthermore, the optical power levels become much larger when wavelength division multiplexing packs many signal channels into one single-mode fiber such that the overall power level is the summation of the individual channel optical powers.

There are two broad categories of nonlinear effects that can be separated based on their characteristics: namely, scattering and Kerr effects.

Fiber alignment and joint loss

A major consideration with all types of fiber–fiber connection is the optical loss encountered at the interface. Even when the two jointed fiber ends are smooth and perpendicular to the fiber axes, and the two fiber axes are perfectly aligned, a small proportion of the light may be reflected back into the transmitting fiber causing attenuation at the joint. This phenomenon, known as Fresnel reflection, is associated with the step changes in refractive index at the jointed interface (i.e. glass–air–glass). The magnitude of this partial reflection of the light transmitted through the interface may be estimated using the classical Fresnel formula for light of normal incidence and is given by

$$r = \left(\frac{n_1 - n}{n_1 + n}\right)^2 \tag{2.59}$$

where r is the fraction of the light reflected at a single interface, $n1$ is the refractive index of the fiber core and n is the refractive index of the medium between the two jointed fibers (i.e. for air n =1). However, in order to determine the amount of light reflected at a fiber joint, Fresnel reflection at both fiber interfaces must be taken into account. The loss in decibels due to Fresnel reflection at a single interface is given by:

$$\text{Loss}_{\text{Fres}} = -10 \log_{10}(1 - r) \tag{2.60}$$

Hence, using the relationships given in Eqs (2.59) and (2.60) it is possible to determine the optical attenuation due to Fresnel reflection at a fiber–fiber joint.

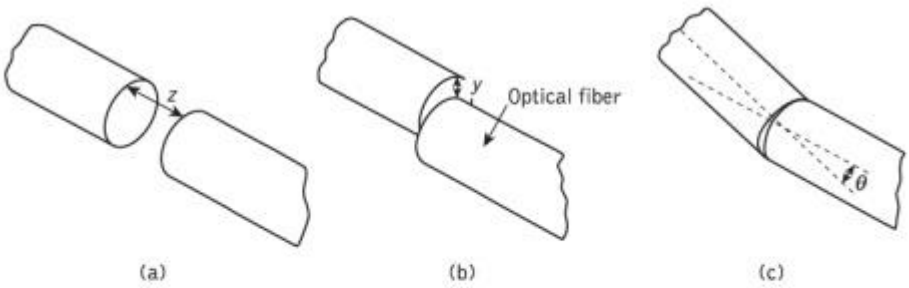

Figure 2.17 The three possible types of misalignment which may occur when jointing compatible optical fibers: (a) longitudinal misalignment; (b) lateral misalignment; (c) angular misalignment

It is apparent that Fresnel reflection may give a significant loss at a fiber joint even when all other aspects of the connection are ideal. However, the effect of Fresnel reflection at a fiber–fiber connection can be reduced to a very low level through the use of an index-matching fluid in the gap between the jointed fibers. When the index-matching fluid has the same refractive index as the fiber core, losses due to Fresnel reflection are in theory eradicated. Unfortunately, Fresnel reflection is only one possible source of optical loss at a fiber joint. A potentially greater source of loss at a fiber–fiber connection is caused by misalignment of the two jointed fibers. In order to appreciate the development and relative success of various connection techniques it is useful to discuss fiber alignment in greater detail.

Any deviations in the geometrical and optical parameters of the two optical fibers which are jointed will affect the optical attenuation (insertion loss) through the connection. It is not possible within any particular connection technique to allow for all these variations.

Hence, there are inherent connection problems when jointing fibers with, for instance

✓⋯different core and/or cladding diameters;

✓⋯different numerical apertures and/or relative refractive index differences;

✓⋯different refractive index profiles;

✓⋯fiber faults (core ellipticity, core concentricity, etc.).

The losses caused by the above factors together with those of Fresnel reflection are usually referred to as intrinsic joint losses. The best results are therefore achieved with compatible (same) fibers which are manufactured to the lowest tolerance.

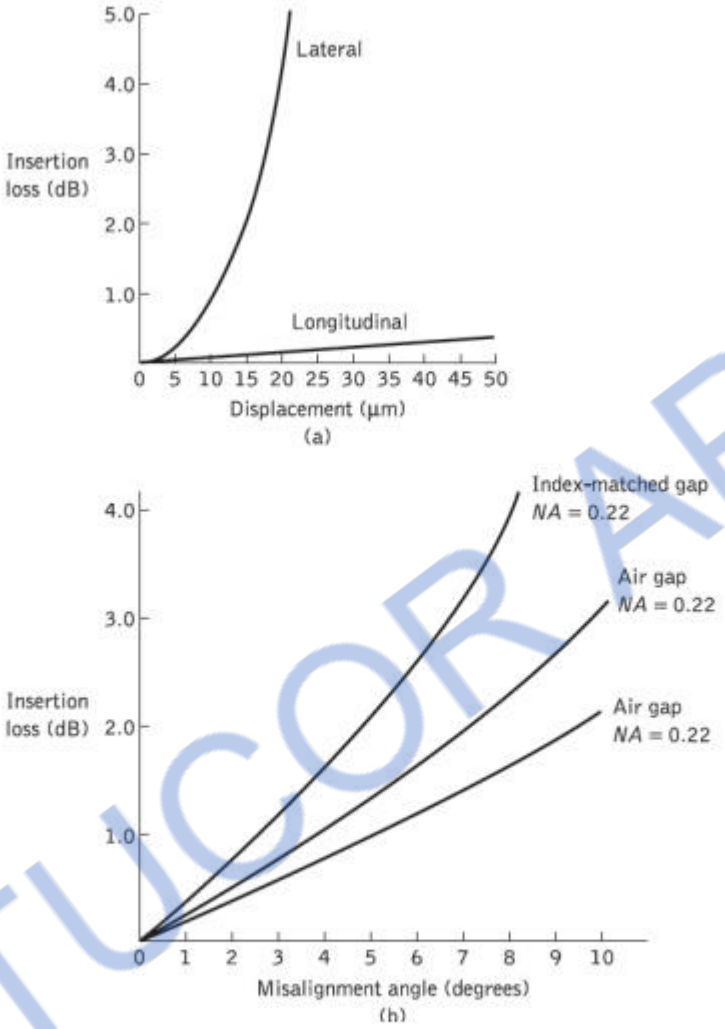

Figure 2.18 Insertion loss characteristics for jointed optical fibers with various types of misalignment: (a) insertion loss due to lateral and longitudinal misalignment for a graded index fiber of 50 μm core diameter.

In this case there is still the problem of the quality of the fiber alignment provided by the jointing mechanism. Examples of possible misalignment between coupled compatible optical fibers are illustrated in Figure 2.17. It is apparent that misalignment may occur in three dimensions: the separation between the fibers (longitudinal misalignment), the offset perpendicular to the fiber core axes (lateral/radial/ axial misalignment) and the angle between the core axes (angular misalignment).

Optical losses resulting from these three types of misalignment depend upon the fiber type, core diameter and the distribution of the optical power between the propagating modes. Examples of the measured optical losses due to the various types of misalignment are shown in Figure 2.18. Figure 2.18(a) shows the attenuation characteristic for both longitudinal and lateral misalignment of a graded index fiber of 50 µm core diameter.

It may be observed that the lateral misalignment gives significantly greater losses per unit displacement than the longitudinal misalignment. For instance, in this case a lateral displacement of 10 µm gives about 1 dB insertion loss whereas a similar longitudinal displacement gives an insertion loss of around 0.1 dB. Figure 2.18(b) shows the attenuation characteristic for the angular misalignment of two multimode step index fibers with numerical apertures of 0.22 and 0.3. An insertion loss of around 1 dB is obtained with angular misalignment of 4° and 5° for the *NA* =0.22 and *NA*=0.3 fibers respectively.

It may also be observed in Figure 2.18(b) that the effect of an index-matching fluid in the fiber gap causes increased losses with angular misalignment. Therefore, it is clear that relatively small levels of lateral and/or angular misalignment can cause significant attenuation at a fiber joint. This is especially the case for fibers of small core diameter (less than 150 µm) which are currently employed for most telecommunication purposes.

1. Multimode fiber joints

Theoretical and experimental studies of fiber misalignment in optical fiber connections allow approximate determination of the losses encountered with the various misalignments of different fiber types. We consider here some of the expressions used to calculate losses due to lateral and angular misalignment of optical fiber joints. Longitudinal misalignment is not discussed in detail as it tends to be the least important effect and may be largely avoided in fiber connection.

Both groups of workers claim good agreement with experimental results, which is perhaps understandable when considering the number of variables involved in the measurement. Also, all groups predict higher losses for fibers with larger numerical

apertures, which is consistent with intuitive considerations (i.e. the larger the numerical aperture, the greater the spread of the output light and the higher the optical loss at a longitudinally misaligned joint).

Theoretical expressions for the determination of lateral and angular misalignment losses are by no means definitive, although in all cases they claim reasonable agreement with experimental results. However, experimental results from different sources tend to vary (especially for angular misalignment losses) due to difficulties of measurement. It is therefore not implied that the expressions given in the text are necessarily the most accurate, as at present the choice appears somewhat arbitrary. Lateral misalignment reduces the overlap region between the two fiber cores. Assuming uniform excitation of all the optical modes in a multimode step index fiber, the overlapped area between both fiber cores approximately gives the lateral coupling efficiency µlat. Hence, the lateral coupling efficiency for two similar step index fibers may be written as

$$\eta_{\text{lat}} \simeq \frac{16(n_1/n)^2}{[1+(n_1/n)]^4}\frac{1}{\pi}\left\{2\cos^{-1}\left(\frac{y}{2a}\right)-\left(\frac{y}{a}\right)\left[1-\left(\frac{y}{2a}\right)^2\right]^{\frac{1}{2}}\right\} \tag{2.61}$$

where $n1$ is the core refractive index, n is the refractive index of the medium between the fibers, y is the lateral offset of the fiber core axes, and a is the fiber core radius. The lateral misalignment loss in decibels may be determined using:

$$\text{Loss}_{\text{lat}} = -10\log_{10}\eta_{\text{lat}}\ \text{dB} \tag{2.62}$$

The predicted losses obtained using the formulas given in Eqs (2.61) and (2.62) are generally slightly higher than the measured values due to the assumption that all modes are equally excited. This assumption is only correct for certain cases of optical fiber transmission. Also, certain authors assume index matching and hence no Fresnel reflection, which makes the first term in Eq. (2.61) equal to unity (as $n1/n = 1$). This may be valid if the two fiber ends are assumed to be in close contact (i.e. no air gap in between) and gives lower predicted losses. Nevertheless, bearing in mind these possible inconsistencies, useful estimates for the attenuation due to lateral misalignment of multimode step index fibers may be obtained.

Lateral misalignment loss in multimode graded index fibers assuming a uniform distribution of optical power throughout all guided modes was calculated by Gloge. He estimated that the lateral misalignment loss was dependent on the refractive index gradient α for small lateral offset and may be obtained from:

$$L_t = \frac{2}{\pi}\left(\frac{y}{a}\right)\left(\frac{\alpha+2}{\alpha+1}\right) \quad \text{for } 0 \le y \le 0.2a \tag{2.63}$$

where the lateral coupling efficiency was given by:

$$\eta_{lat} = 1 - L_t \tag{2.64}$$

Hence Eq. (2.64) may be utilized to obtain the lateral misalignment loss in decibels. With a parabolic refractive index profile where $\alpha = 2$, Eq. (2.63) gives:

$$L_t = \frac{8}{3\pi}\left(\frac{y}{a}\right) = 0.85\left(\frac{y}{a}\right) \tag{2.65}$$

A further estimate including the leaky modes gave a revised expression for the lateral misalignment loss given in Eq. (2.64) of $0.75(y/a)$. This analysis was also extended to step index fibers (where $\alpha = \infty$) and gave lateral misalignment losses of $0.64(y/a)$ and $0.5(y/a)$ for the cases of guided modes only and both guided plus leaky modes respectively.

Factors causing fiber–fiber intrinsic losses were listed in previous Section; the major ones comprising a mismatch in the fiber core diameters, a mismatch in the fiber numerical apertures and differing fiber refractive index profiles are illustrated in Figure 2.19. Connections between multimode fibers with certain of these parameters being different can be quite common, particularly when a pigtailed optical source is used, the fiber pigtail of which has different characteristics from the main transmission fiber. Moreover, as indicated previously, diameter variations can occur with the same fiber type.

Assuming all the modes are equally excited in a multimode step or graded index fiber, and that the numerical apertures and index profiles are the same, then the loss resulting from a mismatch of core diameters (see Figure 2.19(a)) is given by:

$$\text{Loss}_{cd} = \begin{cases} -10 \log_{10}\left(\frac{a_2}{a_1}\right)^2 \text{ (dB)} & a_2 < a_1 \\ 0 \text{ (dB)} & a_2 \geq a_1 \end{cases} \quad (2.66)$$

where $a1$ and $a2$ are the core radii of the transmitting and receiving fibers respectively. It may be observed from Eq. (2.66) that no loss is incurred if the receiving fiber has a larger core diameter than the transmitting one. In addition, only a relatively small loss (0.09 dB) is obtained when the receiving fiber core diameter is 1% smaller than that of the transmitting fiber.

When the transmitting fiber has a higher numerical aperture than the receiving fiber, then some of the emitted light rays will fall outside the acceptance angle of the receiving fiber and they will therefore not be coupled through the joint. Again assuming a uniform modal power distribution, and fibers with equivalent refractive index profiles and core diameters, then the loss caused by a mismatch of numerical apertures (see Figure 2.19(b))

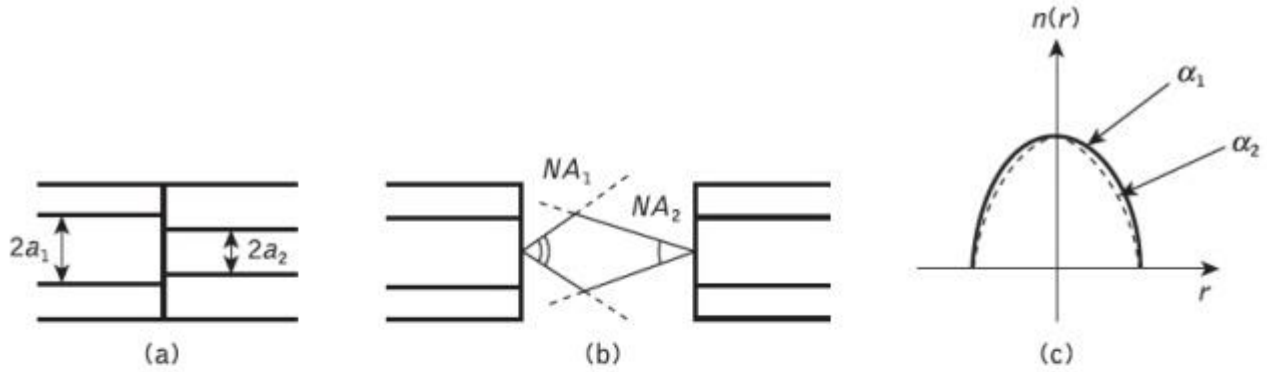

Figure 2.19 Some intrinsic coupling losses at fiber joints: (a) core diameter mismatch; (b) numerical aperture mismatch; (c) refractive index profile difference

$$\text{Loss}_{\text{NA}} = \begin{cases} -10 \log_{10} \left(\dfrac{NA_2}{NA_1} \right)^2 \text{ (dB)} & NA_2 < NA_1 \\ 0 \text{ (dB)} & NA_2 \geq NA_1 \end{cases} \tag{2.67}$$

$$\text{Loss}_{\text{RI}} = \begin{cases} -10 \log_{10} \dfrac{\alpha_2(\alpha_1 + 2)}{\alpha_1(\alpha_2 + 2)} \text{ (dB)} & \alpha_2 < \alpha_1 \\ 0 \text{ (dB)} & \alpha_2 \geq \alpha_1 \end{cases} \tag{2.68}$$

$$\text{Loss}_{\text{int}} = \begin{cases} -10 \log_{10} \dfrac{(a_2 NA_2)^2(\alpha_1 + 2)\alpha_2}{(a_1 NA_1)^2(\alpha_2 + 2)\alpha_1} \text{ (dB)} & a_2 > a_1,\ NA_2 > NA_1,\ \alpha_2 > \alpha_1 \\ 0 \text{ (dB)} & a_2 \leq a_1,\ NA_2 \leq NA_1,\ \alpha_2 \leq \alpha_1 \end{cases} \tag{2.67}$$

2. Single-mode fiber joints

Misalignment losses at connections in single-mode fibers have been theoretically considered by Marcuse and Gambling *et al.* The theoretical analysis which was instigated by Marcuse is based upon the Gaussian or near-Gaussian shape of the modes propagating in single-mode fibers regardless of the fiber type (i.e. step index or graded index). Further development of this theory by Gambling *etal.* gave simplified formulas for both the lateral and angular misalignment losses at joints in single mode fibers. In the absence of angular misalignment Gambling *et al.* calculated that the loss *T*l due to lateral offset *y* was given by:

$$T_l = 2.17 \left(\frac{y}{\omega} \right)^2 \text{dB} \tag{2.68}$$

where ω is the normalized spot size of the fundamental mode.* However, the normalized spot size for the LP01 mode (which corresponds to the HE mode) may be obtained from the empirical formula:

$$\omega = a\frac{(0.65 + 1.62V^{-\frac{3}{2}} + 2.88V^{-6})}{2^{\frac{1}{2}}} \tag{2.69}$$

where ω is the spot size in μm, *a* is the fiber core radius and *V* is the normalized frequency for the fiber. Alternatively, the insertion loss *T*a caused by an angular misalignment θ(in radians) at a joint in a single-mode fiber may be given by

$$T_a = 2.17\left(\frac{\theta\omega\, n_1 V}{aNA}\right)^2 \text{dB} \tag{2.70}$$

where*n*1 is the fiber core refractive index and *NA* is the numerical aperture of the fiber. It must be noted that the formulas given in Eqs (2.69) and (2.70) assume that the spot sizes of the modes in the two coupled fibers are the same. Gambling *et al.* also derived a somewhat complicated formula which gave a good approximation for the combined losses due to both lateral and angular misalignment at a fiber joint. However, they indicate that for small total losses (less than 0.75 dB) a reasonable approximation is obtained by simply combining Eqs (2.68) and (2.70).

Assuming that no losses are present due to the extrinsic factors, the intrinsic coupling loss is given by

$$\text{Loss}_{\text{int}} = -10\log_{10}\left[4\left(\frac{\omega_{02}}{\omega_{01}} + \frac{\omega_{01}}{\omega_{02}}\right)^{-2}\right] \text{(dB)} \tag{2.71}$$

where ω01 and ω02 are the spot sizes of the transmitting and receiving fibers respectively. Equation (2.71) therefore enables the additional coupling loss resulting from mode-field diameter mismatch between two single-mode fibers to be calculated.

Fiber splices

A permanent joint formed between two individual optical fibers in the field or factory is known as a fiber splice. Fiber splicing is frequently used to establish long-haul optical fiber links where smaller fiber lengths need to be joined, and there is no requirement for repeated connection and disconnection. Splices may be divided into two broad categories depending upon the splicing technique utilized. These are fusion splicing or welding and mechanical splicing.

Fusion splicing is accomplished by applying localized heating (e.g. by a flame or an electric arc) at the interface between two butted, prealigned fiber ends causing them to soften and fuse. Mechanical splicing, in which the fibers are held in alignment by some mechanical means, may be achieved by various methods including the use of tubes around the fiber ends (tube splices) or V-grooves into which the butted fibers are placed (groove splices). All these techniques seek to optimize the splice performance (i.e. reduce the insertion loss at the joint) through both fiber end preparation and alignment of the two joint fibers. Typical average splice insertion losses for multimode fibers are in the range 0.1 to 0.2 dB which is generally a better performance than that exhibited by demountable connections.

It may be noted that the insertion losses of fiber splices are generally much less than the possible Fresnel reflection loss at a butted fiber–fiber joint. This is because there is no large step change in refractive index with the fusion splice as it forms a continuous fiber connection, and some method of index matching (e.g. a fluid) tends to be utilized with mechanical splices

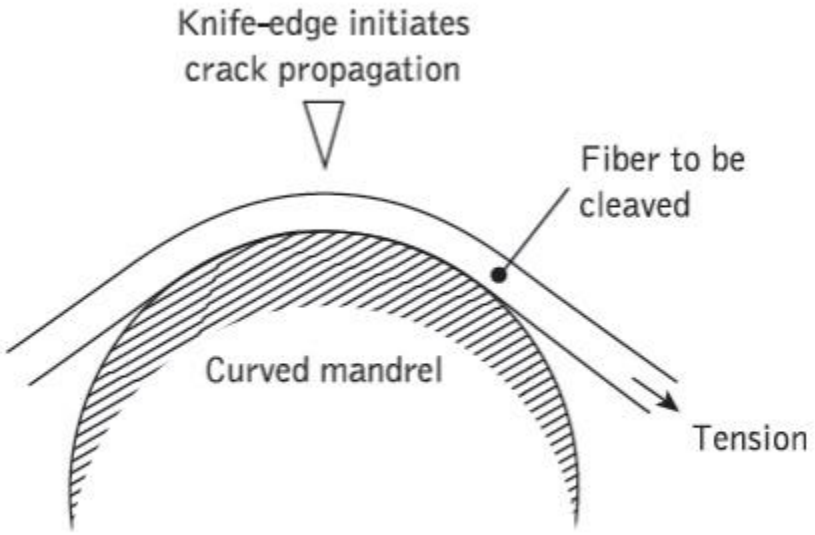

Figure 2.20 Optical fiber end preparation: the principle of scribe and break cutting

A requirement with fibers intended for splicing is that they have smooth and square end faces. In general this end preparation may be achieved using a suitable tool which cleaves the fiber as illustrated in Figure 2.20. This process is often referred to as scribe and break or score and break as it involves the scoring of the fiber surface under tension with a cutting tool (e.g. sapphire, diamond, tungsten carbide blade). The surface scoring creates failure as the fiber is tensioned and a clean, reasonably square fiber end can be produced.

Figure 2.20 illustrates this process with the fiber tensioned around a curved mandrel. However, straight pull, scribe and break tools are also utilized, which arguably give better results.

1. Fusion splices

The fusion splicing of single fibers involves the heating of the two prepared fiber ends to their fusing point with the application of sufficient axial pressure between the two optical fibers. It is therefore essential that the stripped (of cabling and buffer coating) fiber ends are adequately positioned and aligned in order to achieve good continuity of the transmission medium at the junction point. Hence the fibers are usually positioned and clamped with the aid of an inspection microscope.

Flame heating sources such as microplasma torches (argon and hydrogen) and oxhydricmicroburners (oxygen, hydrogen and alcohol vapor) have been utilized with some success. However, the most widely used heating source is an electric arc. This technique offers advantages of consistent, easily controlled heat with adaptability for use under field conditions.

A schematic diagram of the basic arc fusion method is given in Figure 2.21(a) illustrating how the two fibers are welded together. Figure 2.21(b) shows a development of the basic arc fusion process which involves the rounding of the fiber ends with a low-energy discharge before pressing the fibers together and fusing with a stronger arc.

This technique, known as prefusion, removes the requirement for fiber end preparation which has a distinct advantage in the field environment. It has been utilized with multimode fibers giving average splice losses of 0.09 db.

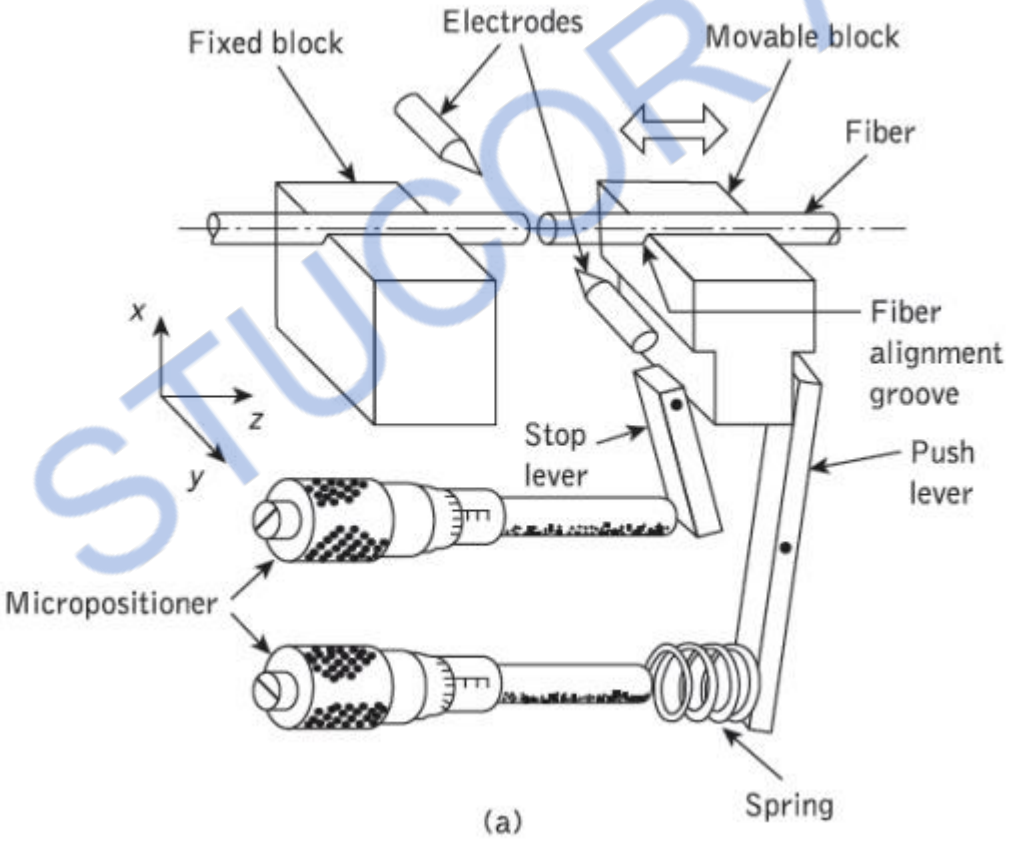

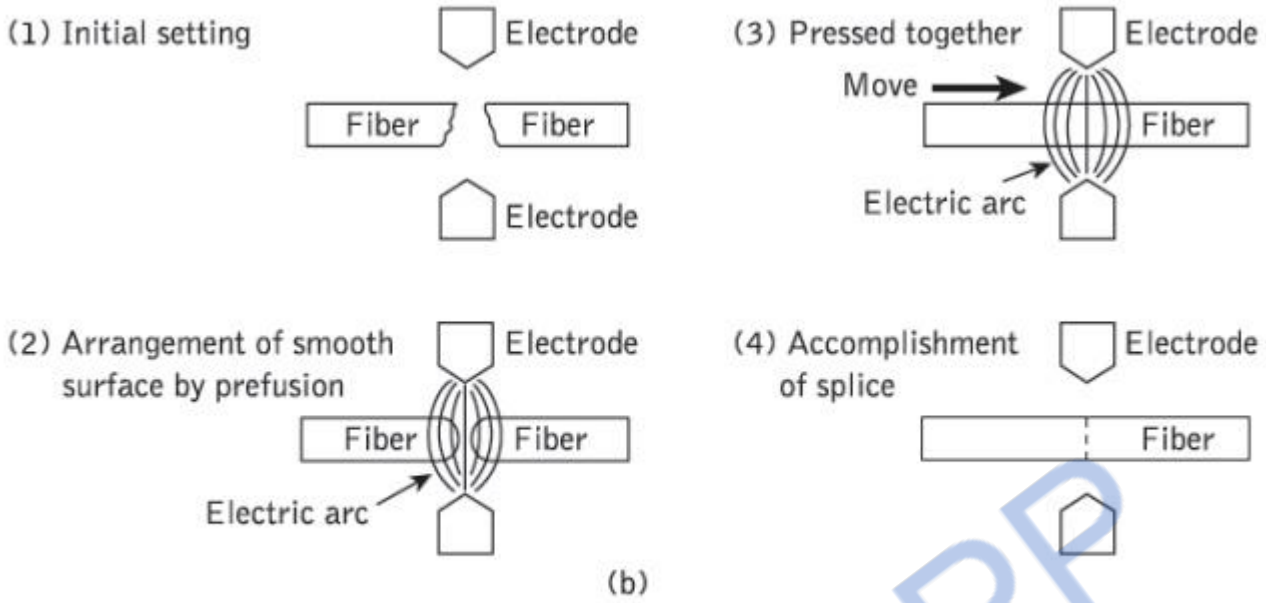

Figure 2.21 Electric arc fusion splicing: (a) an example of fusion splicing apparatus; (b) schematic illustration of the prefusion method for accurately splicing optical fibers

Fusion splicing of single-mode fibers with typical core diameters between 5 and 10 µm presents problems of more critical fiber alignment (i.e. lateral offsets of less than 1 µm are required for low loss joints). However, splice insertion losses below 0.3 dB may be achieved due to a self-alignment phenomenon which partially compensates for any lateral offset.

Self-alignment, illustrated in Figure 2.22, is caused by surface tension effects between the two fiber ends during fusing. An early field trial of single-mode fiber fusion splicing over a 31.6 km link gave mean splice insertion losses of 0.18 and 0.12 dB at wavelengths of 1.3 and 1.55 µm respectively. Mean splice losses of only 0.06 dB have also been obtained with a fully automatic single-mode fiber fusion splicing machine weaken the fiber in the vicinity of the splice. It has been found that even with careful handling, the tensile strength of the fused fiber may be as low as 30% of that of the uncoated fiber before fusion.

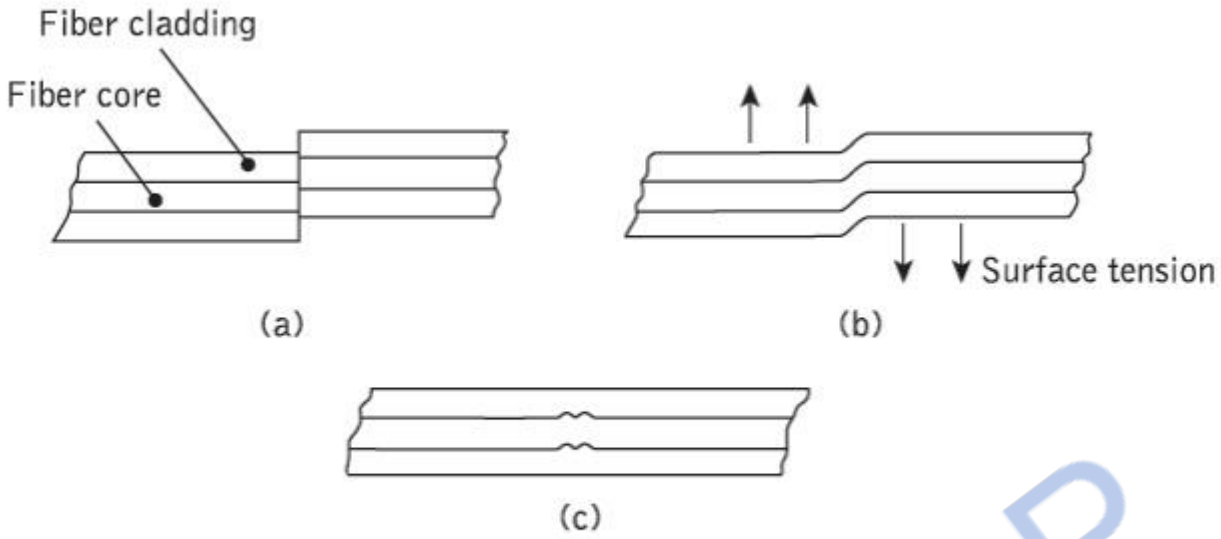

Figure 2.22 Self-alignment phenomenon which takes place during fusion splicing: (a) before fusion; (b) during fusion; (c) after fusion

The fiber fracture generally occurs in the heat affected zone adjacent to the fused joint. The reduced tensile strength is attributed to the combined effects of surface damage caused by handling, surface defect growth during heating and induced residential stresses due to changes in chemical composition. It is therefore necessary that the completed splice is packaged so as to reduce tensile loading upon the fiber in the vicinity of the splice.

2. Mechanical splices

A number of mechanical techniques for splicing individual optical fibers have been developed. A common method involves the use of an accurately produced rigid alignment tube into which the prepared fiber ends are permanently bonded. This snug tube splice is illustrated in Figure 2.23(a) and may utilize a glass or ceramic capillary with an inner diameter just large enough to accept the optical fibers. Transparent adhesive (e.g. epoxy resin) is injected through a transverse bore in the capillary to give mechanical sealing and index matching of the splice. Average insertion losses as low as 0.1 dB have been obtained with multimode graded index and single-mode fibers using ceramic capillaries. However, in general, snug tube splices exhibit problems with capillary tolerance requirements. Hence as a commercial product they may exhibit losses of up to 0.5 dB.

Mechanical splicing technique which avoids the critical tolerance requirements of the snug tube splice is shown in Figure 2.23(b). This loose tube splice uses an oversized square-section metal tube which easily accepts the prepared fiber ends. Transparent adhesive is first inserted into the tube followed by the fibers. The splice is self-aligning when the fibers are curved in the same plane, forcing the fiber ends simultaneously into the same corner of the tube, as indicated in Figure 2.23(b). Mean splice insertion losses of 0.073 dB have been achieved using multimode graded index fibers with the loose tube approach.

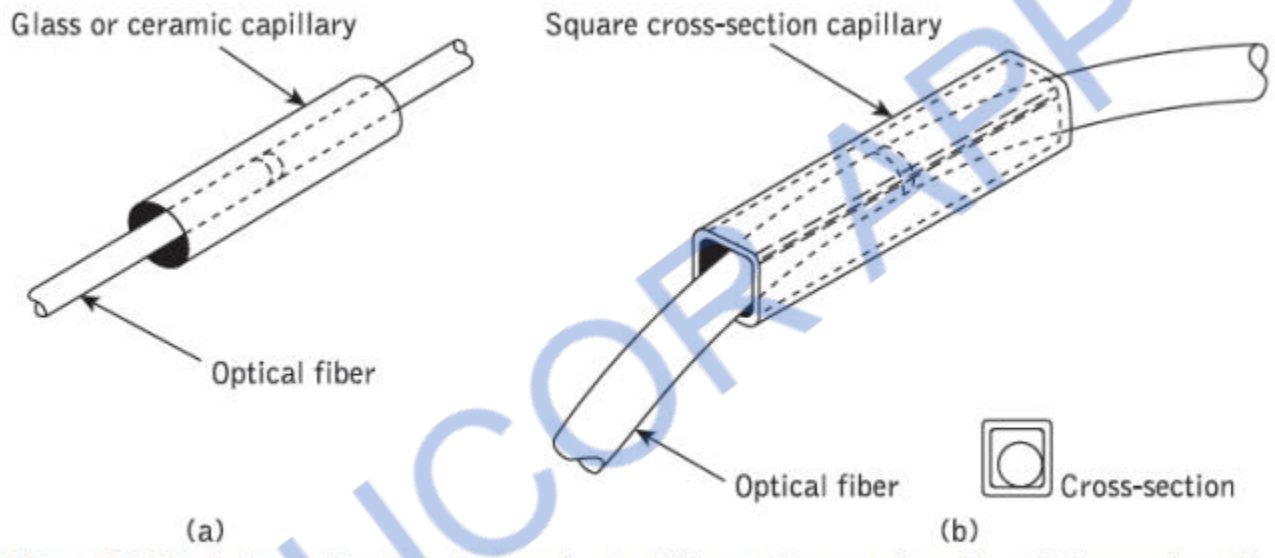

Figure 2.23 Techniques for tube splicing of optical fibers: (a) snug tube splice; (b) loose tube splice utilizing square cross-section capillary

Other common mechanical splicing techniques involve the use of grooves to secure the fibers to be jointed. A simple method utilizes a V-groove into which the two prepared fiber ends are pressed. The V-groove splice which is illustrated in Figure 2.24(a) gives alignment of the prepared fiber ends through insertion in the groove. The splice is made permanent by securing the fibers in the V-groove with epoxy resin. Jigs for producing Vgroove splices have proved quite successful, giving joint insertion losses of around 0.1 dB

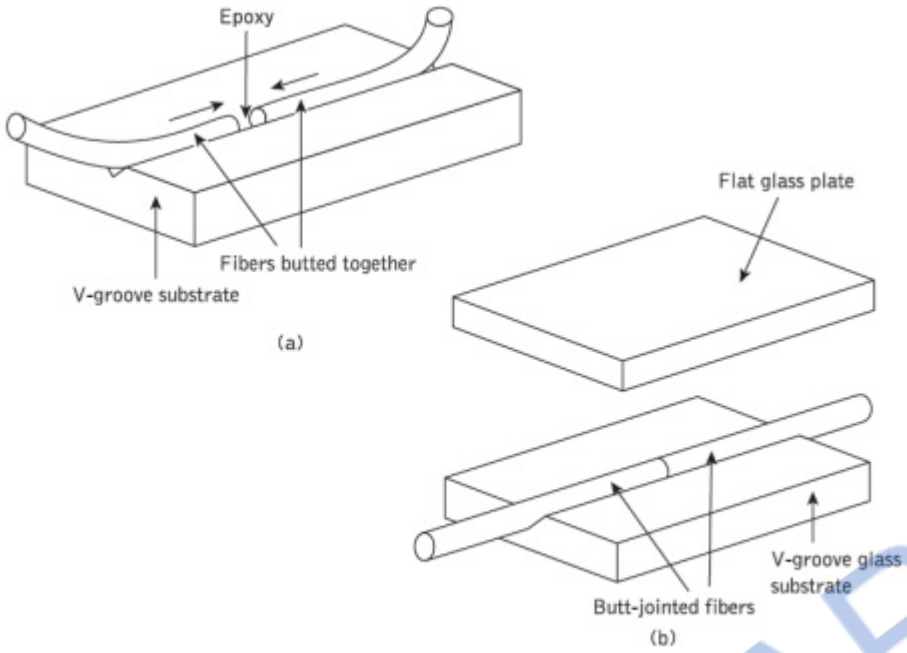

Figure 2.24 V-groove splices

V-groove splices formed by sandwiching the butted fiber ends between a V-groove glass substrate and a flat glass retainer plate, as shown in Figure 2.24(b), have also proved very successful in the laboratory. Splice insertion losses of less than 0.01 dB when coupling single-mode fibers have been reported using this technique. However, reservations are expressed regarding the field implementation of these splices with respect to manufactured fiber geometry, and housing of the splice in order to avoid additional losses due to local fiber bending.

A further variant on the V-groove technique is the elastic tube or elastomeric splice shown in Figure 2.25. The device comprises two elastomeric internal parts, one of which contains a V-groove. An outer sleeve holds the two elastic parts in compression to ensure alignment of the fibers in the V-groove, and fibers with different diameters tend to be centered and hence may be successfully spliced. Although originally intended for multimode fiber connection, the device has become a widely used commercial product which is employed with single-mode fibers, albeit often as a temporary splice for laboratory investigations. The splice loss for the elastic tube device was originally reported as 0.12 dB or less but is generally specified as around 0.25 dB for the commercial product. In addition, index-matching gel is normally employed within the device to improve its performance.

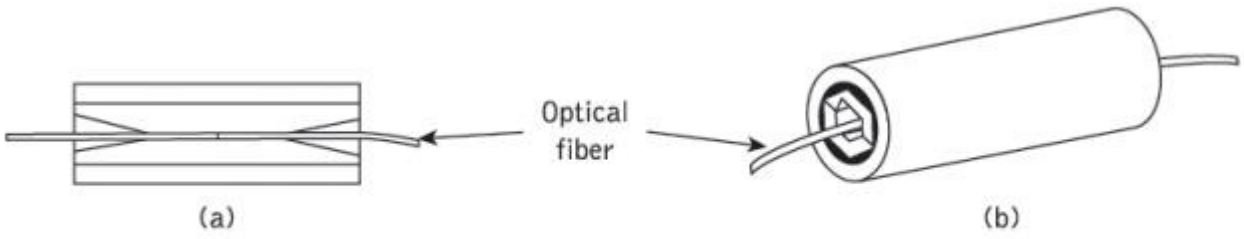

Figure 2.25 The elastomeric splice: (a) cross-section; (b) assembly

A slightly more complex groove splice known as the Springroove® splice utilized a bracket containing two cylindrical pins which serve as an alignment guide for the two prepared fiber ends. The cylindrical pin diameter was chosen to allow the fibers to protrude above the cylinders, as shown in Figure 2.26(a). An elastic element (a spring) was used to press the fibers into a groove and maintain the fiber end alignment, as illustrated in Figure 2.26(b). The complete assembly was secured using a drop of epoxy resin. Mean splice insertion losses of 0.05 dB were obtained using multimode graded index fibers with the Springroove splice. This device found practical use in Italy.

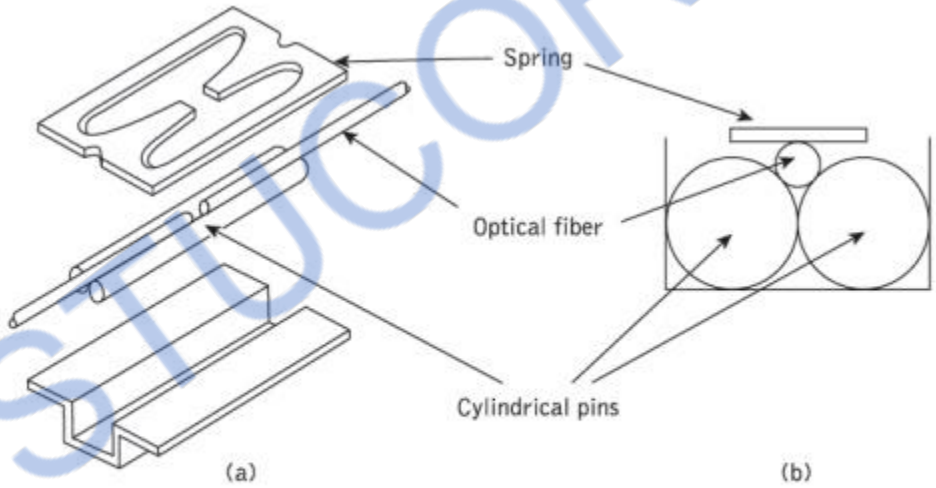

Figure 2.26 The Springroove splice: (a) expanded overview of the splice; (b) schematic cross-section of the splice

An example of a secondary aligned mechanical splice for multimode fiber is shown in Figure 2.27. This device uses precision glass capillary tubes called ferrules as the secondary elements with an alignment sleeve of metal or plastic into which the glass tubed fibers are inserted. Normal assembly of the splice using 50 μm core diameter fiber yields an average loss of around 0.2 dB.

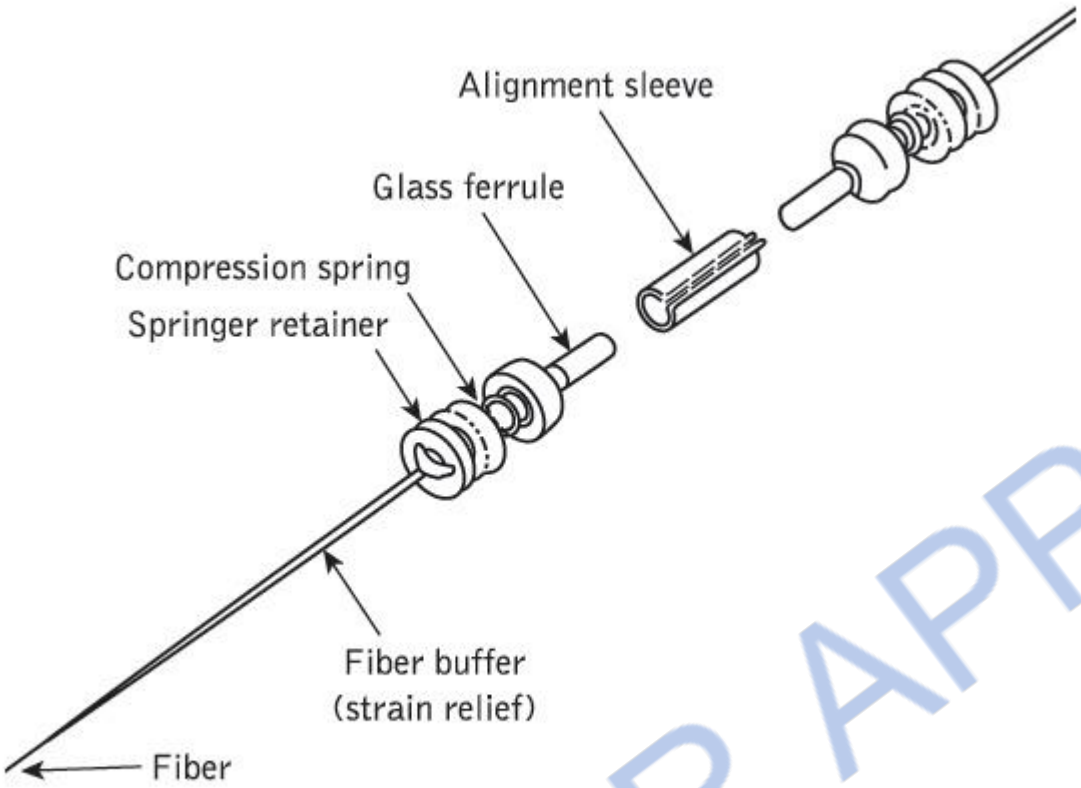

Figure 2.27 Multimode fiber mechanical splice using glass capillary tubes

3. Multiple splices

Multiple simultaneous fusion splicing of an array of fibers in a ribbon cable has been demonstrated for both multimode and single-mode fibers. In both cases a 12-fiber ribbon was prepared by scoring and breaking prior to pressing the fiber ends onto a contact plate to avoid difficulties with varying gaps between the fibers to be fused.

An electric are fusing device was then employed to provide simultaneous fusion. Such a device is now commercially available to allow the splicing of 12 fibers simultaneously in a time of around 6 minutes, which requires only 30 seconds per splice. Splice losses using this device with multimode graded index fiber range from an average of 0.04 dB to a maximum of 0.12 dB, whereas for single-mode fiber the average loss is 0.04 dB with a 0.4 dB maximum.

A simple technique employed for multiple simultaneous splicing involves mechanical splicing of an array of fibers, usually in a ribbon cable. The V-groove multiple-splice secondary element comprising etched silicon chips has been used extensively in the United States for splicing multimode fibers. In this technique a 12-fiber splice is prepared by stripping the ribbon and coating material from the fibers. Then the 12 fibers are laid into the trapezoidal* grooves of a silicon chip using a comb structure, as shown in Figure 2.28. The top silicon chip is then positioned prior to applying epoxy to the chip–ribbon interface. Finally, after curing, the front end face is ground and polished.

The process is normally carried out in the factory and the arrays are clipped together in the field, putting index-matching silica gel between the fiber ends. The average splice loss obtained with this technique in the field is 0.12 dB, with the majority of the loss resulting from intrinsic fiber mismatch. Major advantages of this method are the substantial reduction in splicing time (by more than a factor of 10) per fiber and the increased robustness of the final connection. Although early array splicing investigations using silicon chips demonstrated the feasibility of connecting 12*12 fiber arrays, in practice only single 12-fiber ribbons have been spliced at one time due to concerns in relation to splice tolerance and the large number of telecommunication channels which would be present in the two-dimensional array.

An alternative V-groove flat chip molded from a glass-filled polymer resin has been employed in France. Moreover, direct mass splicing of 12-fiber ribbons has also been accomplished [Ref. 63]. In this technique simultaneous end preparation of all 24 fibers was achieved using a ribbon grinding and polishing procedure. The ribbons were then laid in guides and all 12 fibers were positioned in grooves in the glass-filled plastic

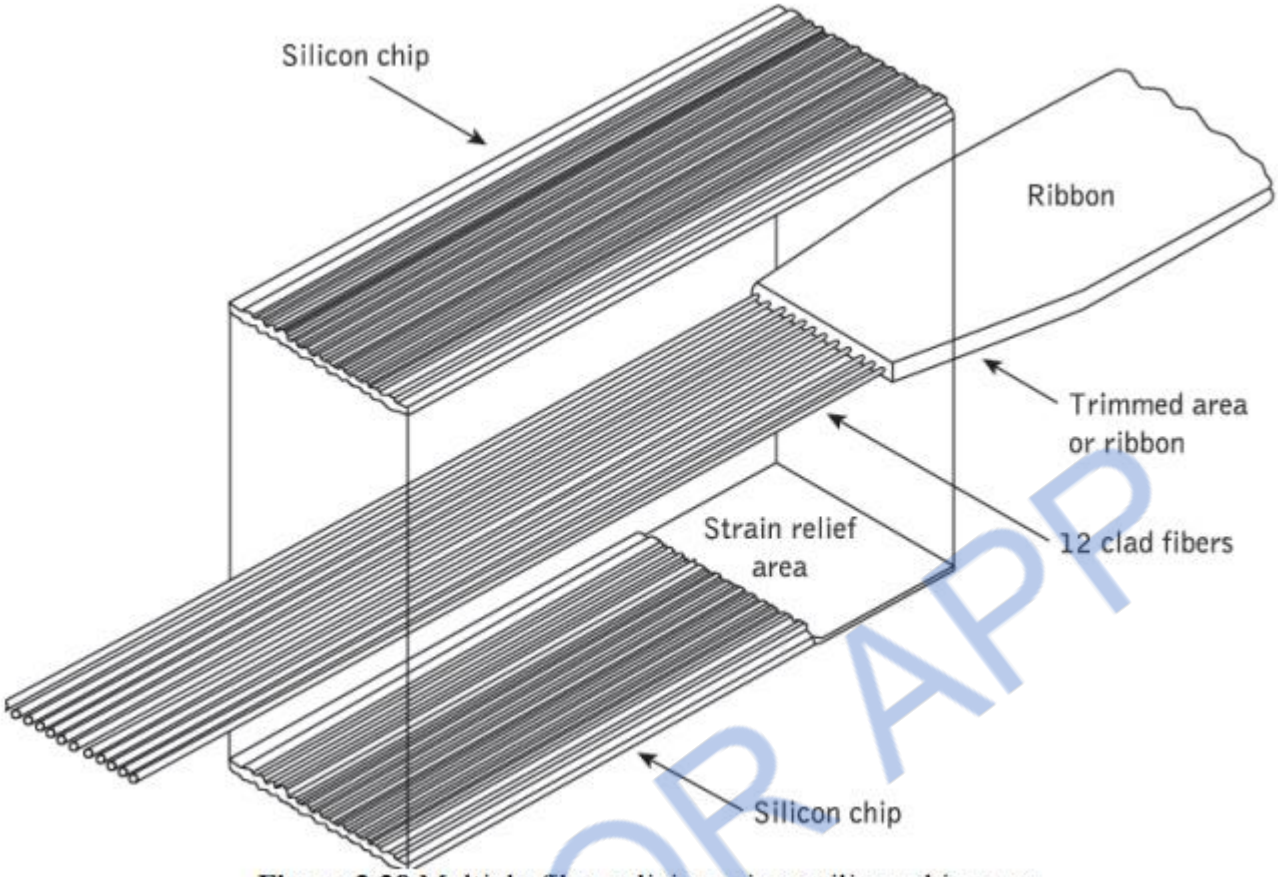

Figure 2.28 Multiple-fiber splicing using a silicon chip array

Fiber couplers

An optical fiber coupler is a device that distributes light from a main fiber into one or more branch fibers.* The latter case is more normal and such devices are known as multiport fiber couplers. Requirements are increasing for the use of these devices to divide or combine optical signals for application within optical fiber information distribution systems including data buses, LANs, computer networks and telecommunication access networks.

Optical fiber couplers are often passive devices in which the power transfer takes place either:

(a) through the fiber core cross-section by butt jointing the fibers or by using some form of imaging optics between the fibers (core interaction type); or

(b) through the fiber surface and normal to its axis by converting the guided core modes to both cladding and refracted modes which then enable the power-sharing mechanism (surface interaction type).

Multiport optical fiber couplers can also be subdivided into the following three main groups, as illustrated in Figure 2.32.

1. Three- and four-port* couplers, which are used for signal splitting, distribution and combining.

2. Star couplers, which are generally used for distributing a single input signal to multiple outputs.

3. Wavelength division multiplexing (WDM) devices, which are a specialized form of coupler designed to permit a number of different peak wavelength optical signals to be transmitted in parallel on a single fiber.

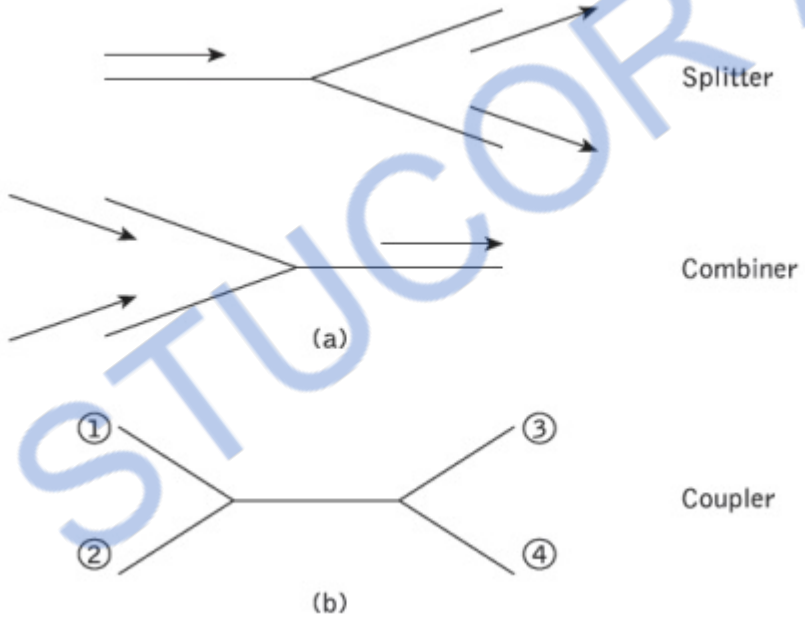

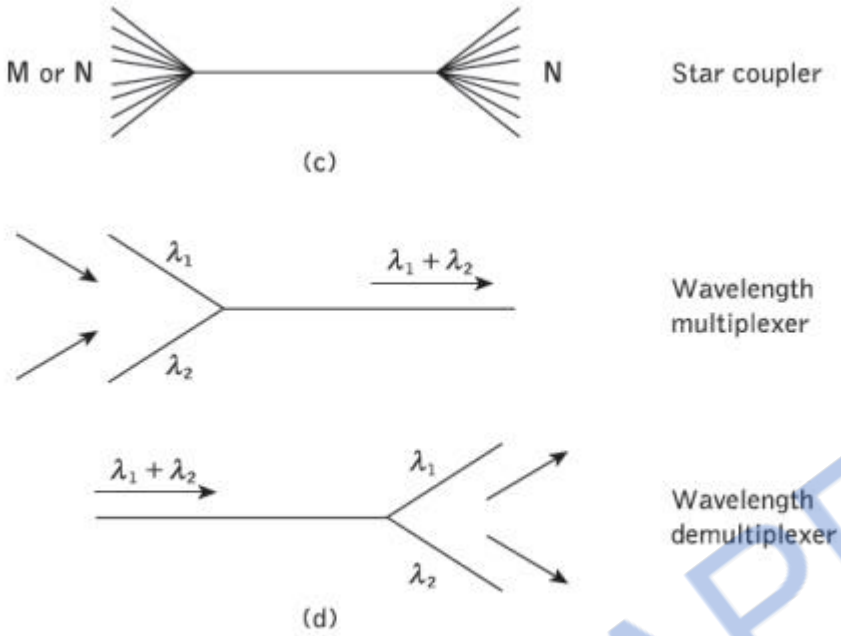

Figure 2.32 Optical fiber coupler types and functions: (a) three-port couplers; (b) four-port coupler; (c) star coupler; (d) wavelength division multiplexing and demultiplexing couplers

In this context WDM couplers either combine the different wavelength optical signal onto the fiber (i.e. multiplex) or separate the different wavelength optical signals output from the fiber (i.e. demultiplex). Ideal fiber couplers should distribute light among the branch fibers with no scattering loss† or the generation of noise, and they should function with complete insensitivity to factors including the distribution of light between the fiber modes, as well as the state of polarization of the light. Unfortunately, in practice passive fiber couplers do not display all of the above properties and hence the characteristics of the devices affect the performance of optical fiber networks.

* Four-port couplers may also be referred to as 2*2 star couplers.

† The scattering loss through the coupler is often referred to as the excess loss.

1. Three- and four-port couplers

Several methods are employed to fabricate three- and four-port optical fiber couplers. The lateral offset method, illustrated in Figure 2.33(a), relies on the overlapping of the fiber end faces. Light from the input fiber is coupled to the output fibers according to the degree of overlap. Hence the input power can be distributed in a welldefined proportion

by appropriate control of the amount of lateral offset between the fibers. This technique, which can provide a bidirectional coupling capability, is well suited for use with multimode step index fibers but may incur higher excess losses than other methods as all the input light cannot be coupled into the output fibers.

Another coupling technique is to incorporate a beam splitter element between the fibers. The semitransparent mirror method provides an ingenious way to accomplish such a fiber coupler, as shown in Figure 2.33(b). A partially reflecting surface can be applied directly to the fiber end face cut at an angle of 45° to form a thin-film beam splitter.

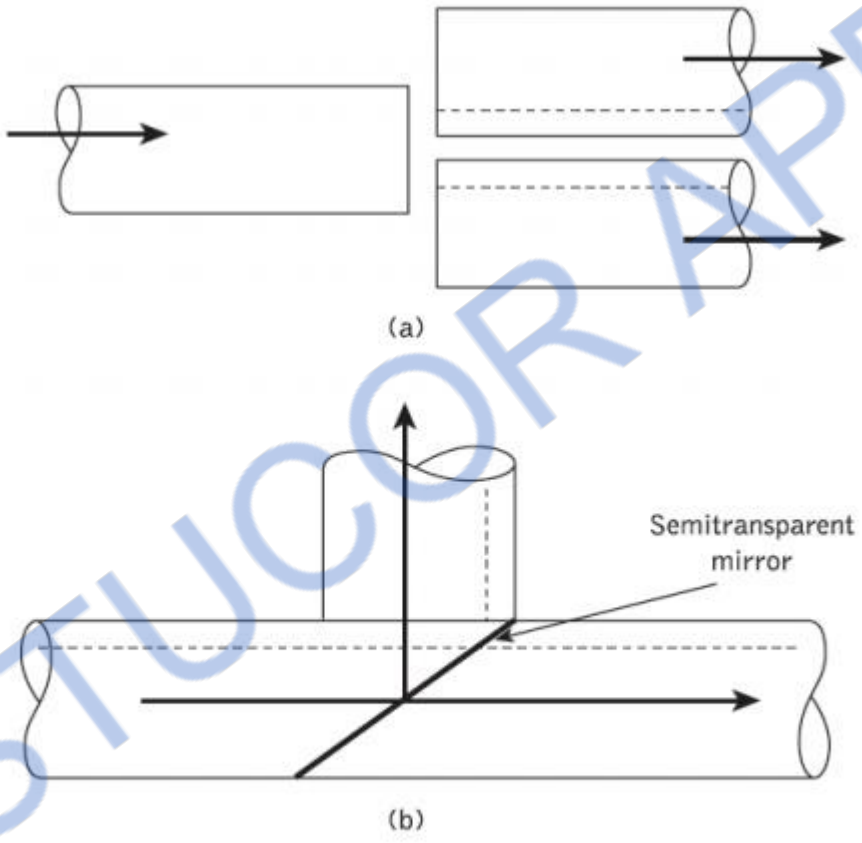

Figure 2.33 Fabrication techniques for three-port fiber couplers: (a) the lateral offset method; (b) the semitransparent mirror method

A fast-growing category of optical fiber coupler is based on the use of micro-optic components. In particular, a complete range of couplers has been developed which utilize the beam expansion and collimation properties of the GRIN-rod lens combined with spherical retro-reflecting mirrors. These devices, two of which are displayed in Figure 2.34, are miniature optical assemblies of compact construction which generally

exhibit low insertion loss (typically less than 1 dB) and are insensitive to modal power distribution. Figure 2.34(a) shows the structure of a parallel surface type of GRIN-rod lens three port coupler which comprises two quarter pitch lenses with a semitransparent mirror in between. Light rays from the input fiber *F*1 collimate in the first lens before they are incident on the mirror. A portion of the incident beam is reflected back and is coupled to fiber *F*2, while the transmitted light is focused in the second lens and then coupled to fiber *F*3. The slant surface version of the similar coupler is shown in Figure 2.34(b).

The parallel surface type, however, is the most attractive due to its ease of fabrication, compactness, simplicity and relatively low insertion loss. Finally, the substitution of the mirror by an interference filter* offers application of these devices to WDM

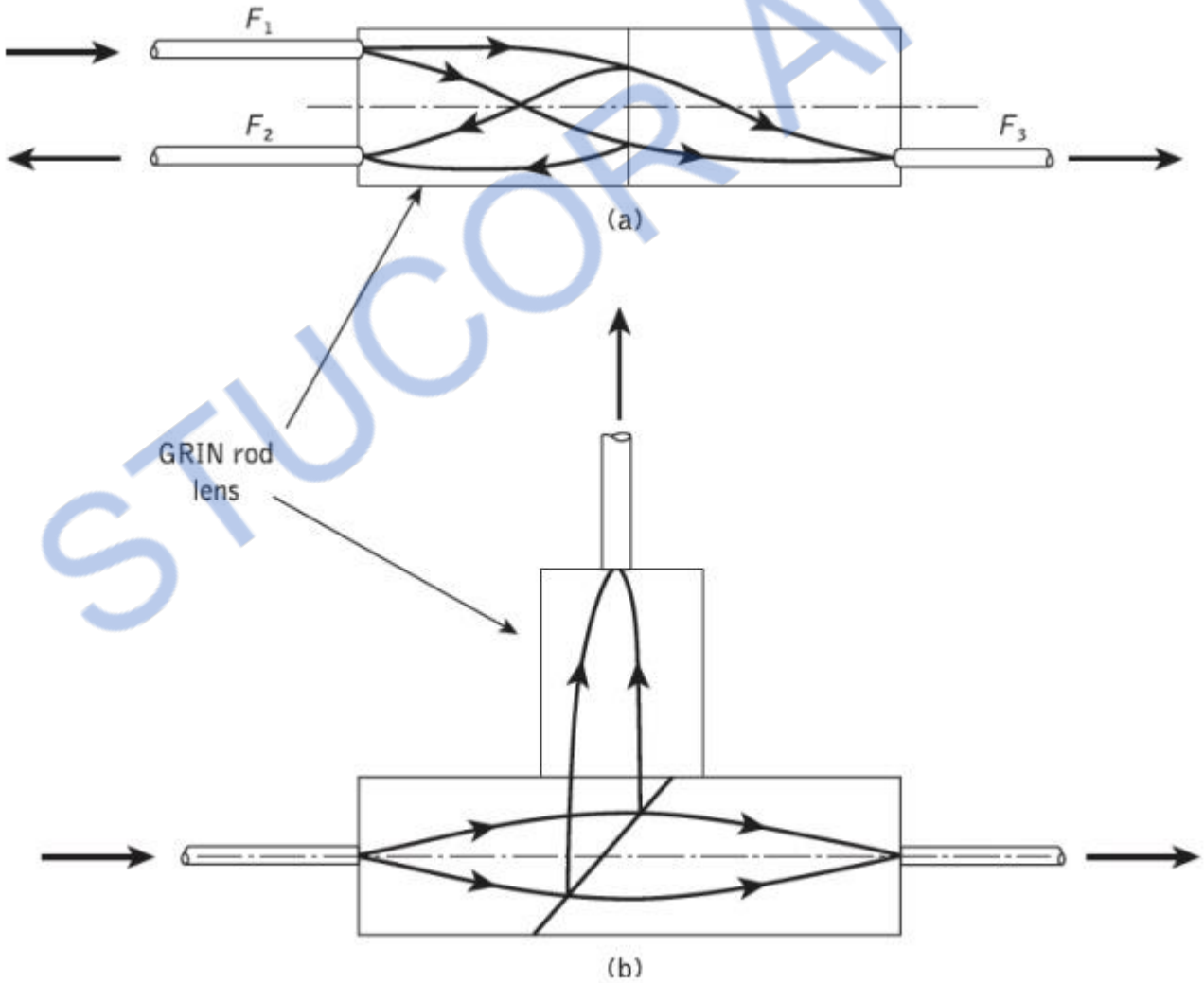

Figure 2.34 GRIN-rod lens micro-optic fiber couplers: (a) parallel surface type; (b) slant surface type

Perhaps the most common method for manufacturing couplers is the fused biconical taper (FBT) technique. In this method the fibers are generally twisted together and then spot fused under tension such that the fused section is elongated to form a biconical taper structure. A three-port coupler is formed by removing one of the input fibers. Optical power launched into the input fiber propagates in the form of guided core modes.

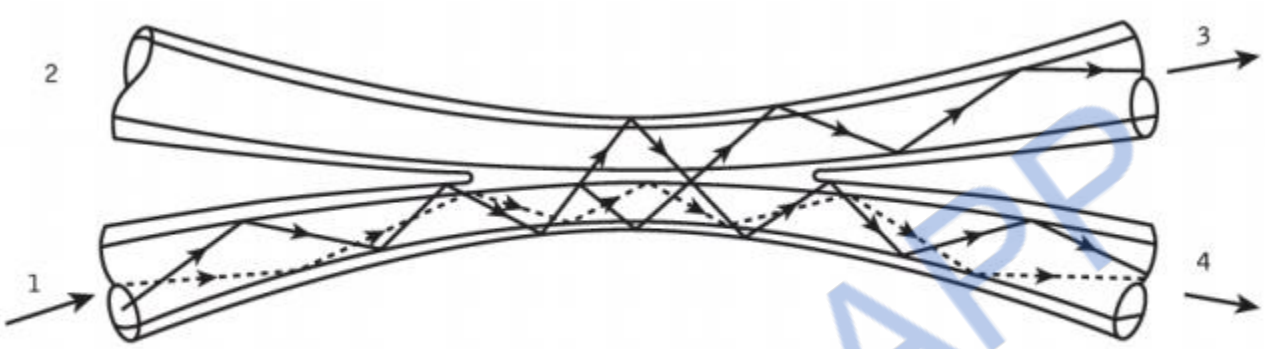

Figure 2.35 Structure and principle of operation for the fiber fused biconical taper coupler

The higher order modes, however, leave the fiber core because of its reduced size in the tapered-down region and are therefore guided as cladding modes. These modes transfer back to guided core modes in the tapered-up region of the output fiber with an approximately even distribution between the two fibers. Often only a portion of the total power is coupled between the two fibers because only the higher order modes take part in the process, the lower order modes generally remaining within the main fiber. In this case a mode-dependent (and therefore wavelength-dependent) coupling ratio is obtained. However, when the waist of the taper is made sufficiently narrow, then the entire mode volume can be encouraged to participate in the coupling process and a larger proportion of input power can be shared between the output fibers. This strategy gives an improvement in both the power and modal uniformity of the coupler. The various loss parameters associated with four-port couplers may be written down with reference to Figure 2.35. Hence, the excess loss which is defined as the ratio of power input to power output is given by:

$$\text{Excess loss (four-port coupler)} = 10 \log_{10} \frac{P_1}{(P_3 + P_4)} \text{ (dB)}$$

$$\text{Insertion loss (ports 1 to 4)} = 10 \log_{10} \frac{P_1}{P_4} \text{ (dB)}$$

$$\text{Crosstalk (four-port coupler)} = 10 \log_{10} \frac{P_2}{P_1} \text{ (dB)}$$

Finally, the splitting or coupling ratio indicates the percentage division of optical power between the output ports. Again referring to Figure 2.35:

$$\text{Split ratio} = \left[\frac{P_3}{(P_3 + P_4)}\right] \times 100\%$$

$$= \left[1 - \frac{P_4}{(P_3 + P_4)}\right] \times 100\%$$

2. Star couplers

Star couplers distribute an optical signal from a single-input fiber to multiple-output fibers. The two principal manufacturing techniques for producing multimode fiber star couplers are the mixer-rod and the FBT methods. In the mixer-rod method illustrated in Figure 2.36 a thin platelet of glass is employed, which effectively mixes the light from one fiber, dividing it among the outgoing fibers. This method can be used to produce a transmissive star coupler or a reflective star coupler, as displayed in Figure 2.36. The typical insertion loss for an 8 * 8 mixer-rod transmissive star coupler with fiber pigtails is 12.5 dB with port-to-port uniformity of ±0.7 dB.

Thus the fibers which constitute the star coupler are bundled, twisted, heated and pulled, to form the device illustrated in Figure. 2.37. With multimode fiber this method relies upon the coupling of higher order modes between the different fibers. It is therefore highly mode dependent, which results in a relatively wide port-to-port output variation in comparison with star couplers based on the mixer-rod technique. In an ideal star coupler the optical power from any input fiber is evenly distributed among the output fibers. The total loss associated with the star coupler comprises its theoretical splitting

loss together with the excess loss. The splitting loss is related to the number of output ports N following:

$$\text{Splitting loss (star coupler)} = 10 \log_{10} N \text{ (dB)}$$

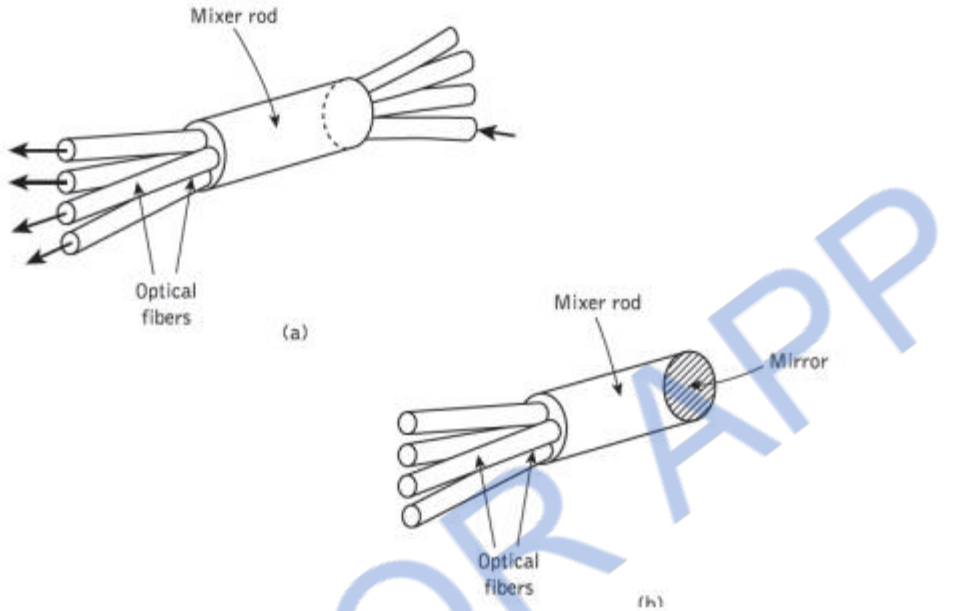

Figure 2.36 Fiber star couplers using the mixer-rod technique: (a) transmissive star coupler; (b)reflective star coupler

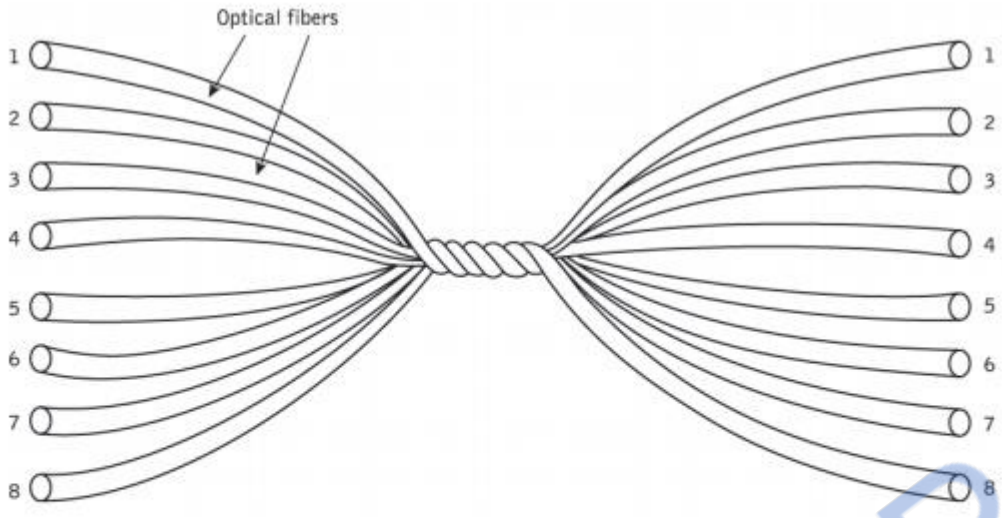

Figure 2.37 Fiber fused biconical taper 8 × 8 port star coupler

For a single input port and multiple output ports where $j = 1, N$, then the excess loss is given by:

$$\text{Excess loss (star coupler)} = 10 \log_{10}\left(P_i \Big/ \sum_{1}^{N} P_j\right) \text{(dB)}$$

TRANSMISSION CHARACTERISTICS OF OPTICAL FIBERS

1. What is Intra Modal Dispersion?

Intra Modal dispersion is pulse spreading that occurs within a single mode. The spreading arises from finite spectral emission width of an optical source. This phenomenon is also called as group velocity dispersion.

2. What are the causes of intra modal dispersion?

There is two main causes of intra modal dispersion. They are:

- Material dispersion
- Wave guide dispersion

3. What is material dispersion?

Material dispersion arises from the variation of the refractive index of the core material as a function of wavelength. Material dispersion is also referred to as chromatic dispersion. This causes a wavelength dependence of group velocity of given mode. So it occurs because the index of refraction varies as a function of optical wavelength.

Material dispersion is an intra modal dispersion effect and is for particular importance for single ode wave-guide.

4. What is waveguide dispersion?

Wave guide dispersion which occurs because of a single mode fiber confines only about 80% of optical power to the core. Dispersion this arises since 20% of light propagates in cladding travels faster than the light confined to the core. Amount of wave-guide dispersion depends on fiber design. Other factor for pulse spreading is inter modal delay

5. What is group velocity?

If L is the distance traveled by the pulse, β is the propagation constant along axis then the group velocity in the velocity at which energy is a pulse travels along the fiber.

$Vg = C. (d\beta / dk)$

6. What is group delay?

In an optical fiber there are various modes present. Then the optical input, which is propagated along the fiber, will travel in various modes. Because of these modes the velocity of the signal will vary also there may be a delay in the optical signal of these various modes. This is called as the 'Group Delay'.

7. What is polarization?

It is a fundamental property of an optical signal .It refers to the electric field orientation of a light signal which can vary significantly along the length of a fibre.

8. What is pulse Broadening?

Dispersion induced signal distortion is that a light pulse will broaden as it travels along the fiber. This pulse broadening causes a pulse to overlap with neighboring pulses. After a time't'the adjacent pulses can no longer be individually distinguished at the receiver and error will occur.

9. What is polarization Mode Dispersion (PMD)?

The difference in propagation times between the two orthogonal polarization modes will result in pulse spreading. This is called as polarization Mode Dispersion.

10. What is Mode Coupling?

It is another type of pulse distortion which is common in optical links. The pulse distortion will increase less rapidly after a certain initial length of fiber due to this mode coupling and differential mode losses. In initial length coupling of energy from one mode to another arises because of structural irregularities, fiber dia. etc.

11. What is Profile Dispersion?

A fiber with a given index profile (alpha) will exhibit different pulse spreading according to the source wavelength used. This is called as Profile Dispersion.

12. What is M-C fiber?

Fibers that have a uniform refractive index throughout the cladding is called as M-C fiber or Matched-cladding fiber.

13. What is D-C fiber?

In depressed cladding fiber the cladding portion next to the core has a lower index than the outer cladding region.

14. Define depresion shifted fiber.

By creating a fiber with large negative waveguide dispersion & assuming the same values for material dispersion as in a standard single mode fiber the addition of waveguide & material dispersion can then shifted to zero dispersion point to long wavelength. The resulting optical fiber are known as dispersion shifted fiber.

15. Define dispersion flattening?

The reduction of fiber dispersion by spreading the dispersion minimum out over a wide range .this approach is known as dispersion flattering.

16. What is effective cut-off wavelength?

It is defined as the largest wavelength at which the higher order LP11 mode power relative to the fundamental LP01 mode power is reduced to 0.1db.

17. What is intramodal dispersion?

The intramodal dispersion depends on wavelength and its effect on signal distortion increases with the spectral width of the optical source. (It is a band of wavelength over which the source emits light

18. Write a note on scattering losses.

Scattering losses in glass arise from microscopic variation in the material density from compositional fluctuation and from structural in homogeneities or defects occurring during fiber manufacture

19. What is Rayleigh scattering?

The index variation causes a Rayleigh type of scattering of light. Rayleigh scattering in glass in the same phenomenon that scatters light from sun in the atmosphere, giving rise to blue sky. The expression for Rayleigh scattering loss is given by

$\alpha scat = (8\pi^3/3\lambda^2)(n^2-1)^2 k_B T_f \beta_T$

n = refractive index

k_B = boltzman constant

β_T= isothermal compressibility

T_f =fictive temperature,

λ =operative wavelength

20. What is intermodal dispersion?

Intermodal dispersion is a pulse spreading that occurs within a single mode. The spreading arises from finite spectral emission width of an optical source. it is called group velocity dispersion or intermodal dispersion

21. What is intramodal delay?

The other factor giving rise to pulse spreading is intramodal delay which is a result of each mode having a different value of Group velocity at a single frequency.

22. What is the measure of information capacity in optical wave guide?

It is usually specified by bandwidth distance product in MHz For a step index fiber the various distortion effects tend to limit the bandwidth distance product to 20MHz.

23. Mention the losses responsible for attenuation in optical fibers.

Absorption losses, Scattering losses and bending losses

24. .What do you meant by Extrinsic absorption?

Absorption phenomena due to impurity atoms present in the fiber.

25. Define microscopic bending?

Fiber losses occur due to small bending arise while the fiber is inserted into a cable.

26. Define macroscopic bending?

If any bending present in the fiber while cabling, the optical power get radiated

GLOSSARY

1. Intra Modal Dispersion.

Intra Modal dispersion is pulse spreading that occurs within a single mode. The spreading arises from finite spectral emission width of an optical source. This phenomenon is also called as group velocity dispersion.

2. Material dispersion.

Material dispersion arises from the variation of the refractive index of the core material as a function of wavelength. Material dispersion is also referred to as chromatic dispersion. This causes a wavelength dependence of group velocity of given mode. So it occurs because the index of refraction varies as a function of optical wavelength. Material dispersion is an intra modal dispersion effect and is for particular importance for single ode wave-guide.

3. Waveguide dispersion.

Wave guide dispersion which occurs because of a single mode fiber confines only about 80% of optical power to the core. Dispersion this arises since 20% of light propagates in

cladding travels faster than the light confined to the core. Amount of wave-guide dispersion depends on fiber design. Other factor for pulse spreading is inter modal delay

4. Group velocity.

If L is the distance traveled by the pulse, β is the propagation constant along axis then the group velocity in the velocity at which energy is a pulse travels along the fiber.

$Vg = C. (d\beta / dk)$

5. Group delay.

In an optical fiber there are various modes present. Then the optical input, which is propagated along the fiber, will travel in various modes. Because of these modes the velocity of the signal will vary also there may be a delay in the optical signal of these various modes. This is called as the 'Group Delay'.

6. Polarization

It is a fundamental property of an optical signal .It refers to the electric field orientation of a light signal which can vary significantly along the length of a fibre.

7. Pulse Broadening.

Dispersion induced signal distortion is that a light pulse will broaden as it travels along the fiber. This pulse broadening causes a pulse to overlap with neighboring pulses. After a time't'the adjacent pulses can no longer be individually distinguished at the receiver and error will occur.

8. Polarization Mode Dispersion (PMD).

The difference in propagation times between the two orthogonal polarization modes will result in pulse spreading. This is called as polarization Mode Dispersion.

9. Mode Coupling.

It is another type of pulse distortion which is common in optical links. The pulse distortion will increase less rapidly after a certain initial length of fiber due to this mode coupling and differential mode losses. In initial length coupling of energy from one mode to another arises because of structural irregularities, fiber dia. etc.

10. Profile Dispersion.

A fiber with a given index profile (alpha) will exhibit different pulse spreading according to the source wavelength used. This is called as Profile Dispersion.

11. M-C fiber.

Fibers that have a uniform refractive index throughout the cladding is called as M-C fiber or Matched-cladding fiber.

12. D-C fiber.

In depressed cladding fiber the cladding portion next to the core has a lower index than the outer cladding region.

13. Dispersion shifted fiber.

By creating a fiber with large negative waveguide dispersion & assuming the same values for material dispersion as in a standard single mode fiber the addition of waveguide & material dispersion can then shifted to zero dispersion point to long wavelength. The resulting optical fiber are known as dispersion shifted fiber.

14. Dispersion flattening.

The reduction of fiber dispersion by spreading the dispersion minimum out over a wide range .this approach is known as dispersion flattering.

15. Effective cut-off wavelength.

It is defined as the largest wavelength at which the higher order LP11 mode power relative to the fundamental LP01 mode power is reduced to 0.1db.

16. Intramodal dispersion?

The intramodal dispersion depends on wavelength and its effect on signal distortion increases with the spectral width of the optical source. (It is a band of wavelength over which the source emits light

17. Scattering losses.

Scattering losses in glass arise from microscopic variation in the material density from compositional fluctuation and from structural in homogeneities or defects occurring during fiber manufacture

18. Rayleigh scattering.

The index variation causes a Rayleigh type of scattering of light. Rayleigh scattering in glass in the same phenomenon that scatters light from sun in the atmosphere, giving rise to blue sky.

19. Intermodal dispersion.

Intermodal dispersion is a pulse spreading that occurs within a single mode. The spreading arises from finite spectral emission width of an optical source. it is called group velocity dispersion or intermodal dispersion

20. Intramodal delay.

The other factor giving rise to pulse spreading is intramodal delay which is a result of each mode having a different value of Group velocity at a single frequency.

UNIT – 3

OPTICAL SOURCES AND DETECTORS

SOURCES AND DETECTORS

Introduction

The optical source is often considered to be the active component in an optical fiber communication system. Its fundamental function is to convert electrical energy in the form of a current into optical energy (light) in an efficient manner which allows the light output to be effectively launched or coupled into the optical fiber. Three main types of optical light source are available. These are:

✓⋯wideband ‘continuous spectra’ sources (incandescent lamps);

✓⋯monochromatic incoherent sources (light-emitting diodes, LEDs);

✓⋯monochromatic coherent sources (lasers).

To aid consideration of the sources currently in major use, the historical aspect must be mentioned. In the early stages of optical fiber communications the most powerful narrowband coherent light sources were necessary due to severe attenuation and dispersion in the fibers. Therefore, gas lasers (helium-neon) were utilized initially. However, the development of the semiconductor injection laser and the LED, together with the substantial improvement in the properties of optical fibers, has given prominence to these two specific sources

LEDs

Spontaneous emission of radiation in the visible and infrared regions of the spectrum from a forward-biased*p–n* junction was discussed. The normally empty conduction band of the semiconductor is populated by electrons injected into it by the forward current through the junction, and light is generated when these electrons recombine with holes in the valence band to emit a photon. This is the mechanism by which light is emitted from an LED, but stimulated emission is not encouraged, as it is in the injection laser, by the addition of an optical cavity and mirror facets to provide feedback of photons.

The LED can therefore operate at lower current densities than the injection laser, but the emitted photons have random phases and the device is an incoherent optical source. Also, the energy of the emitted photons is only roughly equal to the band gap energy of the semiconductor material, which gives a much wider spectral line width (possibly by a factor of 100) than the injection laser. The line width for an LED corresponds to a range of photon energy between 1 and 3.5*KT*, where *K* is Boltzmann's constant and *T* is the absolute temperature.

This gives linewidths of 30 to 40 nm for GaAs-based devices operating at room temperature. Thus the LED supports many optical modes within its structure and is therefore often used as a multimode source, although the coupling of LEDs to single-mode fibers has been pursued with success, particularly when advanced structures are employed. Also, LEDs have several further drawbacks in comparison with injection lasers.

These include:

✓⋯generally lower optical power coupled into a fiber (microwatts);

✓⋯usually lower modulation bandwidth;

✓⋯harmonic distortion.

However, although these problems may initially appear to make the LED a less attractive optical source than the injection laser, the device has a number of distinct advantages which have given it a prominent place in optical fiber communications:

✓⋯*Simpler fabrication*. There are no mirror facets and in some structures no striped geometry.

✓⋯*Cost*. The simpler construction of the LED leads to much reduced cost which is always likelyto be maintained.

✓⋯*Reliability*. The LED does not exhibit catastrophic degradation and has proved far lesssensitive to gradual degradation than the injection laser. It is also immune to self-pulsation and modal noise problems.

✓⋯*Generally less temperature dependence*. The light output against current characteristic is lessaffected by temperature than the corresponding characteristic for the injection laser. Furthermore, the LED is not a threshold device and therefore raising the temperature does not increase the threshold current above the operating point and hence halt operation.

✓⋯*Simpler drive circuitry*. This is due to the generally lower drive currents and reducedtemperature dependence which makes temperature compensation circuits unnecessary.

✓⋯*Linearity*. Ideally, the LED has a linear light output against current characteristic, unlike theinjection laser. This can prove advantageous where analog modulation is concerned.

The planar LED is the simplest of the structures that are available and is fabricated by either liquid- or vapor-phase epitaxial processes over the whole surface of a GaAs substrate. This involves a *p*-type diffusion into the *n*-type substrate in order to create the junction illustrated in Figure 3.1. Forward current flow through the junction gives Lambertian spontaneous emission and the device emits light from all surfaces. However, only a limited amount of light escapes the structure due to total internal reflection, and therefore the radiance is low.

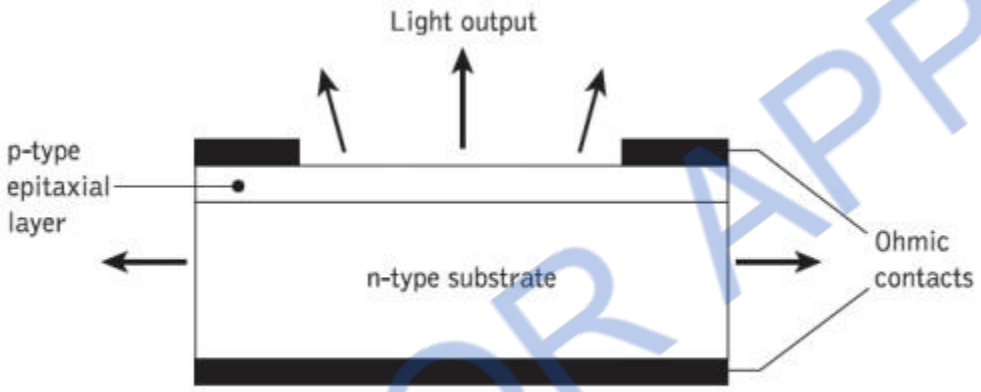

Figure 3.1 The structure of a planar LED showing the emission of light from all surfaces

The absence of optical amplification through stimulated emission in the LED tends to limit the internal quantum efficiency (ratio of photons generated to injected electrons) of the device. Reliance on spontaneous emission allows nonradiative recombination to take place within the structure due to crystalline imperfections and impurities giving, at best, an internal quantum efficiency of 50% for simple homojunction devices. However, as with injection lasers, double-heterojunction (DH) structures have been implemented which recombination lifetime measurements suggest give internal quantum efficiencies of 60 to 80%.

The power generated internally by an LED may be determined by consideration of the excess electrons and holes in the *p*- and *n*-type material respectively (i.e. the minority carriers) when it is forward biased and carrier injection takes place at the device contacts. The excess density of electrons Δn and holesΔp is equal since the injected

carriers are created and recombined in pairs such thatcharge neutrality is maintained within the structure.

LED STRUCTURES

1. Surface emitter LEDs

A method for obtaining high radiance is to restrict the emission to a small active region within the device. The technique pioneered by Burrus and Dawson with homostructure devices was to use an etched well in a GaAs substrate in order to prevent heavy absorption of the emitted radiation, and physically to accommodate the fiber. These structures have a low thermal impedance in the active region allowing high current densities and giving high-radiance emission into the optical fiber. Furthermore, considerable advantage may be obtained by employing DH structures giving increased efficiency from electrical and optical confinement as well as less absorption of the emitted radiation.

This type of surface emitter LED (SLED) has been widely employed within optical fiber communications. The structure of a high-radiance etched well DH surface emitter* for the 0.8 to 0.9μm wavelength band is shown in Figure 3.2. The internal absorption in this device is very low due to the larger bandgap-confining layers, and the reflection coefficient at the back crystal face is high giving good forward radiance. The emission from the active layer is essentially isotropic, although the external emission distribution may be considered Lambertian with a beam width of 120° due to refraction from a high to a low refractive index at the GaAs–fiber interface. The power coupled *P*c into a multimode step index fiber may be estimated from the relationship:

$$P_c = \pi (1 - r) A R_D (NA)^2 \qquad (3.1)$$

where *r* is the Fresnel reflection coefficient at the fiber surface, *A* is the smaller of the fiber core cross-section or the emission area of the source and*R*D is the radiance of the source.

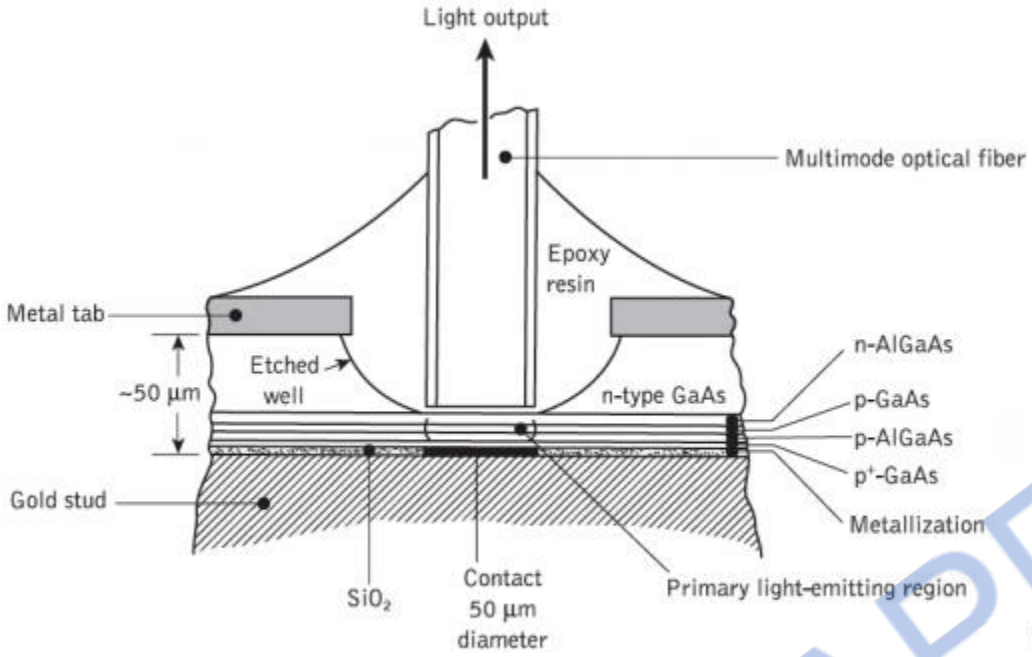

Figure 3.2 The structure of an AlGaAs DH surface-emitting LED (Burrus type).

However, the power coupled into the fiber is also dependent on many other factors including the distance and alignment between the emission area and the fiber, the SLED emission pattern and the medium between the emitting area and the fiber. For instance, the addition of epoxy resin in the etched well tends to reduce the refractive index mismatch and increase the external power efficiency of the device. Hence, DH surface emitters often give more coupled optical power than predicted by Eq. (3.1).

However, for graded index fiber optimum direct coupling requires that the source diameter be about one-half the fiber core diameter. In both cases lens coupling may give increased levels of optical power coupled into the fiber but at the cost of additional complexity. Other factors which complicate the LED fiber coupling are the transmission characteristics of the leaky modes or large angle skew rays. Much of the optical power from an incoherent source is initially coupled into these large-angle rays, which fall within the acceptance angle of the fiber but have much higher energy than meridional rays. Energy from these rays goes into the cladding and may be lost.

Hence much of the light coupled into a multimode fiber from an LED is lost within a few hundred meters. It must therefore be noted that the effective optical power coupled into a short length of fiber significantly exceeds that coupled into a longer length.

The planar structure of the Burrus-type LED and other nonetched well SLEDs allows significant lateral current spreading, particularly for contact diameters less than 25 μm. This current spreading results in a reduced current density as well as an effective emission area substantially greater than the contact area.

2. Edge emitter LEDs

Another basic high-radiance structure currently used in optical communications is the stripe geometry DH edge emitter LED (ELED). This device has a similar geometry to a conventional contact stripe injection laser, as shown in Figure 3.3.

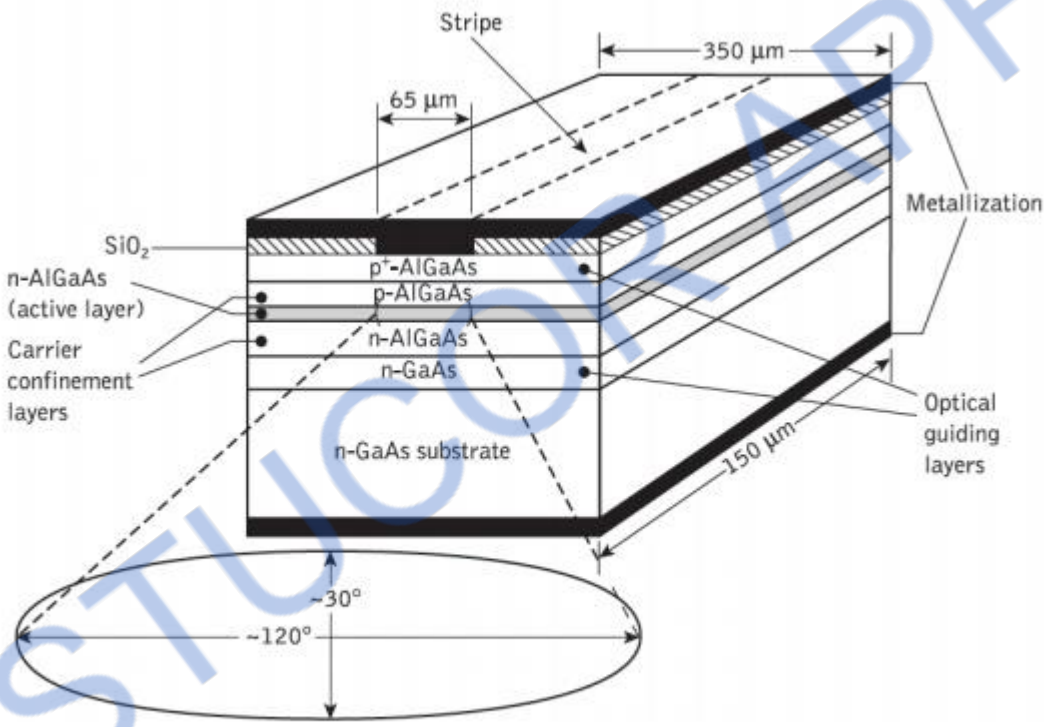

Figure 3.3 Schematic illustration of the structure of a stripe geometry DH AlGaAs edge-emitting LED

It takes advantage of transparent guiding layers with a very thin active layer (50 to 100 μm) in order that the light produced in the active layer spreads into the transparent guiding layers, reducing self-absorption in the active layer. The consequent waveguiding narrows the beam divergence to a half-power width of around 30° in the plane perpendicular to the junction. However, the lack of waveguiding in the plane of the junction gives a Lambertian output with a half-power width of around 120°, as

illustrated in Figure3.3. Most of the propagating light is emitted at one end face only due to a reflector on the other end face and an antireflection coating on the emitting end face. The effective radiance at the emitting end face can be very high giving an increased coupling efficiency into small-*NA* fiber compared with the surface emitter. However, surface emitters generally radiate more powerinto air (2.5 to 3 times) than edge emitters since the emitted light is less affected by reabsorption and interfacial recombination. Comparisons have shown that edge emitters couple more optical power into low *NA* (less than 0.3) than surface emitters, whereas the opposite is true for large *NA* (greater than 0.3).

The enhanced waveguiding of the edge emitter enables it in theory to couple 7.5 times more power into low-*NA* fiber than a comparable surface emitter. However, in practice the increased coupling efficiency has been found to be slightly less than this (3.5 to 6 times). Similar coupling efficiencies may be achieved into low-*NA* fiber with surface emitters by the use of a lens. Furthermore, it has been found that lens coupling with edge emitters may increase the coupling efficiencies by comparable factors (around five times).

The stripe geometry of the edge emitter allows very high carrier injection densities for given drive currents. Thus it is possible to couple approaching a milliwatt of optical power into low-*NA* (0.14) multimode step index fiber with edge-emitting LEDs operating at high drive currents (500 mA).

Edge emitters have also been found to have a substantially better modulation bandwidth of the order of hundreds of megahertz than comparable surface-emitting structures with the same drive level. In general it is possible to construct edge-emitting LEDs with a narrower linewidth than surface emitters, but there are manufacturing problems with the more complicated structure (including difficult heat-sinking geometry) which moderate the benefits of these devices.

The Semiconductor Injection Laser

The electroluminescent properties of the forward-biased *p–n* junction diode have been considered in the preceding sections. Stimulated emission by the recombination of the injected carriers is encouraged in the semiconductor injection laser (also called the

injection laser diode (ILD) or simply the injection laser) by the provision of an optical cavity in the crystal structure in order to provide the feedback of photons. This gives the injection laser several major advantages over other semiconductor sources (e.g. LEDs) that may be used for optical communications. These are as follows:

1. High radiance due to the amplifying effect of stimulated emission. Injection lasers will generally supply milliwatts of optical output power.

2. Narrow linewidth on the order of 1 nm (10 Å) or less which is useful in minimizing the effects of material dispersion.

3. Modulation capabilities which at present extend up into the gigahertz range and will undoubtedly be improved upon.

4. Relative temporal coherence which is considered essential to allow heterodyne (coherent) detection in high-capacity systems, but at present is primarily of use in single-mode systems

5. Good spatial coherence which allows the output to be focused by a lens into a spot which has a greater intensity than the dispersed unfocused emission.

This permits efficient coupling of the optical output power into the fiber even for fibers with low numerical aperture. The spatial fold matching to the optical fiber which may be obtained with the laser source is not possible with an incoherent emitter and, consequently, coupling efficiencies are much reduced

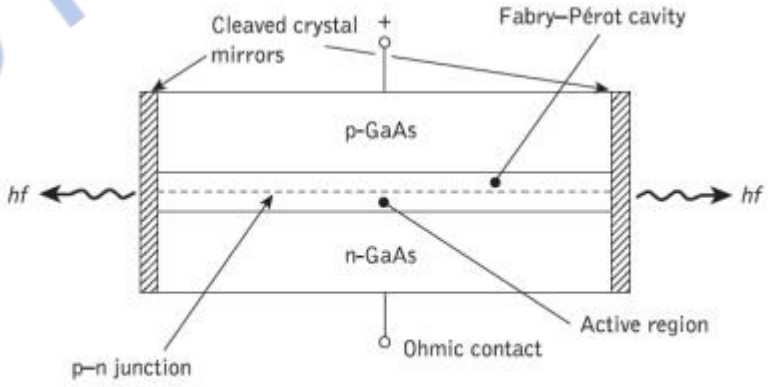

Figure 3.4 Schematic diagram of a GaAs homojunction injection laser with a Fabry–Pérot cavity

These advantages, together with the compatibility of the injection laser with optical fibers (e.g. size), led to the early developments of the device in the 1960s. Early injection lasers had the form of a Fabry–Pérot cavity often fabricated in gallium arsenide which was the major III–V compound semiconductor with electroluminescent properties at the appropriate wavelength for first-generation systems. The basic structure of this homojunction device is shown in Figure 3.4, where the cleaved ends of the crystal act as partial mirrors in order to encourage stimulated emission in the cavity when electrons are injected into the *p*-type region. However, as mentioned previously these devices had a high threshold current density (greater than 104 A cm−2) due to their lack of carrier containment and proved inefficient light sources.

High current densities required dictated that these devices when operated at 300 K were largely utilized in a pulsed mode in order to minimize the junction temperature and thus avert damage. Improved carrier containment and thus lower threshold current densities (around 103 A cm−2) were achieved using heterojunction structures.

The DH injection laser fabricated from lattice-matched III–V alloys provided both carrier and optical confinement on both sides of the *p–n* junction, giving the injection laser a greatly enhanced performance. This enabled these devices with the appropriate heat sinking to be operated in a CW mode at 300 K with obvious advantages for optical communications (e.g. analog transmission). However, in order to provide reliable CW operation of the DH injection laser it was necessary to provide further carrier and optical confinement which led to the introduction of stripe geometry DH laser configurations. Prior to discussion of this structure, however, it is useful to consider the efficiency of the semiconductor injection laser as an optical source.

Stripe geometry

The DH laser structure provides optical confinement in the vertical direction through the refractive index step at the heterojunction interfaces, but lasing takes place across the whole width of the device. This situation is illustrated in Figure 3.5 which shows the broad-area DH laser where the sides of the cavity are simply formed by roughening the edges of the device in order to reduce unwanted emission in these directions and limit the number of horizontal transverse modes. However, the broad emission area creates

several problems including difficult heat sinking, lasing from multiple filaments in the relatively wide active area and unsuitable light output geometry for efficient coupling to the cylindrical fibers.

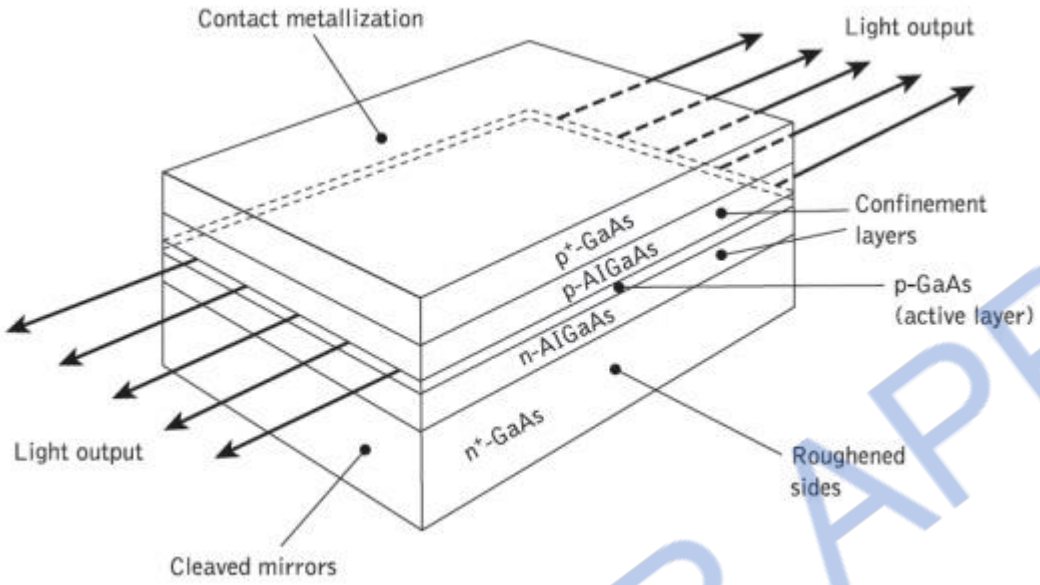

Figure 3.5 A broad-area GaAs/AlGaAs DH injection laser

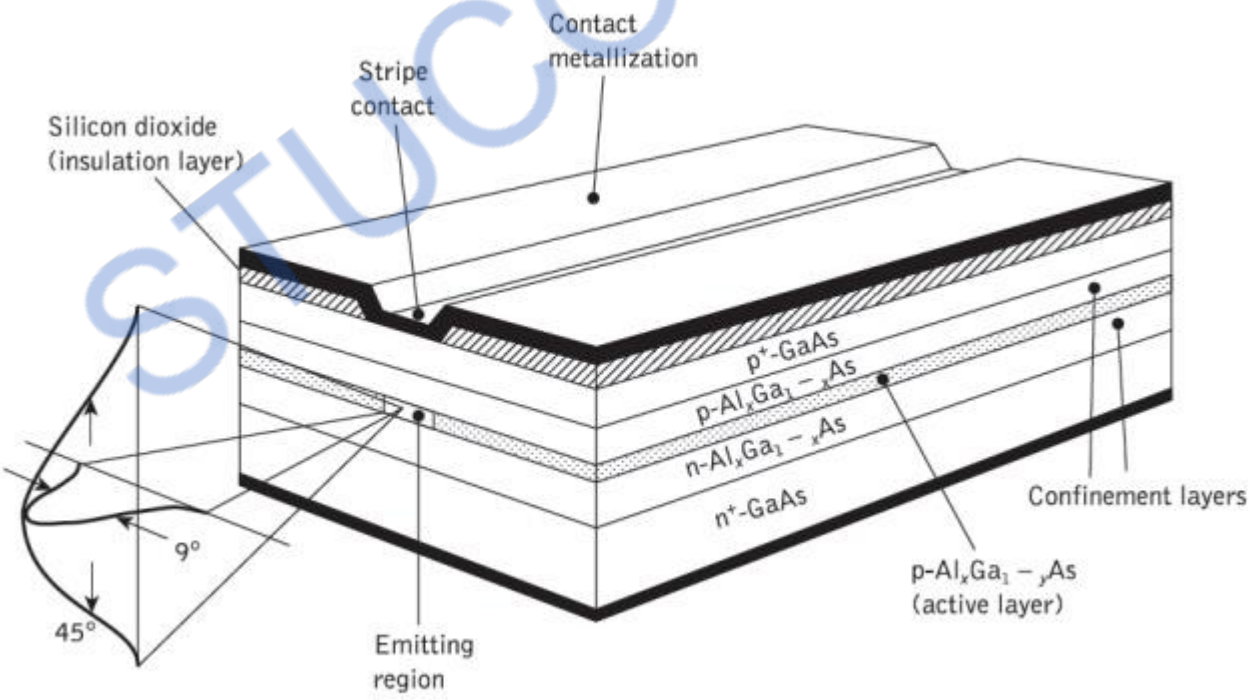

Figure 3.6 Schematic representation of an oxide stripe AlGaAs DH injection laser

To overcome these problems while also reducing the required threshold current, laser structures in which the active region does not extend to the edges of the device were developed. A common technique involved the introduction of stripe geometry to the structure to provide optical containment in the horizontal plane. The structure of a DH stripe contact laser is shown in Figure 3.6 where the major current flow through the device and hence the active region is within the stripe. Generally, the stripe is formed by the creation of high-resistance areas on either side by techniques such as proton bombardment or oxide isolation.

The stripe therefore acts as a guiding mechanism which overcomes the major problems of the broad-area device. However, although the active area width is reduced the light output is still not particularly well collimated due to isotropic emission from a small active region and diffraction within the structure. The optical output and far-field emission pattern are also illustrated in Figure 6.21. The output beam divergence is typically 45° perpendicular to the plane of the junction and 9° parallel to it. Nevertheless, this is a substantial improvement on the broad-area laser.

Injection Laser Structures

1. Gain-guided lasers

Fabrication of multimode injection lasers with a single or small number of lateral modes is achieved by the use of stripe geometry. These devices are often called gain-guided lasers. The constriction of the current flow to the stripe is realized in the structure either by implanting the regions outside the stripe with protons (protonisolated stripe) to make them highly resistive, or by oxide or *p–n* junction isolation. The structure for an aluminum gallium arsenide oxide isolated stripe DH laserwas shown in Figure 3.6. It has an active region of gallium arsenide bounded on both sides by aluminum gallium arsenide regions. This technique has been widely applied, especially for multimode laser structures used in the shorter wavelength region. The current is confined by etching a narrow stripe in a silicon dioxide film.

Two other basic techniques for the fabrication of gain-guided laser structures are illustrated in Figure3.7(a) and (b) which show the proton-isolated stripe and the *p–n* junction isolated stripe structures respectively. In Figure 3.7(a) the resistive region formed by the proton bombardment gives better current confinement than the simple oxide stripe and has superior thermal properties due to the absence of the silicon dioxide layer; *p–n* junction isolation involves a selective diffusion through the *n*-type surface region in order to reach the *p*-type layers, as illustrated in Figure 1(b). None of thesestructures confines all the radiation and current to the stripe region and spreading occurs on both sides of the stripe.

With stripe widths of 10 μm or less, such planar stripe lasers provide highly efficient coupling into multimode fibers, but significantly lower coupling efficiency is achieved into small-core-diameter single-mode fibers. However, with certain practical laser diodes the characteristic is not linear in the simulated emission region, but exhibits kinks. This phenomenon is particularly prevalent with gain-guided injection laser devices. The kinks may be classified into two broad categories.

The first type of kink results from changes in the dominant lateral mode of the laser as the current is changed. The output characteristic for laser *A* in Figure 3.8(a) illustrates this type of kink where lasing from the device changes from the fundamental lateral mode to a higher order lateral mode (second order) in a current region corresponding to a change in slope. The second type of kink involves a ‘spike’, as observed for laser *B* of Figure 3.8(a). These spikes have been shown to be associated with filamentary behavior within the active region of the device. The filaments result from defects within the crystal structure. Both these mechanisms affect the near- and far-field intensity distributions (patterns) obtained from the laser. A typical near-field intensity distribution corresponding to a single optical output power level in the plane of the junction is shown in Figure 3.8(b).

As this distribution is in the lateral direction, it is determined by the nature of the lateral waveguide. The single intensity maximum shown indicates that the fundamental lateral mode is dominant. To maintain such a near-field pattern the stripe geometry of the device is important. In general, relatively narrow stripe devices (< 10 μm) formed by a planar process allow the fundamental lateral mode to dominate.

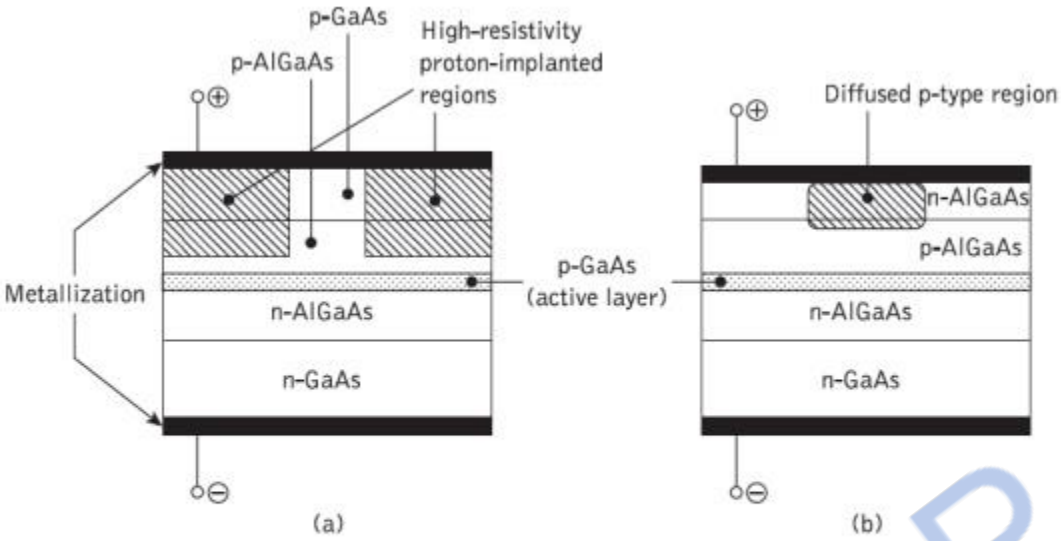

Figure 3.7 Schematic representation of structures for stripe geometry injection lasers: (a) proton-isolated stripe GaAs/AlGaAs laser; (b) *p–n* junction isolated (diffused planar stripe) GaAs/AlGaAs laser

This is especially the case at low power levels where near-field patterns similar to Figure 3.8(b) may be obtained. Although gain-guided lasers are commercially available for operation in both the shorter wavelength range (using GaAs active regions) and the longer wavelength range (using InGaAsP active regions) they exhibit several undesirable characteristics.

Apart from the nonlinearities in the light output versus current characteristics discussed above, gain-guided injection lasers have relatively high threshold currents (100 to 150 mA) as well as low differential quantum efficiency. These effects are primarily caused by the small carrier-induced refractive index reduction within the devices which results in the movement of the optical mode along the junction plane. The problems can be greatly reduced by introducing some real refractive index variation into the lateral structure of the laser such that the optical mode along the junction plane is essentially determined by the device structure.

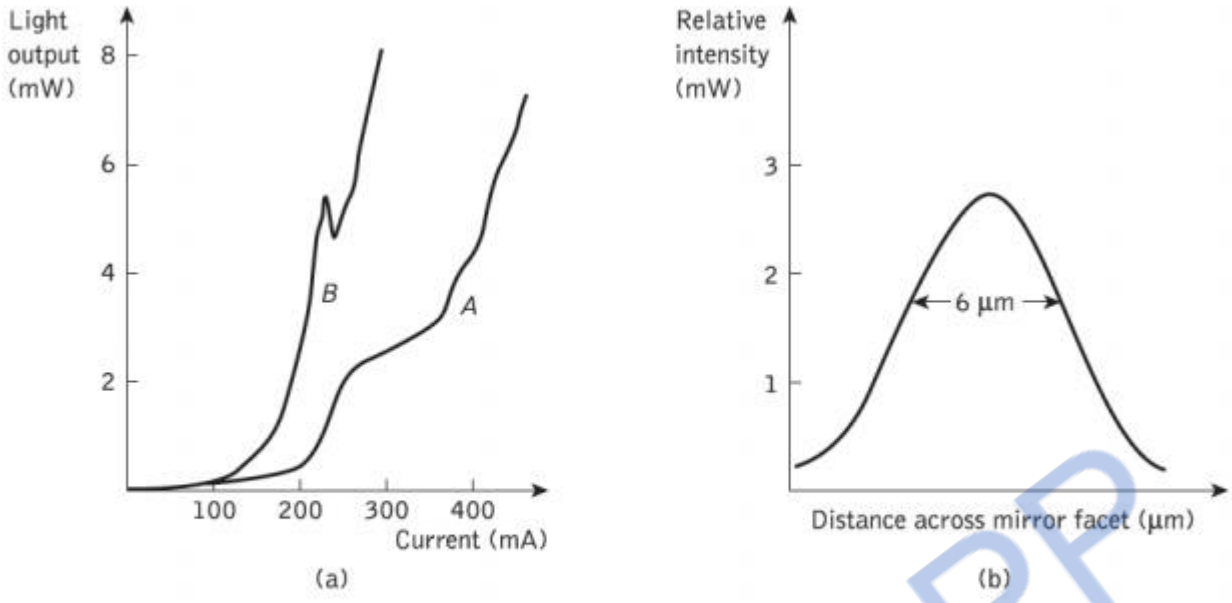

Figure 3.8 (a) The light output against current characteristic for an injection laser with nonlinearities or a kink in the stimulated emission region. (b) A typical near-field intensity distribution (pattern) in the plane of the junction for an injection laser

2. Index-guided lasers

The drawbacks associated with the gain-guided laser structures were largely overcome through the development of index-guided injection lasers. In some such structures with weak index guiding, the active region waveguide thickness is varied by growing it over a channel or ridge in the substrate. A ridge is produced above the active region and the surrounding areas are etched close to it (i.e. within 0.2 to 0.3 µm). Insulating coatings on these surrounding areas confine the current flow through the ridge and active stripe while the edges of the ridge reflect light, guiding it within the active layer, and thus forming a waveguide. Hence in the ridge waveguide laser shown in Figure 3.9 (a), the ridge not only provides the location for the weak index guiding but also acts as the narrow current confining stripe. These devices have been fabricated to operate at various wavelengths with a single lateral mode, and room temperature CW threshold currents as low as 18 mA with output powers of 25 mW have been reported.

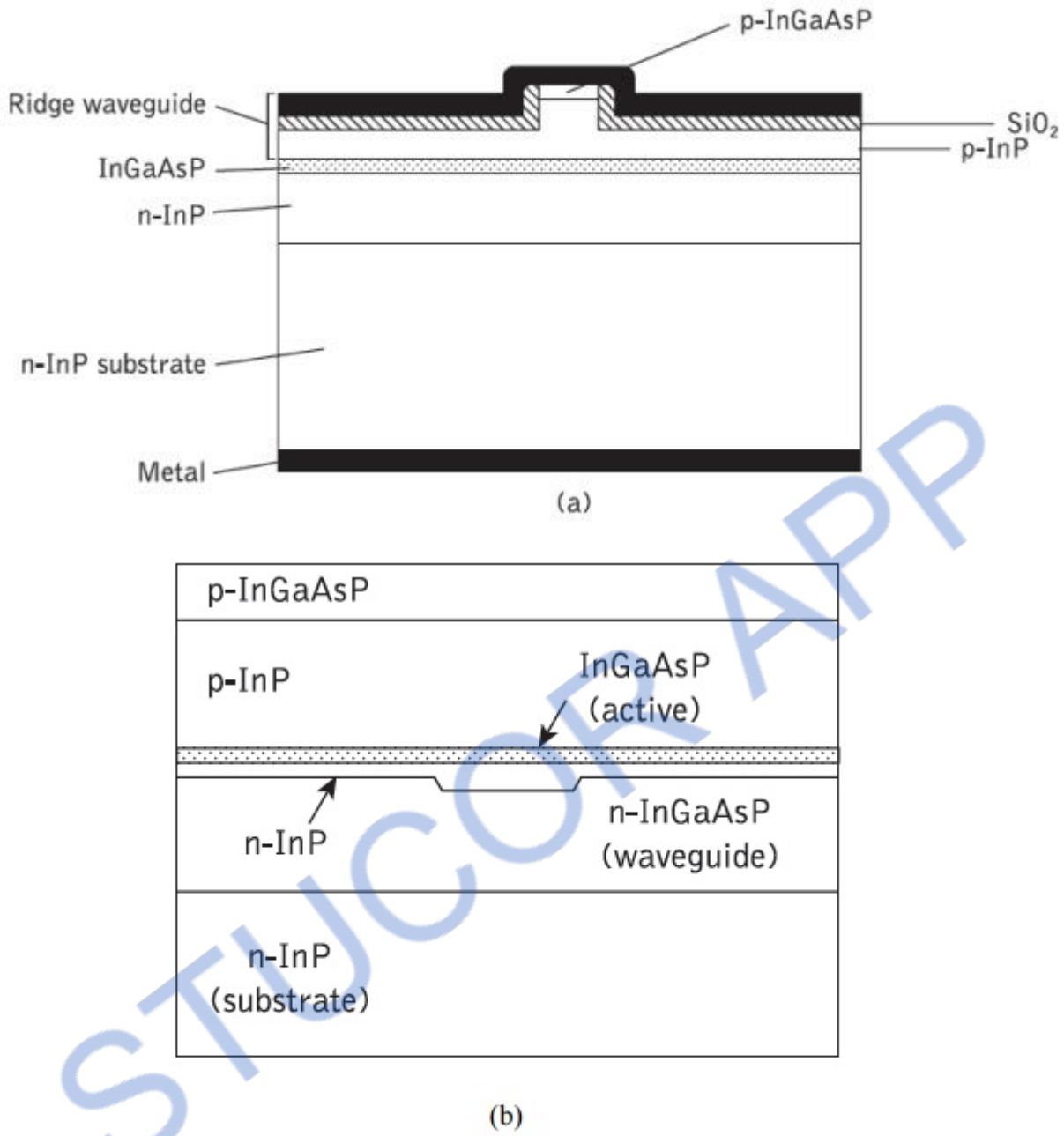

Figure 3.9 Index-guided lasers: (a) ridge waveguide injection laser structures; (c) rib (plano-convex) waveguide injection laser structure

More typically, the threshold currents for such weakly index-guided structures are in the range 40 to 60 mA, which compares a light output versus current characteristic for a ridge waveguide laser with that of an oxide stripe gain-guided device. Alternatively, the application of a uniformly thick, planar active waveguide can be achieved through lateral variations in the confinement layer thickness or the refractive index. However,

room temperature CW threshold currents are between 70 and 90 mA with output powers of around 20 mW for InGaAsP devices operating at a wavelength of 1.3 μm.

3. Quantum-well lasers

DH lasers have also been fabricated with very thin active layer thicknesses of around 10 nm instead of the typical range for conventional DH structures of 0.1 to 0.3 μm. The carrier motion normal to the active layer in these devices is restricted, resulting in a quantization of the kinetic energy into discrete energy levels for the carriers moving in that direction. This effect is similar to the well-known quantum mechanical problem of a one dimensional potential well and therefore these devices are known as quantumwell lasers. In this structure the thin active layer causes drastic changes to the electronic and optical properties in comparison with a conventional DH laser.

These changes are due to the quantized nature of the discrete energy levels with a step-like density of states which differs from the continuum normally obtained. Hence, quantum-well lasers exhibit an inherent advantage over conventional DH devices in that they allow high gain at low carrier density, thus providing the possibility of significantly lower threshold currents. Both single-quantum-well (SQW), corresponding to a single active region, and multiquantum-well (MQW), corresponding to multiple active regions, lasers are utilized. In the latter structure, the layers separating the active regions are called barrier layers. Energy band diagrams for the active regions of these structures are displayed in Figure 3.10. It may be observed in Figure 3.10(c) that when the bandgap energy of the barrier layer differs from the cladding layer in an MQW device, it is usually referred to as a modified multiquantum-well laser.

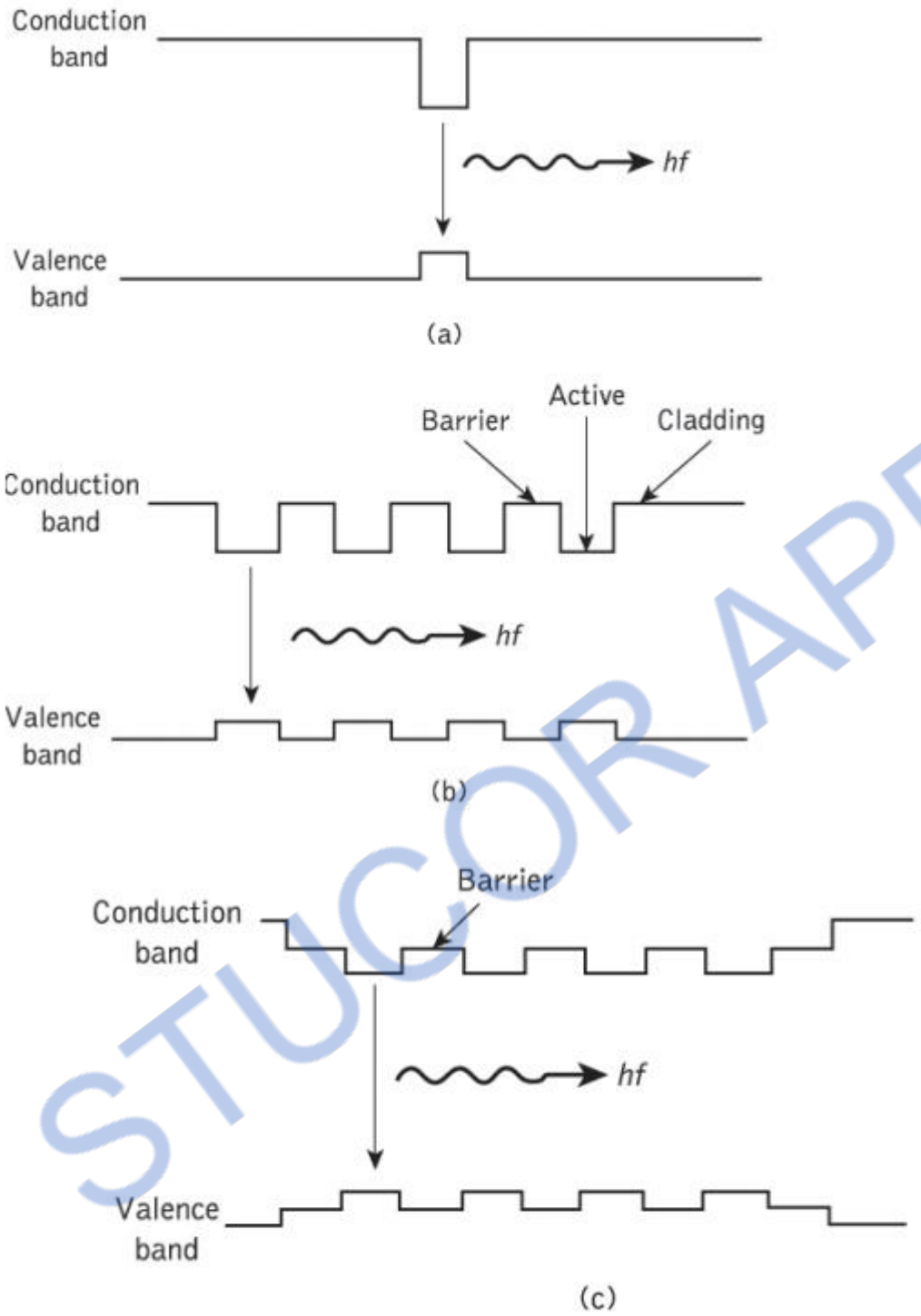

Figure 3.10 Energy band diagrams showing various types of quantum-well structure: (a) single quantum well; (b) multiquantum well; (c) modified multiquantum well

Better confinement of the optical mode is obtained in MQW lasers in comparison with SQW lasers, resulting in a lower threshold current density for these devices. A substantial amount of experimental work has been carried out on MQW lasers using the

AlGaAs/GaAs material system. It has demonstrated the superior characteristics of MQW devices over conventional DH lasers in relation to lower threshold currents, narrower line widths, higher modulation speeds, lower frequency chirp and less temperature dependence.

Optical Detectors

The basic detection process in an intrinsic absorber is illustrated in Figure 3.11 which shows a *p*–*n* photodiode. This device is reverse biased and the electric field developed across the *p*–*n* junction sweeps mobile carriers (holes and electrons) to their respective majority sides (*p*- and *n*-type material). A depletion region or layer is therefore created on either side of the junction. This barrier has the effect of stopping the majority carriers crossing the junction in the opposite direction to the field.

However, the field accelerates minority carriers from both sides to the opposite side of the junction, forming the reverse leakage current of the diode. Thus intrinsic conditions are created in the depletion region.

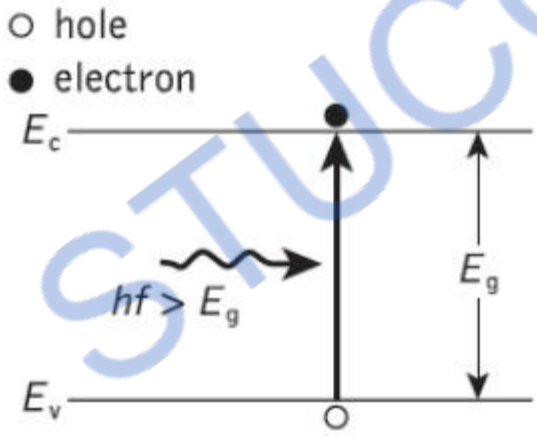

(a)

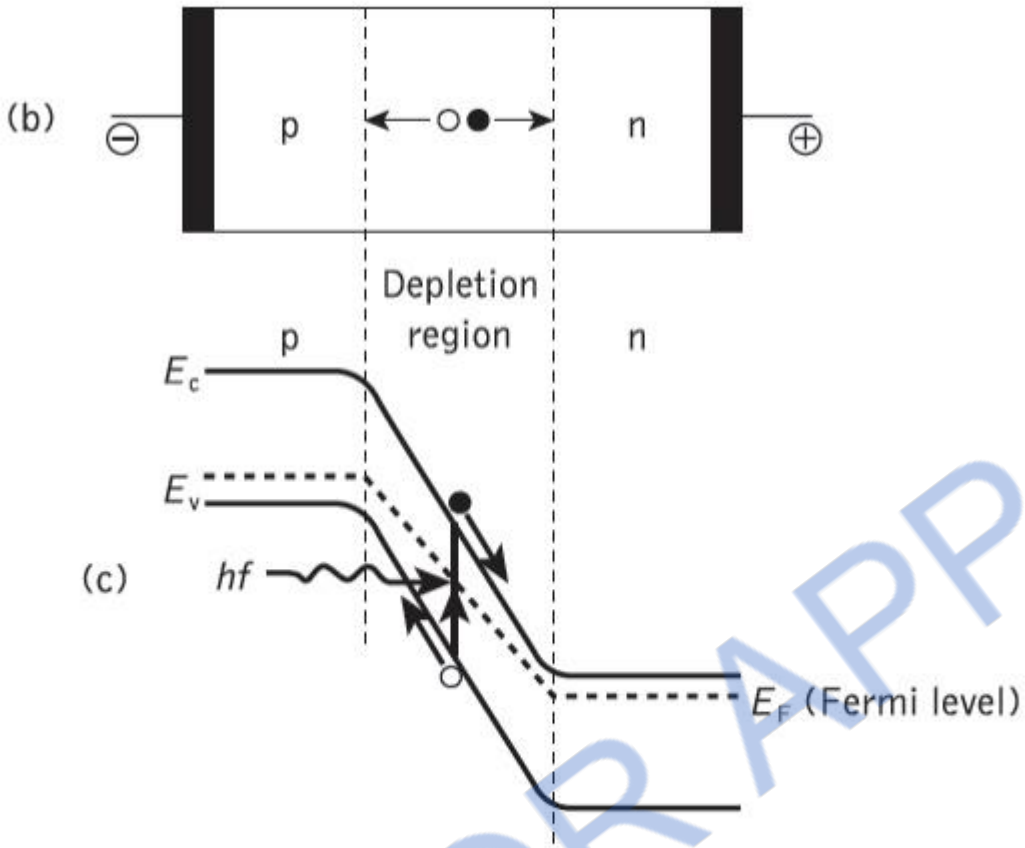

Figure 3.11 Operation of the *p–n* photodiode: (a) photogeneration of an electron–hole pair in an intrinsic semiconductor; (b) the structure of the reverse-biased *p–n* junction illustrating carrier drift in the depletion region; (c) the energy band diagram of the reverse-biased *p–n* junction showing photogeneration and the subsequent separation of an electron–hole pair

1. PIN Photo detectors

In order to allow operation at longer wavelengths where the light penetrates more deeply into the semiconductor material, a wider depletion region is necessary. To achieve this then*n*-type material is doped so lightly that it can be considered intrinsic, and to make a low resistance contact a highly doped*n*-type (n+) layer is added. This creates a *p–i–n* (or PIN) structure, as may be seen in Figure 3.12 where all the absorption takes place in the depletion region.

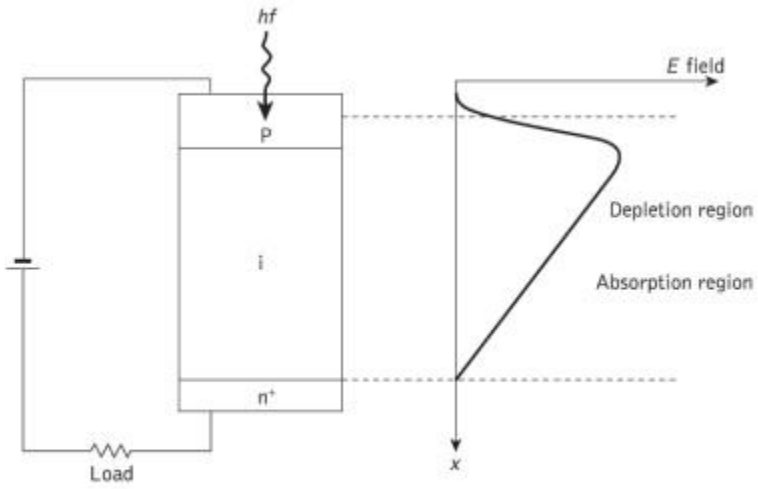

Figure 3.12 The *p–i–n* photodiode showing the combined absorption and depletion region

Figure 3.13 shows the structures of two types of silicon *p–i–n* photodiode for operation in the shorter wavelength band below 1.09 μm. The front-illuminated photodiode, when operating in the 0.8 to 0.9 μm band (Figure 3.13(a)), requires a depletion region of between 20 and 50 μm in order to attain high quantum efficiency (typically 85%) together with fast response (less than 1 ns) and low dark current (1 nA). Dark current arises from surface leakage currents as well as generation– recombination currents in the depletion region in the absence of illumination.

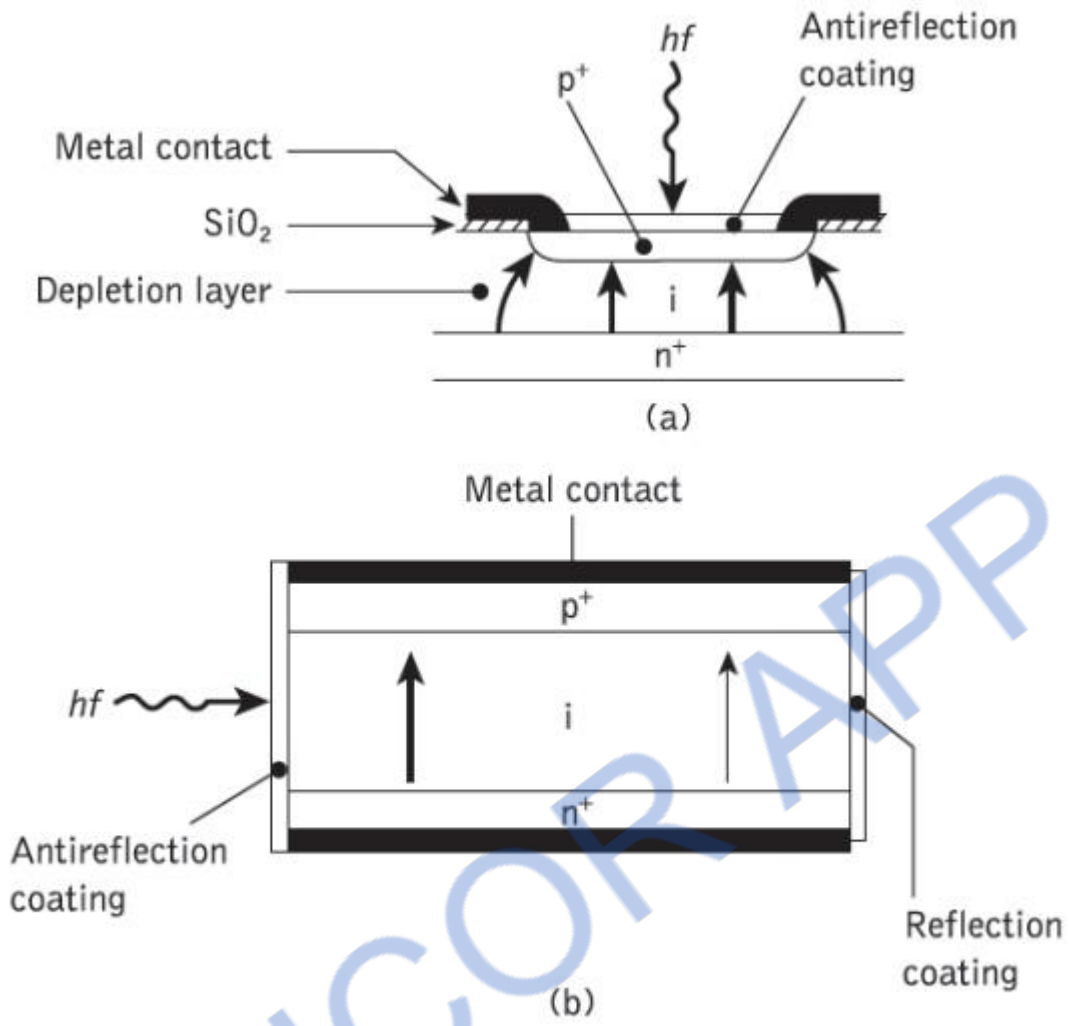

Figure 3.13 (a) Structure of a front-illuminated silicon *p–i–n* photodiode. (b) Structure of a side-illuminated (parallel to junction) *p–i–n* photodiode

The side-illuminated structure (Figure 3.13(b)), where light is injected parallel to the junction plane, exhibits a large absorption width (_500 μm) and hence is particularly sensitive at wavelengths close to the bandgap limit (1.09 μm) where the absorption coefficient is relatively small. Germanium *p–i–n* photodiodes which span the entire wavelength range of interest are also commerciallyavailable, but as mentioned previously the relatively high dark currents are a problem (typically 100 nA at 20 °C increasing to 1 μA at 40 °C).

The favored material is the lattice-matched In0.53Ga0.47As/InP system which can detect at wavelengths up to 1.67 μm. A typical planar device structure is shown in Figure 3.14(a) which requires epitaxial growth of several layers on an *n*-type InP substrate. The incident light is absorbed in the low-doped *n*-type InGaAs layer generating carriers, as

illustrated in the energy band diagram Figure 3.14(b). The discontinuity due to the homojunction between the n+-InP substrate and the n-InGaAs absorption region may be noted. This can be reduced by the incorporation of an *n*-type InP buffer layer.

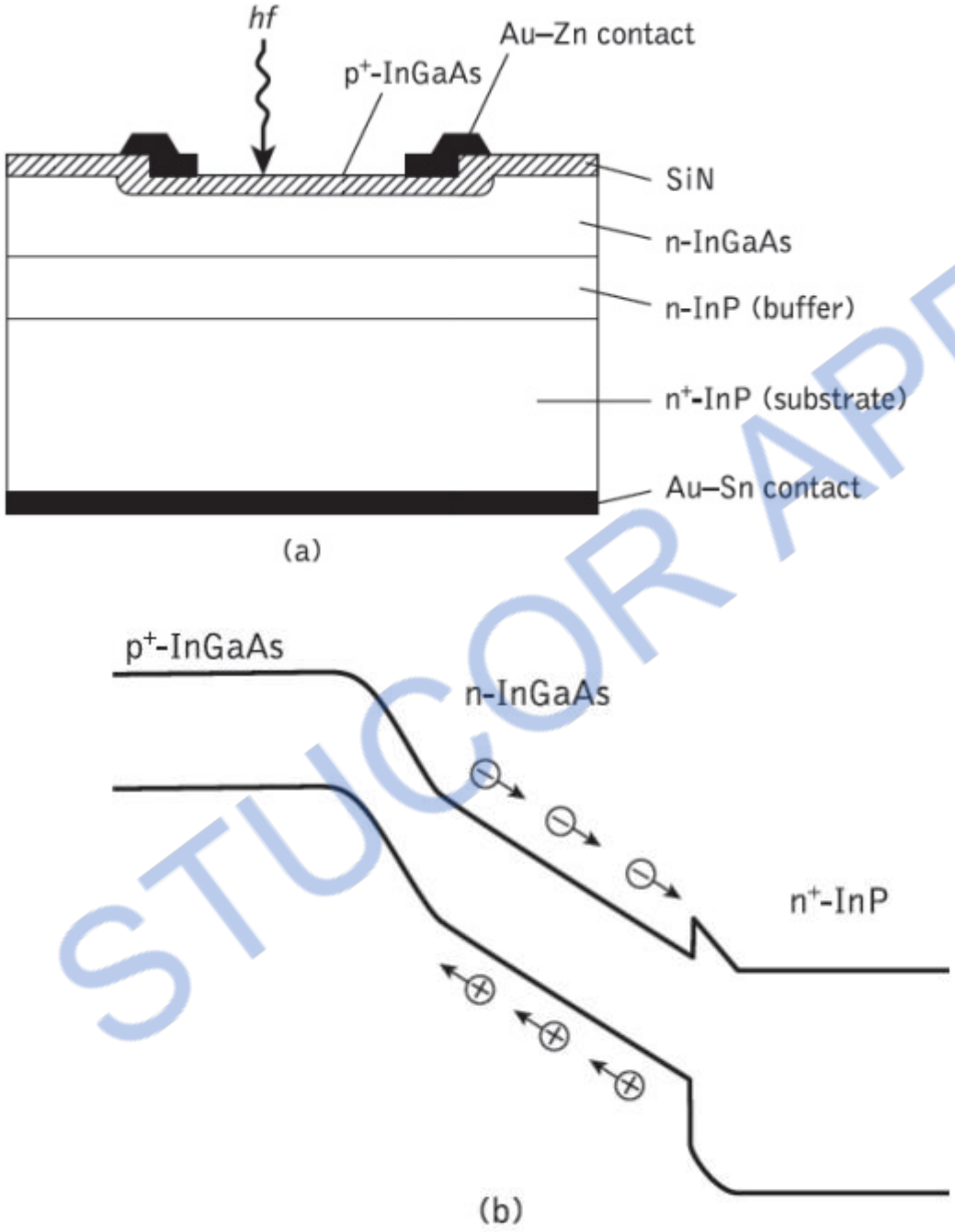

Figure 3.14 Planar InGaAs *p–i–n* photodiode: (a) structure; (b) energy band diagram showing homojunction associated with the conventional *p–i–n* structure

The top entry* device shown in Figure 3.14(a) is the simplest structure, with the light being introduced through the upper p+-layer. However, a drawback with this structure is

a quantum efficiency penalty which results from optical absorption in the undepleted p+-region. In addition, there is a limit to how small such a device can be fabricated as both light access and metallic contact are required on the top. To enable smaller devices with lower capacitances to be made, a substrate entry technique is employed. In this case light enters through a transparent InP substrate and the device area can be fabricated as small as may be practical for bonding.

2. Avalanche photodiodes

The second major type of optical communications detector is the avalanche photodiode (APD). This has a more sophisticated structure than the *p–i–n*photodiode in order to create an extremely high electric field region (approximately 3 × 105 V cm−1), as may be seen in Figure 3.15(a). Therefore, as well as the depletion region where most of the photons are absorbed and the primary carrier pairs generated, there is a high-field region in which holes and electrons can acquire sufficient energy to excite new electron–hole pairs.

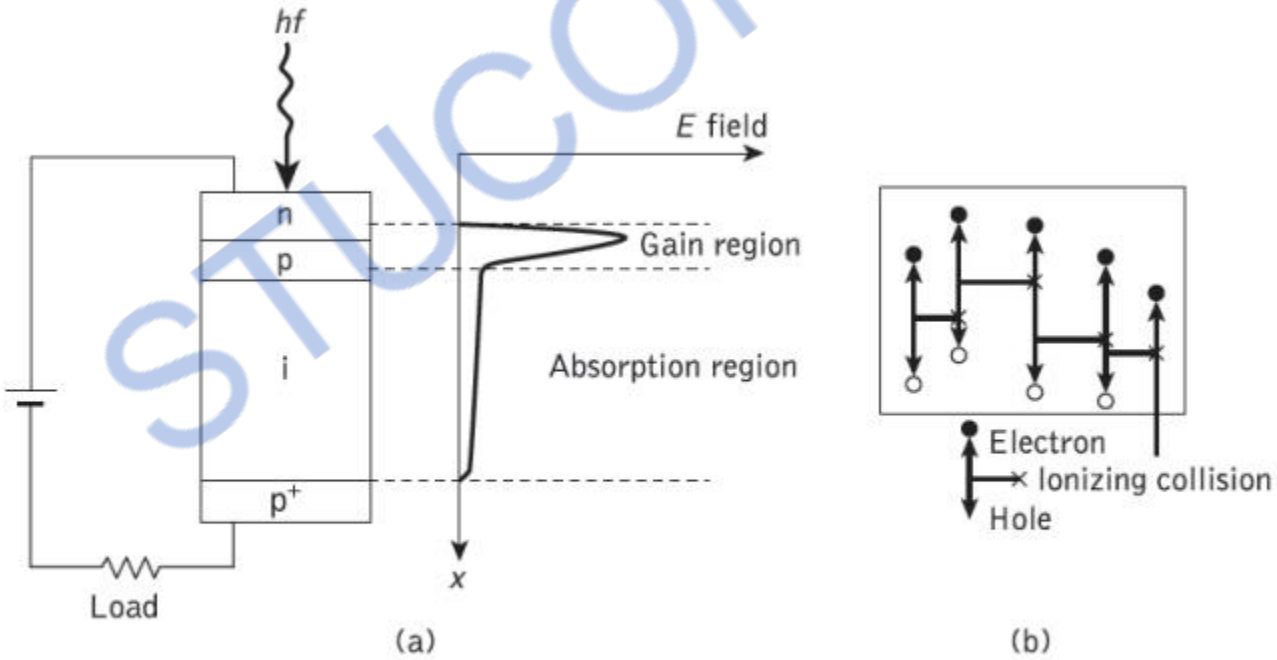

Figure 3.15 (a) Avalanche photodiode showing high electric field (gain) region. (b) Carrier pair multiplication in the gain region of an avalanche photodiode

This process is known as impact ionization and is the phenomenon that leads to avalanche breakdown in ordinary reverse-biased diodes. It often requires high reverse

bias voltages (50 to 400 V) in order that the new carriers created by impact ionization can themselves produce additional carriers by the same mechanism as shown in Figure 3.15(b). More recently, however, it should be noted that devices which will operate at much lower bias voltages (15 to 25 V) have become available.

Carrier multiplication factors as great as 104 may be obtained using defect-free materials to ensure uniformity of carrier multiplication over the entire photosensitive area. However, other factors affect the achievement of high gain within the device. Microplasmas, which are small areas with lower breakdown voltages than the remainder of the junction, must be reduced through the selection of defect-free materials together with careful device processing and fabrication.

In addition, excessive leakage at the junction edges can be eliminated by the use of a guard ring structure as shown in Figure 3.16. At present silicon, germanium and InGaAs APDs are generally available.

Operation of these devices at high speed requires full depletion in the absorption region. When carriers are generated in undepleted material, they are collected somewhat slowly by the diffusion process. This has the effect of producing a long ‘diffusion tail’ on a short optical pulse. When the APD is fully depleted by employing electric fields in excess of 104 Vm−1, all the carriers drift at saturation-limited velocities. In this case the response time for the device is limited by three factors. These are:

(a)the transit time of the carriers across the absorption region (i.e. the depletion width);

(b) the time taken by the carriers to perform the avalanche multiplication process; and

(c) the*RC* time constant incurred by the junction capacitance of the diode and its load.

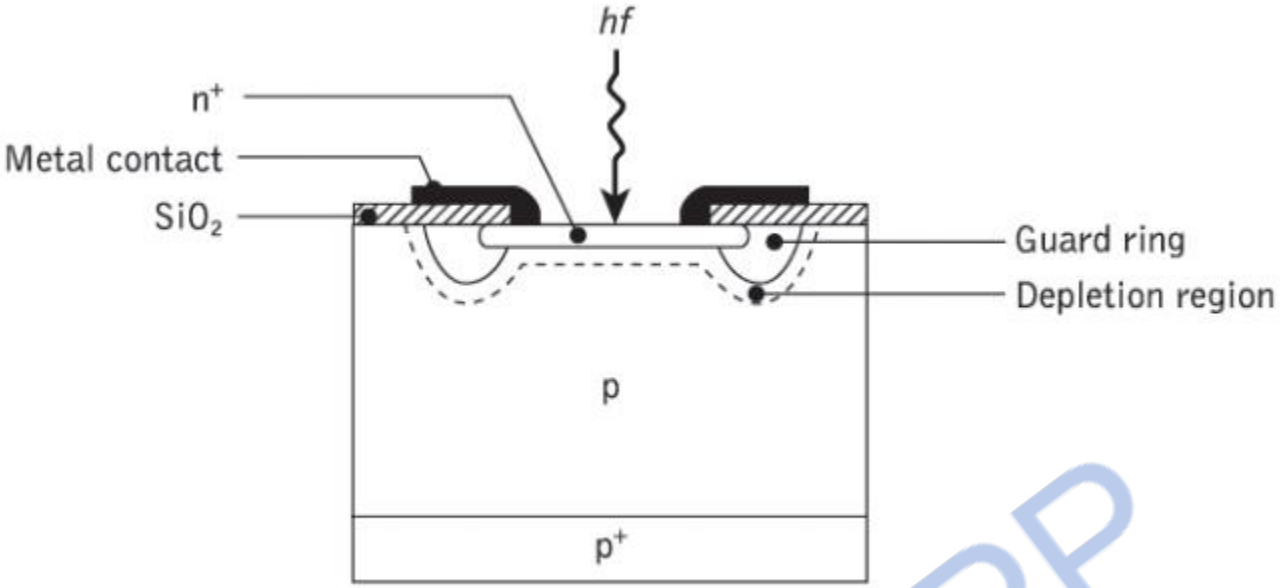

Figure 8.16 Structure of a silicon avalanche photodiode (APD) with guard ring

At low gain the transit time and *RC* effects dominate giving a definitive response time and hence constant bandwidth for the device. However, at high gain the avalanche build up time dominates and therefore the device bandwidth decreases proportionately with increasing gain. Such APD operation is distinguished by a constant gain–bandwidth product. Often an asymmetric pulse shape is obtained from the APD which results from a relatively fast rise time as the electrons are collected and a fall time dictated by the transit time of the holes traveling at a slower speed. Hence, although the use of suitable materials and structures may give rise times between 150 and 200 ps, fall times of 1 ns or more are quite common and limit the overall response of the device.

Photodetector Noise & S/N:

Detection of weak optical signal requires that the photodetector and its following amplification circuitry be optimized for a desired signal-to-noise ratio.

It is the noise current which determines the minimum optical power level that can be detected. This minimum detectable optical power defines the**sensitivity** of photodetector. That is the optical power that generates a photocurrent with the amplitude equal to that of the total noise current (*S/N=1*)

$$\frac{S}{N} = \frac{\text{signal power from photocurrent}}{\text{photodetector noise power} + \text{amplifier noise power}}$$

1. Signal Calculation:

Consider the modulated optical power signal *P(t)* falls on the photodetector with the form of

$$P(t) = P_0[1 + ms(t)]$$

Where *s(t)* is message electrical signal and *m* is modulation index. Therefore the primary photocurrent is (for pin photodiode *M=1*):

$$i_{ph} = \frac{\eta q}{h\nu} MP(t) = I_P[\text{DC value}] + i_p(t)[\text{AC current}]$$

The root mean square signal current is then

$$\langle i_s^2 \rangle = \langle i_p^2 \rangle M^2 = \sigma_s^2$$

$$\langle i_p^2 \rangle = \sigma_p^2 = \frac{m^2 I_P^2}{2} \quad \text{for sinusoidal signal}$$

Noise Sources in Photodetecors :

The principal noises associated with photodetectorsare :

1- Quantum (Shot) noise: arises from statistical nature of the production and collection of photo-generated electrons upon optical illumination. It has been shown that the statistics follow a Poisson process.

2- Dark current noise: is the current that continues to flow through the bias circuit in the absence of the light. This is the combination of bulk dark current, which is due to thermally generated e and h in the *pn* junction, and the surface dark current, due to surface defects, bias voltage an surface area.

• In order to calculate the total noise presented in photodetector, we should sum up the root mean square of each noise current by assuming that those are uncorrelated.

• Total photodetector noise current=quantum noise current +bulk dark current noise + surface current noise

Noise calculation :

Quantum noise current (lower limit on the sensitivity):

$$\langle i_Q^2 \rangle = \sigma_Q^2 = 2qI_P BM^2 F(M)$$

B: Bandwidth, *F(M)* is the noise figure and generally is

$$F(M) \approx M^x \quad 0 \le x \le 1.0$$

Bulk dark current noise:

$$\langle i_{DB}^2 \rangle = \sigma_{DB}^2 = 2qI_D BM^2 F(M)$$

Surface dark current noise

$$\langle i_{DS}^2 \rangle = \sigma_{DS}^2 = 2qI_L B$$

The total rms photodetector noise current is:

$$\langle i_N^2 \rangle = \sigma_N^2 = \langle i_Q^2 \rangle + \langle i_{DB}^2 \rangle + \langle i_{DS}^2 \rangle$$
$$= 2q(I_P + I_D) BM^2 F(M) + 2qI_L B$$

The thermal noise of amplifier connected to the photodetector is:

$$\langle i_T^2 \rangle = \sigma_T^2 = \frac{4k_B TB}{R_L}$$

2. S/N Calculation:

Having obtained the signal and total noise, the signal-to-noise-ratio can be written as:

$$\frac{S}{N}=\frac{\langle i_P^{\,2}\rangle M^2}{2q(I_P+I_D)BM^2F(M)+2qI_LB+4k_BTB/R_L}$$

Since the noise figure *F(M)* increases with M, there always exists an optimum value of *M* that maximizes the S/N. For sinusoidally modulated signal with *m=1* and *F*(*M*) = *Mx*

$$M_{\text{opt}}^{x+2}=\frac{2qI_L+4k_BT/R_L}{xq(I_P+I_D)}$$

Photodetector Response Time

The response time of a photodetector with its output circuit depends mainly on the following three factors:

1- The transit time of the photocarriers in the depletion region. The transit time depends on the carrier drift velocity and the depletion layver width *w*, and is given by:

$$t_d=\frac{W}{v_d}$$

2- Diffusion time of photocarriers outside depletion region.

3- *RC* time constant of the circuit

$$B=\frac{1}{2\pi R_TC_T}$$

$$R_T=R_s\parallel R_L \text{ and } C_T=C_a+C_d$$

SOURCES AND DETECTORS

1. What are the advantages of optical communication?

1. Low transmission loss.

2 Small size and weight.

3. No electromagnetic interference.

4. Electrical isolation.

2. Define direct band gap materials and indirect band gap materials.

In direct band gap materials direct transition is possible from valence band to conduction band.e.g.GaAs,InP,InGaAs In indirect band gap materials direct transition is not possible from valence band to conduction.e.g.silicon,germanium.

3. What are the advantages of LED?

1. LEDs are less complex circuits than Laser diodes.

2. Fabrication is easier.

3. They have long life.

4. What are the two types of confinement used in LEDs?

1. Optical confinement.

2. Carrier confinement.

5. What are the two types of LED configurations?

1. Homo junction

2. Single and double hetero junction.

6. What are the three requirements of Laser action?

1. Absorption

2. Spontaneous emission

3. stimulated emission.

7. What are the three types of Laser diode structures?

1. Gain indexed guide

2. Positive indexed guide

3.Negative indexed guide

8. What are the fundamental structures of Index guided lasers?

1. buried hetero structure.

2. Selectively diffused construction

3. Varying thickness structure

4. Bent layer configuration.

9. What are the three basic methods of current confinement?

1. Preferential dopant diffusion.

2. Proton implantation

3. Inner strip confinement

4. Re growth of back biased PN junction.

10. Define modulation.

The process of imposing information on a light stream is called modulation. This can be achieved by varying the laser drive current.

11. Define external quantum efficiency.

The external quantum efficiency is defined as the number of photons emitted per radiative electron-hole pair recombination above threshold.

12. Define threshold current.

The threshold current is conventionally defined by extrapolation of the lasing region of the power-versus-current curve. At high power outputs, the slope of the curve decreases because of junction heating.

13. Define longitudinal modes.

Longitudinal modes are associated with the length of the cavity and determine the typical spectrum of the emitted radiation.

14. Define lateral modes.

These modes lie in the plane o f t he p n junction. They depend on the side wall preparation and the width of the cavity. It determines the shape of the lateral profile of the laser beam.

15. Define transverse modes.

Transverse modes are associated with the electromagnetic field and beam profile in the direction perpendicular to the plane of the pn junction. They determine the laser characteristics as the radiation pattern and the threshold current density.

16. Define population inversion.

Stimulated emission will exceed absorption only if the population of the excited states is greater than that of the ground state. This condition is called as population inversion

17. Define internal quantum efficiency.

The internal quantum efficiency is the fraction of the electron-hole pairs that recombine radiatively. If the radiative recombination rate is R and the non-radiative recombination rate is Rnr, then the internal quantum efficiency is the ratio of the ratio of the radiative recombination rate to the total recombination rate.

18. Differentiate LEDs and Laserdiodes.

LED

1. The output obtained is incoherent.
2. Less expensive and less complex

3. Long lifetime.

Laser diode

1. The output obtained is coherent.
2. More expensive and more complex.
3. Less lifetime.

Where p-- concentration of holes.

n concentration of electrons.

Ni intrinsic concentration.

20. What is an intrinsic and extrinsic semiconductor material?

Intrinsic semiconductors have no impurities.

Extrinsic semiconductors contain impurities like boron and phosphorus.

21. Define responsivity

The performance o f an avalanche photodiode is characterized by its responsivity

RAPD= $\frac{\eta q M}{h v}$ = Ro M hv

where

Ro is the unity gain responsivity.

22. Define long wavelength cut off related to photodiode.

The upper wavelength cutoff (λc) is determined by the band gap energy Eg of the material. If Eg is expressed in units of electron volts(eV),then λc is given in units of micrometers (μm) by

$$\lambda c(\mu m) = \frac{hc}{Eg} = \frac{1.24}{Eg(eV)}$$

23. Give some types of photodetectors.

- Photomultipliers

- Pyroelectric detectors
- Semiconductor- based detectors
- Phototransistors
- Photodiodes

24. What are the advantages of photodiodes?

a. Small size

b. Suitable material c. High sensitivity

d. Fast response time

25. What are the types of photodiodes?

- PIN photodetector
- Avalanche photodiode(APD)

26. Define photocurrent.

The high electric field present in the depletion region causes the carriers to separate and be collected across the reverse-biased junction. This gives to a current flow in the external circuit, with one electron flowing for every carrier pair generated. This current flow is known as photocurrent.

27. Define quantum efficiency.

It is defined as the number of the electron – hole pairs generated per incident photon of energy hv and is given by

n=No.of electron-hole pairs generated / No. of incident photons

28. Define impact ionization.

In order for carrier multiplication to take place, the photo generated carriers must traverse a region where a very high electric field is present. In this high field region, a photo generated electron or hole can gain energy so that it ionizes bound electrons in the valence band upon colliding with them. This carrier multiplication mechanism is known as impact ionization.

29. Define avalanche effect.

The newly created carriers are accelerated by the high electric field, thus gaining enough energy to cause further impact ionization. This phenomenon is called avalanche effect.

30. What is p+ ∏ p n+ reach- through structure?

The reach –through avalanche photodiode (RAPD) is composed of a high resistivity p-type material deposited as an epitaxial layer on a p+ substrate. A p- type diffusion is then made in the high resistivity material, followed by the construction of an n+ layer. The configuration is called p+ ∏ p n+ reach- through structure.

GLOSSARY

1. Direct band gap materials and indirect band gap materials.

In direct band gap materials direct transition is possible from valence band to conduction band.e.g.GaAs,InP,InGaAs In indirect band gap materials direct transition is not possible from valence band to conduction.e.g.silicon,germanium.

2. Advantages of LED.

1. LEDs are less complex circuits than Laser diodes.
2. Fabrication is easier.
3. They have long life.

3. Two types of confinement used in LEDs.

1. Optical confinement.
2. Carrier confinement.

4. Modulation.

The process of imposing information on a light stream is called modulation. This can be achieved by varying the laser drive current.

5. External quantum efficiency.

The external quantum efficiency is defined as the number of photons emitted per radiative electron-hole pair recombination above threshold.

6. Threshold current.

The threshold current is conventionally defined by extrapolation of the lasing region of the power-versus-current curve. At high power outputs, the slope of the curve decreases because of junction heating.

7. Longitudinal modes.

Longitudinal modes are associated with the length of the cavity and determine the typical spectrum of the emitted radiation.

8. Lateral modes.

These modes lie in the plane of the p n junction. They depend on the side wall preparation and the width of the cavity. It determines the shape of the lateral profile of the laser beam.

9. Transverse modes.

Transverse modes are associated with the electromagnetic field and beam profile in the direction perpendicular to the plane of the pn junction. They determine the laser characteristics as the radiation pattern and the threshold current density.

10. Population inversion.

Stimulated emission will exceed absorption only if the population of the excited states is greater than that of the ground state. This condition is called as population inversion

11. Internal quantum efficiency.

The internal quantum efficiency is the fraction of the electron-hole pairs that recombine radiatively. If the radiative recombination rate is R and the non-radiative recombination rate is Rnr, then the internal quantum efficiency is the ratio of the ratio of the radiative recombination rate to the total recombination rate.

12. Intrinsic and extrinsic semiconductor material.

Intrinsic semiconductors have no impurities.

Extrinsic semiconductors contain impurities like boron and phosphorus.

13. Responsivity

The performance o f an avalanche photodiode is characterized by its responsivity

RAPD= ηqM = Ro M hv

where

Ro is the unity gain responsivity.

14. Long wavelength cut off related to photodiode.

The upper wavelength cutoff (λc) is determined by the band gap energy Eg of the material. If Eg is expressed in units of electron volts(eV),then λc is given in units of micrometers (μm) by

$$\lambda c(\mu m) = \frac{hc}{Eg} = \frac{1.24}{Eg(eV)}$$

15. Photocurrent.

The high electric field present in the depletion region causes the carriers to separate and be collected across the reverse-biased junction. This gives to a current flow in the external circuit, with one electron flowing for every carrier pair generated. This current flow is known as photocurrent.

16. Quantum efficiency.

It is defined as the number of the electron – hole pairs generated per incident photon of energy hv and is given by

n=No.of electron-hole pairs generated /No. of incident photons

17. Impact ionization.

In order for carrier multiplication to take place, the photo generated carriers must traverse a region where a very high electric field is present. In this high field region, a photo generated electron or hole can gain energy so that it ionizes bound electrons in the

valence band upon colliding with them. This carrier multiplication mechanism is known as impact ionization.

18. Avalanche effect.

The newly created carriers are accelerated by the high electric field, thus gaining enough energy to cause further impact ionization. This phenomenon is called avalanche effect.

UNIT – 4

OPTICAL RECEIVER, MEASUREMENTS AND COUPLING

Fundamental Receiver Operation

✓…Digital Signal Transmission

✓…Error Sources

• Digital Receiver Performance

✓…Probability of Error

✓…Receiver Sensitivity

✓…The Quantum Limit

• Coherent Detection

• Analog Receiver

1. Optical Receiver Operation

Digital Signal Transmission

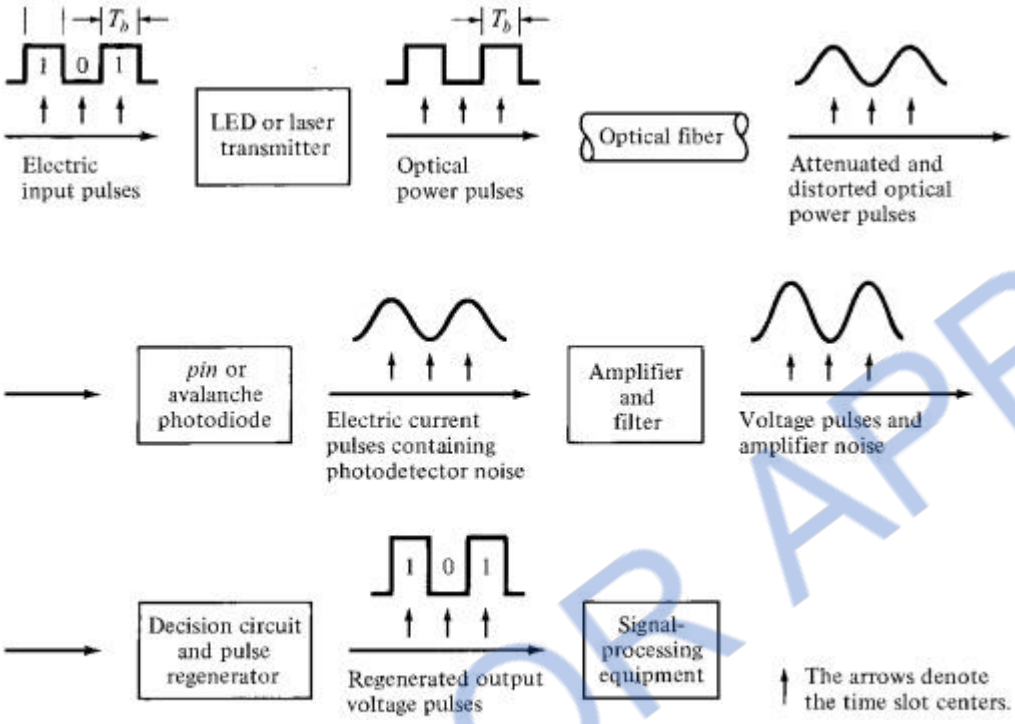

Figure 4.1 Signal path through an optical data link.

✓⋯A typical digital fiber transmission link is shown in Figure 4.1. The transmitted signal is a two-level binary data stream consisting of either a '0' or a '1' in a *bit period* *T*b.

✓⋯The simplest technique for sending binary data is *amplitude-shift keying*, wherein a voltage level is switched between *on* or *off* values.

✓⋯The resultant signal wave thus consists of a voltage pulse of amplitude *V* when a binary 1 occurs and a zero-voltage-level space when a binary 0 occurs.

✓⋯An electric current $i(t)$ can be used to modulate directly an optical source to produce an optical output power $P(t)$.

✓⋯In the optical signal emerging from the transmitter, a '1' is represented by a light pulse of duration *T*b,whereas a '0' is the absence of any light.

✓…The optical signal that gets coupled from the light source to the fiber becomes attenuated and distorted as it propagates along the fiber waveguide. Upon reaching the receiver, either a PIN or an APD converts the optical signal back to an electrical format.

✓…A decision circuit compares the amplified signal in each time slot with a *threshold level*.

✓…If the received signal level is greater than the threshold level, a '1' is said to have been received.

✓…If the voltage is below the threshold level, a '0' is assumed to have been received.

2. Error Sources

✓…Errors in the detection mechanism can arise from various noises and disturbances associates with the signal detection system.

✓…The two most common samples of the spontaneous fluctuations are shot noise and thermal noise.

✓…Shot noise arises in electronic devices because of the discrete nature of current flow in the device.

✓…Thermal noise arises from the random motion of electrons in a conductor.

✓…The random arrival rate of signal photons produces a quantum (or shot) noise at the photodetector. This noise depends on the signal level.

✓…This noise is of particular importance for PIN receivers that have large optical input levels and for APD receivers.

✓…When using an APD, an additional shot noise arises from the statistical nature of the multiplication process. This noise level increases with increasing avalanche gain *M*.

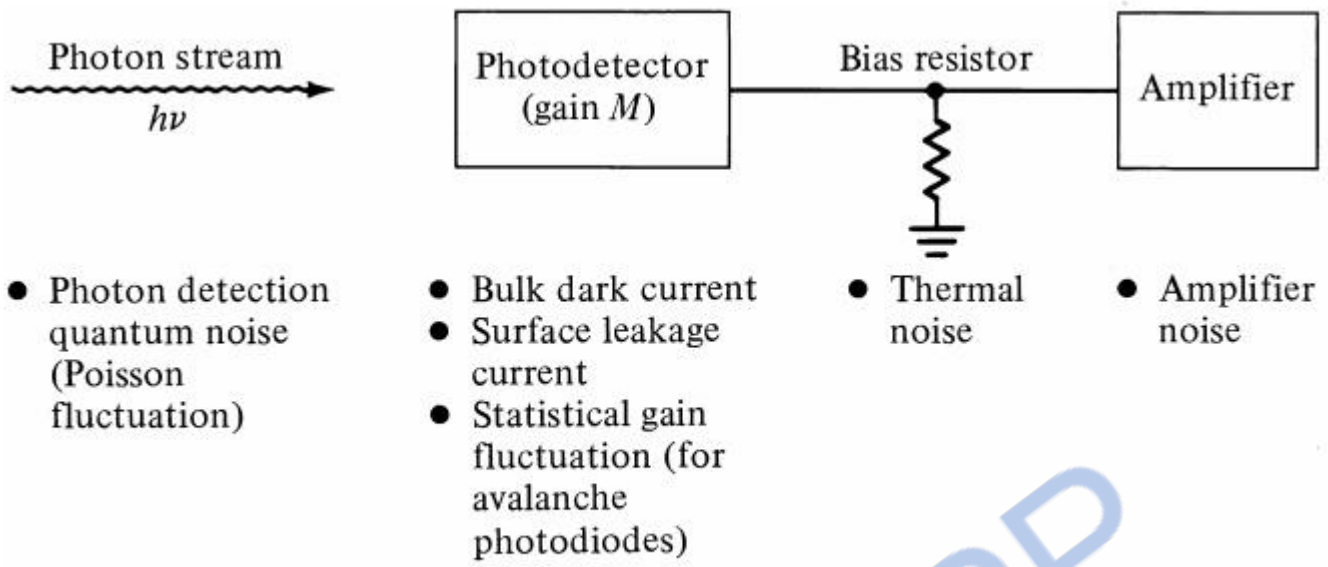

Figure 4.2 Noise sources and disturbances in the optical pulse detection mechanism.

✓⋯Thermal noises arising from the detector load resistor and from the amplifier electronics tend to dominate in applications with low SNR when a PIN photodiode is used.

✓⋯When an APD is used in low-optical-signallevel applications, the optimum avalanche gain is determined by a design tradeoff between the thermal noise and the gain-dependent quantum noise.

✓⋯The primary photocurrent generated by the photodiode is a time-varying Poisson process.

✓⋯If the detector is illuminated by an optical signal $P(t)$, then the average number of electron-hole pairs generated in a time t is

$$\overline{N} = \frac{\eta}{h\nu}\int_0^{\tau} P(t)dt = \frac{\eta E}{h\nu}$$

where h is the detector quantum efficiency, *h*n is the photon energy, and E is the energy received in a time interval .

✓⋯The actual number of electron-hole pairs n that are generated fluctuates from the average according to the Poisson distribution

$$P_r(n) = \overline{N}^n \frac{e^{-\overline{N}}}{n!}$$

where *P*r(*n*) is the probability that *n* electrons are emitted in an interval t

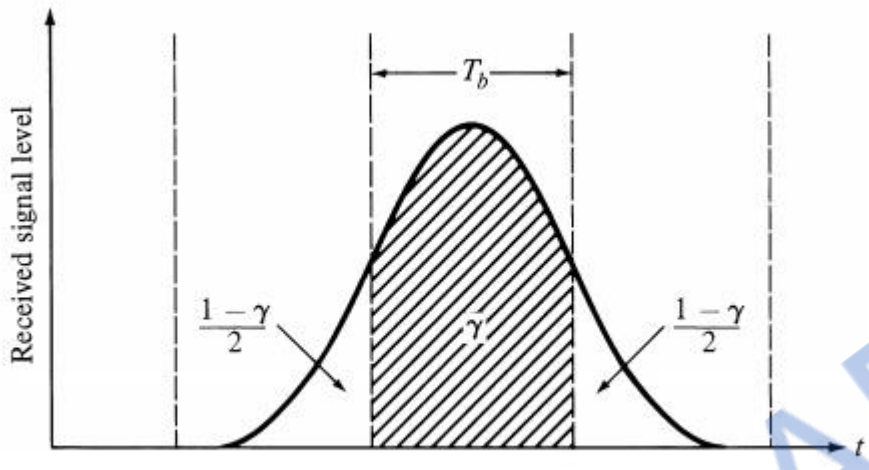

Figure 4.3 Pulse spreading in an optical signal that leads to ISI.

✓⋯For a detector with a mean avalanche gain *M* and an ionization rate ratio *k*, the excess noise factor *F*(*M*) for electron injection is

$$F(M) = kM + \left(2 - \frac{1}{M}\right)(1-k)$$

Or

$$F(M) \cong M^x$$

where the factor *x* ranges between 0 and 1.0 depending on the photodiode material.

✓⋯A further error source is attributed to *intersymbol interference* (ISI), which results from pulse spreading in the optical fiber.

✓⋯The fraction of energy remaining in the appropriate time slot is designated by g, so that 1-g is the fraction of energy that has spread into adjacent time slots.

Receiver Configuration

✓⋯A typical optical receiver is shown in Figure 4.4. The three basic stages of the receiver are a photodetector, an amplifier, and an equalizer.

✓⋯The photo-detector can be either an APD with a mean gain *M* or a PIN for which *M*=1.

✓⋯The photodiode has a quantum efficiency h and a capacitance *C*d.

✓⋯The detector bias resistor has a resistance *R*b which generates a thermal noise current *i*b(*t*).

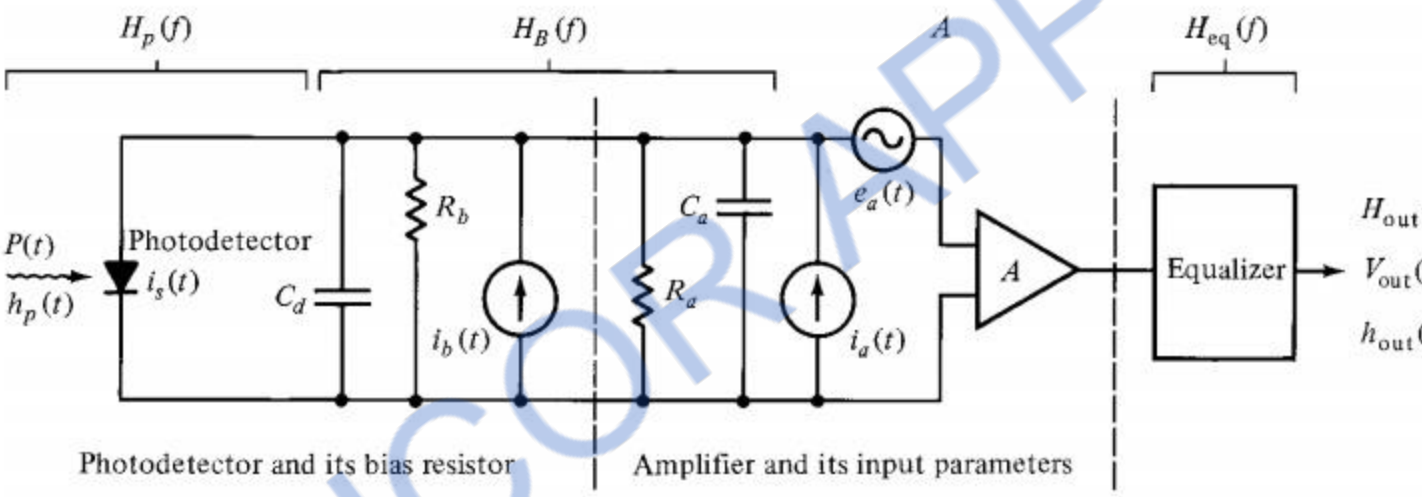

Figure 4.4 Schematic diagram of a typical optical receiver.

Amplifier Noise Sources:

✓⋯The input noise current source *i*a(*t*) arises from the thermal noise of the amplifier input resistance *R*a;

✓⋯The noise voltage source *ea*(*t*) represents the thermal noise of the amplifier channel.

✓⋯The noise sources are assumed to be Gaussian in statistics, flat in spectrum (which characterizes *white* noise), and uncorrelated (statistically independent).

The Linear Equalizer:

✓⋯The equalizer is normally a linear frequency shaping filter that is used to mitigate the effects of signal distortion and inter symbol interference (ISI).

✓⋯The equalizer accepts the combined frequency response of the transmitter, the fiber, and the receiver, and transforms it into a signal response suitable for the following signal processing electronics.

✓⋯The binary digital pulse train incident on the photo-detector can be described by

$$P(t) = \sum_{n=-\infty}^{\infty} b_n h_p(t - nT_b)$$

✓⋯Here, $P(t)$ is the received optical power, Tb is the bit period, bn is an amplitude parameter representing the nth message digit, and hp(t) is the received pulse shape.

✓ Let the nonnegative photodiode input pulse hp(t) be normalized to have unit area

$$\int_{-\infty}^{\infty} h_p(t)dt = 1$$

then bn represents the energy in the nth pulse.

✓⋯The mean output current from the photodiode at time t resulting from the pulse train given previously is

$$\langle i(t) \rangle = \frac{\eta q}{h\nu} MP(t) = R_0 \sum_{n=-\infty}^{\infty} b_n h_p(t - nT_b)$$

where Ro = hq/hn is the photodiode responsivity.

✓⋯The above current is then amplified and filtered to produce a mean voltage at the output of the equalizer.

PROBABLITY OF ERROR

•□□□□□□□□□□The digital receiver performance can be evolved by measuring of error and quantum limit.

•□□□□□□□□□□In practice, several standard ways are available to measuring the rate of error occurences in a digital data stream.

•□□□□□□□□□□**Bit error rate or the error rate [BER]**

Bit error rate is defined by the ratio between number of errors (Ne) occurring over a certain time interval t to the number of error (Nt) during this interval.

$$BER = \frac{N_e}{N_t} = \frac{N_e}{B_t}$$

Where B=1/T_b is the bit rate (is the pulse transmission rate).

•□□□□□□□□□□The error rates the optical fiber telecommunication system range from 10^{-9} to 10^{-12}.

•□□□□□□□□□□The probability distribution of signal at the equalizer output should be known to compute BER. Here the decision is made as to whether a 0 or a 1 is sent.

$$P_1(v) = \int_{-\infty}^{v} p(y/1)dy$$

$$P_0(v) = \int_{v}^{\infty} p(y/0)dy$$

P_1 (v) is the probability that the equalizer output voltage is less than v when log"1" is sent.

P_0 (v) is the probability that the equalizer output voltage exceeds "v" when logic 'o' is sent.

•□□□□□□□□□□The figure shows the probability distribution for received logic 0 and 1.The function P(y/1) and P(y/0) are the conditional probability distribution functions,

that is P(y/x) is the probability that the output voltage is y, given that an x was transmitted.

•□□□□□□□□□□If the threshold voltage is v_{th} then the error probability P_e is defined as

$$P_e = a\,P_1(v_{th}) + b\,P_0(v_{th})$$

•□□□□□□□□□□The weighing factors a and b determined by the priori distribution of the data and b are the probabilities that either a 1 or 0 occurs.

•□□□□□□□□□□To calculate the "p_e", the mean and standard deviation of the output voltage V_{out} (t) should be known.

•□□□□□□□□□□Thus, let us assume that a signal S (Which can be either a noise disturbance or a desired information bearing signal) has a Gaussian probability distribution function with a mean value m.

$$f(s)\,ds = \frac{1}{\sqrt{2\pi\sigma^2}}\,e^{-(s-m)^2/2\sigma^2}\cdot ds$$

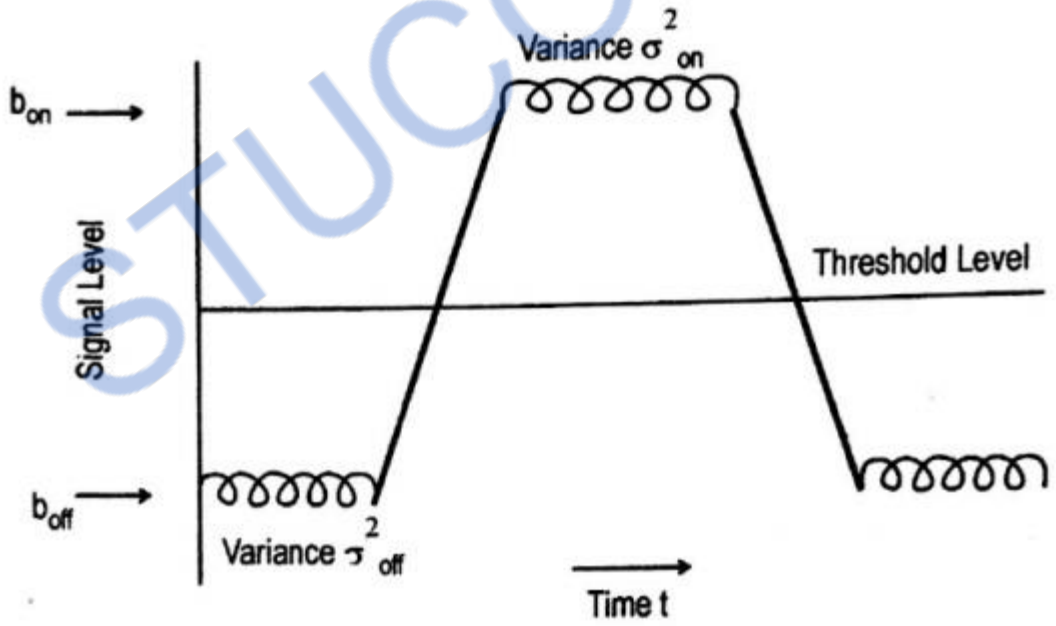

Figure 4.5 Gaussian Noise Statistics of a Binary Signal

•□□□□□□□□□□Now, we can use the probability density function to determine the probability of error for a data stream in which the 1 pulse are all of amplitude V.

•□□□□□□□□□□The above figure shows, the mean and variance of the Gaussian output for a 1 pulse are b_{on} and σ_{on2}, respectively, whereas for a 0 pulse they are b_{off} and σ_{off2}, respectively.

PROBABILITY OF ERROR WHEN 0 PULSE SENT

•□□□□□□□□□□Let us first consider the case of o pulse being sent. So that no pulse is present at the decoding time. The probability that noise will exceed the threshold voltage v_{th} and be 1 pulse.

$$P_0(v_{th}) = \int_{v_{th}}^{\infty} p(y/0)dy = \int_{v_{th}}^{\infty} f_0(y)dy$$

$$= \frac{1}{\sqrt{2\pi}\,\sigma_{off}} \int_{v_{th}}^{\infty} \exp\left[-\frac{(v-b_{off})^2}{2\sigma_{off}^2}\right] dv$$

•□□□□□□□□□□Where the subscript 0 denotes the presence of a 0 bit.

PROBABILITY OF ERROR WHEN 1 PULSE SENT

•□□□□□□□□□□Transmitted pulse 1 is misinterpreted as a o by the electronics following the equalizer.

$$P_1(v_{th}) = \int_{-\infty}^{v_{th}} p(y/1)dy = \int_{-\infty}^{v_{th}} f_1(v)dv$$

$$= \frac{1}{\sqrt{2\pi}\,\sigma_{on}} \int_{-\infty}^{v_{th}} \exp\left[-\frac{(b_{on}-v)^2}{2\sigma_{on}^2}\right] dv$$

Where the subscript 1 denotes the presence of a 1 bit.

QUANTUM LIMIT

•□□□□□□□□□□An ideal photodetector which has unity quantum efficiency and which produces no dark current, that is no electron holde pairs are generated in the absence of an optical pulse.

QUANTUM LIMIT

•□□□□□□□□□□This condition, it is possible to find the minimum received optical power required for a specific nit error rate performance in a digital syatem. This minimum received power level is known as the quantum limit.

•□□□□□□□□□□Assume an optical pulse of energy E falls on the photodeetector in a time interval τ. This can only be interpreted by the receiver as a 0 pulse if no electron hole pairs are generated with the pulse with the pulse present.

•□□□□□□□□□□The probability that n=0 electrons are emitted in a time interval τ is

$$P_r(o) = e^{-\overline{N}}$$

where the average number of electron-hole pairs, $\overline{N} = \eta E / hv$.

•□□□□□□□□□□Thus for a given probability $P_r(o)$, we can find the minimum energy E required at a specific wavelength λ.

Pre Amplifier

The receiver amplifier are the front end preamplifier. The three basic preamplifier structures are:

(1) Low impedance preamplifier

(2) High impedance preamplifier

(3) Trans impedance preamplifier

Advantages Of Pre-Amplifier

A preamplifier should satisfy the following requirements: low noise level, high bandwidth, high dynamic range, high sensitive and high gain.

1. Low Impedance Preamplifier

•□□□□□□□□□□□Photo diode operates in to a low impedance amplifier bias or load resistor "Rb" is used to match the amplifier impedance.

•□□□□□□□□□□□Rb along with the input capacitance of amplifier decides the bandwidth of amplifier.

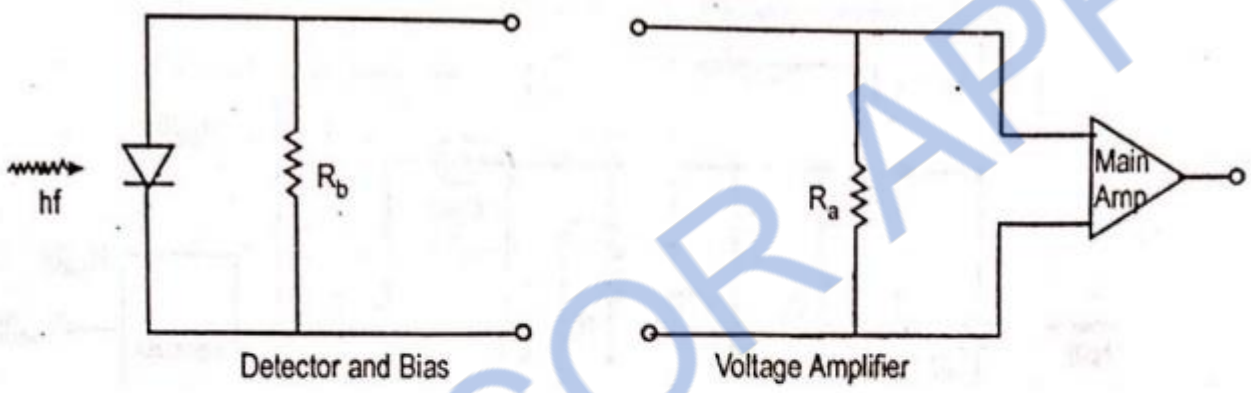

Figure 4.6 Simple Low Impedance Preamplifier Design

$$\text{The total load resistance, } R_{TL} \doteq \frac{R_b R_a}{R_b + R_a}$$

•□□□□□□□□□□□Low impedance preamplifier can operate over a wide bandwidth but they have poor receiver sensitivity.

•□□□□□□□□□□□They are used in special short distance application where high sensitivity is not a major concern.

2. High Impedance Preamplifier

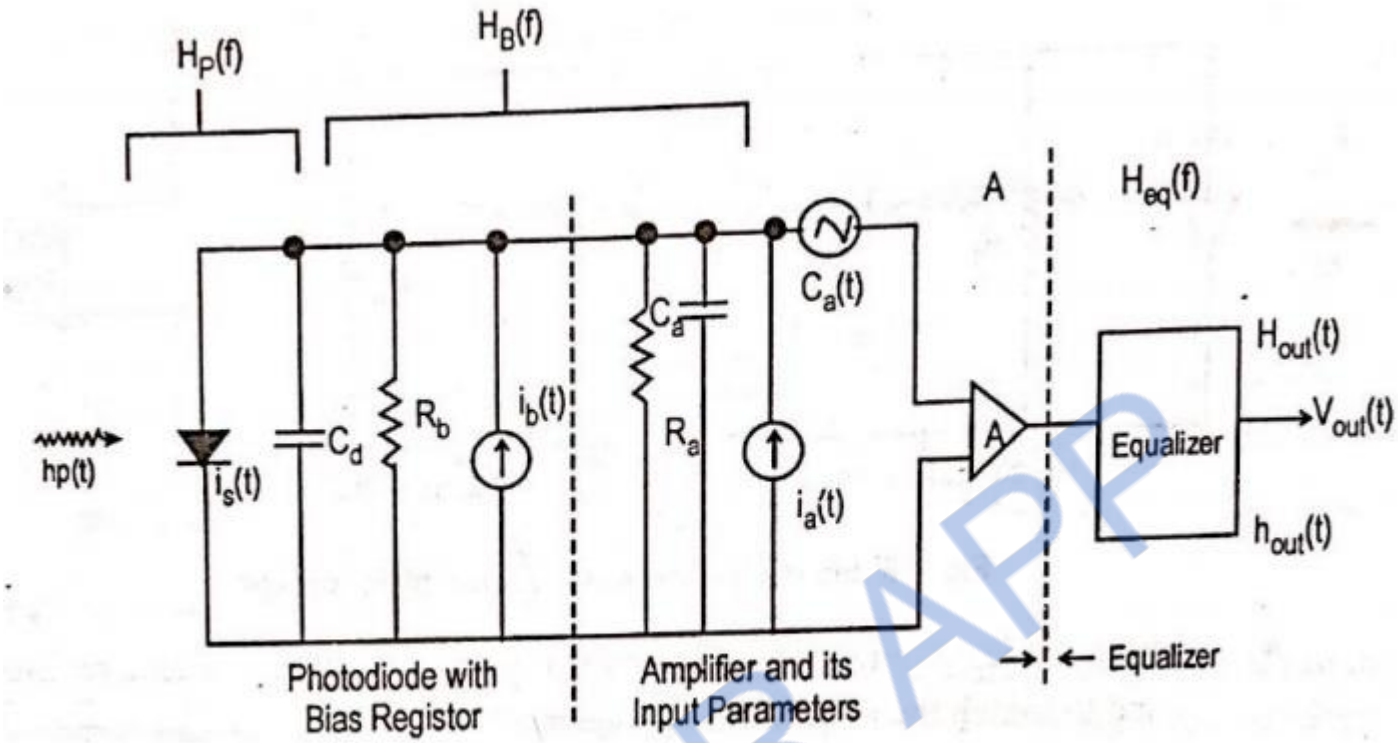

Figure 4.7 Preamplifier Design High Impedance.

•□□□□□□□□□□The second configuration consists of a high input impedance amplifier together with a large detector bias resistor (R_a) in order to reduce the effect of thermal noise.

•□□□□□□□□□□In high impedance preamplifier, the goal is to reduce all sources of noise to the absolute minimum. This can be achieved by reducing input capacitance through the selection of low capacitance high frequency devices.

•□□□□□□□□□□Selecting detectors with low dark currents.

•□□□□□□□□□□Minimizing thermal noise of biasing resistors.

•□□□□□□□□□□Using high impedance amplifier with large R_b (eg., a dipolar transistor or a field effect transistor (FET)).

•□□□□□□□□□□The high impedance procedure a large input RC time constant, the front end bandwidth is less than signal bandwidth. Thus, the input signal is integrated and equalization techniques must be employed to compensate for this.

High Impedance FET Preamplifier

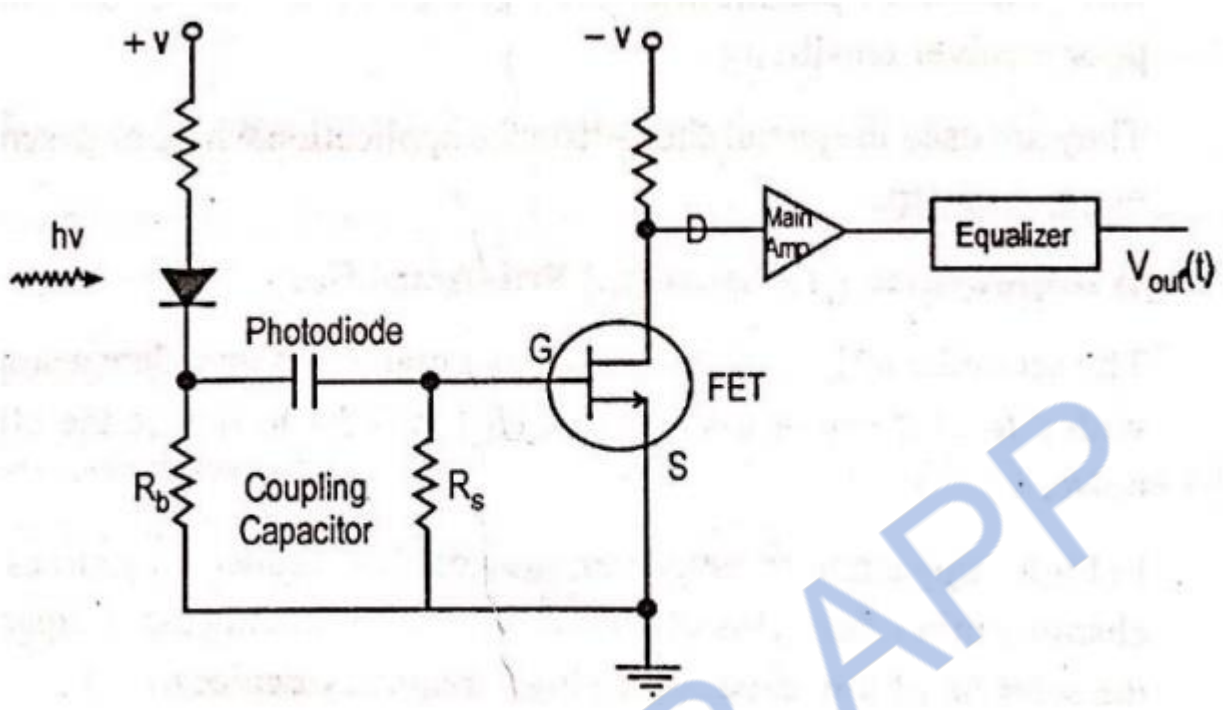

Figure 4.8 High Impedance Preamplifier Design Using FET

•□□□□□□□□□□□For giga bit per second data rates, the lowest noise receivers are made using GaAs MOSFET (metal oxide semiconductor field effect transistor) preamplifiers.

•□□□□□□□□□□□At low frequencies, silicon MOSFETs (metal oxide semiconductor field effect transistors) or JFET are generally used.

Basic Noise Sources in the Circuit are:

•□□□□□□□□□□□Thermal noise associated with FET channel conductance.

•□□□□□□□□□□□Thermal noise from load or feedback resistor.

•□□□□□□□□□□□Shot noise due to gate leakage current.

•□□□□□□□□□□□A fourth noise source is FET 1/*f* noise.

•□□□□□□□□□□□This (1/*f* noise) was not include in the above analyses because it contributes to the overall noise only at very low bit rates.

•□□□□□□□□□□□As he amplifier input resistance is very high, the input current noise spectral density S_1 is

$$S_{I,\,FET} = \frac{4K_BT}{R_a} + 2q\,I_{gate}$$

•□□□□□□□□□□□FET has very large input resistance "R_a" usually greater than $10^6\Omega$ for practical purpose R_e=infinity.

$$S_{I,\,FET} \approx 2\,q\,I_{gate}$$

Where I_{gate} is the channel noise factor.

•□□□□□□□□□□□The thermal noise of the conducting channel resistance is characterized by the transconductance g_m.

•□□□□□□□□□□□The voltage noise spectral density is

$$S_E = \frac{4K_BT\Gamma}{g_m}$$

where Γ is the channel-noise factor.

•□□□□□□□□□□□Γ́ is a numerical that accounts for thermal noise and gate included noise plus the correlation between these two noises.

•□□□□□□□□□□□Thermal noise characteristic equation Ω is a very useful figure of merit for a receiver as it measures

$$W = \frac{1}{q^2 B}\left(S_I + \frac{4K_B T}{R_b} + \frac{S_E}{R^2}\right) I_2 + \frac{(2\pi c)^2}{q^2} S_E I_3 B ,$$

Substituting S_I and S_E, the equalizer output w is

$$W = \frac{1}{q^2 B}\left(2q\, I_{gate} + \frac{4K_B T}{R_b} + \frac{4K_B T\Gamma}{g_m R_b^2}\right) I_2 + \left(\frac{2\pi c}{q}\right)^2 \frac{4K_B T\Gamma}{g_m} I_3 B$$

where $C = C_d + C_{gs} + C_{gd} + C_a$

C_{gs} is the FET gate-source capacitance.

C_{gd} is the FET gate-drain capacitance.

•□□□□□□□□□□□The 1/*f* noise corner frequency f_c is defined as the frequency at which 1/*f* noise, which dominates the FET noise at low frequencies and has 1/*f*power spectrum, becomes equal frequency channel noise described by Γ́.

•□□□□□□□□□□□To minimize the noise in a high impedance design, the bias resistor shoud be very large. The effect of this is the detector output signal is integrated by the amplifier input resistance.

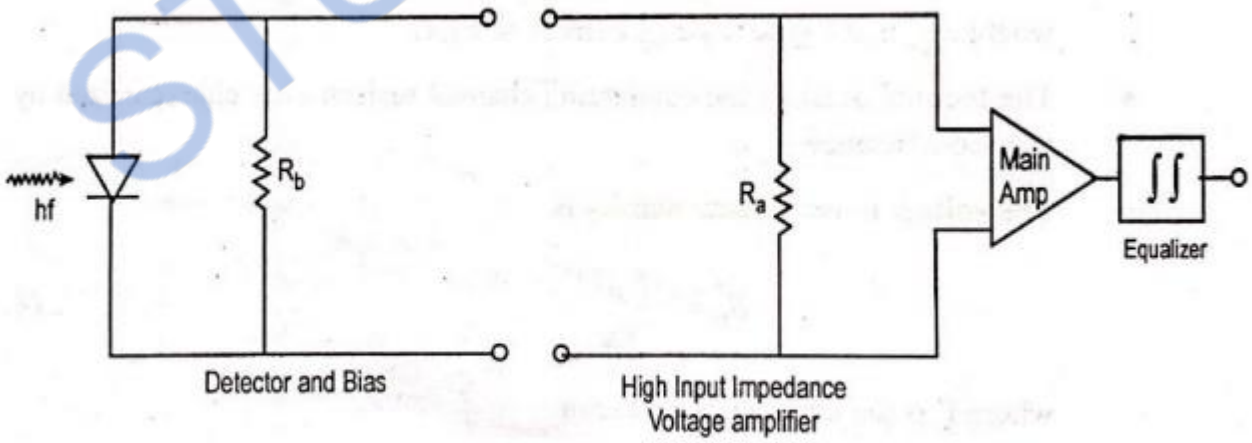

Figure 4.9 Equivalent Circuit to Minimize Noise

•□□□□□□□□□□It is compensated by differentiation in the equalizing fitter. This integration differentiation approach is known as the high impedance amplifier design technique.

High Impedance BJT Preamplifier

•□□□□□□□□□□The circuit shows a simple bipolar grounded emitter transistor amplifier.

•□□□□□□□□□□The input (R_{in}) of a bipolar transistor is given as

$$R_{in} = \frac{K_B T}{q I_{BB}}$$

where I_{BB} is base bias current.

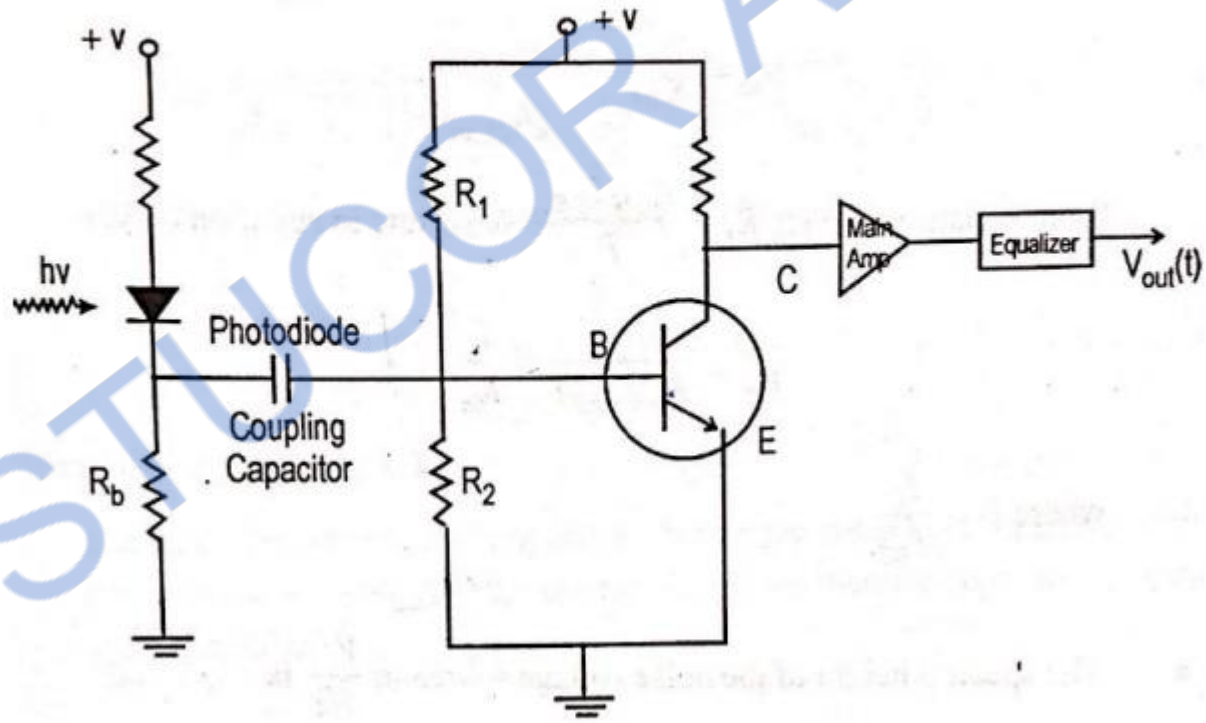

Figure 4.10 High Impedance Preamplifier Design Using FET

•□□□□□□□□□□The amplifier input resistance R_a is given by the parallel combination of the bias resistor R_1 and R_2 and the transistor input resistance R_{in}.

•□□□□□□□□□□□For low noise design ($R_1+R_2>>R_{in}$)

$R_a \sim = R_{in}$

•□□□□□□□□□□□The spectral density (A^2/Hz) of the input noise current source which results from shot noise of the base current is

$$S_I = 2q\ I_{BB}$$

W.K.T $q = \dfrac{K_B T}{R_{in} I_{BB}}$

Now

$$S_I = \frac{2K_B T}{R_{in}}$$

•□□□□□□□□□□□The transconductance g_m is related to the shot noise and is given by

$$g_m = \frac{q I_c}{K_B I}$$

W.K.T $K_B = \dfrac{R_{in} q I_{BB}}{T}$

Now

$$g_m = \frac{q I_c T}{R_{in} q I_{BB} T} = \frac{\beta}{R_{in}}$$

where $\beta = \dfrac{I_C}{I_{BB}}$.

•□□□□□□□□□□□The spectral height of the noise voltage source in V^2/Hz is

$$S_E = \frac{2K_B T}{g_m}$$

Where k_b is the boltzmann's constant.

Thermal Noise Characteristic Equation for Receiver Amplifier

•□□□□□□□□□□The performance of receiver isexpressed by thermal noise characteristic equation (W).

$$W = \frac{1}{q^2 B}\left(S_I + \frac{4K_B T}{R_b} + \frac{S_E}{R^2}\right) I_2 + \frac{(2\pi c)^2}{q^2} S_E I_3 B$$

Substituting R_{in}, S_1,S_E in characteristic equation

Substitute B & g_m in W, We get:

$$W = \frac{T_b}{q^2} 2K_B T \left[\left(\frac{1}{R_{in}} + \frac{2}{R_b} + \frac{R_{in}}{\beta R^2}\right)\right] I_2 + \frac{(2\pi c)^2}{T_b q^2}\left(\frac{R_{in}}{\beta}\right) I_3$$

If $R_b >> R_a$ then $R_a \approx R_{in}$,

$$W = \frac{2K_B T}{q^2}\left[\frac{T_b}{R_{in}} \cdot \frac{\beta+1}{\beta} I_2 + \frac{(2\pi c)^2}{\beta T_b} R_{in} I_3\right]$$

Transimpedance Preamplifier

•□□□□□□□□□□The transimpedance amplifier is nothing but the low noise high impedance amplifier with a negative feedback 'R_f' resistor, the device therefore operates as a current mode amplifier.

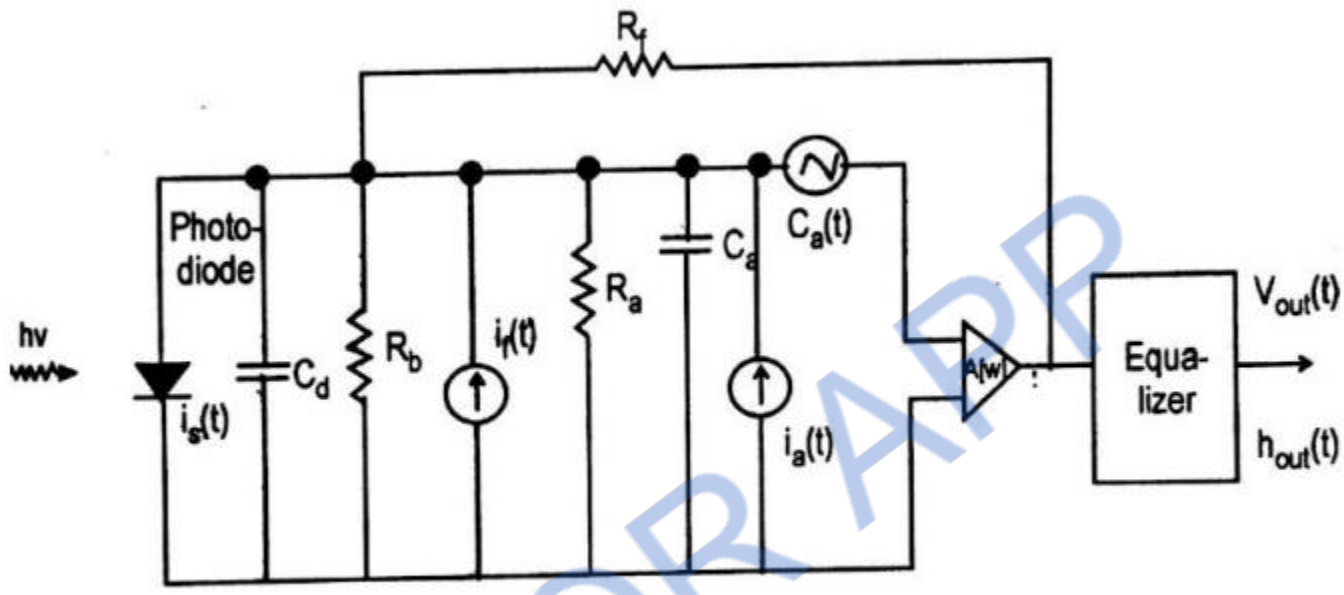

Figure 4.11 Equivalent Circuit of the Transimpedance Receiver Design

•□□□□□□□□□□Transimpedance amplifier design overcomes the drawbacks of high impedance amplifier. Such as

(1) For broadband applications, equalization is required.

(2) It has limited dynamic range.

•□□□□□□□□□□The thermal noise characteristic 'W_{TZ}' at equalizer output can be found by replacing R_b and R_b'.

•□□□□□□□□□□□The thermal noise characteristics are the sum of output noise of a non-feedback amplifier plus the thermal noise associated with the feedback resistance.

Transfer Function of Non-Feedback Amplifier

•□□□□□□□□□□□The transfer function of non-feedback amplifier is given by

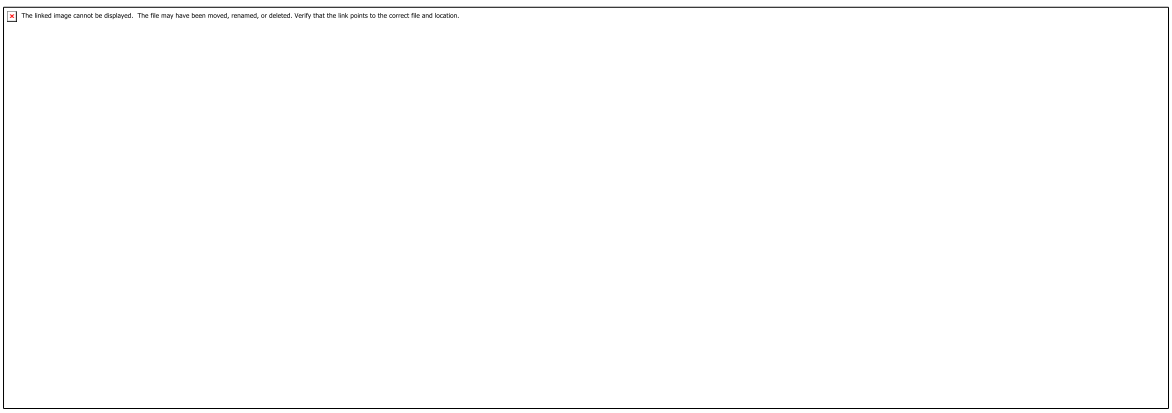

•□□□□□□□□□□□The bandwidth of non-feedback amplifier is B=1/4RC

Advantages of Transimpedance Amplifier:

(1) Wide dynamic range.

(2) Little or no equalization is required.

(3) Less susceptible to pick up noise, cross talk, EMI.

(4) It is very easily controllable and stable.

(5) Loss sensitivity.

(6) Output resistance is small.

Fiber attenuation measurements

Fiber attenuation measurement techniques have been developed in order to determine the total fiber attenuation of the relative contributions to this total from both absorption losses and scattering losses. The overall fiber attenuation is of greatest interest to the system designer, but the relative magnitude of the different loss mechanisms is important in the development and fabrication of low-loss fibers. Measurement techniques to obtain the total fiber attenuation give either the spectral loss characteristic or the loss at a single wavelength (spot measurement).

1. Total fiber attenuation

A commonly used technique for determining the total fiber attenuation per unit length is the cut-back or differential method. Figure 4.5 shows a schematic diagram of the typical experimental setup for measurement of the spectral loss to obtain the overall attenuation spectrum for the fiber. It consists of a ‘white’ light source, usually a tungsten halogen or xenon are lamp. The focused light is mechanically chopped at a low frequency of a few hundred hertz. This enables the lock-in amplifier at the receiver to perform phase-sensitive detection.

The chopped light is then fed through a monochromator which utilizes a prism or diffraction grating arrangement to select the required wavelength at which the attenuation is to be measured. Hence the light is filtered before being focused onto the fiber by means of a microscope objective lens. A beam splitter may be incorporated before the fiber to provide light for viewing optics and a reference signal used to compensate for output power fluctuations.

When the measurement is performed on multimode fibers it is very dependent on the optical launch conditions. Therefore unless the launch optics are arranged to give the steady-state mode distribution at the fiber input, or a dummy fiber is used, then a mode scrambling device is attached to the fiber within the first meter.

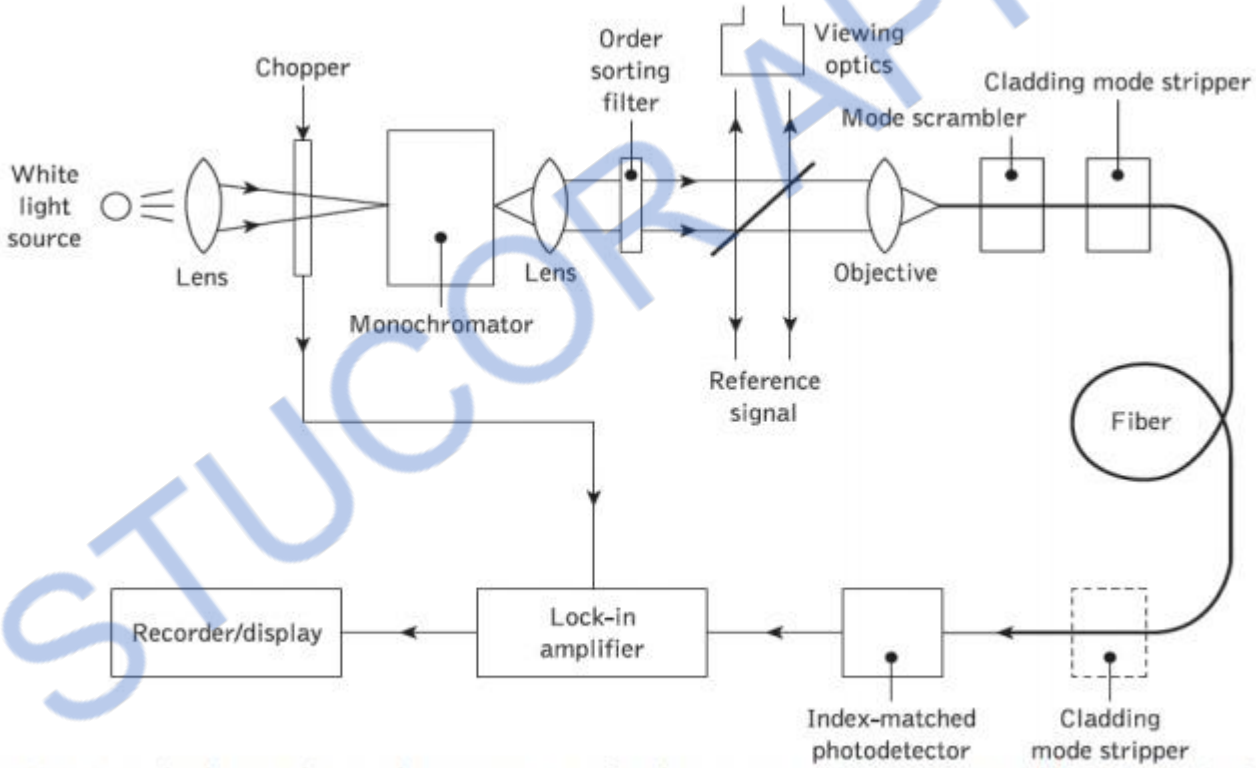

Figure 4.5 A typical experimental arrangement for the measurement of spectral loss in optical fibers using the cut-back technique

The fiber is also usually put through a cladding mode stripper, which may consist of an S-shaped groove cut in the Teflon and filled with glycerine. This device removes light launched into the fiber cladding through radiation into the index-matched (or slightly higher refractive index) glycerine. A mode stripper can also be included at the fiber output end to remove any optical power which is scattered from the core into the

cladding down the fiber length. This tends to be pronounced when the fiber cladding consists of a low-refractive-index silicone resin.

The optical power at the receiving end of the fiber is detected using a *p–i–n* or avalanche photodiode. In order to obtain reproducible results the photodetector surface is usually index matched to the fiber output end face using epoxy resin or an index-matching gell. Finally, the electrical output from the photodetector is fed to a lock-in amplifier, the output of which is recorded.

The cut-back method* involves taking a set of optical output power measurements over the required spectrum using a long length of fiber (usually at least a kilometer). This fiber is generally uncabled having only a primary protective coating. Increased losses due to cabling do not tend to change the shape of the attenuation spectrum as they are entirely radiative, and for multimode fibers are almost wavelength independent.

The fiber is then cut back to a point 2 m from the input end and, maintaining the same launch conditions, another set of power output measurements is taken.

$$\alpha_{\mathrm{dB}} = \frac{10}{L_1 - L_2} \log_{10} \frac{P_{02}}{P_{01}}$$

$L1$ and L_2 are the original and cut-back fiber lengths respectively, and P_{01} and P_{02} are the correspondingoutput optical powers at a specific wavelength from the original and cut-back fiber lengths. Hence when

$L1$ and L_2 are measuredin kilometers, αdB has units of dB km^{-1}.

$$\alpha_{\mathrm{dB}} = \frac{10}{L_1 - L_2} \log_{10} \frac{V_2}{V_1}$$

where V_1 and V_2 correspond to output voltage readings from the original fiber length and the cut-back fiber length respectively.

2. Fiber absorption loss measurement

It was indicated in the preceding section that there is a requirement for the optical fiber manufacturer to be able to separate the total fiber attenuation into the contributions from

the major loss mechanisms. Material absorption loss measurements allow the level of impurity content within the fiber material to be checked in the manufacturing process.

The measurements are based on calorimetric methods which determine the temperature rise in the fiber or bulk material resulting from the absorbed optical energy within the structure. The apparatus shown in Figure 4.6, which is used to measure the absorption loss in optical fibers, was modified from an earlier version which measured the absorption losses in bulk glasses. This temperature measurement technique, illustrated diagrammatically in Figure 4.6(b), has been widely adopted for absorption loss measurements.

The two fiber samples shown in Figure 4.6(b) are mounted in capillary tubes surrounded by a low-refractive-index liquid (e.g. methanol) for good electrical contact, within the same enclosure of the apparatus shown in Figure 4.6(a). A thermocouple is wound around the fiber containing capillary tubes using one of them as a reference junction (dummy fiber).

Light is launched from a laser source (Nd : YAG or krypton ion depending on the wavelength of interest) through the main fiber (not the dummy), and the temperature rise due to absorption is measured by the thermocouple and indicated on a nanovoltmeter. Electrical calibration may be achieved by replacing the optical fibers with thin resistance wires and by passing known electrical power through one. Independent measurements can then be made using the calorimetric technique and with electrical measurement instruments.

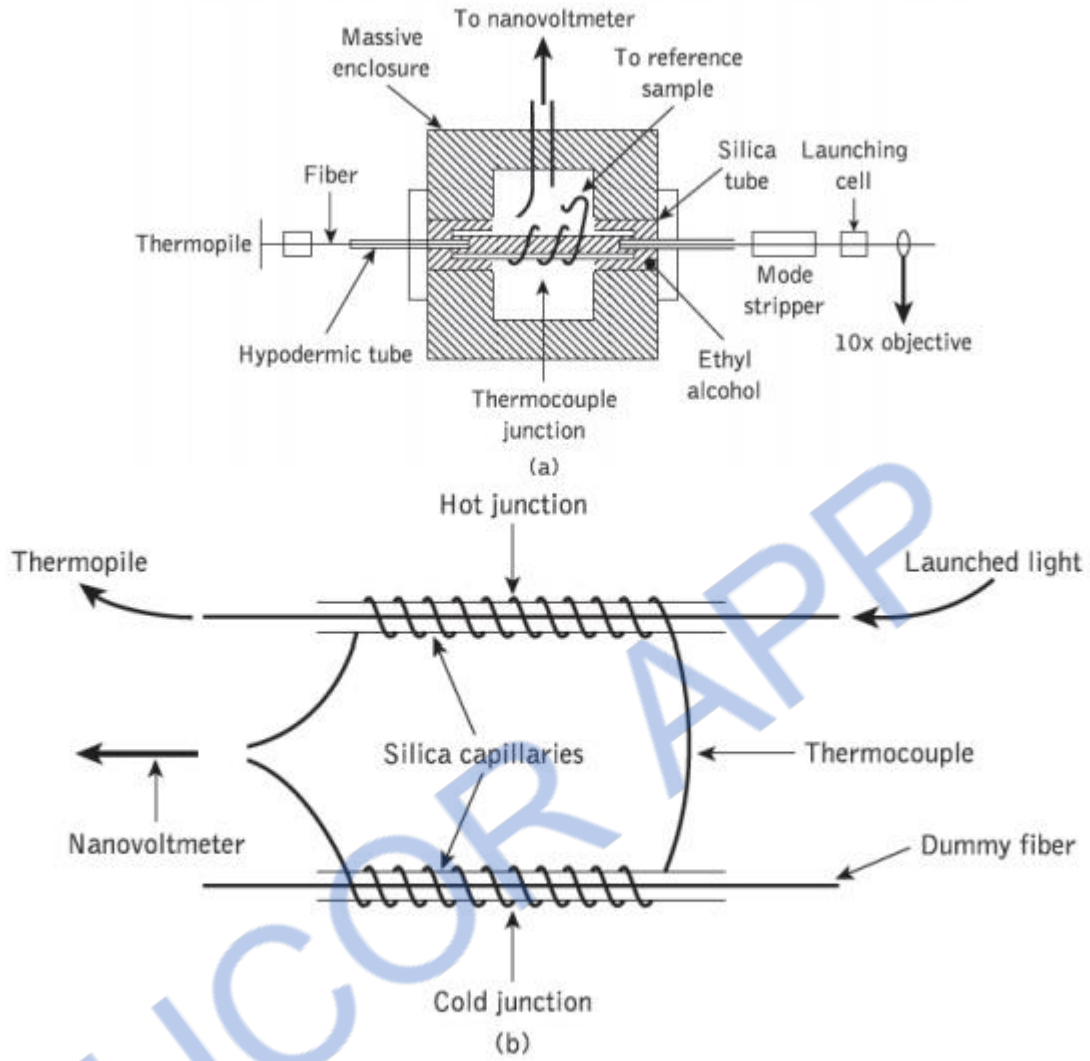

Figure 4.6 Calorimetric measurement of fiber absorption losses: (a) schematic diagram of a version the apparatus; (b) the temperature measurement technique using a thermocouple

The calorimetric measurements provide the heating and cooling curve for the fiber sample used. A typical example of this curve is illustrated in Figure 4.7(a). The attenuation of the fiber due to absorption αabs may be determined from this heating and cooling characteristic. A time constant *t*c can be obtained from a plot of ($T\infty$ -*Tt*) on a logarithmic scale against the time *t*, an example of which shown in Figure 4.7(c) was obtained from the heating characteristic displayed in Figure 4.7(b). $T\infty$ corresponds to the maximum temperature rise of the fiber under test and *Tt* is the temperature rise at a time *t*.

It may be observed from Figure 4.7(a) that $T\infty$ corresponds to a steady-state temperature for the fiber when the heat loss to the surroundings balances the heat generated in the fiber resulting from absorption at a particular optical power level. The time constant tc may be obtained from the slope of the straight line plotted in Figure 4.7(c) as:

$$t_c = \frac{t_2 - t_1}{\ln(T_\infty - T_{t_1}) - \ln(T_\infty - T_{t_2})} \quad (14.3$$

$$\alpha_{abs} = \frac{CT_\infty}{P_{opt} t_c} \text{ dB km}^{-1} \quad (14.4$$

where C is proportional to the thermal capacity per unit length of the silica capillary and the low-refractive-index liquid surrounding the fiber, and$P$opt is the optical power propagating in the fiber under test. The thermal capacity per unit length may be calculated, or determined by the electrical calibration utilizing the thin resistance wire.

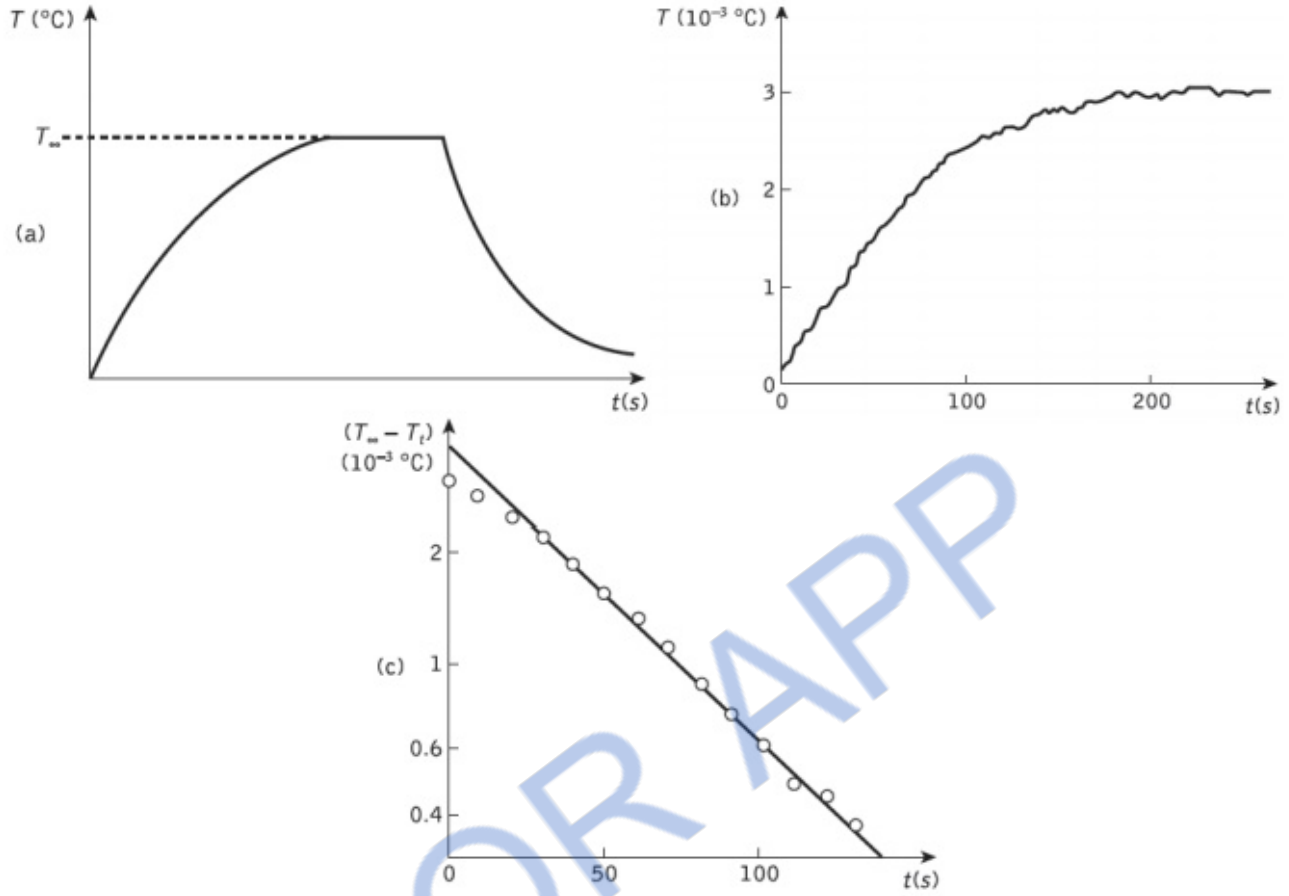

Figure 4.7 (a) A typical heating and cooling curve for a glass fiber sample. (b) A heating curve. (c) The corresponding plot of ($T\infty - Tt$) against time for a sample glass rod

3. Fiber scattering loss measurement

The usual method of measuring the contribution of the losses due to scattering within the total fiber attenuation is to collect the light scattered from a short length of fiber and compare it with the total optical power propagating within the fiber.

Light scattered from the fiber may be detected in a scattering cell as illustrated in the experimental arrangement shown in Figure 4.8. This may consist of a cube of six square solar cells or an integrating sphere and detector. The solar cell cube which contains index-matching fluid surrounding the fiber gives measurement of the scattered light, but careful balancing of the detectors is required in order to achieve a uniform response.

This problem is overcome in the integrating sphere which again usually contains indexmatching fluid but responds uniformly to different distributions of scattered light.

However, the integrating sphere does exhibit high losses from internal reflections. Other variations of the scattering cell include the internally reflecting cell and the sandwiching of the fiber between two solar cells.

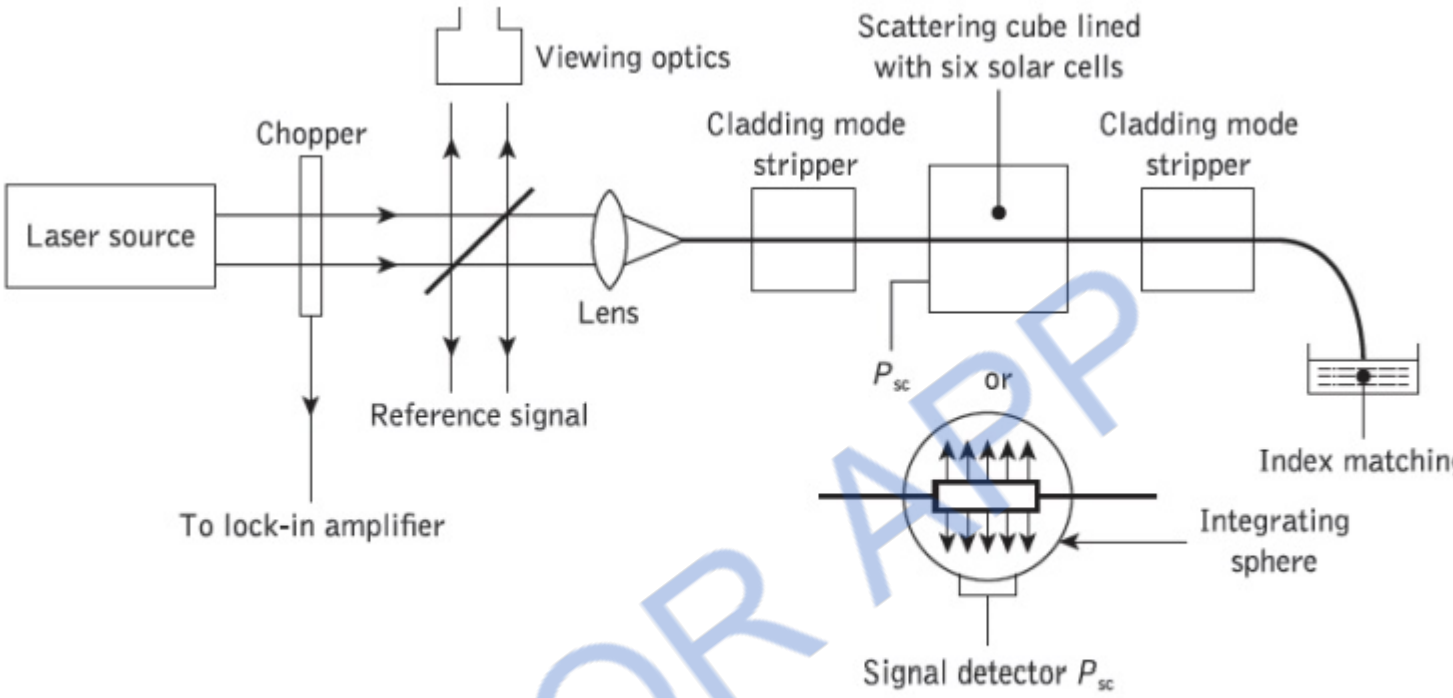

Figure 4.8 An experimental setup for measurement of fiber scattering loss illustrating both the solar cell cube and integrating sphere scattering cells

A laser source (i.e. He–Ne, Nd : YAG, krypton ion) is utilized to provide sufficient optical power at a single wavelength together with a suitable instrument to measure the response from the detector. In order to avoid inaccuracies in the measurement resulting from scattered light which may be trapped in the fiber, cladding mode strippers are placed before and after the scattering cell. These devices remove the light propagating in the cladding so that the measurements are taken only using the light guided by the fiber core. Also, to avoid reflections contributing to the optical signal within the cell, the output fiber end is index matched using either a fluid or suitable surface.

The loss due to scattering αsc is given by:

$$\alpha_{sc} = \frac{10}{l(\text{km})} \log_{10}\left(\frac{P_{opt}}{P_{opt} - P_{sc}}\right) \text{dB km}^{-1} \qquad (4.3)$$

where l(km) is the length of the fiber contained within the scattering cell, Popt is the optical power propagating within the fiber at the cell and Psc is the optical power scattered from the short length of fiber l within the cell. As Popt>>Psc, then the logarithm in Eq. (4.3) may be expanded to give:

$$\alpha_{sc} = \frac{4.343}{l(\text{km})}\left(\frac{P_{sc}}{P_{opt}}\right) \text{dB km}^{-1} \quad (4.4$$

Since the measurements of length are generally in centimeters and the optical power is normally registered in volts, Eq. (4.4) can be written as:

$$\alpha_{sc} = \frac{4.343 \times 10^5}{l(\text{cm})}\left(\frac{V_{sc}}{V_{opt}}\right) \text{dB km}^{-1} \quad (4.5)$$

where Vsc and Vopt are the voltage readings corresponding to the scattered optical power and the total optical power within the fiber at the cell. The relative experimental accuracy (i.e. repeatability) for scatter loss measurements is in the range ±0.2 dB using the solar cell cube and around 5% with the integrating sphere. However, it must be noted that the absolute accuracy of the measurements is somewhat poorer, being dependent on the calibration of the scattering cell and the mode distribution within a multimode fiber.

Fiber dispersion measurements

Dispersion measurements give an indication of the distortion to optical signals as they propagate down optical fibers. The delay distortion which, for example, leads to the broadening of transmitted light pulses limits the information-carrying capacity of the fiber. The measurement of dispersion allows the bandwidth of the fiber to be determined. Therefore, besides attenuation, dispersion is the most important transmission characteristic of an optical fiber. As discussed in Section 3.8, there are three major mechanisms which produce dispersion in optical fibers (material dispersion, waveguide dispersion and intermodal dispersion). The importance of these different mechanisms to the total fiber dispersion is dictated by the fiber type. For instance, in multimode fibers (especially step index), intermodal dispersion tends to be the dominant mechanism,

whereas in single-mode fibers intermodal dispersion is nonexistent as only a single mode is allowed to propagate. In the single-mode case the dominant dispersion mechanism is chromatic (i.e. intramodal dispersion). The dominance of intermodal dispersion in multimode fibers makes it essential that dispersion measurements on these fibers are performed only when the equilibrium mode distribution has been established within the fiber, otherwise inconsistent results will be obtained. Therefore devices such as mode scramblers or filters must be utilized in order to simulate the steady state mode distribution.

Dispersion effects may be characterized by taking measurements of the impulse response of the fiber in the time domain, or by measuring the baseband frequency response in the frequency domain. If it is assumed that the fiber response is linear with regard to power, a mathematical description in the time domain for the optical output power Po(t) from the fiber may be obtained by convoluting the power impulse response $h(t)$ with the optical input power Pi(t) as:

$$P_o(t) = h(t) * P_i(t) \tag{4.6}$$

where the asterisk * denotes convolution. The convolution of $h(t)$ with Pi(t) shown in Eq. (4.6) may be evaluated using the convolution integral where:

$$P_o(t) = \int_{-\infty}^{\infty} P_i(t-x)h(x)\,dx \tag{4.7}$$

In the frequency domain the power transfer function $H(\omega)$ is the Fourier transform of $h(t)$ and therefore by taking the Fourier transforms of all the functions in Eq. (4.6) we obtain:

$$\mathcal{P}_o(\omega) = H(\omega)\mathcal{P}_i(\omega) \tag{4.8}$$

1. Time domain measurement

The most common method for time domain measurement of pulse dispersion in multimode optical fibers is illustrated in Figure 4.9. Short optical pulses (100 to 400 ps)

are launched into the fiber from a suitable source (e.g. A1GaAs injection laser) using fast driving electronics. The pulses travel down the length of fiber under test (around 1 km) and are broadened due to the various dispersion mechanisms. However, it is possible to take measurements of an isolated dispersion mechanism by, for example, using a laser with a narrow spectral width when testing a multimode fiber. In this case the chromatic dispersion is negligible and the measurement thus reflects only intermodal dispersion.

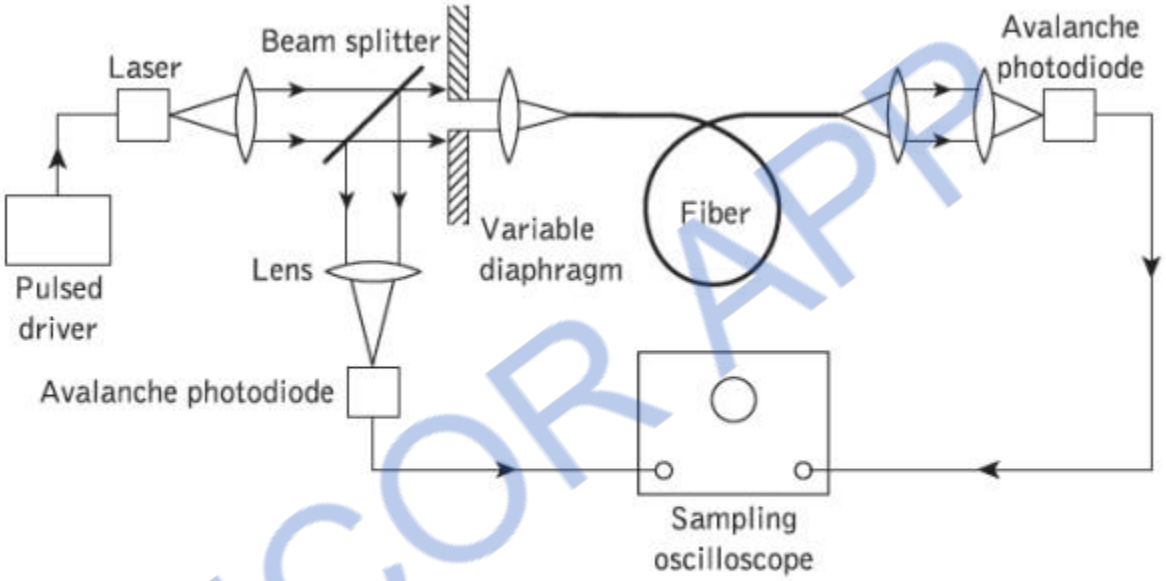

Figure 4.9 Experimental arrangement for making multimode fiber dispersion measurements in the time domain.

The pulses are received by a high-speed photodetector (i.e. avalanche photodiode) and are displayed on a fast sampling oscilloscope. A beam splitter is utilized for triggering the oscilloscope and for input pulse measurement. After the initial measurement of output pulse width, the long fiber length may be cut back to a short length and the measurement repeated in order to obtain the effective input pulse width. The fiber is generally cut back to the lesser of 10 m or 1% of its original length . As an alternative to this cut-back technique, the insertion or substitution method similar to that used in fiber loss measurement can be employed. This method has the benefit of being nondestructive and only slightly less accurate than the cut-back technique.

The fiber dispersion is obtained from the two pulse width measurements which are taken at any convenient fraction of their amplitude. If *P*i(*t*) and*P*o(*t*) of Eq. (4.6) are assumed to have a Gaussian shape then Eq. (4.6) may be written in the form:

$$\tau_o^2(3\text{ dB}) = \tau^2(3\text{ dB}) + \tau_i^2(3\text{ dB}) \tag{4.9}$$

where τi(3 dB) and τo(3 dB) are the 3 dB pulse widths at the fiber input and output, respectively, and τ (3 dB) is the width of the fiber impulse response again measured at half the maximum amplitude. Hence the pulse dispersion in the fiber (commonly referred to as the pulse broadening when considering the 3 dB pulse width) in ns km−1 is given by:

$$\tau(3\text{ dB}) = \frac{(\tau_o^2(3\text{ dB}) - \tau_i^2(3\text{ dB}))^{\frac{1}{2}}}{L}\ \text{ns km}^{-1} \tag{4.10}$$

where τ(3 dB), τi(3 dB) and τo(3 dB) are measured in ns and *L* is the fiber length in km.

It must be noted that if a long length of fiber is cut back to a short length in order to take the input pulse width measurement, then *L* corresponds to the difference between the two fiber lengths in km.

2. Frequency domain measurement

Frequency domain measurement is the preferred method for acquiring the bandwidth of multimode optical fibers. This is because the baseband frequency response *H*(ω) of the fiber may be obtained directly from these measurements using Eq. (4.8) without the need for any assumptions of Gaussian shape, or alternatively, the mathematically complex deconvolution of Eq. (4.8) which is necessary with measurements in the time domain. Thus the optical bandwidth of a multimode fiber is best obtained from frequency domain measurements.

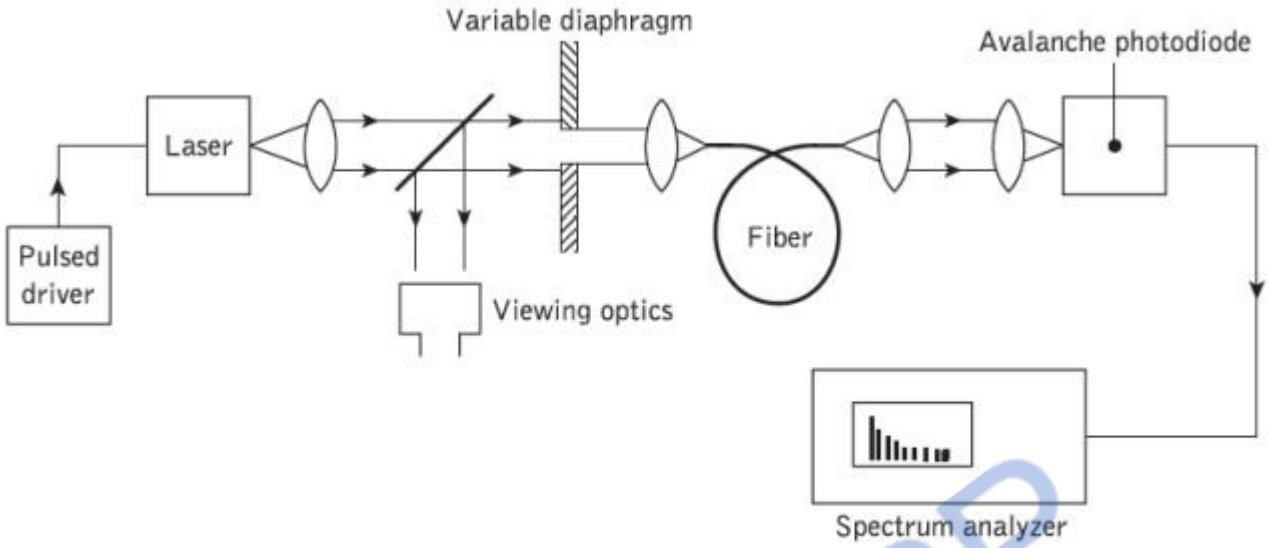

Figure 4.10 Experimental setup for making fiber dispersion measurements in the frequency domain using a pulsed laser source

One of two frequency domain measurement techniques is generally used. The first utilizes a similar pulsed source to that employed for the time domain measurements shown in Figure 4.9. However, the sampling oscilloscope is replaced by a spectrum analyzer which takes the Fourier transform of the pulse in the time domain and hence displays its constituent frequency components. The experimental arrangement is illustrated in Figure 4.10. Comparison of the spectrum at the fiber output Po(ω) with the spectrum at the fiber input Pi(ω) provides the baseband frequency response for the fiber under test where:

$$H(\omega) = \frac{\mathcal{P}_o(\omega)}{\mathcal{P}_i(\omega)} \qquad (4.11)$$

The second technique involves launching a sinusoidally modulated optical signal at different selected frequencies using a sweep oscillator. Therefore the signal energy is concentrated in a very narrow frequency band in the baseband region, unlike the pulse measurement method where the signal energy is spread over the entire baseband region.

Fiber refractive index profile measurements

The refractive index profile of the fiber core plays an important role in characterizing the properties of optical fibers. It allows determination of the fiber's numerical aperture and

the number of modes propagating within the fiber core, while largely defining any intermodal and/or profile dispersion caused by the fiber. Hence a detailed knowledge of the refractive index profile enables the impulse response of the fiber to be predicted.

Also, as the impulse response and consequently the information-carrying capacity of the fiber is strongly dependent on the refractive index profile, it is essential that the fiber manufacturer is able to produce particular profiles with great accuracy, especially in the case of graded index fibers (i.e. optimum profile). There is therefore a requirement for accurate measurement of the refractive index profile. These measurements may be performed using a number of different techniques each of which exhibit certain advantages and drawbacks.

In this section we will discuss some of the more popular methods which may be relatively easily interpreted theoretically, without attempting to review all the possible techniques which have been developed.

1. Interferometric methods

Interference microscopes (e.g. Mach–Zehnder, Michelson) have been widely used to determine the refractive index profiles of optical fibers. The technique usually involves the preparation of a thin slice of fiber (slab method) which has both ends accurately polished to obtain square (to the fiber axes) and optically flat surfaces. The slab is often immersed in an index-matching fluid, and the assembly is examined with an interference microscope. Two major methods are then employed, using either a transmitted light interferometer or a reflected light interferometer.

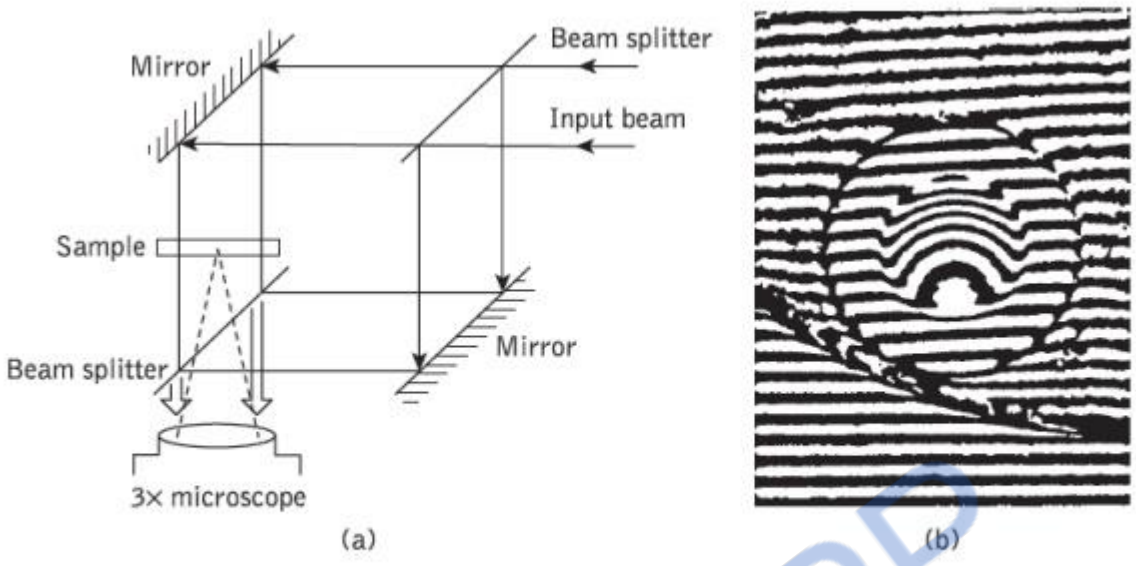

Figure 4.11 (a) The principle of the Mach–Zehnder interferometer. (b) The interference fringe pattern obtained with an interference microscope from a graded index fiber

In both cases light from the microscope travels normal to the prepared fiber slice faces (parallel to the fiber axis), and differences in refractive index result in different optical path lengths. This situation is illustrated in the case of the Mach–Zehnder interferometer in Figure 4.11(a). When the phase of the incident light is compared with the phase of the emerging light, a field of parallel interference fringes is observed. A photograph of the fringe pattern may then be taken, an example of which is shown in Figure 4.11(a).

The fringe displacements for the points within the fiber core are then measured using as reference the parallel fringes outside the fiber core (in the fiber cladding). The refractive index difference between a point in the fiber core (e.g. the core axis) and the cladding can be obtained from the fringe shift q, which corresponds to a number of fringe displacements.

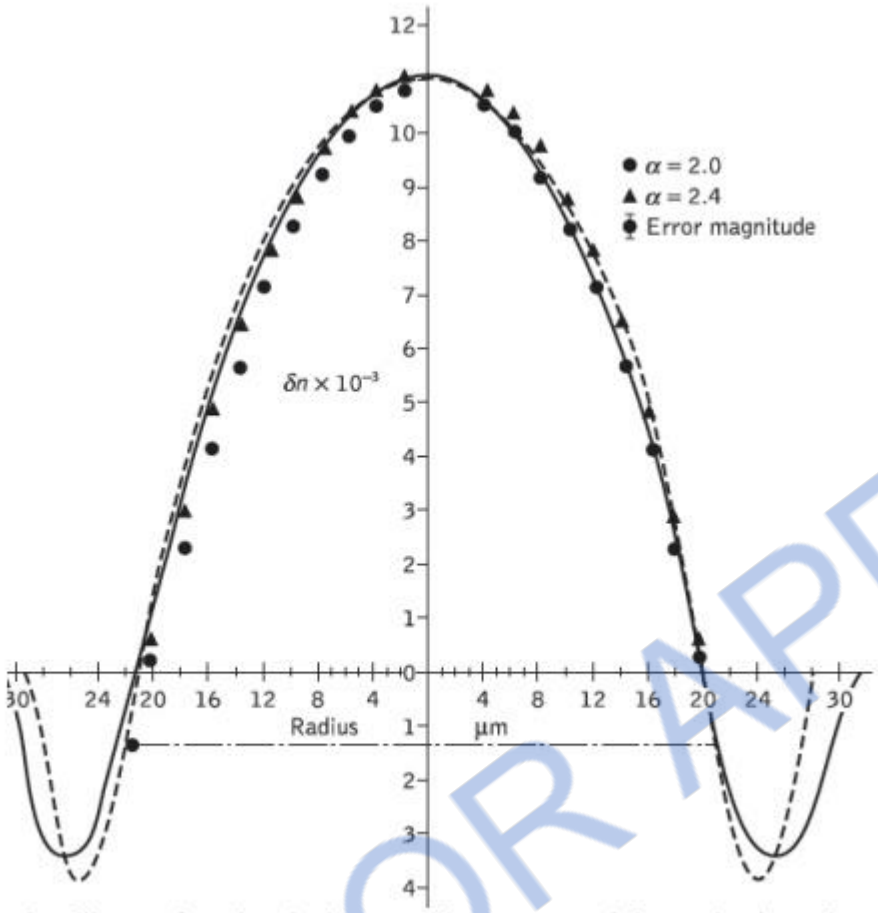

Figure 4.12 The fiber refractive index profile computed from the interference pattern

This difference in refractive index δn is given by:

$$\delta n = \frac{q\lambda}{x} \qquad (4.12$$

where x is the thickness of the fiber slab and λ is the incident optical wavelength. The slab method gives an accurate measurement of the refractive index profile, although computation of the individual points is somewhat tedious unless an automated technique is used.

Figure 4.13 shows the experimental setup used to observe an IGA response using a nonlinear optical loop mirror interferometer. It consists of a laser source and a combination of optical lenses and mirrors where a beam splitter separates the signal creating the delayed path. The two optical signals (i.e. original and delayed signals) combine at a point where a photorefractive crystal is placed which is the mixing element

employed in this method. Several crystalline material systems, known as photorefractive crystals, can be used to produce a diffraction grating in order to implement IGA. Photorefraction is, however, an electro-optic phenomenon in which the local index of refraction is modified by spatial variations of the light intensity.

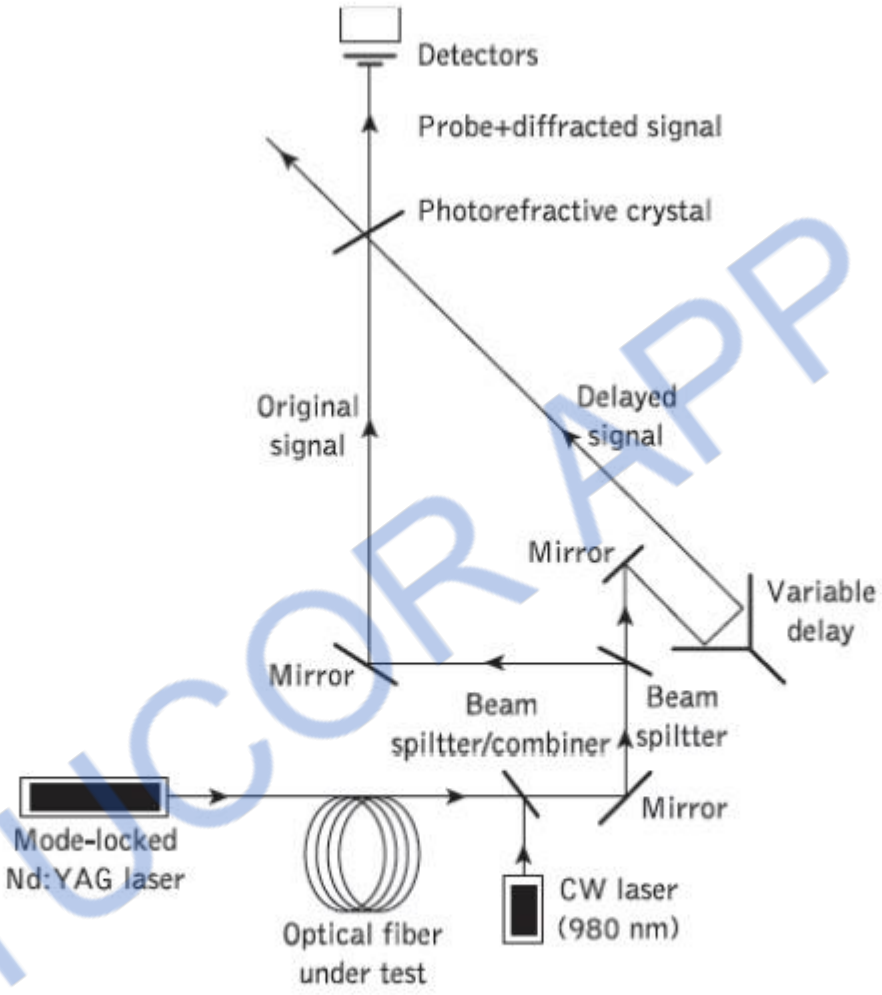

Figure 4.13 Experimental setup for the measurement of the refractive index of silica fiber using the induced-grating autocorrelation function technique

2. Near-field scanning method

The near-field scanning or transmitted near-field method utilizes the close resemblance that exists between the near-field intensity distribution and the refractive index profile, for a fiber with all the guided modes equally illuminated. It provides a reasonably straightforward and rapid method for acquiring the refractive index profile.

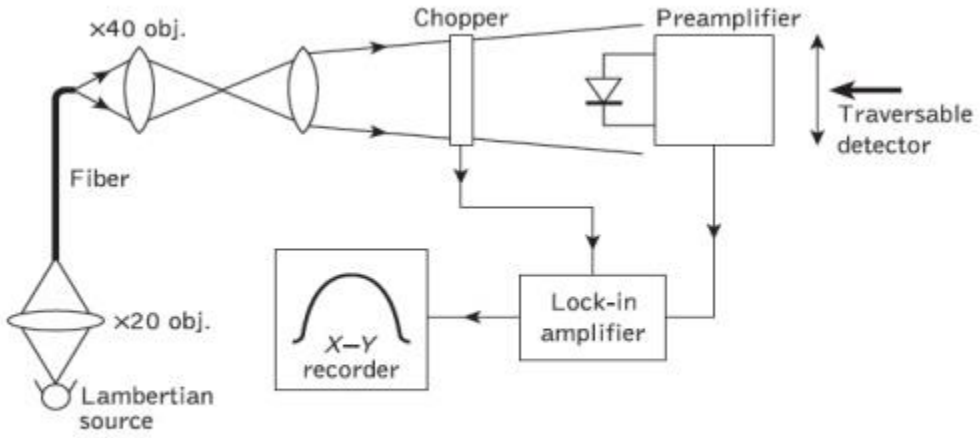

Figure 4.14 Experimental setup for the near-field scanning measurement of the refractive index profil

When a diffuse Lambertian source (e.g. tungsten filament lamp or LED) is used to excite all the guided modes then the near-field optical power density at a radius r from the core axis $P\mathrm{D}(r)$ may be expressed as a fraction of the core axis near-field optical power density $P\mathrm{D}(0)$ following:

$$\frac{P_{\mathrm{D}}(r)}{P_{\mathrm{D}}(0)} = C(r, z)\left[\frac{n_1^2(r) - n_2^2}{n_1^2(0) - n_2^2}\right] \tag{4.13}$$

where $n1(0)$ and $n1(r)$ are the refractive indices at the core axis and at a distance r from the core axis respectively, $n2$ is the cladding refractive index and $C(r, z)$ is a correction factor. The correction factor which is incorporated to compensate for any leaky modes present in the short test fiber may be determined analytically.

The transmitted near-field approach is, however, not similarly recommended for single-mode fiber. An experimental configuration is shown in Figure 4.14. The output from a Lambertian source is focused onto the end of the fiber using a microscope objective lens. A magnified image of the fiber output end is displayed in the plane of a small active area photodetector (e.g. silicon p–i–n photodiode). The photodetector which scans the field transversely receives amplification from the phase-sensitive combination of the optical chopper and lock-in amplifier. Hence the profile may be plotted directly on an X–Y recorder. However, the profile must be corrected with regard to $C(r, z)$ as illustrated in Figure 4.15(a) which is very time consuming. Both the scanning and data acquisition can be automated with the inclusion of a minicomputer.

The test fiber is generally 2 m in length to eliminate any differential mode attenuation and mode coupling. A typical refractive index profile for a practical step index fiber measured by the near-field scanning method is shown in Figure 4.15(b). It may be observed that the profile dips in the center at the fiber core axis. This dip was originally thought to result from the collapse of the fiber preform before the fiber is drawn in the manufacturing process but has been shown to be due to the layer structure inherent at the deposition stage.

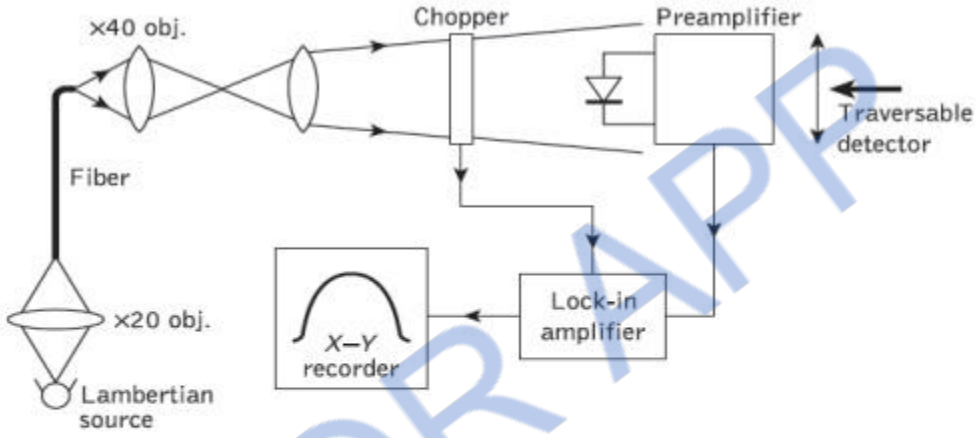

Figure 4.14 Experimental setup for the near-field scanning measurement of the refractive index profi

When a diffuse Lambertian source (e.g. tungsten filament lamp or LED) is used to excite all the guid modes then the near-field optical power density at a radius r from the core axis $P\mathrm{D}(r)$ may be express as a fraction of the core axis near-field optical power density $P\mathrm{D}(0)$ following:

Fiber cutoff wavelength measurements

A multimode fiber has many cutoff wavelengths because the number of bound propagating modes is usually large. For example, considering a parabolic refractive index graded fiber, the number of guided modes Mg is:

$$M_g = \left(\frac{\pi a}{\lambda}\right)^2 (n_1^2 - n_2^2) \qquad (4.14$$

where a is the core radius and $n1$ and $n2$ are the core peak and cladding indices respectively. It may be observed from Eq. (4.14) that operation at longer wavelengths

yields fewer guided modes. Therefore it is clear that as the wavelength is increased, a growing number of modes are cutoff where the cutoff wavelength of aLP*lm* mode is the maximum wavelength for which the mode is guided by the fiber.

Usually the cutoff wavelength refers to the operation of single-mode fiber in that it is the cutoff wavelength of the LP11 mode (which has the longest cutoff wavelength) which makes the fiber single moded when the fiber diameter is reduced to 8 or 9 μm. Hence the cutoff wavelength of the LP11 is the shortest wavelength above which the fiber exhibits single-mode operation and it is therefore an important parameter to measure.

The theoretical value of the cutoff wavelength can be determined from the fiber refractive index profile. Because of the large attenuation of the LP11 mode near cutoff, however, the parameter which is experimentally determined is called the effective cutoff wavelength, which is always smaller than the theoretical cutoff wavelength by as much as 100 to 200 nm. It is this effective cutoff wavelength which limits the wavelength region for which the fiber is 'effectively' single-mode.

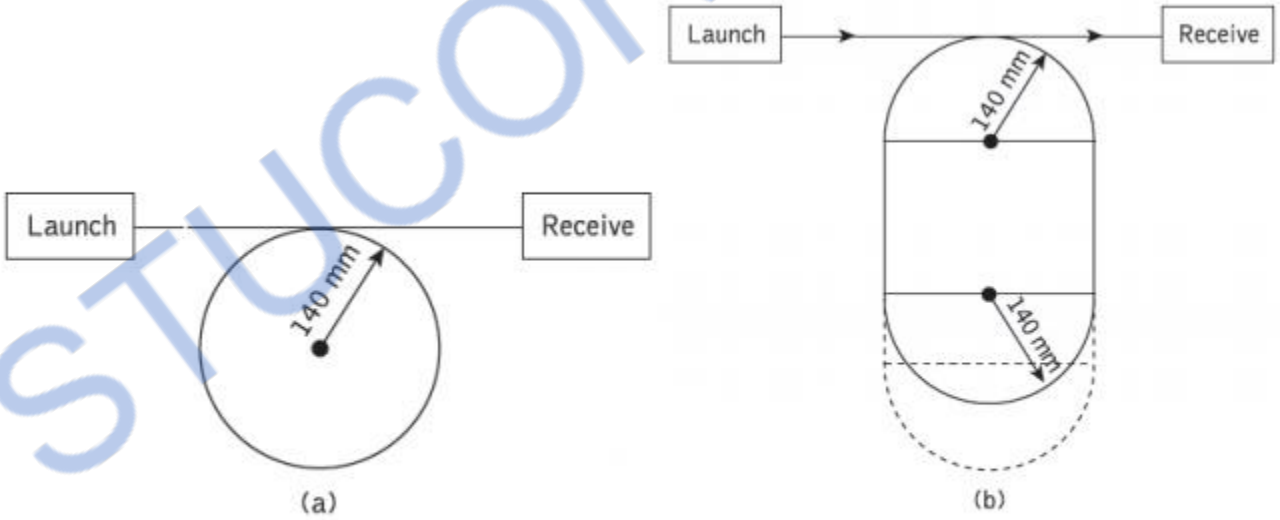

Figure 4.16 Configurations for the measurement of uncabled fiber cutoff wavelength: (a) single turn; (b) split mandrell

In the bending-reference technique the power *P*s(λ) transmitted through the fiber sample in the configurations shown in Figure 4.16 is measured as a function of wavelength. Thus the quantity *P*s(λ) corresponds to the total power, including launched higher order modes, of the ITU-T definition for cutoff wavelength. Then keeping the launch conditions fixed, at least one additional loop of sufficiently small radius (60 mm or less)

is introduced into the test sample to act as a mode filter to suppress the secondary LP11 mode without attenuating the fundamental mode at the effective cutoff wavelength. In this case the smaller transmitted spectral power *P*b(λ) is measured which corresponds to the fundamental mode power referred to in the definition. The bend attenuation *a*b(λ) comprising the level difference between the total power and the fundamental power is calculated as:

$$a_b(\lambda) = 10 \log_{10} \frac{P_s(\lambda)}{P_b(\lambda)} \tag{4.15}$$

The bend attenuation characteristic exhibits a peak in the wavelength region where the radiation losses resulting from the small loop are much higher for the LP11 mode than for the LP01 fundamental mode, as illustrated in Figure 4.17.

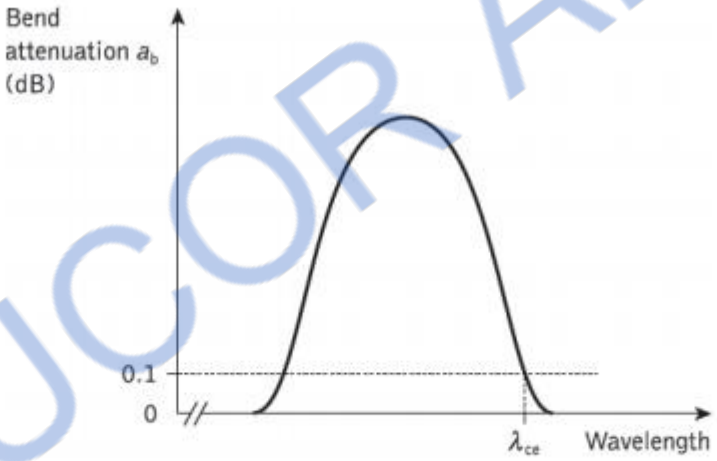

Figure 4.17 Bend attenuation against wavelength in the bending method for the measurement of cutoff wavelength λce

It should be noted that the shorter wavelength side of the attenuation maximum corresponds to the LP11 mode, being well confined in the fiber core, and hence negligible loss is induced by the 60 mm diameter loop, whereas on the longer wavelength side the LP11 mode is not guided in the fiber and therefore, assuming that the loop diameter is large enough to avoid any curvature loss to the fundamental mode, there is also no increase in loss.

The relative attenuation *a*m(λ) or level difference between the powers launched into the multimode and single-mode fibers may be computed as:

$$a_m(\lambda) = 10 \log_{10} \frac{P_s(\lambda)}{P_m(\lambda)} \quad (4.16)$$

Fiber numerical aperture measurements

The numerical aperture is an important optical fiber parameter as it affects characteristics such as the light-gathering efficiency and the normalized frequency of the fiber (*V*). This in turn dictates the number of modes propagating within the fiber (also defining the singlemode region) which has consequent effects on both the fiber dispersion (i.e. intermodal) and, possibly, the fiber attenuation (i.e. differential attenuation of modes). The numerical aperture (*NA*) is defined for a step index fiber as:

$$NA = \sin \theta_a = (n_1^2 - n_2^2)^{\frac{1}{2}} \quad (4.17$$

where Θa is the maximum acceptance angle, *n*1 is the core refractive index and *n*2 is the cladding refractive index.

It is assumed that the light is incident on the fiber end face from air with a refractive index (*n*0) of unity. Although Eq. (4.17) may be employed with graded index fibers, the numerical aperture thus defined represents only the local *NA* of the fiber on its core axis (the numerical aperture for light incident at the fiber core axis). The graded profile creates a multitude of local *NA*s as the refractive index changes radially from the core axis

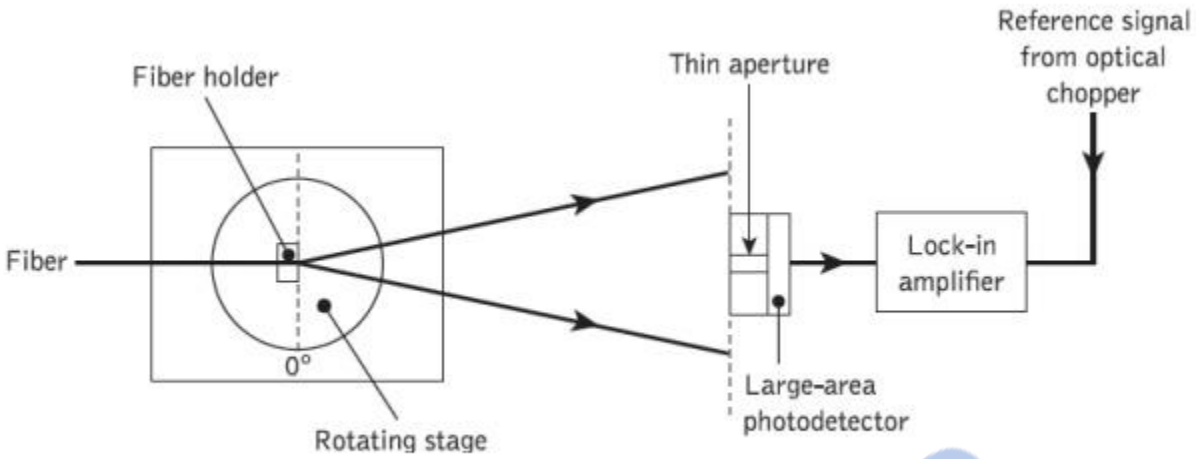

Figure 4.18 Fiber numerical aperture measurement using a scanning photodetector and a rotating stage

For the general case of a graded index fiber these local numerical apertures NA(r) at different radial distances r from the core axis may be defined by:

$$NA(r) = \sin \theta_a(r) = (n_1^2(r) - n_2^2)^{\frac{1}{2}} \qquad (4.18$$

Therefore, calculations of numerical aperture from refractive index data are likely to be less accurate for graded index fibers than for step index fibers unless the complete refractive index profile is considered. The numerical aperture may be determined by calculation.

` An example of an experimental arrangement with a rotating stage is shown in Figure 4.18. A 2 m length of the graded index fiber has its faces prepared in order to ensure square smooth terminations.

The fiber output end is then positioned on the rotating stage with its end face parallel to the plane of the photodetector input, and so that its output is perpendicular to the axis of rotation. Light at a wavelength of 0.85 μm is launched into the fiber at all possible angles (overfilling the fiber) using an optical system similar to that used in the spot attenuation measurements.

The photodetector, which may be either a small-area device or an apertured large-area device, is placed 10 to 20 cm from the fiber and positioned in order to obtain a maximum signal with no rotation (0°). Hence when the rotating stage is turned the limits of the far-field pattern may be recorded. The output power is monitored and plotted as a

function of angle, the maximum acceptance angle being obtained when the power drops to 5% of the maximum intensity. Thus the numerical aperture of the fiber can be obtained from Eq. (4.17).

A less precise measurement of the numerical aperture can be obtained from the far-field pattern by trigonometric means. The experimental apparatus is shown in Figure 4.19.

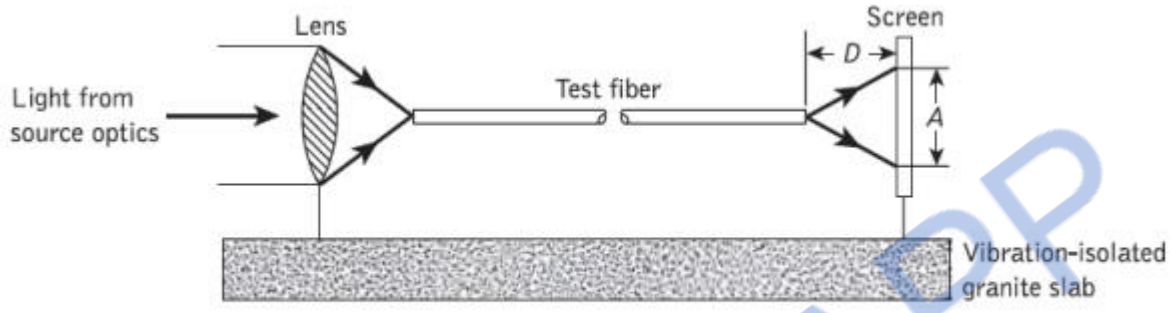

Figure 4.19 Apparatus for trigonometric fiber numerical aperture measurement

where the end prepared fiber is located on an optical base plate or slab. Again light is launched into the fiber under test over the full range of its numerical aperture, and the farfield pattern from the fiber is displayed on a screen which is positioned a known distance D from the fiber output end face. The test fiber is then aligned so that the optical intensity on the screen is maximized. Finally, the pattern size on the screen A is measured using a calibrated vernier caliper. The numerical aperture can be obtained from simple trigonometrical relationships where:

$$NA = \sin\theta_a = \frac{A/2}{[(A/2)^2 + D^2]^{\frac{1}{2}}} = \frac{A}{(A^2 + 4D^2)^{\frac{1}{2}}} \tag{4.19}$$

It must be noted that the accuracy of this measurement technique is dependent upon the visual assessment of the far-field pattern from the fiber. The above measurement techniques are generally employed with multimode fibers only, as the far-field patterns from single-mode fibers are affected by diffraction phenomena

Fiber diameter measurements

1. Outer diameter

It is essential during the fiber manufacturing process (at the fiber drawing stage) that the fiber outer diameter (cladding diameter) is maintained constant to within 1%. Any diameter variations may cause excessive radiation losses and make accurate fiber–fiber connection difficult. Hence on-line diameter measurement systems are required which provide accuracy better than 0.3% at a measurement rate greater than 100 Hz (i.e. a typical fiber drawing velocity is 1 ms $^{-1}$). Use is therefore made of noncontacting optical methods such as fiber image projection and scattering pattern analysis.

The most common on-line measurement technique uses fiber image projection (shadow method) and is illustrated in Figure 4.20. In this method a laser beam is swept at a constant velocity transversely across the fiber and a measurement is made of the time interval during which the fiber intercepts the beam and casts a shadow on a photodetector.

In the apparatus shown in Figure 4.20 the beam from a laser operating at a wavelength of 0.6328 μm is collimated using two lenses ($G1$ and $G2$). It is then reflected off two mirrors ($M1$ and $M2$), the second of which ($M2$) is driven by a galvanometer which makes it rotate through a small angle at a constant angular velocity before returning to its original starting position. Therefore, the laser beam which is focused in the plane of the fiber by a lens ($G3$) is swept across the fiber by the oscillating mirror, and is incident on the photodetector unless it is blocked by the fiber. The velocity ds/dt of the fiber shadow thus created at the photodetector is directly proportional to the mirror velocity $d\phi/dt$ following:

$$\frac{ds}{dt} = l\frac{d\phi}{dt} \quad (14.31) \qquad (4.20)$$

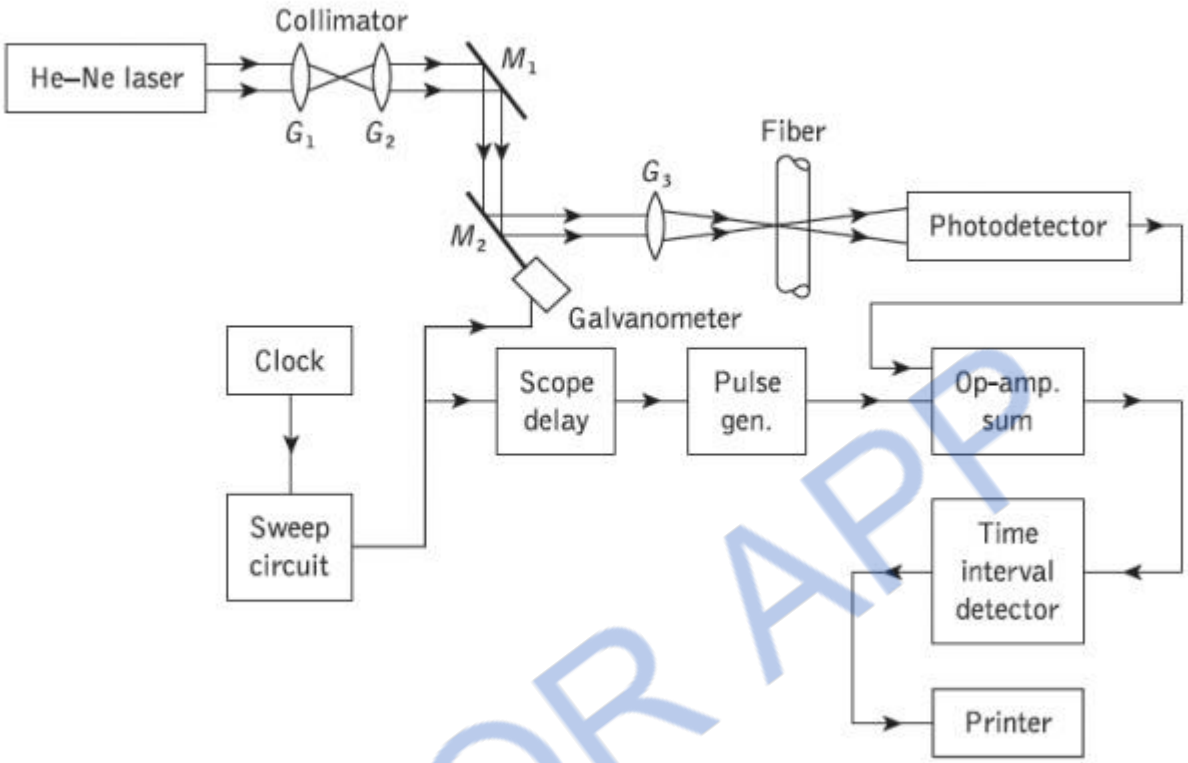

Figure 4.20 The shadow method for the on-line measurement of the fiber outer diameter.

where *l* is the distance between the mirror and the photodetector. Furthermore, the shadow is registered by the photodetector as an electrical pulse of width *We* which is related to the fiber outer diameter *do* as:

$$d_0 = W_e\frac{ds}{dt} \qquad (4.21$$

Thus the fiber outer diameter may be quickly determined and recorded on the printer. The measurement speed is largely dictated by the inertia of the mirror rotation and its accuracy by the rise time of the shadow pulse.

Other on-line measurement methods, enabling faster diameter measurements, involve the analysis of forward or backward far-field patterns which are produced when a plane wave is incident transversely on the fiber. These techniques generally require measurement of the maxima in the center portion of the scattered pattern from which the

diameter can be calculated after detailed mathematical analysis. They tend to give good accuracy (e.g. ±0.25 μm) even though the theory assumes a perfectly circular fiber cross-section. Also, for step index fibers the analysis allows determination of the core diameter, and core and cladding refractive indices. Measurements of the fiber outer diameter after manufacture (off-line) may be performed using a micrometer or dial gage. These devices can give accuracies of the order of ±0.5 μm. Alternatively, off-line diameter measurements can be made with a microscope incorporating a suitable calibrated micrometer eyepiece.

2. Core diameter

The core diameter for step index fibers is defined by the step change in the refractive index profile at the core–cladding interface. Therefore the techniques employed for determining the refractive index profile (interferometric, near-field scanning, refracted ray, etc.) may be utilized to measure the core diameter. Graded index fibers present a more difficult problem as, in general, there is a continuous transition between the core and the cladding.

In this case it is necessary to define the core as an area with a refractive index above a certain predetermined value if refractive index profile measurements are used to obtain the core diameter. Core diameter measurement is also possible from the near-field pattern of a suitably illuminated (all guided modes excited) fiber. The measurements may be taken using a microscope equipped with a micrometer eyepiece similar to that employed for off-line outer diameter measurements.

FIBER OPTIC RECEIVER AND MEASUREMENTS

1. **Define minimum detectable optical power.**

It is defined as the optical power necessary to produce a photocurrent of the same magnitude as the root mean square of the total current.

2. **Define quantum noise.**

It is not possible to predict exactly how many electron-hole pairs are generated by a known optical power incident on the detector is the origin of the type of short noise called quantum noise.

3. What is meant by error rate?

An approach is to divide the number Ne of errors occurring over a certain time interval t by the number Nt of pulses transmitted during this interval. This is called either the error rate or the bit error rate.

$$\text{Bit error rate BER} = \frac{Ne}{Nt} = \frac{Ne}{Bt}$$

$$\text{Where } B = \frac{1}{Tb}$$

4. Define quantum limit

It is possible to find the minimum received optical power required for a specific bit error rate performance in a digital system. This minimum received power level is known as quantum limit.

5. Give the classifications of preamplifiers.

- Low impedence(LZ) preamplifier
- High impedence(HZ) preamplifier
- Transimpedence preamplifier

6. What is meant by excess noise factor?

The ratio of the actual noise generated in an avalanche photodiode to the noise that would exist if all carrier pairs were multiplied by exactly m is called the excess noise factor (F).

7. What is meant by inter symbol interference (ISI)?

ISI results from pulse spreading in the optical fibre. The presence of this energy in adjacent time slots results in an interfering signal. Hence it is called ISI.

8. Give the advantages of Pin photodiodes.

- Very low reverse bias is necessary
- High quantum efficiency
- Large bandwidth
- Low noise level

9. What do you mean by thermal noise?

Thermal noise is due to the random motion of electrons in a conductor. Thermal noise arising from the detector load resistor and from the amplifier electronics tend to dominate in applications with low signal to noise ratio.

10. Give the equation for mean square shot noise.

The mean square shot noise is given by

$$\langle i_n^2 \rangle = 2qI_B$$

I_B average output current

B bandwidth of the amplifier

11. Define multiplication M .

The multiplication M for all carriers generated in the photodiode is defined by

$M = I_M / I_P$

I_M : average value of the total multiplied output current

I_P : primary unmultiplied photocurrent

12. What is current mode of operation of photodiode?

In photo conducting mode, the photocurrent is slightly dependent on the reverse bias. For a constant reverse bias, the current is linear. This is called current mode of operation of the photodiode.

13. What are the system requirements?

The following are the key system requirements.

- The desired or possible transmission distance
- The data rate or channel bandwidth
- Bit error rate (BER)

14. What are splices? What are the requirements of splices?

The splices are generally permanent fiber joints, whereas connectors are temporar y fiber joints. Splicing is a sort of soldering. The requirements of splices are:

- Should cause low attenuation
- Should be strong & light in weight
- Should have minimum power loss
- Should be easy to install

15. What are the methods of fiber splicing?

There are 3 methods of fiber splicing. They are:

- Electric arc fusion splicing or fusion splicing
- Mechanical splicing
- V-groove splicing or loose tube splicing

16. What are connectors? What are the types of connectors?

The connectors are used to join the optical sources as well as detectors to the optical fiber temporarily. They are also used to join two optical fibers. The 2 major types of connectors are:

- Lensed type expanded beam connector
- Ferrule type connector

17. What are the requirements of a good connector?

The requirements of a good connector are as follows:

- Low loss

- Repeatability
- Predictability
- Ease of assembly and use
- Low cost & reliability
- Compatibility

18. Give the 2 analysis that are used to ensure system performance?

The 2 analysis that are used to ensure system performance are:

- Link power budget analysis
- Rise time budget analysis

19. Explain briefly about link power budget analysis?

In the optical power loss model for a pt-to-pt link, the optical power rxed at the photo detector depends on the amount of light coupled into the fiber & losses occurring in the fiber at the connectors & splices. The link loss budget is derived from the sequential loss contribution of each element in the link.

Loss=10 log (Pout) / (Pin)

The total optical power loss is,

PT = PS - PR

20. Give the range of system margin in link power budget?

The system margin is usually (6-8) db. A positive system margin ensures proper operation of the circuit. A negative value indicates that insufficient power will reach the detector to achieve the required bit error rate, BER.

21. What are the system components of system rise time?

The 4 basic system components that contribute to the system rise time are:

- Transmitter (source) rise time
- Receiver rise time
- Material dispersion time of the fiber

- Modal dispersion time of the fiber link

All these 4 basic elements may significantly limit system speed.

22. **Why the attenuation limit curve slopes downwards to the right**?

As the minimum optical power required at the rxer for a given BER becomes higher for increasing data rates, the attenuation limit curve slopes downward to the right.

23. What are the noise effects on system performance?

The main penalties are modal noise, wavelength chirp, spectral broadening, mode-partition noise.

24. Define modal noise?

It arises when the light from a coherent laser is coupled in to a multimode fiber operating at 400Mbps and higher. It mainly occurs due to mechanical vibrations and fluctuations in the frequency of the optical source.

25. What are the measures to avoid modal noise?

The measures are

- use LEDs
- use LASER having more longitudinal modes
- use a fiber with large numerical aperture
- use a single mode fiber

26. Define mode partition noise?

The mode partition noise is associated with intensit y fluctuations in the longitudinal modes of a laser diode. It becomes more pronounced for the higher bit rates.

27. What is meant by chirping?

It means that the dynamic line broadening (line broadening is a frequency chirp) in the laser which oscillates in the single longitudinal mode under CW operation when the injection current is intensity modulated.

28. What is the best way to minimize the chirping?

It is to choose the laser emission wavelength close to the zero-dispersion of the wavelength of the fiber.

29. What is reflection noise?

It is the optical power that gets reflected at the refractive index discontinuities such as in splices, couplers and filters, or connectors. The reflected signals can degrade both the transmitter and receiver performance.

30. What are the effects of reflection noise in high speed systems?

They cause optical feedback which leads to optical instabilities that may lead to inter symbol interference and intensity noise.

GLOSSARY

1. **Minimum detectable optical power.**

It is defined as the optical power necessary to produce a photocurrent of the same magnitude as the root mean square of the total current.

2. **Quantum noise.**

It is not possible to predict exactly how many electron-hole pairs are generated by a known optical power incident on the detector is the origin of the type of short noise called quantum noise.

3. **Error rate**

An approach is to divide the number Ne of errors occurring over a certain time interval t by the number Nt of pulses transmitted during this interval. This is called either the error rate or the bit error rate.

4. **Quantum limit**

It is possible to find the minimum received optical power required for a specific bit error rate performance in a digital system. This minimum received power level is known as quantum limit.

5. Excess noise factor.

The ratio of the actual noise generated in an avalanche photodiode to the noise that would exist if all carrier pairs were multiplied by exactly m is called the excess noise factor (F).

6. Inter symbol interference (ISI).

ISI results from pulse spreading in the optical fibre. The presence of this energy in adjacent time slots results in an interfering signal. Hence it is called ISI.

7. Thermal noise.

Thermal noise is due to the random motion of electrons in a conductor. Thermal noise arising from the detector load resistor and from the amplifier electronics tend to dominate in applications with low signal to noise ratio.

8. Multiplication M .

The multiplication M for all carriers generated in the photodiode is defined by

M = IM/ IP

IM : average value of the total multiplied output current

IP: primary unmultiplied photocurrent

9. Current mode of operation of photodiode.

In photo conducting mode, the photocurrent is slightly dependent on the reverse bias. For a constant reverse bias, the current is linear. This is called current mode of operation of the photodiode.

10. Splices.

The splices are generally permanent fiber joints, whereas connectors are temporary fiber joints. Splicing is a sort of soldering.

11. Connectors.

The connectors are used to join the optical sources as well as detectors to the optical fiber temporarily. They are also used to join two optical fibers. The 2 major types of connectors are:

- Lensed type expanded beam connector
- Ferrule type connector

12. Link power budget analysis.

In the optical power loss model for a pt-to-pt link, the optical power rxed at the photo detector depends on the amount of light coupled into the fiber & losses occurring in the fiber at the connectors & splices.

13. Modal noise.

It arises when the light from a coherent laser is coupled in to a multimode fiber operating at 400Mbps and higher. It mainly occurs due to mechanical vibrations and fluctuations in the frequency of the optical source.

14. Mode partition noise.

The mode partition noise is associated with intensity fluctuations in the longitudinal modes of a laser diode. It becomes more pronounced for the higher bit rates.

15. Chirping

It means that the dynamic line broadening (line broadening is a frequency chirp) in the laser which oscillates in the single longitudinal mode under CW operation when the injection current is intensity modulated.

16. Reflection noise.

It is the optical power that gets reflected at the refractive index discontinuities such as in splices, couplers and filters, or connectors. The reflected signals can degrade both the transmitter and receiver performance.

UNIT – 5

OPTICAL COMMUNICATION SYSTEMS AND NETWORKS

SONET/SDH

✓⋯SONET is the TDM optical network standard for North America

✓⋯SONET is called Synchronous Digital Hierarchy (SDH) in the rest of the world

✓⋯SONET is the basic phycal layer standard

✓⋯Other data types such as ATM and IP can be transmitted over SONET

✓⋯OC-1 consists of 810 bytes over 125 us; OC-*n* consists of 810*n* bytes over 125 us

✓⋯Linear multiplexing and de-multiplexing is possible with Add-Drop-Multiplexers

✓⋯The SONET/SDH standards enable the interconnection of fiber optic transmission equipment from various vendors through multiple-owner trunk networks.

✓⋯The basic transmission bit rate of the basic SONET signal is

✓⋯In SDH the basic rate is 155.52 Mb/s.

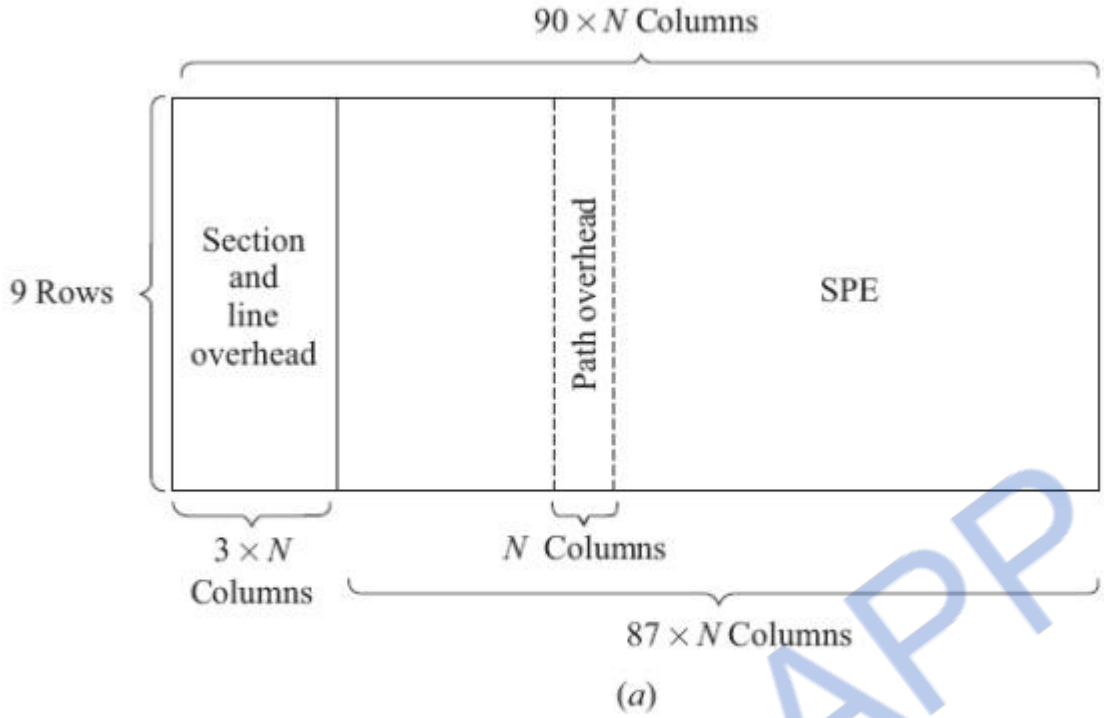

Figure 5.1 Basic formats of an STS-N SONET frame

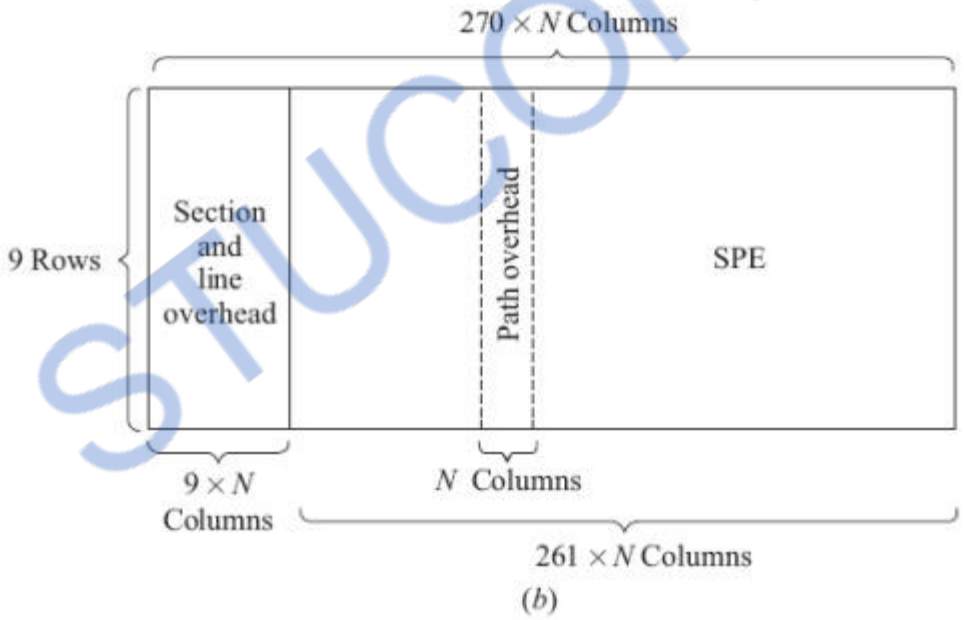

Figure 5.2 Basic formats of an STM-N SDH frame

Common values of OC-N and STM-N:

✓…OC stands for optical carrier. It has become common to refer to SONET links as OC-N links.

✓…The basic SDH rate is 155.52 Mb/s and is called the synchronous transport module—level 1 (STM 1).

SONET level	*Electrical level*	*SDH level*	*Line rate (Mb/s)*	*Common rate name*
OC-N	STS-N	—	N × 51.84	—
OC-1	STS-1	—	51.84	—
OC-3	STS-3	STM-1	155.52	155 Mb/s
OC-12	STS-12	STM-4	622.08	622 Mb/s
OC-48	STS-48	STM-16	2488.32	2.5 Gb/s
OC-192	STS-192	STM-64	9953.28	10 Gb/s
OC-768	STS-768	STM-256	39813.12	40 Gb/s

SONET Add Drop Multiplexers:

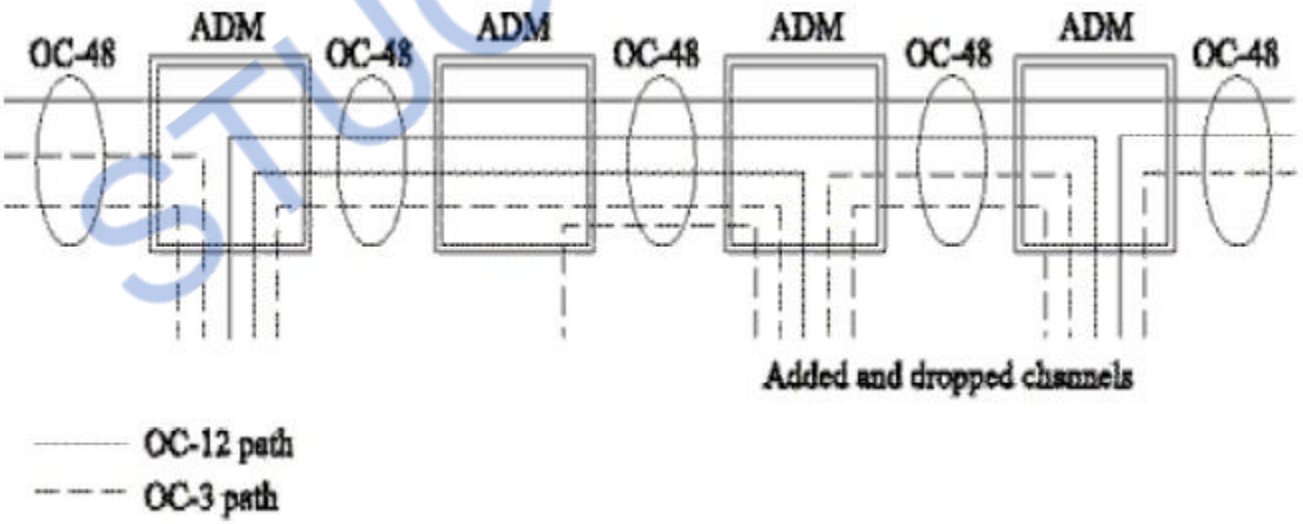

SONET ADM is a fully synchronous, byte oriented device, that can be used add/drop OC sub-channels within an OC-*N* signal

Ex: OC-3 and OC-12 signals can be individually added/dropped from an OC-48 carrier

SONET/SDH Rings:

✓…SONET and SDH can be configured as either a ring or mesh architecture

✓…SONET/SDH rings are *self-healing rings* because the traffic flowing along a certain path can be switched automatically to an alternate or standby path following failure or degradation of the link segment

✓…Two popular SONET and SDH networks:

– 2-fiber, unidirectional, path-switched ring (2-fiber UPSR)

– 2-fiber or 4-fiber, bidirectional, line-switched ring (2-fiber or 4-fiber BLSR)

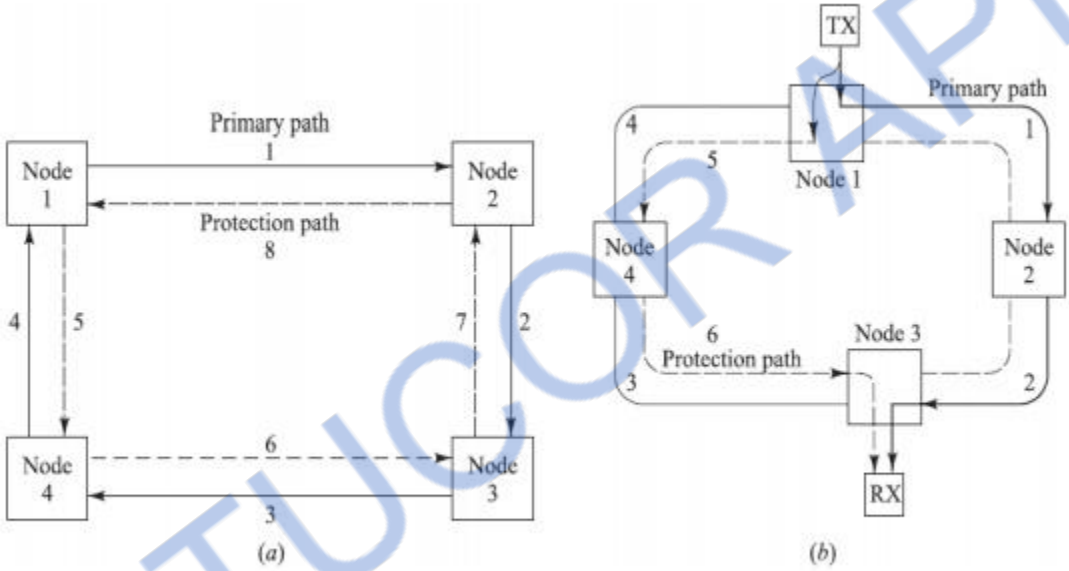

Figure 5.3 Generic 2-fiber UPSR with a counter-rotating protection path

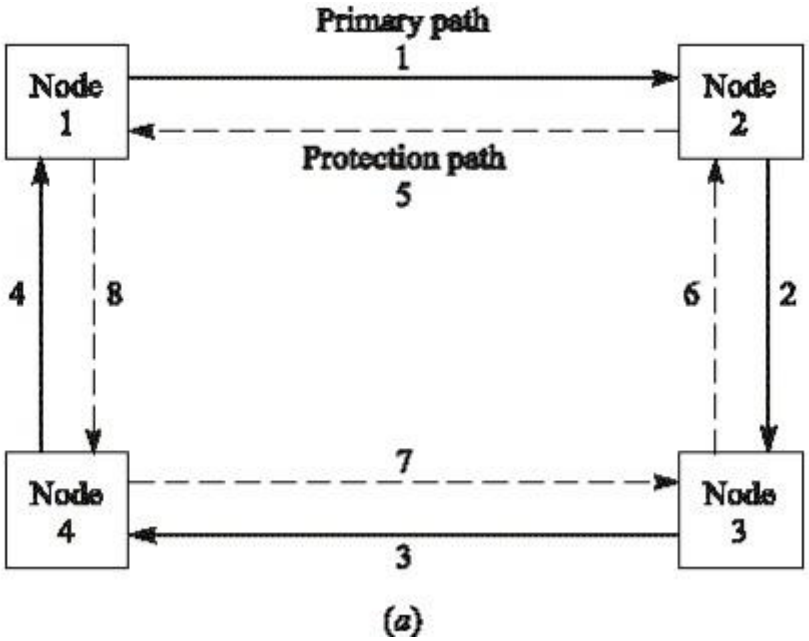

(a)

Ex: Total capacity OC-12 may be divided to four OC-3 streams, the OC-3 is called a path here

2-Fiber UPSR Protection:

✓…Rx compares the signals received via the primary and protection paths and picks the best one

✓…Constant protection and automatic switching

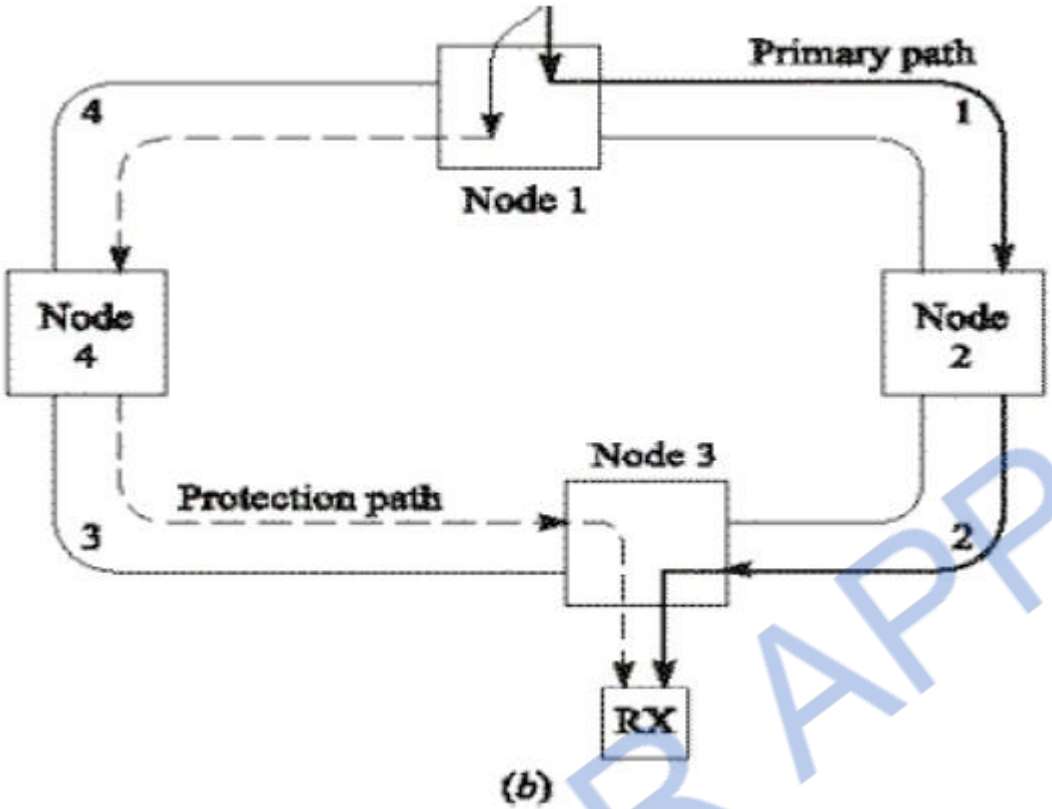

BLSR Recovery from Failure Modes:

✓…If a primary-ring device fails in either node 3 or 4, the affected nodes detect a loss-of-signal condition and switch both primary fibers connecting these nodes to the secondary protection pair

✓…If an entire node fails or both the primary and protection fibers in a given span are severed, the adjacent nodes switch the primary-path connections to the protection fibers, in order to loop traffic back to the previous node.

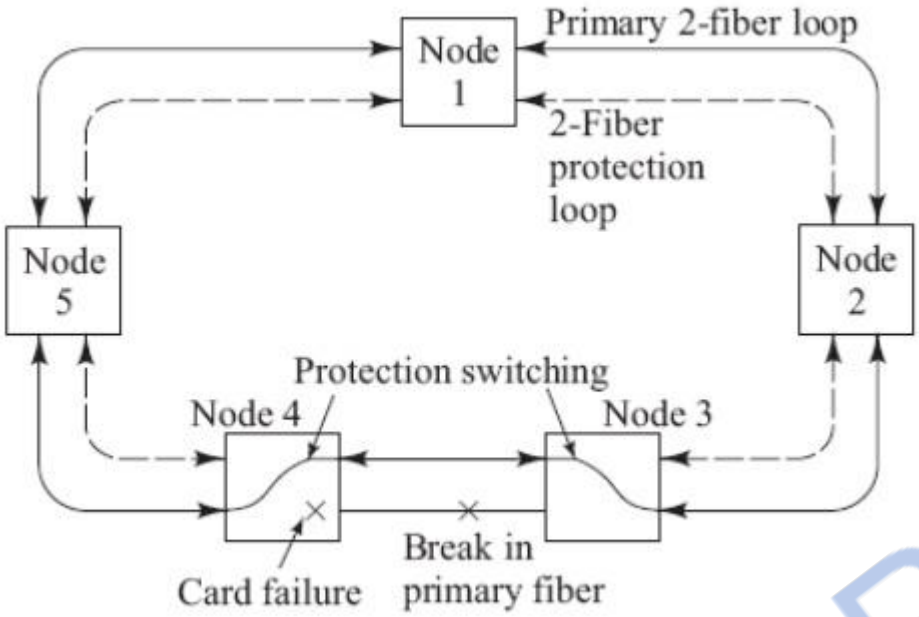

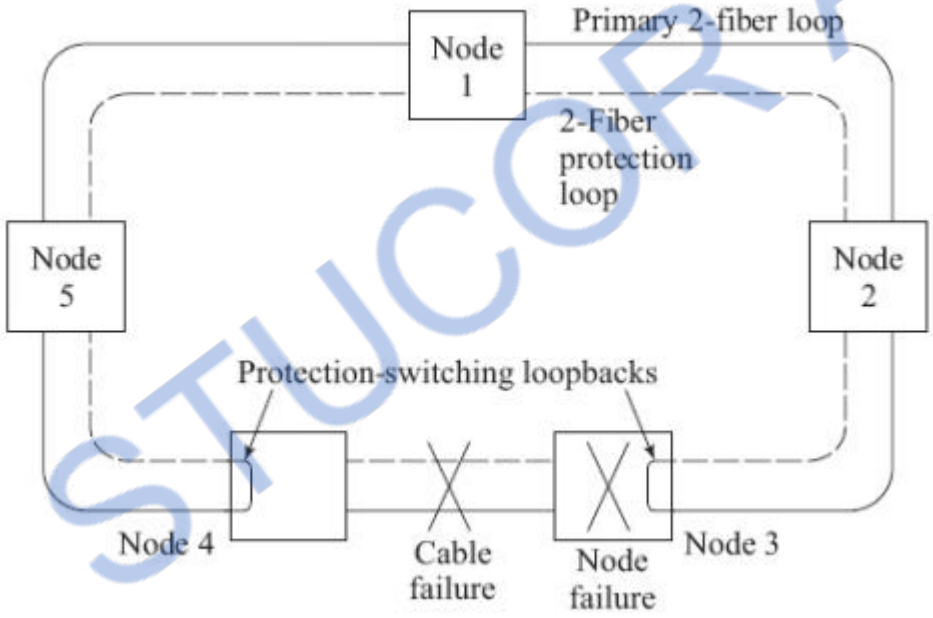

4-Fiber BLSR Basics:

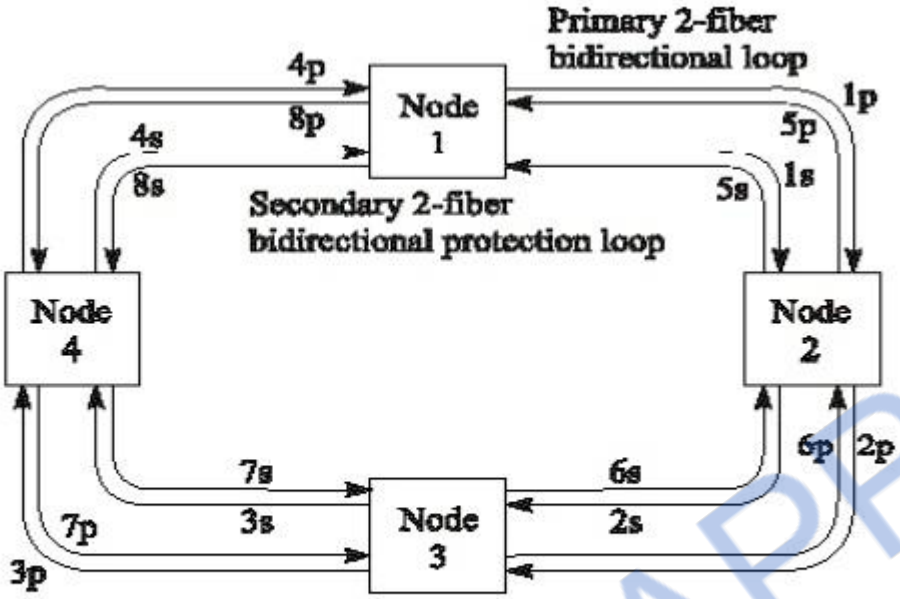

Node 1→3; 1p, 2p Node 3→1; 3p, 4p

BLSR Fiber-Fault Reconfiguration:

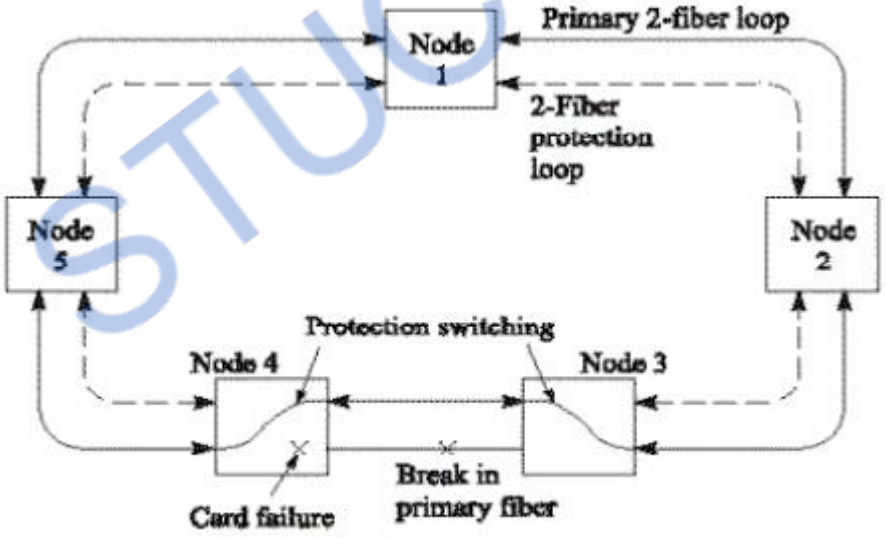

In case of failure, the secondary fibers between only the affected nodes (3 & 4) are used, the other links remain unaffected

BLSR Node-Fault Reconfiguration:

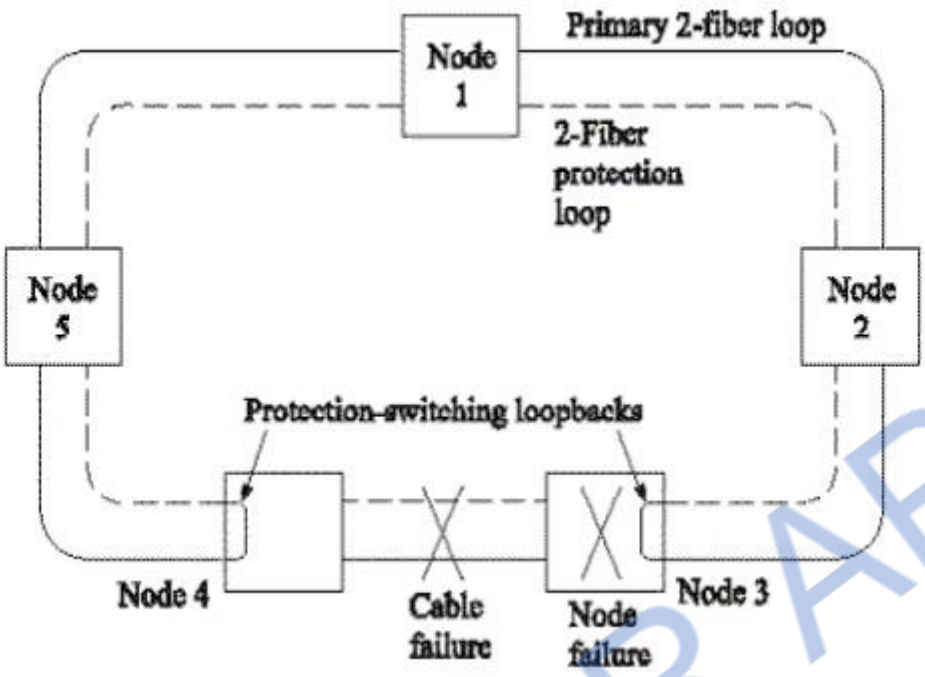

If both primary and secondary are cut, still the connection is not lost, but both the primary and secondary fibers of the entire ring is occupied

Broadcast and Select WDM Networks

•□□□□□□□□□□All-optical WDM networks have full potential of optical transmission capacity and versatility of communication networks beyond SONET architectures.

•□□□□□□□□□□These networks can be classified as

(1) Broadcast-and-select techniques

(2) Wavelength-routing networks.

•□□□□□□□□□□Broadcast-and select techniques employing passive optical stars, buses and wavelength routers are used for local networks can be classified as

(1) Single-hop networks

(2) Multi-hop networks

•□□□□□□□□□□Single hop refers to network where information transmitted in the form of light reaches its destination without being converted to an electrical form at any intermediate point. In a multi hop network, intermediate electro-optical conversion can occurred.

1. Broadcast and Select Signal Hop Network

•□□□□□□□□□□Two alternate physical architectures for a WDM-based local network have n sets of transmitters and receivers are attached to either a star coupler or a passive bus.

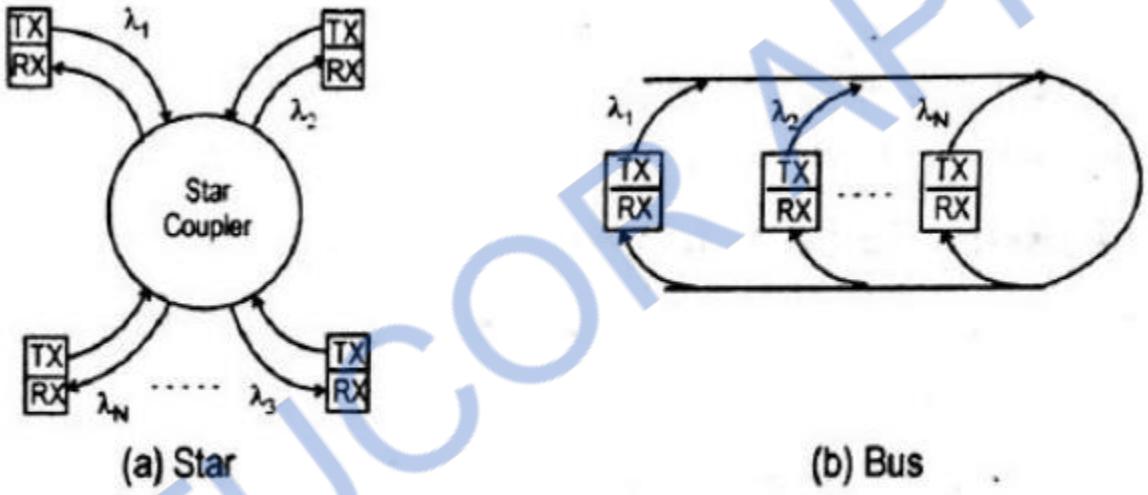

Figure 5.5 Physical architecture of WDM based local network

•□□□□□□□□□□Each transmitter sends its information at a fixed wavelength.

•□□□□□□□□□□All the transmissions from the various nodes are combined in a pasive star. Coupler or coupled onto a bus and sent out to all receivers.

•□□□□□□□□□□An interesting point to note is that the WDM setup is protocol transparent.

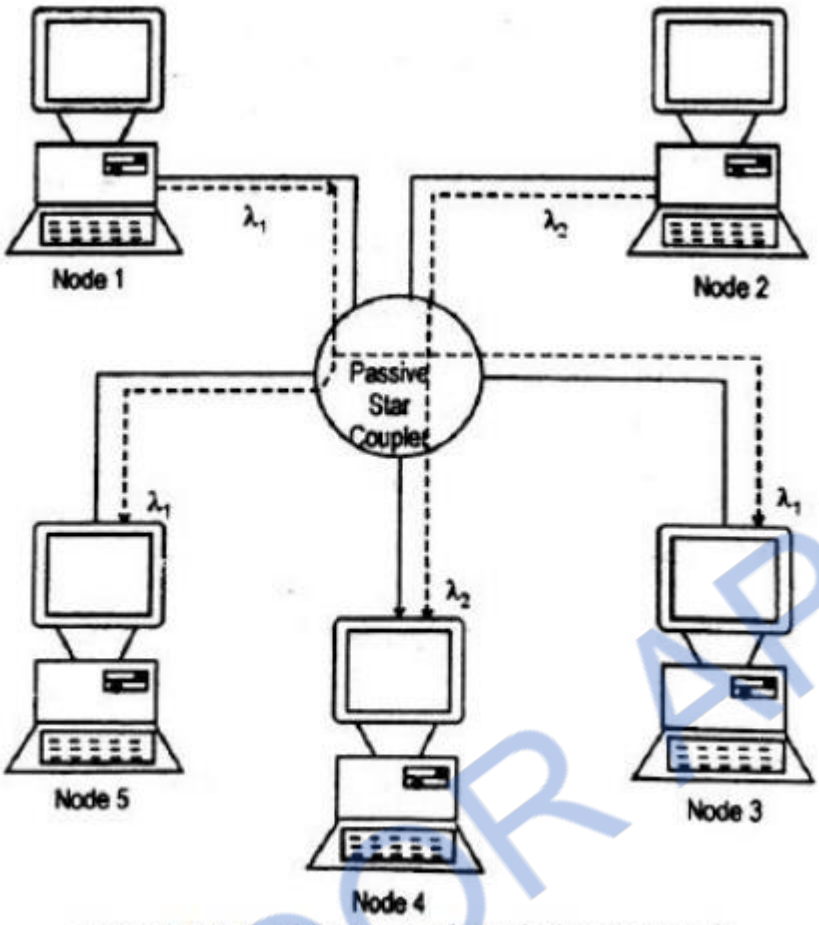

Figure 5.6 Architecture of single hop network

•□□□□□□□□□□□Protocol transparent means that different sets of communicating nodes can use different information exchange rules (protocols) without affecting the other nodes in the network.

•□□□□□□□□□□□The architectures of single-hop broadcast-and-select networks are fairly simple, there needs to be careful dynamic coordination between the nodes.

•□□□□□□□□□□□A transmitter sends its selective filter to that wavelength.

•□□□□□□□□□□□Two sending stations need to coordinate their transmission so tha collisions of information streams at the some wavelength do not occur.

2. Broadcast and Select Multihop Network

•□□□□□□□□□□□Drawback of single-hop networks is the need for rapidlyt unable lasers or receiver optical fibers.

•□□□□□□□□□□This drawback can be overcome by the designs of multihop networks.

•□□□□□□□□□□Multihop networks do not have direct paths between each node pair.

•□□□□□□□□□□Each node has a small number of fixed tuned optical transmitter and receivers.

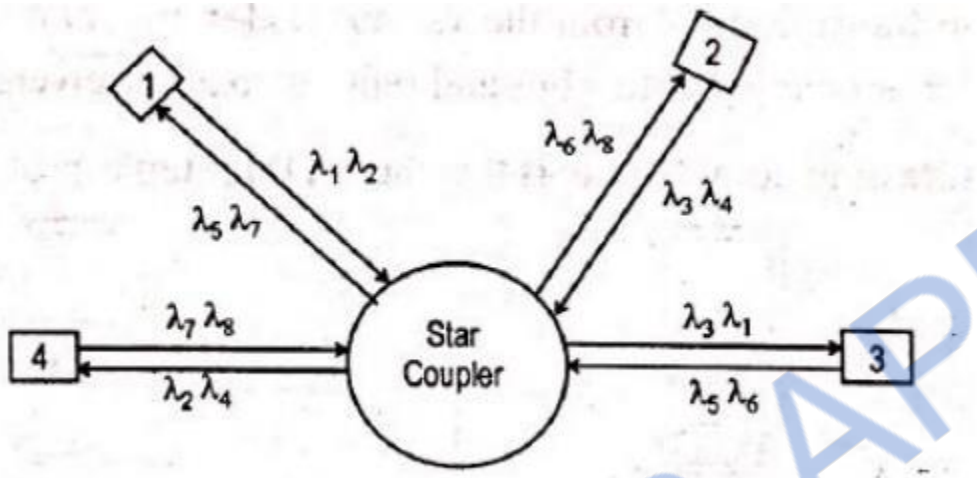

Figure 5.7 Broadcast and select Multihop networks

•□□□□□□□□□□An example, a four node broadcast and select multihop network where each node transmits on one set of two fixed wavelengths and receives on another set of two fixed wavelengths.

•□□□□□□□□□□Information destined for other nodes will have to be routed through intermediate stations.

•□□□□□□□□□□Considering the operation, a simplified transmission shceme in which message are sent as packets with a data field and an address header containing source and destination identifiers (i.e,. routing information) with control bits.

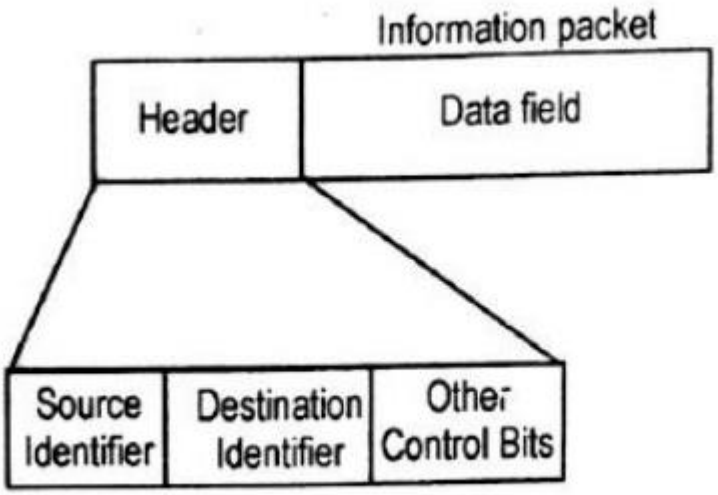

Figure 5.8 Simple representation of fields contained in a data pocket

•□□□□□□□□□□At intermediate node, the optical signal is converted to an electrical format.

•□□□□□□□□□□The address header is decoded to examine the routing information field, which will indicate where the packet should go.

•□□□□□□□□□□Routing information is used to send the electronic packets from optical transmitter to the next node in the logical path toward its final destination.

•□□□□□□□□□□**Advantage:** There are no destination conflicts or packet collisions in the network.

•□□□□□□□□□□For H hops between nodes, there is a network throughput penalty of at least 1/H.

3. The Shuffle Net Multihop Network

•□□□□□□□□□□Various topologies for multihop lighwave networks are

(1) The shuffle net graph

(2) The de Bruijin graph

(3) He toroidal Manhattan street network

•□□□□□□□□□□A scheme called the perfect shuffle is widely used to form processor interconnect patterns in multiprocessors.

•□□□□□□□□□□□For optical networks, the logical configuration consists of a cylindrical arrangement of k column, each having p nodes. Where P is the number of fixed transceiver pairs per node.

•□□□□□□□□□□□The total number of nodes is then

$$N = kp^k \quad \ldots (5.18)$$

where $k = 1, 2, 3, \ldots$

$p = 1, 2, 3, \ldots$

- The total number of wavelengths N_λ needed in the network is

$$N_\lambda = {}_pN = kp^{k+1} \quad \ldots (5.19)$$

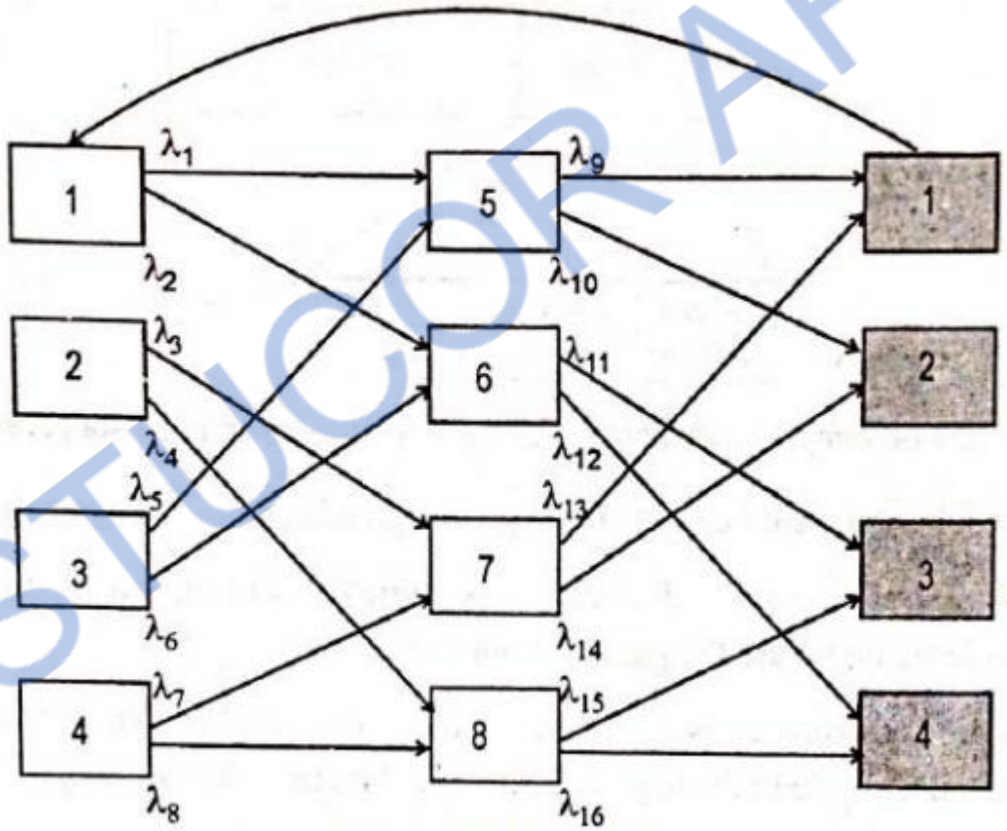

Figure 5.9 Shuffle Net

•□□□□□□□□□□□a (p,k)=(2,2) shuffle net, where the (k+1)th column represents the completion of a trip around the cylinder back to the first column.

•□□□□□□□□□□Performance parameter for the shuffle net is the average number of hops between any randomly chosen nodes.

•□□□□□□□□□□Since, all nodes have p output wavelength, p nodes can be reached from any node in one hop, p^2 additional nodes can be reached in two hope, until all the (p^k-1) other nodes are visited.

•□□□□□□□□□□The maximum number of hops is

$$H_{max} = 2k - 1 \qquad \ldots (5.20)$$

•□□□□□□□□□□Consider figure above, the connections between nodes 1 and 5 and nodes 1 and 7. In first case, the hop number is one.

•□□□□□□□□□□In second case three hops are needed with routes 1- 6 – 7 or 1 – 5 – 2 - 7.?

•□□□□□□□□□□The average of hops Bar H of a shuffle net is

- The average number of hops $\overline{H}$ of a Shuffle Net is

$$\overline{H} = \frac{1}{N-1}\left[\sum_{j=1}^{k-1} j p^j + \sum_{j=0}^{k-1}(k+j)+(p^k - p^j)\right]$$

$$= \frac{kp^k(p-1)(3k-1)-2k(p^k-1)}{2(p-1)(kp^k-1)} \qquad \ldots (5.21)$$

•□□□□□□□□□□In multiphopping, part of the capacity of a particular link directly connecting two nodes is actually utilized for carrying between them.

•□□□□□□□□□□The rest of thelink capacity is used to forward messages from other nodes.

•□□□□□□□□□□The system has $N_p = kp^{K+1}$ links, the total network capacity C is

$$C = \frac{kp^{k+1}}{\overline{H}} \qquad \ldots (5.22)$$

•□□□□□□□□□□The per-user throughput δ is

$$\delta = \frac{C}{N} = \frac{P}{H} \qquad \ldots (5.23)$$

•□□□□□□□□□□Different (p,k) combination result in different throughputs, to get a better network performance.

Wavelength Routed Networks

•□□□□□□□□□□Two problems arise in broadcast and select networks,

•□□□□□□□□□□More wavelengths are needs as the number of nodes in the network grows.

•□□□□□□□□□□Without the widespread are use of optical booster amplifier, due to this splitting losses is high.

•□□□□□□□□□□Wavelength routed networks overcome these limitations through wavelength reuse, wavelength conversion, and optical switching.

•□□□□□□□□□□The physical topology of a wavelength routed network consists of optical wavelength routers interconnected by pair of point-to-point fiber link in an arbitrary mesh configuration.

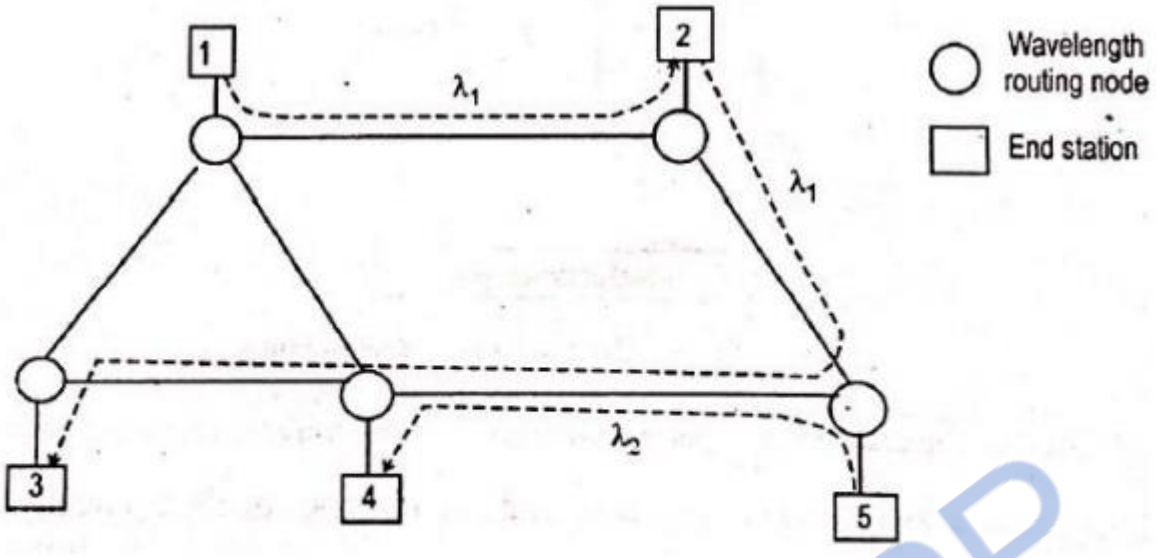

Figure 5.10 Wavelength Reuse on Mesh Network

•□□□□□□□□□□□Each link can carry a certain number off wavelength which can be directed independently to differently output paths at a node.

•□□□□□□□□□□□Each node may have logical connections with several other nodes in the network, where each connection uses a particular wavelength.

•□□□□□□□□□□□The paths taken by any two connections do not overlap, they can use the same wavelength.

1. Optical Cross Connect

•□□□□□□□□□□□The concept of an optical cross connect architecture is the physical path structure, have a high degree of path modularity, capacity scaling, and flexibility in adding or dropping channels at a user site can be achieved.

•□□□□□□□□□□□The physical path structure is called as path layer.

•□□□□□□□□□□□These cross connects (OXCs) operate in the optical domain and can route very high capacity WDM data streams over a network of interconnected optical paths.

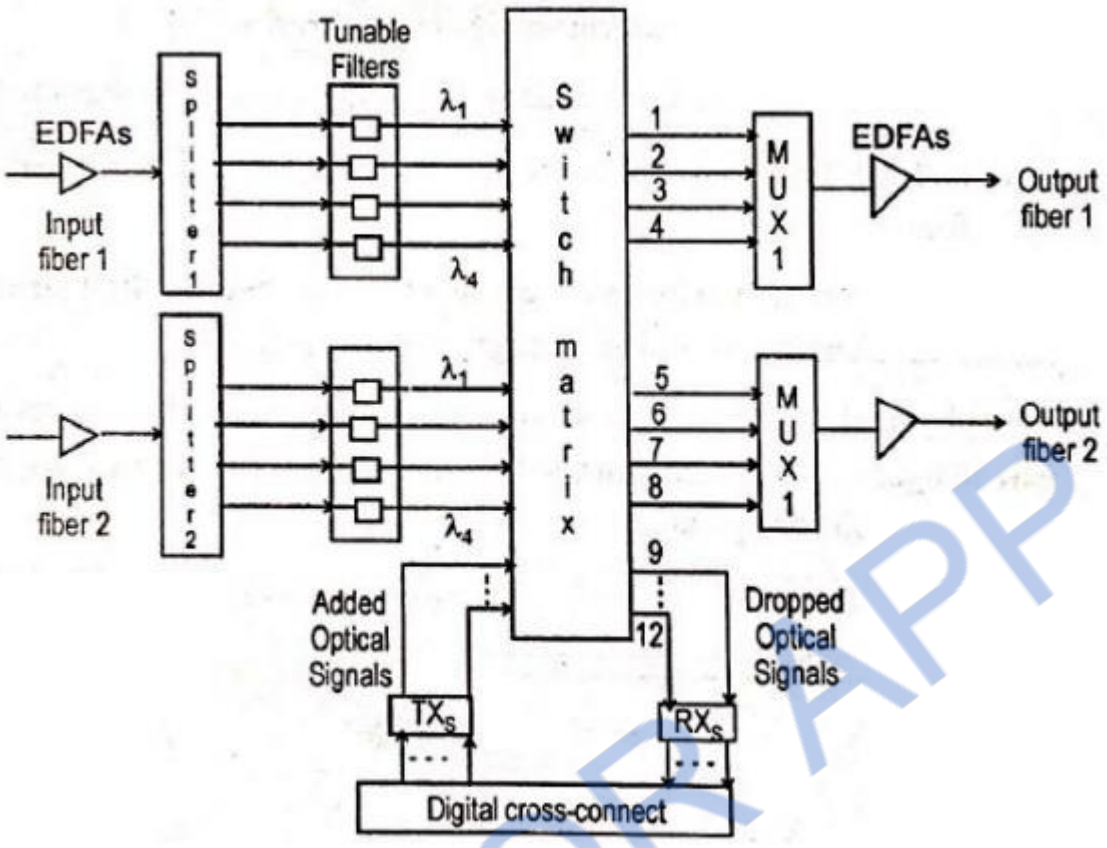

Figure 5.11 Optical Cross Connect Architecture

•□□□□□□□□□□□OXC architecture uses space switching without wavelength conversion.

•□□□□□□□□□□□The space switching can be constructed of a cascade of electronically controlled optical directional-coupler elements or semiconductor-optical-ampliier switching gates.

•□□□□□□□□□□□Each of the input fiber carries a M wavelengths.

•□□□□□□□□□□□The input, arriving aggregate if signal wavelength is amplified and divided into N streams by a power splitter.

•□□□□□□□□□□□Tunable filter then select individual wavelengths, which are directed to an optical space switching matrix.

•□□□□□□□□□□□A waveguide grating demultiplexer could be used to divide the incoming aggregate stream into individual wavelength channels.

•□□□□□□□□□□The switch matrix directs the channels either output lines, or to a particular receiver attached to the OXC at outputs ports 9 through 12.

•□□□□□□□□□□Signals that are generated locally by a user get connected electrically via the digital cross connect matrix (DXC) to an optical transmitter.

•□□□□□□□□□□They enter the switch matrix, which directs them to the appropriate output line.

•□□□□□□□□□□The M output lines, each carrying separate wavelength, are fed into a wavelength multiplexer (‘mux’ and a demultiplexer is ‘demux’) to form a single aggregate output stream.

•□□□□□□□□□□An optical amplifier to boost the signal level for transmission over the trunk fiber.

2. Performance Evaluation of Wavelemgth Conversion

•□□□□□□□□□□These effects are

(1) Probability models

(2) Deterministic algorithms

•□□□□□□□□□□The benefits are greater in a mesh network than in a ring or fully connected network.

The Effect of Wavelength Conversion

•□□□□□□□□□□Simple model, circuit switched networks is used.

•□□□□□□□□□□The probability that a wavelength is blocked along a path.

•□□□□□□□□□□It provides insight into the network performance improvement using wavelength conversion.

•□□□□□□□□□□Assume H links (or hops) between two nodes A and B.

•□□□□□□□□□□The expected number of busy wavelength on any link is ρF, where ρ is a measure of the fiber utilization along the path and F is the number of a available wavelengths per fiber link.

Non Linear Effect on Network Performance

Important Challenges In Designing Non Linear Networks Are:

•□□□□□□□□□□Transmission of the different wavelength channel at the highest possible bit rate.

•□□□□□□□□□□Transmission over the longest possible distance with the smallest number of optical amplifier.

•□□□□□□□□□□Network architectures that allow simple and efficient operation, control and management.

The Various Signal Impairment Effect are as Follows

i. **Group Delay Dispersion (GVD)**, Which limits the bit rate by temporally spreading a transmitted optical pulse, dispersion induced pulse spreading can be minimized by WDM networks operation in a low dispersion window such as 1310 nm and 1550 nm.

ii. Non-uniform gain across the desired wavelength range of EDFAs in WDM links.

iii. **Polarization Mode Dispersion (PMD)**, Which arises from orthogonal polarization modes traveling at a slightly different speeds owing to fiber birefringence.

iv. Reflections from splices and connectors that can cause instabilities in laser sources. These can eliminated by the use of optical isolators.

v. Non-linear inelastic scattering processes, which are interactions between optical signal and molecular or acoustic vibrations in a fiber.

v. Non-linear variations of the refractive index in a silica fiber that occur because the refractive index is dependent on intensity changes in the signal.

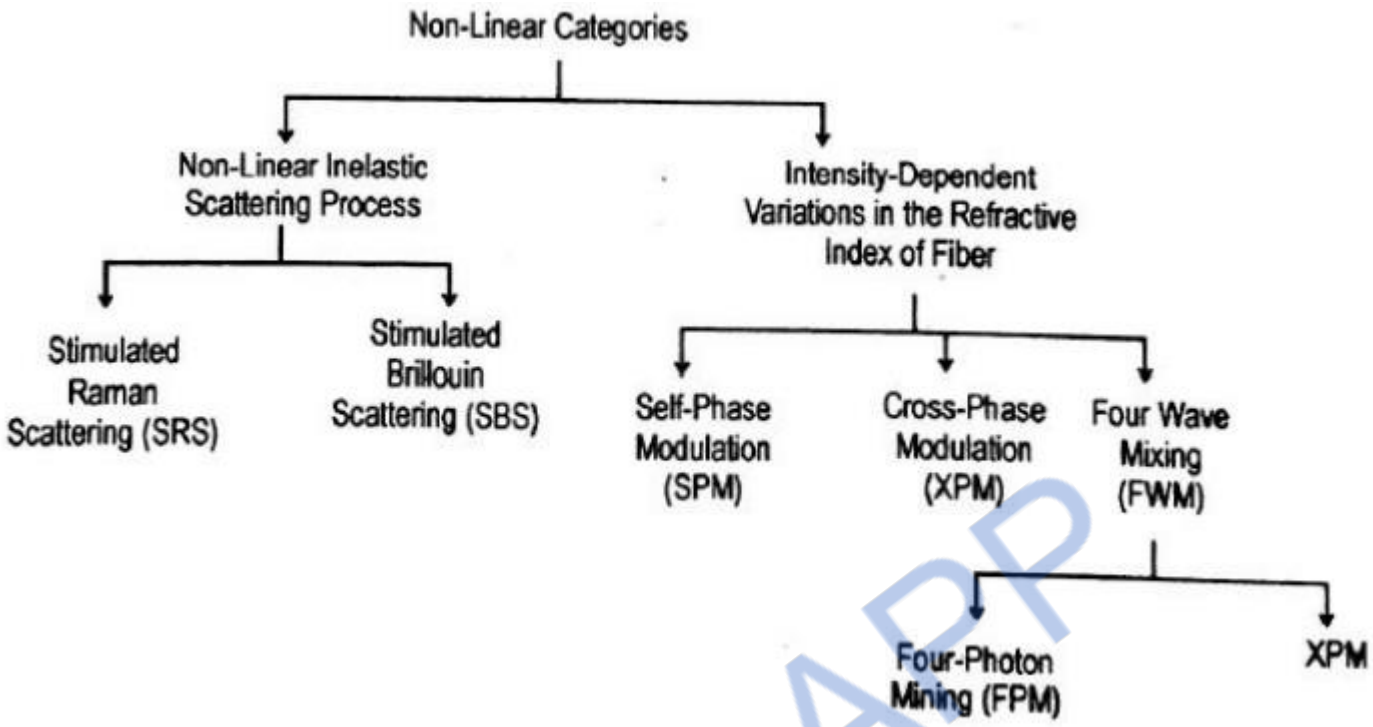

•□□□□□□□□□□□A connection request between modes A and B is blocked if one of the H intervening fibers is full.

•□□□□□□□□□□□The probability P_b' that a the connection request from A to B is blocked is the probabity and fiber link with all wavelength F.

$$P_b' = 1 - (1 - \rho^F)^H \qquad \ldots (5.24)$$

•□□□□□□□□□□□If q is the achievable utilization for a given blocking probability in a network with wavelength conversion.

$$q=\left[1-(1-P_b')^{1/H}\right]^{1/F}\approx\left(\frac{P_b'}{H}\right)^{1/F} \qquad \ldots(5.25)$$

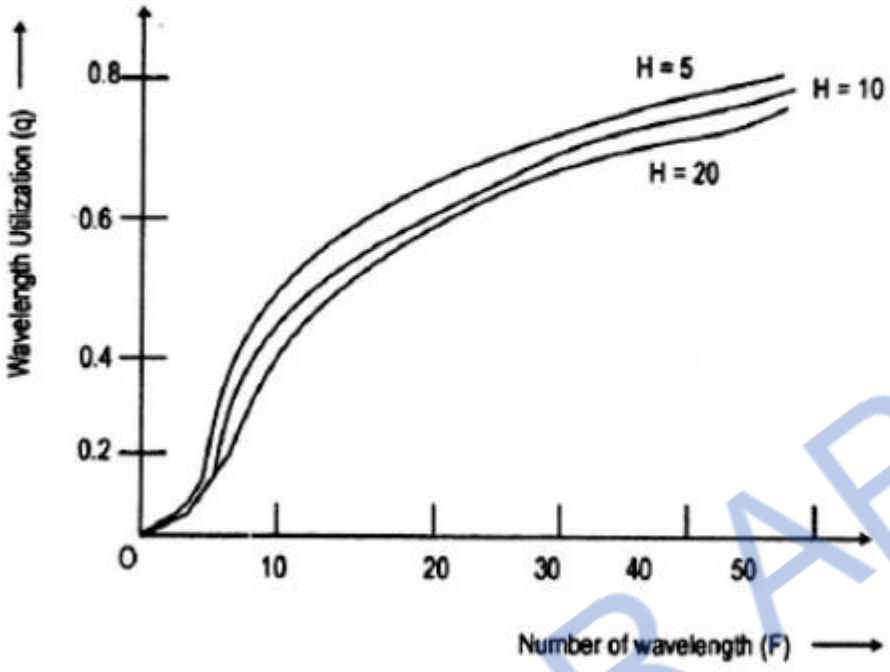

Figure 5.12 Wavelength utilization using wavelength conversion

•□□□□□□□□□□□The effect of path length is small, and q rapidly approaches I as F becomes large.

A Network Without Wavelength Conversion

•□□□□□□□□□□□A connection request between A and B can be honoured only if there is a free wavelength.

•□□□□□□□□□□□The probability P_b that the connection request from A and B is blocked is the probability that each wavelength is used on at least one of the H links,

$$P_b=[1-(1-\rho)^H]^F \qquad \ldots(5.26)$$

•□□□□□□□□□□□Letting P be the achievable utilization for a given blocking probability in a network without wavelength conversions,

$$P = 1 - (1 - P_b^{1/F})^{1/H} \approx -\frac{1}{H} \ln (1 - P_b^{1/F}) \qquad \ldots (5.27)$$

•□□□□□□□□□□Where the approximation holds for large values of H and for $P_{b1/F}$ not too close to unity.

•□□□□□□□□□□In this case, the achievable utilization is inversely proportional to the length of the path H between A and B.

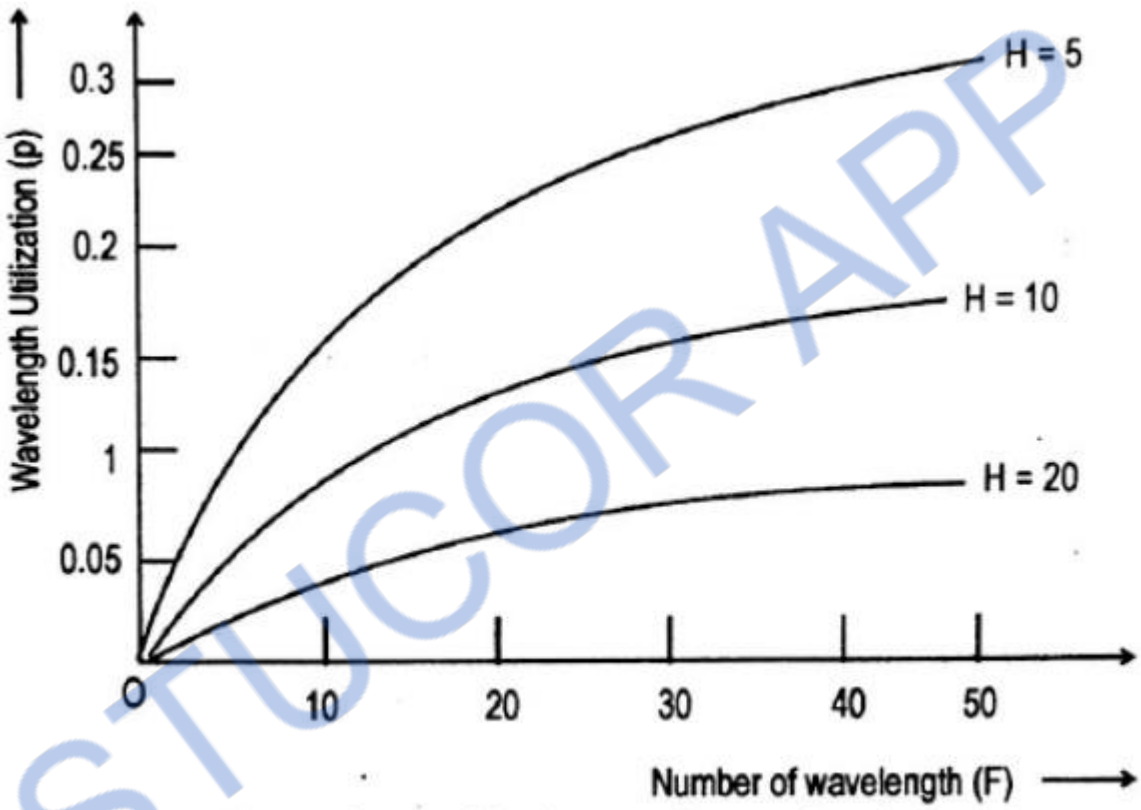

Figure 5.13 Wavelength utilization not using wavelength conversion

•□□□□□□□□□□Here the effect of path length (i.e., the number of links) is dramatic.

To Measure the Benefit of Wavelength Conversion

•□□□□□□□□□□The gain G=q/P to be the increase in fiber or wavelength utilization for the same blocking probability.

- From equation (5.25) and (5.27). Setting $P_b' = p_b$ we have

$$G = q/P$$

$$G \equiv \frac{q}{p} = \frac{1-\left[(1-P_b)^{1/H}\right]^{1/F}}{1-\left(1-P_b^{1/F}\right)^{1/H}}$$

$$\approx H^{1-1/F}\,\frac{P_b^{1/F}}{-\ln\left(1-P_b^{1/F}\right)} \qquad \ldots (5.28)$$

•□□□□□□□□□□□G as a function of H=5, 10 and 20 links for blocking probability for $p_b=10^{-3}$.

•□□□□□□□□□□□F increases, the gain increases, peaks at about H/2

•□□□□□□□□□□□The gain slowly decreases, since large trunking networks are more efficient.

1. Effective Length And Area

•□□□□□□□□□□□The non-linear process can be depend on the transmission length, the cross-sectional area of the fiber, and the optical power level in the fiber.

•□□□□□□□□□□□**Effective Length** L_{eff}: Which takes into account power adsorption along the length of the fiber (i.e., optical power decays exponentially with length) is given by

$$L_{eff} = \frac{1}{p_0}\int_0^L p(z)\,dz = \int_0^L e^{-\alpha z}\,dz = \frac{1-e^{-\alpha L}}{\alpha} \qquad \ldots (5.29)$$

•□□□□□□□□□□□When there is a optical amplifier in a link, the effective length is the sum of the effective lengths of the individual spans between optical amplifiers.

•□□□□□□□□□□□If the total amplified link length is L_A and the span length between amplifier is L, the effective length is

$$L_{eff} = \frac{1 - e^{-\alpha L}}{\alpha} \frac{L_A}{L} \qquad \text{... (5.30)}$$

•□□□□□□□□□□The effects of non-linearities increase with the light intensity in a fiber. This light intensity is inversely propoetional to the cross-sectional area of the fiber.

•□□□□□□□□□□As a rule of thumb, standard non-dispersion-shifted single mode fibers have effective area A_{eff}=80μm^2, dispersion-shifted fibers have effective area A_{eff} is 55μm^2 and dispersion-compenstating fibers have effective areas is 20oμm^2.

2. Stimulated Raman Scattering

•□□□□□□□□□□Stimulated Raman scattering is an interaction between light waves and the vibrational modes of silica molecules.

•□□□□□□□□□□If a photon with energy hv_1 is incident on a molecule having a vibrational frequency v_{in}, the molecule can absorb some energy from the photon.

•□□□□□□□□□□In interaction, the photon is scattered, thereby attaining a lower frequency v_2 a corresponding lower energy hv_2. The modified photon is called as stokes photon.

•□□□□□□□□□□The optical signal wave that is injected into a fiber is the source of the interacting photons, it is often called the pump wave, it supplies power from the generated wave.

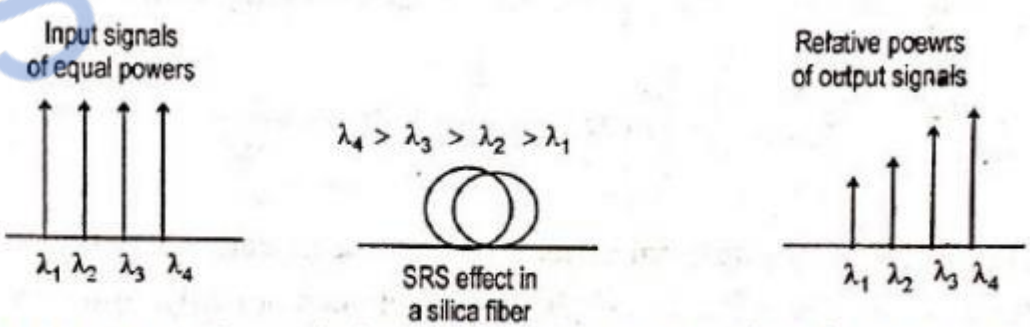

Figure 5.14 SRS Transfers optical power From Shorter Wavelength to Longer Wavelength

•□□□□□□□□□□SRS can severely limit the performance of a multichannel optical communication system by transferring energy from short-wavelength channels to

neighboring higher-wavelength channels. This is a broadband effect that can occur in both dirctions.

•□□□□□□□□□□The effects of SRS, consider WDM system has N channel equally spaced in a 30 nm band cantered at 1545 nm.

•□□□□□□□□□□Assume f_{out} (j) is the fraction of power coupled from channel o to channel j

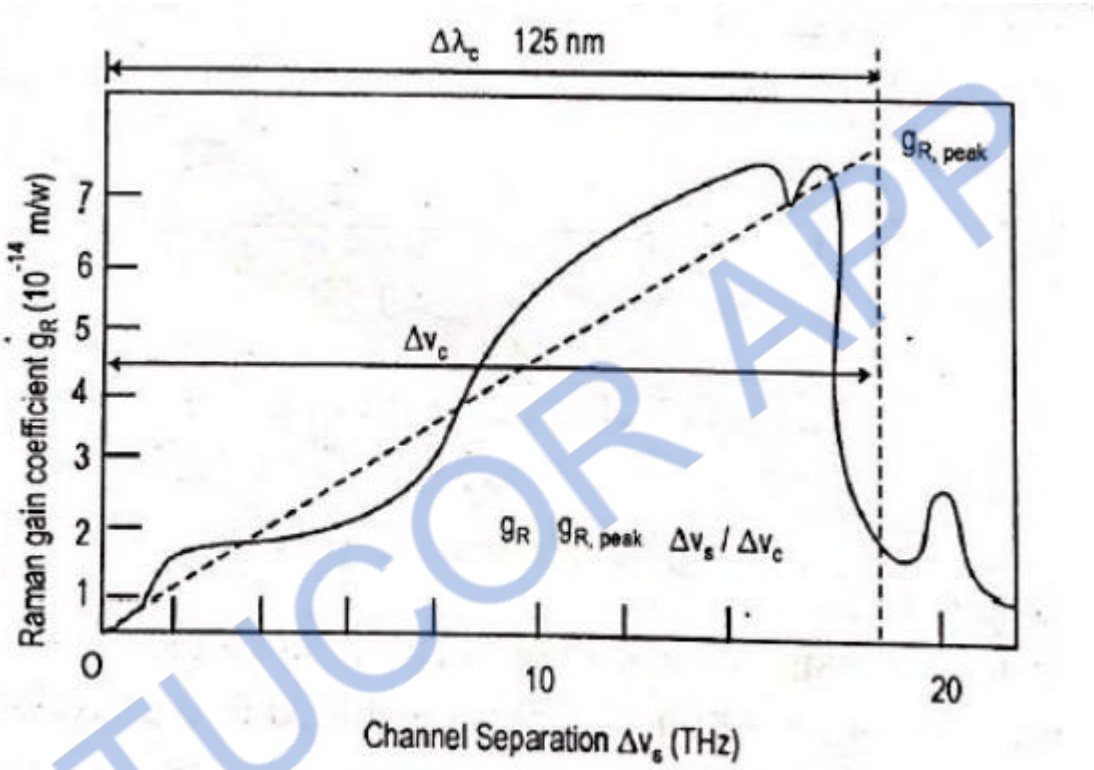

Figure 5.15 Wavelength Channel Separation

•□□□□□□□□□□The total fraction of power coupled out of 0 to all the other channel is

$$F_{out} = \sum_{j=1}^{N-1} F_{out}(j) = \sum_{j=1}^{N-1} g_{R,peak} \frac{j\Delta v_s}{\Delta v_c} \frac{PL_{eff}}{2A_{eff}}$$

$$= \frac{g_{R,peak}\,\Delta v_s\,PL_{eff}}{2\Delta v_c\,A_{eff}} \frac{N(N-1)}{2} \qquad \ldots(5.31)$$

•□□□□□□□□□□The power penalty for this channel is -10 log(1-F_{out})

•□□□□□□□□□□To keep power penalty <0.5 dB and F_{out} <0.1 use equation (5.31) with A_{eff}=55μm2, the criterion.

$$[NP]\,[N-1]\,\Delta v_s\,L_{eff} < 5 \times 10^{-3}\ \text{mW}\ .\ TH_z\ .\ km \qquad \ldots(5.32)$$

where NP is the total power coupled into the fiber,

$(N-1)\Delta v_s$ is the total occupied optical bandwidth.

L_{eff} is the effective length.

3. Stimulated Brillouin Scattering

•□□□□□□□□□□Stimulated Brillouin scattering arises when light waves scatter from acoustic waves.

•□□□□□□□□□□Scattered wave propagates principally in the backward direction in single-mode fibers. This backward light experiences gain from the forward-propagating signals.

•□□□□□□□□□□The frequency of the scattered light experiences a Doppler shift given by

$$v_B = 2n\,V_s/\lambda \qquad \ldots(5.33)$$

Where n is the index refraction, Vs is the velocity of sound in material.

•□□□□□□□□□□Interaction occurs Brillouin linewidth of Δv_g=20MHz at 1550nm.

•□□□□□□□□□□For V_s=5760 m/s in fused silica, the frequency of the backward propagating light at 1550 nm is shifted by 11 GHz(0.99nm) rom the original signal.

•□□□□□□□□□□In a long fiber chain containing optical amplifiers, there are optical isolators to prevent backward scattered signals form entering the amplifier.

•□□□□□□□□□□SBS threshold power P_{th} is defined to be the signal power at which the backward light equal the fiber-input power.

$$P_{th} \approx 21 \frac{A_{eff} b}{g_B L_{eff}} \left(1 + \frac{\Delta v_{source}}{\Delta v_B}\right) \quad \ldots (5.34)$$

where A_{eff} is the effective cross-sectional area of propagating wave.

b is the polarization factor (b = 1 to 2).

L_{eff} is the effective length.

g_B is the Brillouing gain cocefficient (4×10^{-11} m/w).

•□□□□□□□□□□□The SBS threshold power increase as the source linewidth becomes larger.

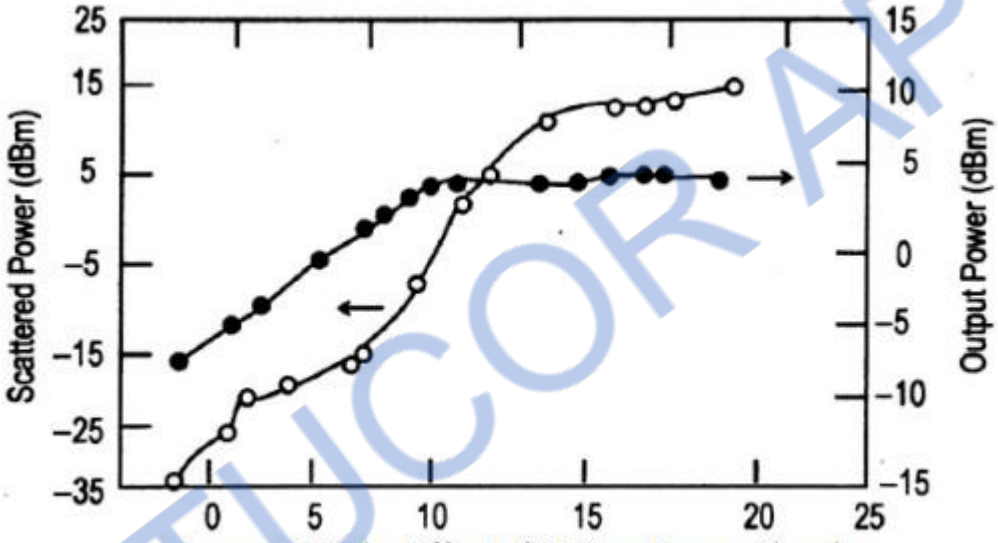

Figure 5.16 The Effect of SBS on Power Signal

•□□□□□□□□□□□Several schemes are available for reducing the power penalty effects of SBS as follows:

- Keeping the optical power per WDM channel below the SBS thresholds, for long-haul systems.
- Increasing the linewidth of the source, smince the gain bandwidth of SBS is very small. This can be achieved through direct modulation of the source.
- Slightly dithering the laser output in frequency, at roughly tens of kilohertz. The dither frequency should scale as the ratio of the injected power to the SBS threshold.

4. Cross Talk

Crosstalk: it is defined us the feed through of one channel signal into another channel.

Types Of Crosstalk:

There are two types of crosstalk that can occur is WDM systems:

(1) Intrachannel crosstalk

(2) Interechannel crosstalk

(I)INTRACHANNEL CROSSTALK;

It arises when interfering signal is at the same wavelength as the desired signal. This effect is more severe than interchannel crosstalk, because the interference falls completely with in the receiver bandwidth.

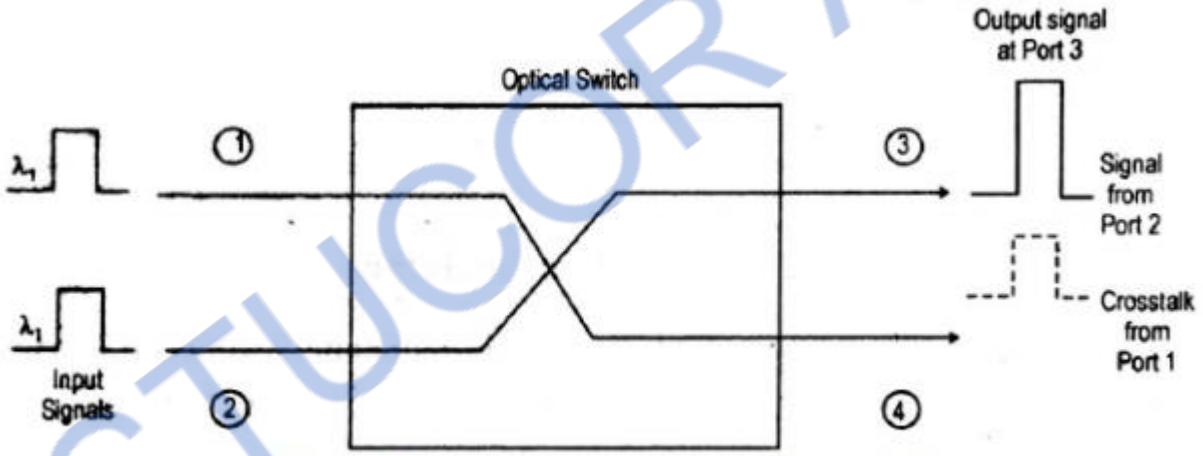

Figure 5.17 Origin of Inter channel Cross Talk

Two independent signals, each at a wavelength λ1, enter an optical switch.

This switch routes the signal entering port 1 to output port 4, and routes the signal entering port 2 to output port 3.

Within the switch, a spurious fraction of the optical power entering port 1 gets coupled to port 3, where it interferes with the signal from port 2.

(II) INTERCHANNEL CROSSTALK

It arises when an interfering signal comes from a neighboring channel that operates at a different wavelength.

Power penalty of interchannel crosstalk is

$$\text{Penalty}_{inter} = -5 \log (1 - \varepsilon) \quad \ldots (5.43)$$

where ε is the a fraction of received crosstalk power.

Average crosstalk power εiP, the factor is from equation (5.43)

$$\varepsilon = \sum_{i=1}^{N} \varepsilon_i \quad \ldots (5.44)$$

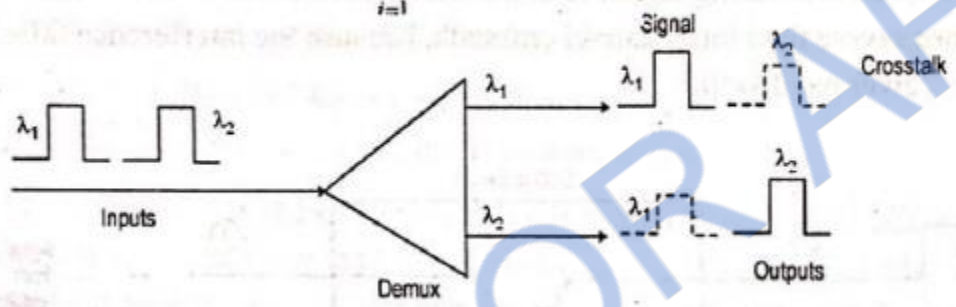

Fig. 5.32: Origin of interchannel crosstalk

Example, a 1 –dB penalty arises when the intrachannel level is 38.7 dB below the signal level and for interchannel crosstalk is 16 dB below the signal.

SOLITONS

Group velocity dispersion (GVD) causes most pulses to broaden in time as they propagate through an fiber.

A ‘solitons’ are pulses that travel along the fiber without change in shape or amplitude or velocity.

Soliton, takes advantage of non-linear effects in silica, particularly self phase modulation (SPM) resulting from the Kerr non-linearity, to overcome the pulse-broadening effects if GVD.

The term “soliton” refers to special kinds of waves that can propagate undistorted over long distances and remain unaffected after collision with each other.

In an optical communication system, solitons are very narrow, high intensity optical pulses that retain their shape through the interaction of balancing pulse dispersion with the non-linear properties of an optical fiber.

In an relative effects of SPM and GVD are controlled just right, and the appropriate pulse shape is chosen, the pulse compression routing from SPM can exactly offset the pulse broadening effect of GVD.

Fundamental Solitons- The family of pulse that do not change in shape are called fundamental solitons.

1. SOLITONS PULSE

When a pulse transverse a medium with a positive GVD parameter β_2 for the constituent frequencies, the leading part of the pulse is shifted toward a longer wavelength (lower frequencies) so that the speed in that portion increases.

In the trailing half, the frequency arises. So the speed decreases. This causes the trailing edge to be further delayed.

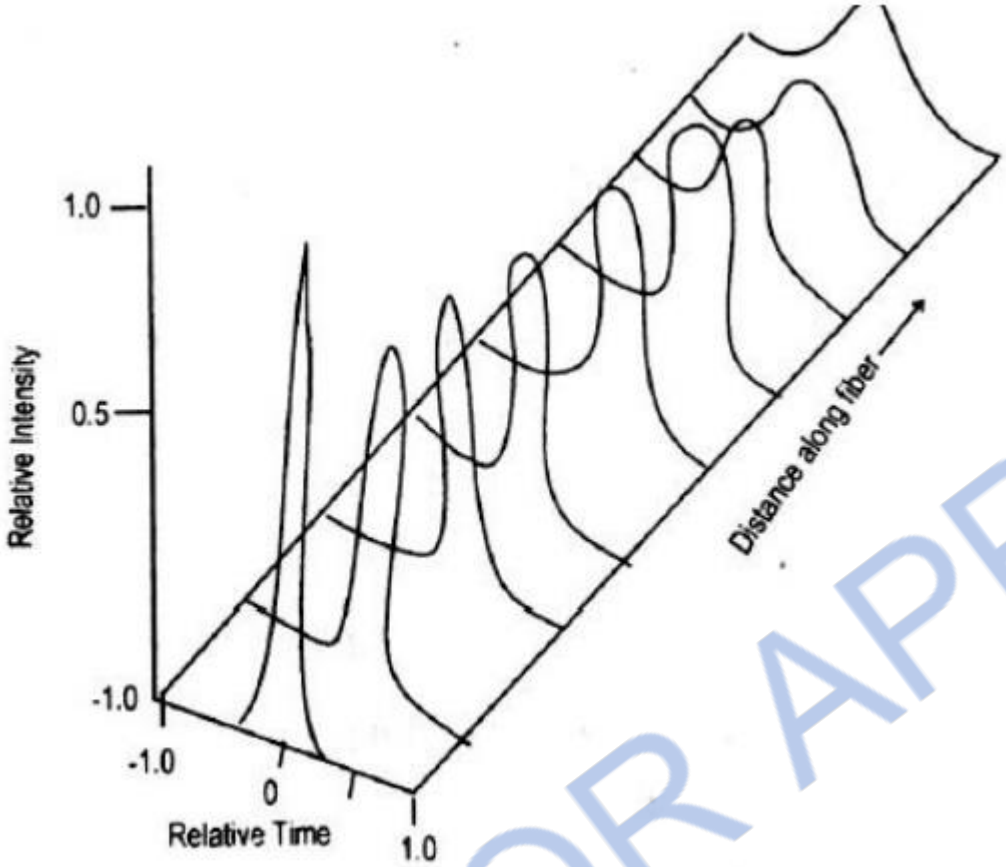

Figure 5.18 Temporal Change in a Narrow High Intensity Pulse

When a narrow high-intensity pulse traverse a medium with a negative GVD parameter for the constituting frequencies, GVD counteracts the chirp produced by SPM.

GND retards the low frequencies in the front end of the pulse and advances the high frequencies at the back.

The result is that the high-intensity sharply peaked soliton pulse changes neither its shape nor its spectrum as it travels along the fiber.

To derive the evolution of the pulse shape required for sodium transmission, one needs to consider the non-linear schrodinger (NLS) equation

$$-j\frac{\partial u}{\partial z}=\frac{1}{2}\frac{\partial^2 u}{\partial t^2}+N^2|u|^2u-j(\alpha/2)u \qquad \ldots(5.45)$$

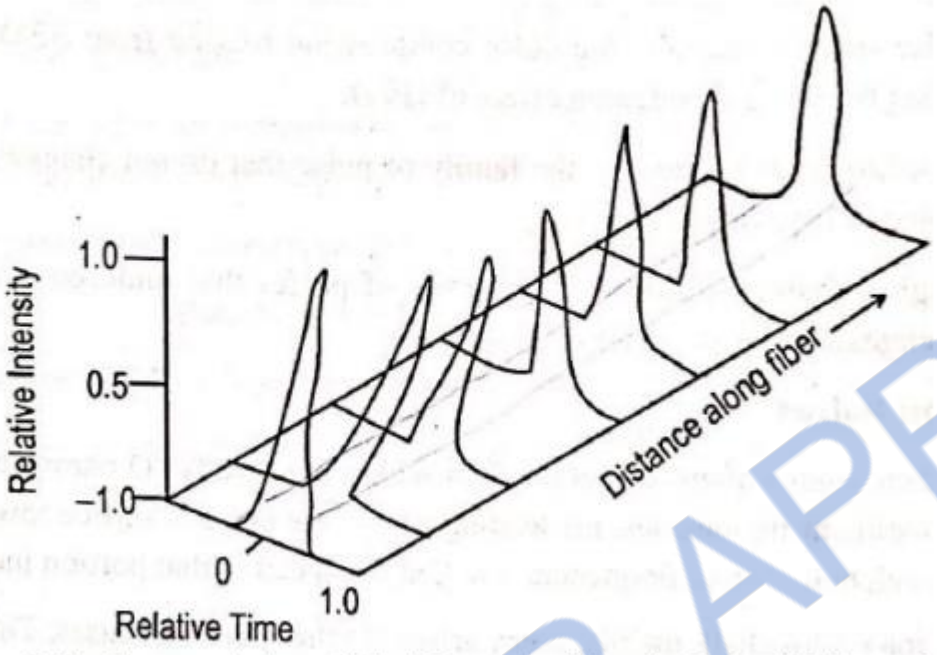

Figure 5.19 Characteristics of High Intensity Sharply Peaked Solitons Pulse

Special soliton units to eliminate scaling constants.

The Three Right-Hand Terms in Equation (5.45)

(1) The first term represents GVD effects of the fiber.

(2) The second non-linear term denotes the fact that the refractive index of the fiber depends on the light intensity.

Through the self-modulation process, this physical phenomenon broadens the frequency spectrum of a pulse.

(3) The third term represents the effects of energy loss or gain.

2. SOLITONS PARAMETERS

Full-Width Half-Maximum (FWHM)

The full-width Half-maximum (FWHM) is a pulse is defined as the full width of the pulse at its half-maximum power level.

The FWHM T_S of the fundamental soliton pulse in normalized time is found from the relationship

$$\text{sech}^2(\tau) = \frac{1}{2}$$

where $\tau = \frac{\tau_s}{(2T_o)}$.

T_0 is the basic normalized time unit.

$$T_0 = \frac{T_S}{2\cosh^{-1}\sqrt{2}} = \frac{T_S}{1.7627} \approx 0.567 T_S \qquad \ldots (5.49)$$

Dispersion Length (L_{disp})

The normalized distance parameter (also called dispersion length) L_{disp} is a characteristic length for the effects of the dispersion term.

L_{disp} is a measure of the period of a soliton

$$L_{disp} = \frac{2\pi c}{\lambda^2}\frac{T_0^2}{D} = \frac{1}{[2\cosh^{-1}\sqrt{2}]^2}\frac{2\pi c}{\lambda^2}\frac{T_s^2}{D}$$

$$\approx 0.322\frac{2\pi c}{\lambda^2}\frac{T_s^2}{D} \qquad \ldots (5.50)$$

where c is the speed of light,

λ is the wavlength in vacuum,

D is the dispersion of the fiber,

L_{disp} is measured in km.

The solition to equation (5.45) for the fundamental solution is given by

$$u(z, t) = \text{sech}(t)\exp(jz/2) \qquad \ldots (5.46)$$

Where sech (t) is the hyperbolic secant function. This is a bell-shaped pulse.

The phase term exp (jz/2) in equation (5.46) has no influence on the shape of the pulse, the soliton is independent of z and hence is non-dispersive in the time domain.

For the NLS equation, to find the first-order effects of the dispersive and non-linear terms are just complementary phase shifts.

For a given by equation (5.46), these phase shifts are

$$d\phi_{\text{non-line}} = |u(t)|^2\, dz = \text{sech}^2(t)dz \qquad \ldots (5.47)$$

For the non-linear process, and

$$d\phi_{disp} = \left(\frac{1}{2u}\frac{\partial^2 u}{\partial t^2}\right)dz = \left[\frac{1}{2} - \text{sec}\, h^2(t)\right]dz \qquad \ldots (5.48)$$

Dispersion and non-linear phase shifts of a soliton pulse which sum is constant, which yields a common phase shift of z\2 for the entire pulse.

Since such a phase shift changes neither the temporal nor the spectral shape of a pulse, the soliton remains completely non-dispersive in both the temporal and frequency domain.

Optical CDMA

The simplest configuration,CDMA achieves multiple access by assigning a unique code to each user.

To communicate with another node, user imprint their agreed upon code onto the data. The receiver can then decode the bit stream by locking onto the code sequence.

The principle of optical CDMA is based on spread-spectrum techniques.

The concept is to spread the energy of the optical signal over a frequency band that is much wider than the minimum bandwidth required to send the information.

Spreading is done by a code that is independent of the signal itself.

On optical encoder is used to map each bit of information into the high-rate (longer-code-length) optical sequence.

The symbols is the spreading code are called chips.

The energy density of the transmitted waveform is distributed more or less uniformly over the entire spread-spectrum bandwidth.

The set of optical sequences becomes a set of unique 'address codes or signature sequences' the individual network users.

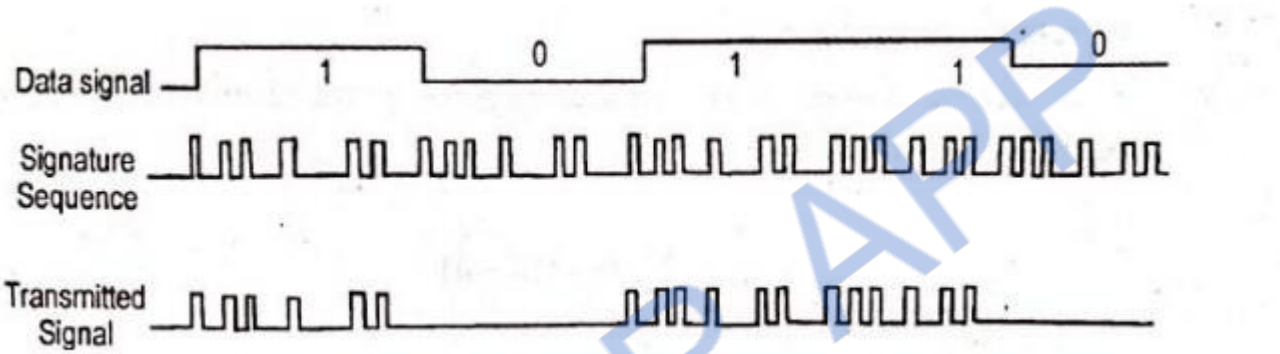

Figure 5.20 Six Chip optical CDMA Encoding Scheme

The signature sequence contains six chips. When the data signal contains 1 data bit, the six-chip sequence is transmitted, no chips are sent for a 0 data bit.

Time-domain optical CDMA allows a number of users to access a network simultaneously, through the use of a common wavelength.

Both asynchronous and synchronous optical CDMA techniques. In synchronous accessing schemes follow rigorous transmission schdules, the produce more successful transmission (higher throughputs) than asynchronous methods where network access is random and collisions between users can occurs.

An optical CDMA network is based on the use of a coded sequence of pulses.

The setup consists of N transmitter and receiver pairs interconnected in a star

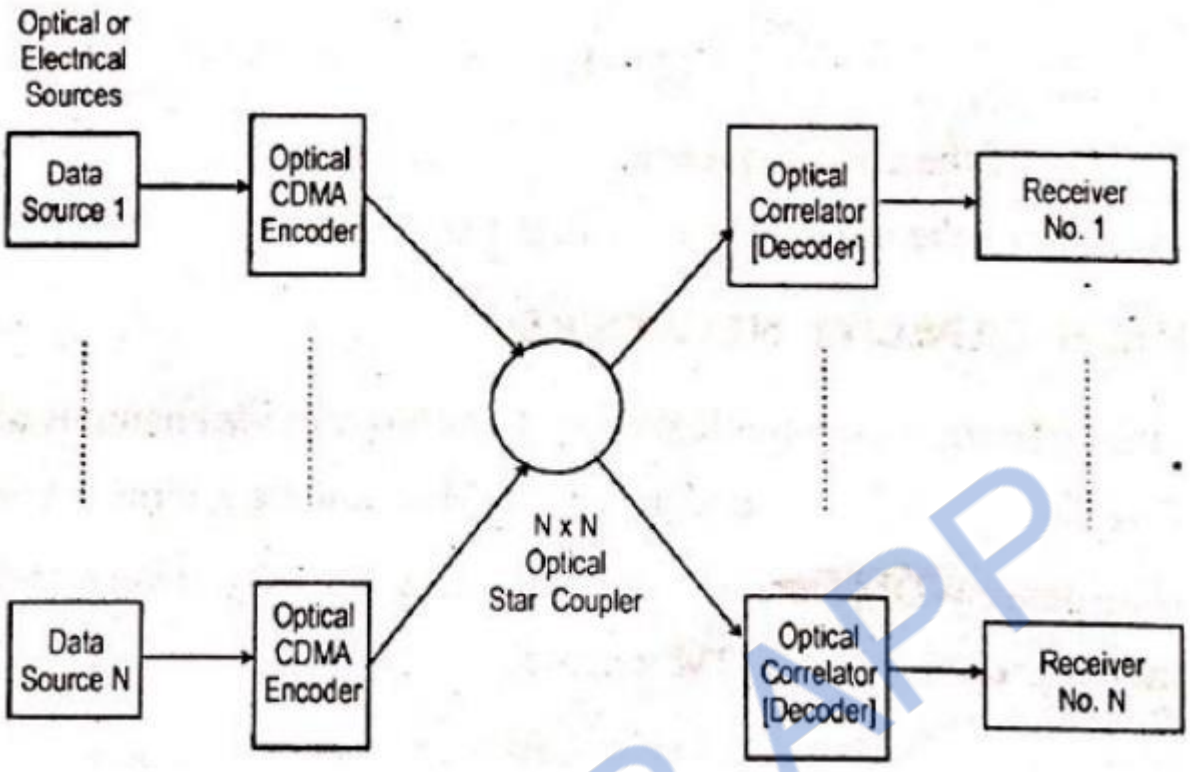

Figure 5.21 Optical CDMA Network Based on Using a Coded Sequence Pulse

To send information from node j to node k, the address code for node k is impressed upon the data by the encoder at node j.

At the destination, the receiver differentiates between codes by means of correlation detection.

Each receiver correlates its own address f(n) with the received signal s(n). The receiver output r(n) is

$$r(n) = \sum_{k=1}^{N} s(k) f(k-n) \qquad \ldots (5.57)$$

If the received signal arrives at the correct destination, then s(n)=f(n).

Equation (5.57) represents an autocorrelation function, if s(n) not equal to f(n) the equation (5.57) represents a cross-correlation function.

For a receiver to be able to distinguish the proper address correctly, it is necessary to maximize the autocorrelation function and minimize the cross-correlation function.

Prime-sequence codes and optical orthogonal codes (OOCs) are the commonly used spreading sequences in optical CDMA systems.

An OOC systems the number of simultaneous user an is bounded by

$$N \leq \left\lfloor \frac{F-1}{K(K-1)} \right\rfloor \qquad \ldots (5.58)$$

ULTRA HIGH CAPACITY NETWORKS

Advance of optical communication systems has provide channels with enormous bandwidth at least 25THz and dense WDM technology, ultrafast optical TDM.

To using dense WDM techniques to increase the capacity of long-haul transmission link and ultrafast optical TDM schemes.

These are particularly attractive in LAN or MANs

TDM Schemes To Shared-Media Local Neteorks Have Two Methods:

(1) Bit-interleaved TDM.

(2) Time-slotted TDM.

1. Ultra High Capacity WDM Networks

Two popular approaches are used to achieve increased capacity.

(a) to widen the spectral bandwidth of EDFAs from 30 to 80 nm, by using broadening techniques.

Increasing the capacity of a WDM link is to improve the spectral efficiency of the WDM signals.

Most of the demonstrations use a rate of 20 Gb/s for each individual wavelength to avoid non-linear effects.

Examples are,

(1) A 50-channel WDM system operating at an aggregated 1-Tb/s rate over a 600 km link.

(2) A 132-channel WDM system operating at an aggregated 2.6 Tb/s rate over a 120-km/link.

2. Bit-Interleaved Optical TDM

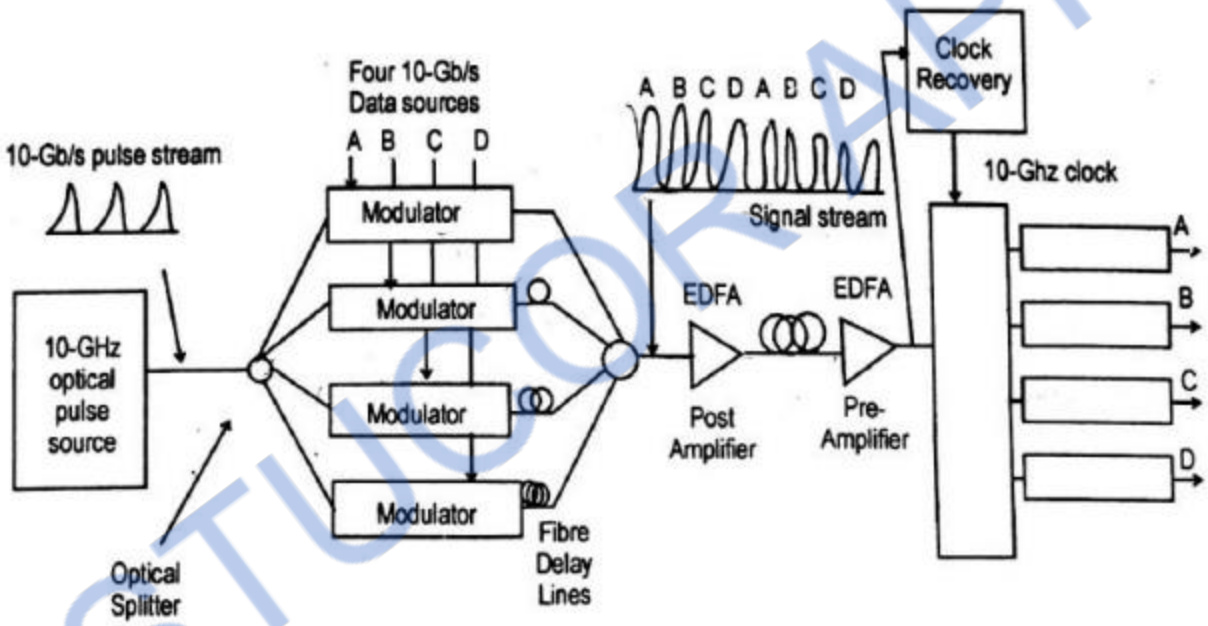

Figure 5.22 Ultrafast Point – Point Transmission System Using Optical TDM

Repetition rate typically ranges from 2.5 to 10 Gb/S, which corresponds to the bit rate of the electric data tributaries feeding the system.

An optical splitter divides the pulse train into N separate streams.

The pulse streams is 10 Gb/S and N=4, each of these channels is then individually modulated by an electrical tributary data source at a bit rate B.

The modulated outputs are delayed individually by different fractions of the clock period, and are then interleaved through an optical combiner to produce an aggregate bitrate of NXB.

Optical post amplifier and preamplifier are generally included in the link to compenstate for splitting and attenuation loss.

At the receiving end, the aggregate pulse stream is demultiplexed into the original N independent data channels for further signal processing.

A clock-recovery mechanism operating at the base bit rate B is required at the receiver to drive and synchronize the demultiplexer.

OPTICAL NETWORKS

1. What are the techniques to reduce optical feedback?

- Fiber end faces with a curved surface to the laser emitting facet.
- Index matching oil or gel at air glass interfaces.
- PC connectors
- Optical isolators within the transmitter module.

2. What are the basic performances of the WDM?

- Insertion loss
- Channel width
- Cross talk

3. What is WDM? Define.

WDM is wave length division multiplexing. The optical beam consists of different wavelengths and several channel information is transmitted over a single channel.

4. What is meant as bidirectional WDM?

A single WDM which operates as both multiplexing and De multiplexing Devices is said as the bidirectional WDM.

5. Define Radiance.

Radiance (or brightness) is a measure, in Watts, of the optical power radiated into a unit solid angle per unit area of the emitting surface.

6. What is meant by 'population inversion'?

In thermal equilibrium, the density of excited electrons is very small. Most photons incident on the system will therefore be absorbed, so that stimulated emission is essentially negligible. Stimulated emission will exceed absorption only if the population of the excited states is greater than that of the ground state. This condition is known as population inversion.

7. What are the factors to be considered in link power budget?

The factors to be considered in link power budget are:

- Transmission speed
- Optical sources & detectors
- Optical fiber

8. What are the causes of absorption?

Normally, the system is in the ground state. When a photon of energy hγ12 impinges on the system, an electron in state E1 can absorb the photon energy & be excited to state E2.

9. What is meant by hetero junction?

In hetero junction, two different alloy layers are on each side of the active region. Because of the sandwich structure of differently composed alloy layers, both the carriers & optical field are confined in the central active layer.

10. What is meant by indirect band gap semiconductor material?

For indirect band gap materials, the conduction-band minimum & the valence- band maximum energy levels occur at different values of momentum. Here, band-to- band recombination must involve a third particle to conserve momentum, since the photon momentum is very small. Phonons serve this purpose.

11. What is meant by 'modal noise'?

It arises when light from a laser is coupled into the multimode fiber.

12. .What is the necessity of cladding for an optical fiber?

a) To provide proper light guidance inside the core

b) To avoid leakage of light from the fiber

c) To avoid mechanical strength for the fiber

d) To protect the core from scratches and other mechanical damages

GLOSSARY

1. Techniques to reduce optical feedback.

Fiber end faces with a curved surface to the laser emitting facet.

Index matching oil or gel at air glass interfaces.

PC connectors

Optical isolators within the transmitter module.

2. Performances of the WDM.

• Insertion loss

• Channel width

• Cross talk

3. WDM.

WDM is wave length division multiplexing. The optical beam consists of different wavelengths and several channel information is transmitted over a single channel.

4. Bidirectional WDM.

A single WDM which operates as both multiplexing and De multiplexing Devices is said as the bidirectional WDM.

5. Radiance.

Radiance (or brightness) is a measure, in Watts, of the optical power radiated into a unit solid angle per unit area of the emitting surface.

6. Population inversion

In thermal equilibrium, the density of excited electrons is very small. Most photons incident on the system will therefore be absorbed, so that stimulated emission is essentially negligible. Stimulated emission will exceed absorption only if the population of the excited states is greater than that of the ground state. This condition is known as population inversion.

7. Causes of absorption

Normally, the system is in the ground state. When a photon of energy hγ12 impinges on the system, an electron in state E1 can absorb the photon energy & be excited to state E2.

8. Hetero junction

In hetero junction, two different alloy layers are on each side of the active region. Because of the sandwich structure of differently composed alloy layers, both the carriers & optical field are confined in the central active layer.

9. Indirect band gap semiconductor material

For indirect band gap materials, the conduction-band minimum & the valence- band maximum energy levels occur at different values of momentum. Here, band-to- band recombination must involve a third particle to conserve momentum, since the photon momentum is very small. Phonons serve this purpose.

10. PON.

A system that brings optical fiber cabling and signals all or most of the way to the end user. Depending on where the PON terminates, the system can be described as fiber-to-the-curb (FTTC), fiber-tothe- building (FTTB), or fiber-to-the-home (FTTH).